Techno-economic evaluation of bio-hydrogen production

via membrane reforming and cryogenic co2 separation.

TU Delft

TNO innovation for life

S. Tomar

Techno-economic evaluation of bio-hydrogen production

via membrane reforming and cryogenic CO_2 separation

by

S. Tomar

in partial fulfillment of the requirements for the degree of
Master of Science
in Sustainable Energy Technology
at the Delft University of Technology,
to be defended publicly on Monday September 14, 2020 at 03:00 PM.

Student number:	4798570	
Project duration:	January 6, 2020 – September 14, 2020	
Thesis committee:	Prof. dr. ir. W. de Jong,	TU Delft, Chair and supervisor
	Prof. dr. D. J. E. M. Roekaerts,	TU Delft
	Dr. ir. R. M. Stikkelman,	TU Delft

TU Delft

In all you do,
absolutely everything,
may love be the core.

-Christopher Poindexter

Acknowledgements

I wish to express my greatest gratitude to my daily advisor Francesco Sebastiani for giving me the opportunity to work on my graduation project at TNO and guiding me throughout the course of my project. Without his guidance and help this wouldn't have been possible.

I wish to thank my supervisor and committee chair Prof. Wiebren de Jong, for his guidance and support whenever I needed it. I also wish to thank all the people whose assistance was a milestone in the completion of this project. Jan Wilco Dijkstra for his expert advise on process modelling and basic membrane reactor development is Aspen Plus. Henk van Veen and Juriaan Boon for their valuable feedback and suggestions on my project scope and results. Marija Saric for the basic understanding of the ACM Membrane reactor model. I thank my committee members Prof. Dirk Roekaerts and Dr. Rob Stikkelman for agreeing to be a part of my graduation.

Furthermore, I wish to thank TU Delft and TNO for the wonderful experience throughout my studies and graduation project. I have evolved professionally and personally with all the knowledge and experience I have gained during this course of time.

Finally, I must express my very profound gratitude to my family and friends for providing me with unfailing support and continuous encouragement throughout my years of study and through the process of researching and writing this thesis. This accomplishment would not have been possible without them. Thank you.

Abstract

Transport sector CO_2 emissions are on the rise and responsible for nearly 30% of the EU's total CO_2 emissions (European Parliament, 2019). An attractive way to reduce the CO_2 emissions by transport is by changing the fuel used. Hydrogen is expected to play a key role in a clean, secure and affordable energy future (IEA). However, a clean, widespread use of hydrogen in global energy transitions faces several challenges. Currently, the global hydrogen production is approximately 7.2 EJ per year, 96% of which comes from fossil fuels. To harness the potential of hydrogen on the way to a clean energy future requires the capture of CO_2 from hydrogen production from fossil fuels and greater supplies of hydrogen from renewable energy sources. This study focuses on assessing the techno-economic potential of the membrane technology coupled with carbon capture technology, to produce decentralized bio-hydrogen in realizing a low carbon society in The Netherlands.

A literature survey was performed to determine the performance of the membrane reactor & cryogenic capture technologies and expected technological advancements. With the information obtained, a basic process of membrane reforming with carbon capture was modelled in Aspen Plus. Different configurations of the basic process were developed. In the first stage, thermodynamic key performance indicators were used to compare the performance of the different configurations developed. Secondly, one promising configuration was chosen and the levelized cost of hydrogen was used to optimize the process parameters like sweep ratio, permeate pressure, feed pressure etc. Finally, the optimum configuration was used to determine its economic and CO_2 emissions potential compared to the conventional steam methane reforming process. Exergy analysis for the optimum configuration was also performed.

The optimum levelized cost of hydrogen of the decentralized hydrogen production system developed in this work is calculated to be 4.19 €/$kg\ H_2$. The levelized cost of hydrogen for the equivalent centralized steam methane reforming system is 5.98 €/$kg\ H_2$. Therefore, the decentralized system developed is more attractive than the centralized system. The higher costs of the centralized system are due to the hydrogen transportation costs. Furthermore, the carbon capture unit costs 0.68 €/kg H_2 and an additional dehydration unit at 0.4 €/kg H_2 is required to meet the PEM fuel-cell hydrogen specifications. The efficiency and carbon capture rate of the developed configuration is 66.07% and 72.13% respectively, higher than the conventional process. The exergy efficiency of the developed process is 65.1%. The CO_2 emissions for the decentralized system across the value chain are calculated to be 1.4 kg CO_2/kg H_2. Future scenarios with renewable energy in the electricity mix result in negative CO_2 emissions, making the system attractive to limit the climate change and also benefit financially from the EU-ETS. The CO_2 emissions of the centralized system are 5.45 kg CO_2/kg H_2 with post-combustion carbon capture and 10.14 kg CO_2/kg H_2 with state-of-the-art reforming. With a carbon tax to be implemented soon, the costs of this system will rise making the decentralized system even more attractive. However, uncertainties in the development of an integrated hydrogen transport infrastructure, fuel-grade hydrogen demand, technological advancements in membrane reactors etc. may affect the comparative attractiveness of the systems.

Contents

List of Figures ix

List of Tables xiii

Nomenclature xviii

1 Introduction 1
- 1.1 Scope of the research . . . 2
- 1.2 Methodology . . . 3

2 Theoretical Background 5
- 2.1 Hydrogen . . . 5
- 2.2 Conventional hydrogen production process . . . 6
- 2.3 Membrane reforming for hydrogen production . . . 7
- 2.4 Feed . . . 9
  - 2.4.0.1 **Biogas in the Netherlands** . . . 9
  - 2.4.1 Feed pre-treatment . . . 9
    - 2.4.1.1 **Effect of impurities in the feed** . . . 9
    - 2.4.1.2 **Pre-treatment technologies** . . . 10
- 2.5 Membrane technology . . . 10
  - 2.5.1 Membranes for hydrogen separation . . . 12
    - 2.5.1.1 **Material & fabrication** . . . 12
    - 2.5.1.2 **Membrane configurations** . . . 14
    - 2.5.1.3 **Hydrogen permeation mechanism** . . . 14
    - 2.5.1.4 **Commercialization of dense metal membranes** . . . 15
  - 2.5.2 Membrane reactors . . . 16
    - 2.5.2.1 **Membrane reactor performance for hydrogen production** . . . 17
- 2.6 Carbon capture and storage . . . 20
  - 2.6.1 Carbon capture with cryogenic technology . . . 21
  - 2.6.2 Transport and storage . . . 23
- 2.7 Industrial processes . . . 24
- 2.8 Key takeaways . . . 25

3 Basis of design 27
- 3.1 Value chain definition . . . 27
  - 3.1.1 Reference system value chain . . . 27
  - 3.1.2 Novel system value chain . . . 28
- 3.2 System description . . . 28
  - 3.2.1 Process description . . . 29
  - 3.2.2 Battery limits . . . 30
  - 3.2.3 Design assumptions . . . 30
  - 3.2.4 Model description . . . 32
    - 3.2.4.1 **Membrane reactor Aspen Plus Point model** . . . 32
    - 3.2.4.2 **Membrane reactor ACM model** . . . 33
  - 3.2.5 Modelling assumptions . . . 34
    - 3.2.5.1 **General process assumptions** . . . 34
    - 3.2.5.2 **Membrane reactor Aspen Plus Point model** . . . 36
    - 3.2.5.3 **Membrane reactor ACM model** . . . 36
  - 3.2.6 Configurations generated . . . 37
- 3.3 Key performance indicators definition . . . 40
- 3.4 Key takeaways . . . 41

4 Process design & optimization **43**
4.1 Method for process configuration selection . . . 43
4.2 Process configuration selection . . . 44
4.3 Process optimization . . . 48
4.3.1 Carbon capture optimization . . . 48
4.3.2 Heat integration . . . 49
4.4 Conclusion . . . 50

5 Techno-economic evaluation **51**
5.1 Economic factors . . . 51
5.1.1 General assumptions . . . 51
5.1.2 Capital expenditure (CAPEX) . . . 52
5.1.3 Operational expenditure . . . 53
5.2 LCOH optimization . . . 55
5.2.1 Method for LCOH optimization . . . 55
5.2.2 Optimization results . . . 55
5.3 (Local) Optimum result . . . 59
5.3.1 Sensitivity analysis on LCOH . . . 60
5.4 Comparison with reference . . . 61
5.4.1 Techno-economic comparison . . . 61
5.4.2 Carbon footprint comparison . . . 63
5.5 Conclusion . . . 65

6 Exergy analysis **67**
6.1 Definition . . . 67
6.2 Physical & chemical exergy . . . 67
6.3 Exergy calculation . . . 68
6.4 Conclusion . . . 70

7 Conclusion and recommendations **71**

Bibliography **73**

A Aspen models **79**

B Performance results of the three configurations **85**
B.1 Process with carbon capture unit before the membrane reactor . . . 85
B.1.1 Sweep ratio: Base case, Case 2.1, Case 2.2 & Case 2.3 . . . 85
B.1.2 Recycle ratio: Base case & Case 3.1 . . . 89
B.1.3 Permeate pressure: Base case, Case 4.1, Case 4.2 & Case 4.3 . . . 94
B.2 Process with carbon capture unit after the membrane reactor: without recycle of off-gases . . . 97
B.2.1 Sweep ratio: Base case, Case 2.1, Case 2.2 & Case 2.3 . . . 98
B.2.2 Permeate pressure: Base case, Case 4.1, Case 4.2 & Case 4.3 . . . 102
B.3 Process with carbon capture unit after the membrane reactor: with recycle of off-gases . . . 104
B.3.1 Sweep ratio: Base case, Case 2.1 & 2.2 & Case 2.3 . . . 105
B.3.2 Recycle ratio: Base case & Case 3.1 . . . 108
B.3.3 Permeate pressure: Base case, Case 4.1, Case 4.2 & Case 4.3 . . . 112

C Pinch analysts: T-Q curves **119**

D Results of the cases formulated for LCOH optimization **121**

E Cases formulated for (local) optimum process determination **125**

F Break-down of cost components for the (local) optimum process **127**

G Break-down of CO_2 emissions of the four cases **131**

H Standard molar chemical exergy of selected substances **135**

I Exergy calculation verification **137**

List of Figures

1.1 CO_2 emissions by sector in The EU (European Parliament, 2019). 1
1.2 Share of the hydrogen production methods (Voldsund et al., 2016). 2

2.1 Process scheme for conventional SMR. 6
2.2 Process scheme for the MR. 7
2.3 Biogas purification methods (Zăbavă et al., 2019). 10
2.4 Membrane unit (Kluiters, 2004) 11
2.5 Co-current set-up (Kluiters, 2004). 11
2.6 Counter-current set-up (Kluiters, 2004). 11
2.7 Co-current set-up (Kluiters, 2004). 11
2.8 Counter-current set-up (Kluiters, 2004). 11
2.9 Membrane unit (Kluiters, 2004). 12
2.10 H_2 solubility (cm^3 of H2/100 g metal) in different metals at 1 atm (Yun and Ted Oyama, 2011). 13
2.11 Mechanism of permeation of hydrogen through metal membranes (Hamstra et al., 2015). 14
2.12 Basis sketch of the reactor used by Van Delft et al. (2009). 17
2.13 Methane conversion with a membrane reactor (MR), fixed-bed reactor (FBR) and equilibrium conversion (thermo) vs feed flow (Van Delft et al., 2009). 17
2.14 Methodology for determining optimum hydrogen cost of a plant (Shafiee et al., 2016). . 18
2.15 Membrane reactor configuration (Chompupun et al., 2018). 19
2.16 Two-dimensional model of the membrane reactor (Chompupun et al., 2018). 19
2.17 Simplified reactor model for scaling-up (Chompupun et al., 2018) 19
2.18 3-D unit cell honeycomb monolith reactor (Chompupun et al., 2018). 19
2.19 Methodology for determining optimum hydrogen cost of a plant (Shafiee et al., 2016). . 20
2.20 CO_2 capture technologies with high concentration of CO_2 (Hartnig and Roth, 2012). . . . 21
2.21 Cryogenic CO_2 capture with flash separators (Atsonios et al.). 22
2.22 Cryogenic CO_2 capture with distillation column (Atsonios et al.). 22
2.23 CO_2 separation and purification process developed by Xu et al. (2014). 22
2.24 Phase diagram of CO_2 (Witkowski et al., 2014). 23
2.25 Process flow of Port Jérôme plant (Terrien et al., 2014). 24
2.26 Senju Hydrogen Station (Shirasaki et al., 2009). 25

3.1 SMR process producing 1.5 million $Nm^3/day\ H_2$ (Spath and Mann, 2001). 28
3.2 Value chain of reference SMR system (Spath and Mann, 2001) & (Katikaneni et al., 2014). 28
3.3 Value chain of novel case 28
3.4 Novel process producing 500 $Nm^3/h\ H_2$. 29
3.5 Sketch of the whole system from biogas production to refueling station. 30
3.6 Process block diagram (PBD) of Configuration 1: Carbon capture unit before the reforming section. 38
3.7 Process block diagram of Configuration 2: Carbon capture unit after the reforming section without recycle stream. 38
3.8 Process block diagram of Configuration 3: Carbon capture unit after the reforming section with recycle stream. 39

4.1 L/S & area vs biogas feed. 44
4.2 Global hydrogen recovery factor for all three configurations varying biogas feed from 9.75 to 10.5 kmol/h. 45
4.3 Carbon capture rate for all three configurations varying biogas feed from 9.75 to 10.5 kmol/h. 45

4.4 Global methane conversion for all three configurations varying biogas feed from 9.75 to 10.5 kmol/h. . . . 46
4.5 Global efficiency for all three configurations varying biogas feed from 9.75 to 10.5 kmol/h. 46
4.6 Per-pass hydrogen recovery factor for all three configurations varying biogas feed from 9.75 to 10.5 kmol/h. . . . 47
4.7 Per-pass methane conversion for all three configurations varying biogas feed from 9.75 to 10.5 kmol/h. . . . 47
4.8 Total work & duties of the three different configurations with biogas feed of 10.5 kmol/h. 48
4.9 Single stage refrigeration cycle using propylene as refrigerant (Luyben, 2017). . . . 49
4.10 Grand composite curve for Base case with biogas feed flow rate of 10.5 kmol/h. . . . 50

5.1 Levelized cost of hydrogen with varying biogas feed flow rate. . . . 56
5.2 Levelized cost of hydrogen with varying sweep ratio. . . . 56
5.3 Membrane surface area vs hydrogen compressor duty for different permeate pressure. 57
5.4 Levelized cost of hydrogen with varying permeate pressure. . . . 57
5.5 OPEX of hydrogen dehydration unit for different permeate pressure. . . . 58
5.6 Levelized cost of hydrogen with varying reactor pressure. . . . 58
5.7 Cost changes in the reforming & carbon capture section with varying reactor pressure. . 59
5.8 Contribution to total annual cost. . . . 60
5.9 LCOH sensitivity for cost variation of $\pm$ 50% from reference value. . . . 61
5.10 Components of LCOH for the four cases. . . . 62
5.11 Future CO_2 emissions scenario. . . . 64

6.1 Exergy in and out distribution of the system. . . . 69
6.2 Grassmann diagram of novel system. . . . 69

A.1 Aspen model of Configuration 1: process with carbon capture unit before the reforming section. . . . 80
A.2 Aspen model of Configuration 2: process with carbon capture unit after the reforming section without recycle stream. . . . 81
A.3 Aspen model of Configuration 3: process with carbon capture unit after the reforming section with recycle stream. . . . 82
A.4 Aspen model of the optimum process. . . . 83
A.5 Aspen model of the carbon capture unit of the optimum process. . . . 84

B.1 Global hydrogen recovery factor vs productivity for different sweep ratios, varying biogas feed from 9.75 to 10.5 kmol/h. . . . 85
B.2 Carbon capture rate vs productivity for different sweep ratios, varying biogas feed from 9.75 to 10.5 kmol/h. . . . 86
B.3 Work & duties (reforming section) for different sweep ratios with biogas feed of 10.5 kmol/h. 87
B.4 Total Work & duties of the process for different sweep ratios with biogas feed of 10.5 kmol/h. . . . 87
B.5 Membrane surface area vs sweep ratio. . . . 88
B.6 Global methane conversion vs productivity for different sweep ratios varying biogas feed from 9.75 to 10.5 kmol/h. . . . 88
B.7 Global efficiency vs productivity for different sweep ratios varying biogas feed from 9.75 to 10.5 kmol/h. . . . 89
B.8 Global hydrogen recovery factor vs productivity for different recycle ratios varying biogas feed from 9.75 to 10.5 kmol/h. . . . 90
B.9 Carbon capture rate vs productivity for different recycle ratios varying biogas feed from 9.75 to 10.5 kmol/h. . . . 90
B.10 Per-pass hydrogen recovery factor vs productivity for different recycle ratios varying biogas feed from 9.75 to 10.5 kmol/h. . . . 91
B.11 Per-pass methane conversion vs productivity for different recycle ratios varying biogas feed from 9.75 to 10.5 kmol/h. . . . 91
B.12 Global methane conversion vs productivity for different recycle ratios varying biogas feed from 9.75 to 10.5 kmol/h. . . . 92

B.13 Global efficiency vs productivity for different recycle ratios varying biogas feed from 9.75 to 10.5 kmol/h. . . . 92
B.14 Total work & duties of the process for different recycle ratios with biogas feed of 10.5 kmol/h. . . . 93
B.15 Work & duties (reforming section) for different recycle ratios with biogas feed of 10.5 kmol/h. . . . 93
B.16 Work & duties (carbon capture unit) for different recycle ratios with biogas feed of 10.5 kmol/h. . . . 94
B.17 Global hydrogen recovery factor vs productivity for different permeate pressures varying biogas feed from 9.75 to 10.5 kmol/h. . . . 95
B.18 Carbon capture rate vs productivity for different permeate pressures varying biogas feed from 9.75 to 10.5 kmol/h. . . . 95
B.19 Global methane conversion vs productivity for different permeate pressures varying biogas feed from 9.75 to 10.5 kmol/h. . . . 96
B.20 Global efficiency vs productivity for different permeate pressures varying biogas feed from 9.75 to 10.5 kmol/h. . . . 96
B.21 Membrane surface area vs hydrogen compression work for different permeate pressures. 97
B.22 Total Work & duties of the process for different permeate pressures with biogas feed of 10.5 kmol/h. . . . 97
B.23 Global hydrogen recovery factor vs productivity for different sweep ratios varying biogas feed from 9.75 to 10.5 kmol/h. . . . 98
B.24 Carbon capture rate vs productivity for different sweep ratios varying biogas feed from 9.75 to 10.5 kmol/h. . . . 98
B.25 Per-pass hydrogen recovery factor vs productivity for different sweep ratios varying biogas feed from 9.75 to 10.5 kmol/h. . . . 99
B.26 Global methane conversion vs productivity for different sweep ratios varying biogas feed from 9.75 to 10.5 kmol/h. . . . 99
B.27 Global efficiency vs productivity for different sweep ratios varying biogas feed from 9.75 to 10.5 kmol/h. . . . 100
B.28 Work & duties (reforming section) for different sweep ratios with biogas feed of 10.5 kmol/h.100
B.29 Total Work & duties of the process for different sweep ratios with biogas feed of 10.5 kmol/h. . . . 101
B.30 Membrane surface area vs sweep ratio. . . . 101
B.31 Global hydrogen recovery factor vs productivity for different permeate pressures varying biogas feed from 9.75 to 10.5 kmol/h. . . . 102
B.32 Carbon capture rate vs productivity for different permeate pressures varying biogas feed from 9.75 to 10.5 kmol/h. . . . 102
B.33 Global methane conversion vs productivity for different permeate pressures varying biogas feed from 9.75 to 10.5 kmol/h. . . . 103
B.34 Global efficiency vs productivity for different permeate pressures varying biogas feed from 9.75 to 10.5 kmol/h. . . . 103
B.35 Membrane surface area vs hydrogen compression work for different permeate pressures.104
B.36 Total Work & duties of the process for different permeate pressures with biogas feed of 10.5 kmol/h. . . . 104
B.37 Global hydrogen recovery factor vs productivity for different sweep ratios varying biogas feed from 9.75 to 10.5 kmol/h. . . . 105
B.38 Carbon capture rate vs productivity for different sweep ratios varying biogas feed from 9.75 to 10.5 kmol/h. . . . 105
B.39 Global methane conversion vs productivity for different sweep ratios varying biogas feed from 9.75 to 10.5 kmol/h. . . . 106
B.40 Global efficiency vs productivity for different sweep ratios varying biogas feed from 9.75 to 10.5 kmol/h. . . . 106
B.41 Work & duties (reforming section) for different sweep ratios with biogas feed of 10.5 kmol/h.107
B.42 Total Work & duties of the process for different sweep ratios with biogas feed of 10.5 kmol/h. . . . 107
B.43 Membrane surface area vs sweep ratio. . . . 108

B.44 Global hydrogen recovery factor vs productivity for different recycle ratios varying biogas feed from 9.75 to 10.5 kmol/h. . . . 108
B.45 Carbon capture rate vs productivity for different recycle ratios varying biogas feed from 9.75 to 10.5 kmol/h. . . . 109
B.46 Per-pass hydrogen recovery factor vs productivity for different recycle ratios varying biogas feed from 9.75 to 10.5 kmol/h. . . . 109
B.47 Per-pass methane conversion vs productivity for different recycle ratios varying biogas feed from 9.75 to 10.5 kmol/h. . . . 110
B.48 Global methane conversion vs productivity for different recycle ratios varying biogas feed from 9.75 to 10.5 kmol/h. . . . 110
B.49 Global efficiency vs productivity for different recycle ratios varying biogas feed from 9.75 to 10.5 kmol/h. . . . 111
B.50 Total Work & duties of the process for different sweep ratios with biogas feed of 10.5 kmol/h. . . . 111
B.51 Global hydrogen recovery factor vs productivity for different permeate pressures varying biogas feed from 9.75 to 10.5 kmol/h. . . . 112
B.52 Carbon capture rate vs productivity for different permeate pressures varying biogas feed from 9.75 to 10.5 kmol/h. . . . 112
B.53 Global methane conversion vs productivity for different permeate pressures varying biogas feed from 9.75 to 10.5 kmol/h. . . . 113
B.54 Global efficiency vs productivity for different permeate pressures varying biogas feed from 9.75 to 10.5 kmol/h. . . . 113
B.55 Membrane surface area vs hydrogen compression work for different permeate pressures. 114
B.56 Total Work & duties of the process for different permeate pressures with biogas feed of 10.5 kmol/h. . . . 114

C.1 T-Q diagram. . . . 119
C.2 Shifted T-Q diagram. . . . 119

D.1 KPI results with varying biogas feed flow rate. . . . 121
D.2 KPI results with varying sweep ratio. . . . 122
D.3 KPI results with varying permeate pressure. . . . 122
D.4 KPI results with varying reactor pressure. . . . 123

F.1 Contribution to capital expenditure. . . . 128
F.2 Contribution to total component cost. . . . 129
F.3 Contribution to annual costs. . . . 129
F.4 Break-down of permeate dehydration component cost. . . . 130
F.5 Break-down of permeate dehydration annual operating cost. . . . 130

G.1 Value chain of $reference\ case_c$ with locations of CO_2 emissions. . . . 131
G.2 Value chain of $novel\ case_c$ with locations of CO_2 emissions. . . . 132

List of Tables

2.1 Maximum allowable limits of contaminants in PEM fuel cells in road vehicles (Ohi et al., 2016). . . . 6
2.2 Properties of common hydrogen selective membranes (Kluiters, 2004) & (Gallucci et al., 2013). . . . 13
2.3 Quality specifications for the CO_2 stream for storage (Alstom UK, 2011) . . . 23
2.4 Key takeaways from the literature study . . . 25

3.1 Input-output specifications. . . . 31
3.2 Typical specifications of molecular sieve 5A (ZR Catalyst). . . . 32
3.3 Modelling assumptions used in Aspen Plus simulation[a] . . . 34
3.4 Regeneration modelling assumptions. . . . 36
3.5 Comparison of the three configurations . . . 39
3.6 Differences between the novel and the reference process across value chain . . . 40

4.1 Process parameters for different cases formulated. . . . 44
4.2 Stream information for pinch analysis. . . . 49

5.1 Cost parameters. . . . 51
5.2 Capital cost of system components. . . . 52
5.3 Relevant CPECI values for this work. . . . 53
5.4 Installation factors. . . . 53
5.5 Operational expenditure factors. . . . 54
5.6 Manipulated variables range. . . . 55
5.7 Different cases analysed. . . . 55
5.8 (Local) Optimum conditions for the novel process. . . . 60
5.9 Manipulated variables range. . . . 61
5.10 Comparison of key results. . . . 62
5.11 Input-output specifications of the cases. . . . 63
5.12 Comparison of carbon footprint of the different cases. . . . 64
5.13 Comparison of novel and reference cases. . . . 65

6.1 Reference state conditions. . . . 68
6.2 Exergy flow results. . . . 68

B.1 Results of configuration 1. . . . 114
B.1 Results of configuration 1. . . . 115
B.2 Results for configuration 2. . . . 115
B.2 Results for configuration 2. . . . 116
B.3 Results of configuration 3. . . . 116
B.3 Results of configuration 3. . . . 117

D.1 Summary of the results. . . . 124

E.1 Formulated cases to determine the optimum process conditions. . . . 125

F.1 Economic analysis of the (local) optimum process. . . . 127

G.1 CO_2 emissions of both the processes across the value chain. . . . 133

H.1 Standard Molar Chemical Exergy, (kJ/kmol), of selected Substances at 298 K and p_0. . . . 135

I.1 Biogas and water feed exergy flow (hand calculation). 137

Nomenclature

Roman Symbols

A	Area	m^2
C	Concentration	$kmol/m^3$
c	Cost	€
D	Diffusion coefficient	m^2/s
DF	Driving force	$Pa^{0.5}$
$\overline{E}$	Mass exergy	kJ/kg
d	After tax rate of return	%
$\dot{E}$	Exergy flow	kW
H	Heat of reaction	$kJ/kmol$
h	Enthalpy	J
i	Inflation	%
J	Flux	$kmol/m^2s$
K_{ads}	Absorption coefficient	
K_{eq}	Equilibrium constant	
K_p	Membrane permeance	$kmol/m^2 s Pa^{0.5}$
k	Rate constant	
$\dot{m}$	Mass flowrate	kg/s
n	Lifetime of plant	$years$
$\dot{n}$	Molar flow rate	kmol/s
p	Partial pressure	Pa
Q	Membrane permeability	$kmol/m\ s\ Pa$
Q_H	Heat flow	W
R	Scale factor	
r	Reaction rate	kmol/hr kg_{cat}
rr	After tax real rate of return	%
S	Surface area	m^2
s	Entropy	J/K
T	Temperature	K
V	Volume	m^3

W	Power	kW
x	Distance	m
y	Mole fraction	

Greek Symbols

α	Annuity factor	%
Δ	Difference	
δ	Membrane thickness	μm
η	Efficiency	%

Subscripts

b	Baseline case
ch	Chemical
c	Carbon reduction case
des	Destroyed
feed	Feed flow
f	Fixed
in	Inflow
mem	Membrane
om	Operation & maintenance
out	Outflow
o	Reference state
perm	Permeate
ph	Physical
ret	Retentate
r	Reactor
T	Total
var	Variable

Abbreviations

ACM	Aspen custom modeler	
ATR	Auto-thermal reforming	
BG	Biogas	
CAC	CO_2 avoidance cost	$€/ton\ CO_2$
CAPEX	Capital expenditure	€
CCS	Carbon capture and storage	
CEPCI	Chemical engineering plant cost index	

CHP	Combined heat and power	
COP	Coefficient of performance	
CVD	Chemical vapour deposition	
EBTF	European Benchmarking Task Force	
ELP	Electroless plating	
EOR	Enhanced oil recovery	
EU-ETS	European union emission trading system	
FBMR	Fluidized bed membrane reactor	
FBR	Fluidized bed reactor	
FCV	Fuel cell vehicle	
GHG	Greenhouse gas	
GWP	Global warming potential	
Hex	Heat exchanger	
HRF	Hydrogen recovery factor	%
ICEV	Internal combustion engine vehicles	
IEA	International Energy Agency	
KPI	Key performance indicator	
L/S	Load-to-surface ratio	
LCOH	Levelized cost of hydrogen	$€/kg\ H_2$
LDV	Light duty vehicle	
LHV	Lower heating value	MJ/kg
MDEA	Methyl diethanolamine	
MEA	Ethanolamine	
MOC	Membrane-on-catalyst	
MRF	Membrane reformer	
MR	Membrane reactor	
NGCC	Natural gas combined cycle	
NG	Natural gas	
O&M	Operations & maintenance	
ODP	Oxygen depletion potential	
OPEX	Operating expenditure	€
PBMR	Packed bed membrane reactor	
PEMFC	Proton-exchange membrane fuel cell	
PFR	Plug flow reactor	

PSA	Pressure swing adsorption	
PVD	Physical vapour deposition	
RR	Reflux ratio	
S/C ratio	Steam-to-carbon ratio	
SMR	Steam methane reformer	
SRK equation of state	Soave-Redlich-Kwong equation of state	
SR	Steam reforming	
TCC	Total component cost	€
TEA	Triethylamine	
TPC	Total plant cost	€
TPD	Tons per day	
TSA	Temperature swing adsorption	
VSA	Vacuum swing adsorption	
WGS	Water-gas shift	

1

Introduction

Our current energy system relies primarily on fossil fuels: non-renewable, depleting resources that release greenhouse gases. The challenges that are now faced by the world's energy system are far greater than those that were faced during the 1970s energy crisis and a shift away from our current reliance on fossil fuels is inevitable. Energy transition from fossil-based to zero-carbon is needed to reduce energy related carbon emissions, limit climate change and meet the Paris Agreement goals of limiting the global temperature rise this century well below 2 °C above pre-industrial levels (UNFCCC).

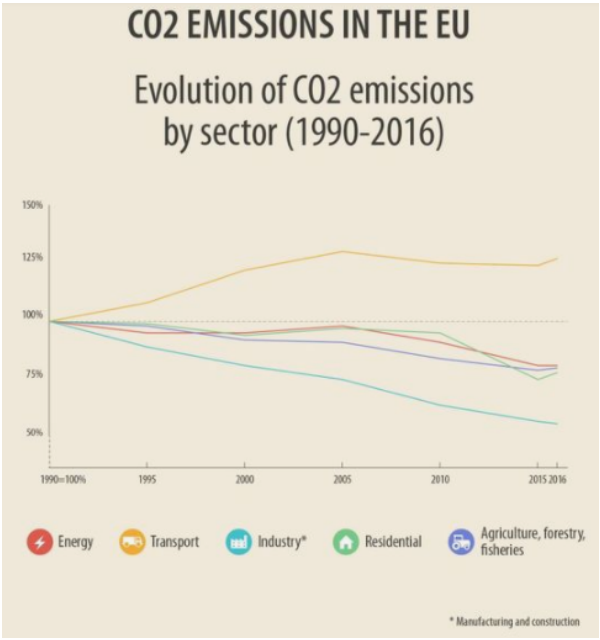

Figure 1.1: CO_2 emissions by sector in The EU (European Parliament, 2019).

Transport sector CO_2 emissions are on the rise and responsible for nearly 30% of the EU's total CO_2 emissions (European Parliament, 2019). Passenger cars are the major polluters accounting for around 60% of the total CO_2 emissions by road transport. As part of efforts to reduce the CO_2 emissions, the EU has set a goal of reducing the transport emissions by 60% by 2050 compared to 1990.

An attractive way to reduce the CO_2 emissions by transport is by changing the fuel used. Hydrogen is expected to play a key role in a clean, secure and affordable energy future (IEA). Today, hydrogen is used mostly in oil refining and the production of fertilizers. To make a significant contribution to clean

energy transition it needs to be adopted in sectors like transport, building and power generation where it is almost absent.

Technologies available today enable hydrogen to produce, store, move and use energy in a number of different ways. It can be transformed into electricity and methane to power homes and feed industry, and also into fuels for cars, trucks, ships etc. A clean, widespread use of hydrogen, however, in global energy transitions faces several challenges. Currently, the global hydrogen production is approximately 7.2 EJ per year, 96% of which comes from fossil fuels and the rest 4% from electrolysis. This results in 500 Mt carbon-dioxide emissions per year (Voldsund et al., 2016). Hydrogen is majorly supplied from natural gas and coal, with steam methane reforming covering around 50% of the global production (Di Marcoberardino et al., 2018). The share of hydrogen production methods is shown in figure 1.2.

To harness the potential of hydrogen on the way to a clean energy future requires the capture of CO_2 from hydrogen production from fossil fuels and greater supplies of hydrogen from renewable energy sources. Furthermore, producing hydrogen from renewable electricity is costly at the moment and the development of hydrogen infrastructure is slow which is holding back widespread adoption (IEA).

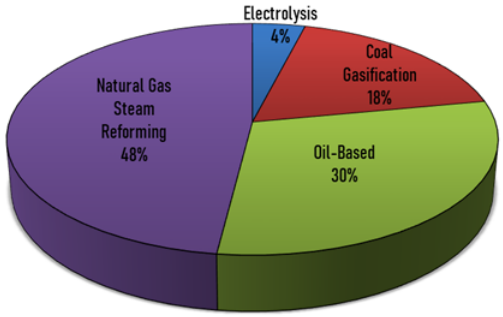

Figure 1.2: Share of the hydrogen production methods (Voldsund et al., 2016).

One near-term opportunity to boost hydrogen on the path towards its clean, widespread use is decentralized production via membrane reforming of biogas integrated with carbon capture technology. Biogas is a renewable energy source and along with carbon capture this process is expected to produce near-zero or even negative CO_2 emissions. Membrane reforming promises economic small-scale hydrogen production combined with inexpensive capture because of the high concentration and pressure of exiting gas stream (Sjardin et al., 2006). Furthermore, decentralized production would result in a higher efficiency on a value chain level due to less transport cost and emissions. This entire system from waste to fuels will enable in creating a circular economy as well. The International Energy Agency (IEA) predicted the deployment of fuel cell vehicles (FCVs) will begin in earnest by 2025 in the passenger light duty vehicles (LDVs) (Voldsund et al., 2016). Therefore, such a system at a refuelling station will exploit the increasing demand for hydrogen as a fuel. This study will assess the techno-economic potential of the membrane technology coupled with carbon capture technology, to produce near-zero or negative emissions hydrogen in realizing a low carbon society in The Netherlands. The integration of these technologies into a process could facilitate capture at small scales, avoid the hydrogen transport costs and therefore contribute to a more rapid reduction in carbon emissions. This potential will be quantitatively assessed in this work by means of process modelling and simulations, sensitivity analysis followed by economic and CO_2 emissions evaluation compared to conventional production processes and finally exergy analysis.

1.1. Scope of the research

Initial research on membrane separation processes for production of hydrogen showed promising results compared to the conventional steam reforming process (Kikuchi, 2000). The integration of this membrane technology with the maturing CCS (carbon capture & storage) technology into a novel sys-

tem has the potential to deliver green hydrogen that will facilitate the transition to a low carbon economy (Sjardin et al., 2006).

The main research question is formulated as follows:

What is the economic potential of PEM fuel-grade hydrogen production by membrane enhanced reforming of biogas with carbon capture to realize a low carbon society and promote sustainable growth for the transportation sector in The Netherlands?

To help answer the main question, a number of sub-questions are formulated:

- What are the different process configurations possible? How do these configurations perform with respect to each other?
- How does the best performing configuration compare to the conventional steam methane reforming process in terms of economic and CO2 avoidance potentials?

These sub-questions are answered by conducting a conceptual process design of a membrane reactor for biogas conversion to hydrogen at FCV grade. The process design is supported by process simulations, to quantitatively compare different process configurations, generate mass and energy balances, as well as enable following economic, emissions and exergy analysis. The results that answer these sub-questions are valid at given design assumptions, that are fixed in the basis of process design. This basis of design is built answering the following main questions, but not only:

- What capacity of the plant is preferable?
- Should the plant be centralized or decentralized?
- What are the battery limits (system boundaries) of the system?
- Is feed gas sufficiently available to produce the capacity chosen?
- Is pre-treatment of feed gas (minor contaminants) required? If yes, to what extent?
- Does the H_2 produced from the membrane reactor meet the fuel-grade specifications? And CO_2 from the carbon capture unit?

1.2. Methodology

The questions addressed for the basis of design were answered with the help of preliminary literature review. First, the capacity and the location of the system were decided. The capacity was chosen depending on the average size of the biogas digester available in The Netherlands, the predicted demand of hydrogen in the near future, membrane performance assumed, and also the availability of performance data of the conventional process to compare with. The location of the system depended majorly on transportation factors.

With literature available on membrane reforming and carbon capture technologies, the suitable process parameters were chosen. With the information obtained, a basic process of membrane reforming with carbon capture was modelled in Aspen Plus. The battery limits of the process developed were decided for a clear performance analysis and comparison. Different configurations of the basic process were developed. In the first stage, before conducting a detailed economic potential estimate, thermodynamic key performance indicators for example, efficiency, carbon capture rate etc. were used to compare the performance of the different configurations developed. Secondly, one promising configuration was chosen and the LCOH (economic performance indicator) was used to optimize the process parameters like sweep ratio, permeate pressure, feed pressure etc. To calculate the LCOH, the cost factors were taken from literature and experts. Finally, the optimum configuration was used to determine its economic and CO_2 emissions potential compared to the conventional steam methane reforming process and also perform exergy analysis to evaluate the process design performance.

2

Theoretical Background

In this chapter, the background information necessary to build the novel process and compare it to the conventional one is discussed. First, the current and future use and importance of hydrogen is mentioned. Following, the conventional production method of hydrogen is introduced. Then, the novel hydrogen production process using membrane technology is discussed, with integration of the carbon capture technology. Each section of the process is explained in detail. Finally, a few industrial processes that use these technologies and their performances are listed.

2.1. Hydrogen

The main use of hydrogen is in petroleum refining and fertilizer production. However, its use in the transportation and utilities market is growing in recent years. This is due to the fact that hydrogen is a clean fuel with zero or near-zero emissions and therefore has high potential to reduce the greenhouse gas emissions in many applications. The major impact will be in its use in a fuel cell, as when consumed in a fuel cell it produces only water, electricity and heat. Hydrogen and fuel cells have a potential for use in a vast number of applications: transportation, industrial, residential, commercial etc. Energy Department-funded analysis states that the maximum reduction in emissions will be in the transportation sector (U.S. Department of Energy, 2017).

It is important to realize that, currently, the hydrogen production plants are centralized and large-scale complementing its use in the petroleum and fertilizer industry. However, if we consider its future applications, decentralized and small-scale production units (closer to the end user) may be the best solution to introduce hydrogen in the short run partly because the initial (in the energy transition) demand for hydrogen will be low (Hartnig and Roth, 2012). Another major reason is the current immature hydrogen pipeline infrastructure. For example, when using hydrogen in a fuel cell vehicle, it is better to have a production plant close to the refuelling station to avoid the transportation costs and easily match the supply to the demand as the vehicle fleet increases. On the other hand, once the demand for hydrogen is large enough, central hydrogen production will become cost-competitive to decentralized production. Research on the hydrogen distribution infrastructure is ongoing as stated by the Department of Energy but it also mentions that a number of technical concerns need to be dealt with before its global deployment (U.S. Department of Energy). At present, the uncertainty and the cost of transport is high.

The future market of hydrogen as a fuel will depend on four primary factors: the cost of hydrogen, rate of advancement of H_2 consuming technologies, the cost of competing energy systems, the potential long-term restrictions on GHGs (Hartnig and Roth, 2012). Katikaneni et al. (2014) compares on-site hydrogen generation using liquid hydrocarbons with natural gas based centralized hydrogen production along with pipeline transportation. The important takeaway from this research is that the centralized production of hydrogen from natural gas costs $ 1.4/kg (1.274 €/kg) but with transportation, the total cost goes to $ 6.23/ kg (5.67 €/kg). The high cost of transport along with the uncertainty of performance has led to increased research on feasibility of small-scale on-site hydrogen production.

When dealing with fuel-grade hydrogen, it is of utmost importance to keep in mind the fuel quality specifications. Below is a table enlisting the maximum allowable limits of contaminants in fuel cells for road vehicles (Ohi et al., 2016). Furthermore, the refuelling pressure for FCVs is 700 bar (U.S. Department of Energy, 2016).

Table 2.1: Maximum allowable limits of contaminants in PEM fuel cells in road vehicles (Ohi et al., 2016).

Characteristics	**Type I, Type II Grade D**
Hydrogen fuel index (minimum mole fraction)	99.97%
Total non-hydrogen gases	300 µmol/mol
Maximum concentration of individual contaminants	
Water (H_2O)	5 µmol/mol
Total hydrocarbons (Methane basis)	2 µmol/mol
Oxygen (O_2)	5 µmol/mol
Helium (He)	300 µmol/mol
Total Nitrogen (N_2) and Argon (Ar)	100 µmol/mol
Carbon dioxide (CO_2)	2 µmol/mol
Carbon monoxide (CO)	0.2 µmol/mol
Total sulphur compounds (H_2S basis)	0.004 µmol/mol
Formaldehyde (HCHO)	0.01 µmol/mol
Formic acid (HCOOH)	0.2 µmol/mol
Ammonia (NH_3)	0.1 µmol/mol
Total halogenated compounds (Halogenate ion basis)	0.05 µmol/mol
Maximum particulates concentration	1 mg/kg

2.2. Conventional hydrogen production process

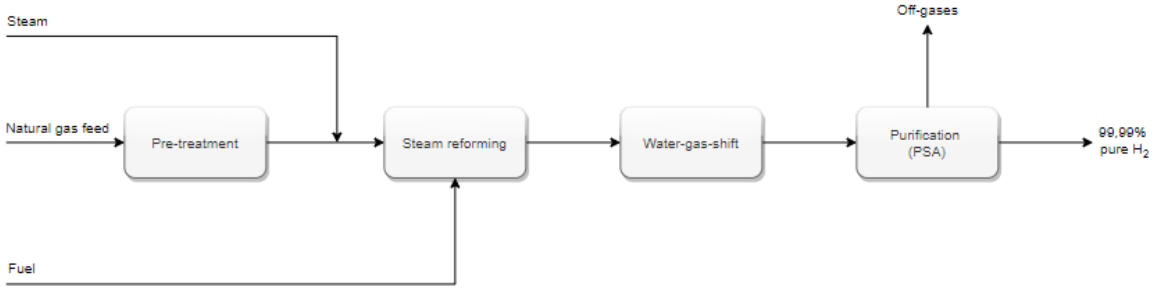

Figure 2.1: Process scheme for conventional SMR.

The conventional process for large-scale hydrogen production in the industry is by steam reforming (Go et al., 2009). More than 50% of the global production is from steam reforming of natural gas (NG). In steam reforming of natural gas, steam reacts with the natural gas in the presence of nickel-based catalyst to produce mainly hydrogen, carbon dioxide and carbon monoxide. The block diagram shows the conventional steam reforming plant for hydrogen production from natural gas. The main reactions that take place in this process are shown below (Hartnig and Roth, 2012):

$$CH_4 + H_2O \rightleftharpoons CO + 3H_2 \quad \Delta H^{\circ}_{298K} = 206.4\ kJ/mol \tag{2.1}$$

$$C_nH_{2n+2} + nH_2O \rightleftharpoons nCO + (2n+1)H_2 \quad \Delta H^{\circ}_{298K} > 0 \tag{2.2}$$

$$CO + H_2O \rightleftharpoons CO_2 + H_2 \qquad \Delta H^{\circ}_{298K} = -41.2\ kJ/mol \tag{2.3}$$

Reaction 1 is the main reforming reaction that takes place and reaction 2 represents the reforming of higher hydrocarbons that maybe present in natural gas. Reaction 3 is called the water-gas shift (WGS) reaction . The first 2 reactions are endothermic whereas reaction 3 is exothermic.

The production process has four important sub-processes. Purification of the feed is required if high amounts of contaminants are present. A desulphurization unit is most commonly employed in a reforming process to remove the sulphur compounds in the natural gas. This step is very important due to the high sulphur sensitivity of catalysts in the reformer.

In the reforming section, the steam reforming reactions take place (reaction 1 & 2). Owing to the endothermic nature of the steam reforming reaction, heat input is required for the process. This heat can either be provided by the off-gases from the PSA unit or additional natural gas. The main operating variables that influence the reaction are temperature, pressure, molar steam-to-carbon ratio. The operating conditions are high temperatures of 800-900 °C, process pressure between 15-30 bar and S/C ratio between 2.5-3. The reactions are catalysed by supported nickel catalysts.

Next, high-temperature WGS reaction takes place where the gas is cooled down to 350 °C and carbon monoxide is converted to hydrogen using iron-oxide based catalysts (reaction 3). The exit gas temperature is around 400-450 °C, because of the exothermic nature of the reaction. To obtain pure hydrogen, purification of the reactor outlet stream is required. The commonly used technology is pressure-swing adsorption (PSA). The gas from the WGS unit is cooled to ambient temperature and the water in the stream is separated before it enters the adsorption column. The hydrogen obtained from this step is >99.95 % pure. The off-gas from the PSA unit is usually burned in the reformer to provide the input heat and decrease the fuel requirements. They can also be recycled into the reformer. In that case, natural gas is used as a fuel for the reformer.

The thermodynamic limitations, the endothermic nature of the reforming reaction and the need for many complex steps to purify hydrogen mean a high capital investment and a reduced process efficiency. Cost of WGS and PSA practically accounts for about 30 % of the total cost for producing H_2 (Go et al., 2009). By integrating hydrogen selective membranes, a high degree of process integration and intensification can be accomplished in the steam reformer. A number of process units can be decreased and total required reactor volume greatly reduced while achieving higher methane conversions, hydrogen yields (beyond thermodynamic limitations) at lower temperatures and with higher energy efficiencies (Gallucci et al., 2008).

2.3. Membrane reforming for hydrogen production

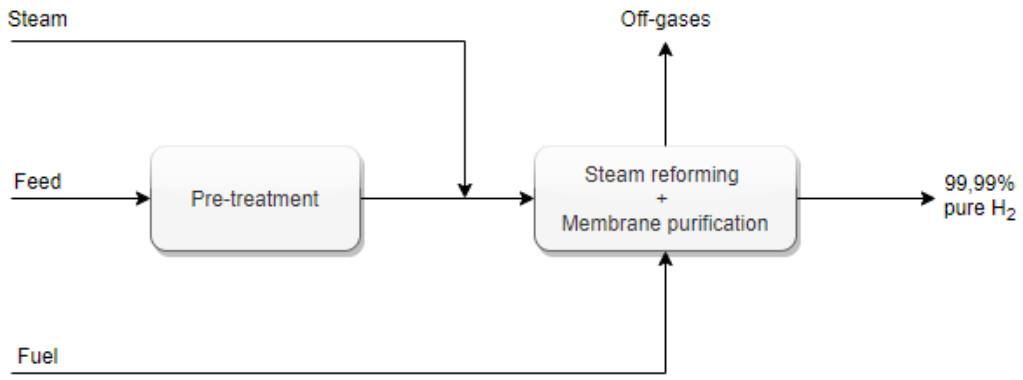

Figure 2.2: Process scheme for the MR.

The feed, depending on its composition, is usually pre-treated before it enters the membrane reactor. Due to the high sulphur sensitivity of the Ni-based catalyst in the reformer, a desulphurization unit is usually employed similar to the conventional production process. Different technologies are available for this purification step, depending on the feed composition, the amount of contaminants needed to be removed etc.

The membrane reactor (MR) can combine the three most crucial steps of the conventional production process into one i.e. steam reforming, water-gas shift as well as produce high purity hydrogen. The latter is because the Pd-based membranes that are placed inside the reforming tubes are highly selective to hydrogen and don't allow other gases to pass through it. The reactions that take place in the reformer are similar to the conventional process.

Compared to the temperature of the conventional process of around 900 °C, the MR can operate at a lower temperature (500- 650 °C) with better methane conversions than the steam methane reformer (SMR). This is due to the continuous removal of hydrogen, which shifts the equilibrium of the reaction to the right. However, a minimum of 500 °C is required for sufficient methane conversion (Sjardin et al., 2006).

In the conventional process, as pressure increases the reaction shifts to the feed side, lowering the methane conversion. Assuming the permeation capacity of the membrane is sufficient and enough hydrogen is removed from the feed side, the effect of increasing pressure in the MR is opposite to the SMR. A higher reaction pressure increases the hydrogen flux through the membrane, increasing the methane conversion. High permeation rate (flux)[1] has a positive effect on membrane area but increases costs for compressors, pumps etc. To further improve the permeation of hydrogen through the membrane, a high pressure difference between the feed and the permeate stream of the reactor is required (For a better understanding refer figure 2.4). This is achieved with the help of a sweep stream (usually steam) at around atmospheric pressure or by using a vacuum pump. The optimal pressure of the feed is between 10-30 bar and the permeate side is atmospheric or lower. An elaborate choice between the two configurations has to be made depending on the results desired. If the sweep configuration is adopted, steam needs to be produced, heated to the reaction temperature and later separated from the hydrogen, which requires energy. If a sweep configuration is chosen, an optimum sweep ratio [2] needs to be determined. Similar performance is achieved with lower reactor pressure and vacuum permeate configuration, however, additional equipments are required i.e. vacuum pump which increase the costs. It also depends on the hydrogen outlet pressure required. Compression costs from vacuum to a very high pressure will be considerably high.

Steam feed is usually added in excess to improve conversion and prevent coke formation which is a pervasive problem in membrane reactors. The coke deactivates the catalyst, causes bed pressure increase as a result of blocking the flow. The optimal steam-to-carbon ratio [3] is 2.7-3.2. Higher values will increase methane conversion but imply lower hydrogen partial pressure and therefore result in increase in the membrane surface area. Also, more steam production will be needed.

The membrane reactor produces two streams: the permeate stream which contains pure hydrogen (in case of vacuum) or hydrogen & steam (if sweep gas is used). This permeate stream is purified to contain at least 99.97% hydrogen and is compressed and stored. The retentate stream contains majorly CO_2, H_20 product, unreacted CH_4, CO and unseparated H_2,

In the conventional SMR, the off-gases from the PSA unit are either recycled or sent to the furnace to raise heat for the endothermic reforming reaction. This can also be done for the MR without the need of the PSA unit. However, if almost complete methane conversion and hydrogen recovery is attained, the retentate stream contains mainly CO_2 and water with small amounts of CH_4, CO, N_2, H_2. To reduce the carbon footprint of the process, the CO_2 can be purified, captured and stored. This technique is called pre-combustion carbon capture as the CO_2 is recovered and stored before combustion.

[1] The amount of permeate the passes through the membrane per unit area per unit time.
[2] The ratio of sweep flow to the permeate hydrogen flow.
[3] The ratio of moles of steam to moles of equivalent carbon in the reactor feed

A number of pre-combustion CO_2 capture technologies are available in the industry and the technology chosen depends on the concentration of CO_2 in the stream, the scale, required pressure and the presence of contaminants (Hartnig and Roth, 2012). Carbon capture and storage technologies will be discussed later in this chapter (refer section 2.6). The gases that remain after CO_2 is captured can be recycled with the feed or burned to produce heat for the membrane reactor.

2.4. Feed

Currently, the conventional feed used by the industry for production of hydrogen is natural gas. It is said to be the earth's "cleanest" fossil fuel, majorly composed of methane. When it burns, mostly carbon dioxide, water vapor and small amounts of nitrogen oxides are produced (American Gas Association). The conventional hydrogen production process produces significant amounts of CO_2 emissions (close to 10 kg CO_2 per kilogram of H_2 product) (Hartnig and Roth, 2012). To reduce the carbon emissions, other sustainable feedstocks are replacing natural gas; one such feedstock is biogas.

Biogas is a mixture of gases that are produced from the decomposition of organic waste (American Gas Association). When the organic matter, such as food waste, agricultural waste, manure etc, break down in an anaerobic environment (in the absence of oxygen) they release a blend of gases, majorly CH_4 and CO_2, water vapour and traces of hydrogen sulfide, nitrogen and ammonia . This process of producing biogas from organic matter is called anaerobic digestion and is facilitate by anaerobic organisms which digest this matter.

Biogas is known as an "environmentally-friendly" energy source because it reduces the dependence on fossil fuels and helps mitigate the global waste epidemic that releases tons of methane in the air. However, it is important to note that feed purification technologies may be different and more severe in the case of biogas as compared to natural gas. This is because, biogas has a lot of contaminants like sulphur, ammonia etc. which are detrimental in the downstream processes and need to be removed. The exact composition of biogas depends on its origin. Although it is comparatively dirtier than natural gas, biogas is increasingly being adopted in the industry as a feed for steam reforming for reduced greenhouse emissions.

Biogas in the Netherlands

In the year 2016, the Netherlands had more than 252 functioning digesters with 219 MW installed electrical capacity and 11,905 Nm^3/h bio-methane upgrading capacity (IEA Bioenergy, 2016). Unlike many other countries, the percentage of energy in biogas utilised as heat is 56% while that as electricity is 33%. 8% of the energy is used as vehicle fuel which is amongst the highest in the world. Furthermore, it was predicted that the biogas sector has a potential to produce 1.2 billion m^3 of biogas or 0.75 billion m^3 bio-methane by 2020 increasing to 3.7 billion m^3 of biogas or 2.2 billion m^3 of bio-methane by 2030 (Green Gas Forum, 2014), with significant growth expected in biogas from manure, sewage sludge, grass and seaweed.

2.4.1. Feed pre-treatment

In this section, the importance of feed pre-treatment and the most harmful impurities that can reduce the performance of the membrane and catalyst are mentioned. Furthermore, commercial feed pre-treatment technologies are listed that could be used to purify the feed.

Effect of impurities in the feed

Some gases present in the feed stream can be harmful for the performance of the membrane and the catalyst in the membrane reactor, and therefore need to be removed. The most harmful is sulphur, usually present as H_2S. Hydrogen sulphide deactivates the reforming catalyst, which is an alloy of Ni. Sulphur adsorbs so strongly on Ni that it causes a substantial loss of surface area of the catalyst and therefore, the activity. Research by experts showed that the sulphur coverage on the catalyst is always greater than 0.5 even when the concentration of H_2S in the feed is less than 0.02 ppm (Hou et al., 1999). Another detrimental effect of H_2S in the stream is corrosive decay of the membranes. The most commonly used membranes are the Pd-Ag alloys due to their high H_2 permeability. These alloys however, show high levels of deterioration when exposed to even trace amounts of H_2S. Studies showed that a reduction in H_2 flux to 80% is seen when exposed to 20 ppm H_2S for 10 minutes (Gabitto

and Tsouris, 2019). Therefore, all the sulphur in the feed needs to be removed to ppb levels for an acceptable catalyst and membrane performance and reduce the replacement costs. Other gases that cause harmful effects are N_2 and NH_3. Sakamoto et al. (1997) studied the effect of 10% N_2 and NH_3 in the gas stream on hydrogen permeation for a few chosen Pd alloy membranes. Optimum operating conditions to minimize the effect of these gases are difficult to determine owing to the different effects of the different gases. Therefore, the best option is to remove these gases from the feed stream to the lowest concentration possible.

Pre-treatment technologies
Biogas is a mixture of gases composed mainly of 40-70% vol CH_4, 30 - 60% vol CO_2, 0-1% vol H_2, 0-3% vol H_2S and 1-5% vol other gases (Zăbavă et al., 2019). The exact composition depends on the source of the biogas, but always contains some amount of contaminants. Prior to use, biogas need to be treated (purified) to remove these impurities. The most common methods used for biogas treating are shown in figure 2.3

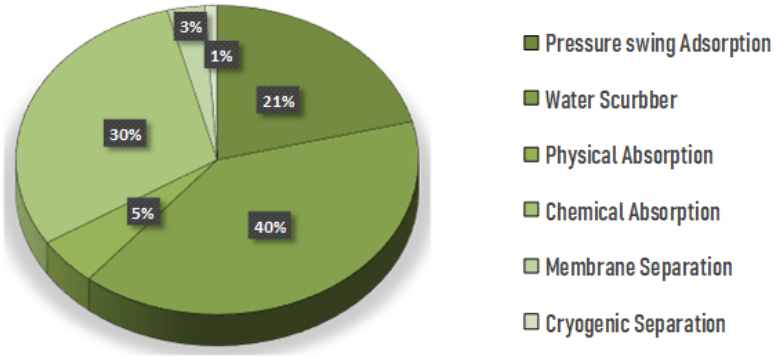

Figure 2.3: Biogas purification methods (Zăbavă et al., 2019).

These methods are based on these four principle cleaning techniques namely, bio-filtration, adsorption, water scrubbing (an absorption process) and refrigeration. The technologies mentioned above are commercial and efficiently clean the biogas, the outlet stream having negligible impurities. A detailed description of these processes is not mentioned as pre-treatment of biogas is out of scope of this study.

2.5. Membrane technology

A membrane is a barrier that allows selective mass transport of substances. It is selective because some substances can pass through it more easily than others. This makes it easy to separate or purify a mixture into different components. The phases can be liquids or gases. Membrane processes are continuous unlike the PSA purification step which is cyclical. They are mainly preferred in small-scale applications because of the scalability cost advantage of PSA processes (IEA, 2017). In this work, we will focus on gas separation membranes.

In the last 60 years, major developments in the membrane technology have taken place. This has made the application of manufactured membranes a viable option. Membrane applications are diverse, from reverse osmosis (to purify water) to micro filtration (to filter bacteria) (Kluiters, 2004).

The popularity of membranes owes largely to the following advantages:

- Mild process conditions
- Low energy consumption
- Continuous separation possible
- Easy scaling up
- No additives

- Easy integration with other separation technologies

It is important to note the disadvantages (depending on the specific membrane type):

- Low lifetime
- Fouling tendency
- Low selectivity or flux
- Linear scaling factor, no economies of scale

Before diving into the membrane characteristics for hydrogen purification, a basic explanation of the membrane configuration is given for a better understanding.

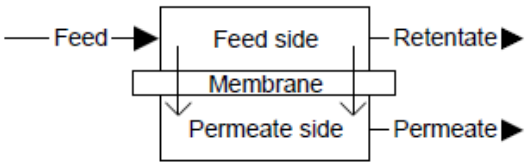

Figure 2.4: Membrane unit (Kluiters, 2004)

Figure 2.4 shows the basic membrane set-up. The two sides of a membrane are called the feed side, from which the feed enters and the permeate side, the downstream side. The general rule is that the most relevant species permeates from the feed side to the permeate side, in this study it's hydrogen. The feed side "flow in" is called the feed flow and the resulting flow after permeation is called the retentate flow. The inlet flow at the permeate side is called the sweep flow and the exit flow is called the permeate.

The two main flow operations of the membrane are co-current and counter-current.

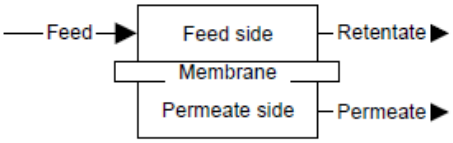

Figure 2.5: Co-current set-up (Kluiters, 2004).

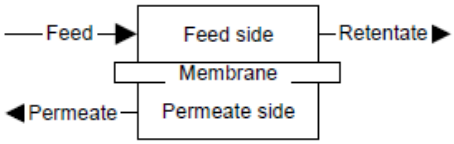

Figure 2.6: Counter-current set-up (Kluiters, 2004).

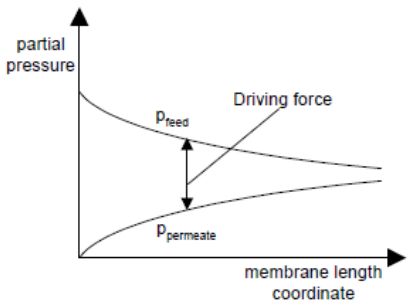

Figure 2.7: Co-current set-up (Kluiters, 2004).

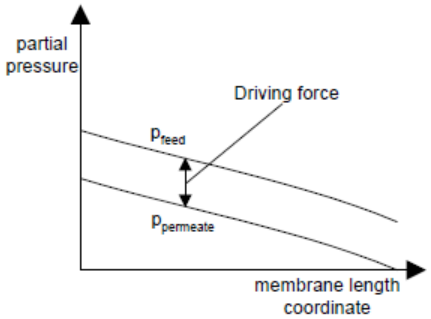

Figure 2.8: Counter-current set-up (Kluiters, 2004).

The co-current set-up is when the feed and the permeate run in the same direction whereas in the counter-current they run in the opposite direction as seen in figure 2.5 & 2.6 respectively. In the co-current operation, the initial driving force is large but it decreases as the permeation takes place, figure 2.7. If the membrane length is long enough, the partial pressures on the feed and permeate side will become almost equal. This means the efficiency will decrease as membrane surface area increases. In contrast, the partial pressure difference between the feed and the permeate is roughly constant throughout the length of the membrane in the counter-current set-up. This results in substantial driving force even at the exit. Therefore, the best membrane results are obtained with the counter-current operation. Another effective way to increase the partial pressure difference between the feed and permeate side is by using a sweep flow as shown in figure 2.9

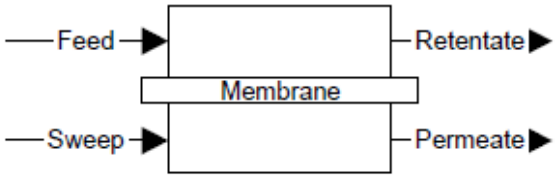

Figure 2.9: Membrane unit (Kluiters, 2004).

The performance and efficiency of a membrane can be measured in terms of flow or flux through the membrane and the selectivity. The selectivity is the measure of the difference in permeability of a substance compared to others in a mixture. For example, if a membrane allows only hydrogen to pass through it, its selectivity is 100 % for hydrogen.

The next sections will focus on research and development of membranes for hydrogen separation and application of membranes for hydrogen production.

2.5.1. Membranes for hydrogen separation

Membranes can be a good alternative for separation of hydrogen from mixtures and can replace PSA and cryogenic separation technologies depending on the scale and purity of the product required (Kluiters, 2004). They perform better as compared to other purification methods when high recovery is required. Furthermore, they can operate at moderate temperatures and pressures. Maintenance requirements are minimal because of a lack of moving parts and have less complex control systems compared to the other hydrogen purification technologies. Since 1979, polymeric membranes are used in the ammonia industry for hydrogen recovery and since the late 1990s palladium membranes are being used for the production of pure hydrogen in the electronics industry (Kluiters, 2004). In the recent decades membrane are being developed and employed in more sectors for hydrogen separation.

Material & fabrication

Hydrogen selective membranes are classified into four categories: metallic, carbon, ceramic (together called inorganic) and polymeric (organic). Polymeric membranes have a wide range of applications and are available at a relatively low cost. They are currently used for refinery separation processes as a primary material. Inorganic membranes can be operated under higher temperatures than polymeric and posses high chemical stability (IEA, 2017). The properties of the most common hydrogen selective membranes are summarized in table 2.2 (Kluiters, 2004) & (Gallucci et al., 2013).

The most important parameters when choosing a membrane type are selectivity, flux and temperature range at which the membranes can be applied. Dense metallic and dense ceramic membranes are the most suitable ones in order to obtain high hydrogen purity because of their very high selectivity towards hydrogen (Gallucci et al., 2013).

Table 2.2: Properties of common hydrogen selective membranes (Kluiters, 2004) & (Gallucci et al., 2013).

	Dense polymer	**Micro porous ceramic**	**Dense metallic**	**Porous carbon**	**Dense ceramic**
Temperature range	< 100 °C	$200 - 600$ °C	$300 - 600$ °C	$500 - 900$ °C	$600 - 900$ °C
H_2 **selectivity**[a]	low	$5 - 139$	> 1000	$4 - 20$	> 1000
H_2 **flux** (10^{-3}**mol/m^{2}s) at dP = 1 bar**	low	$60 - 300$	$60 - 300$	$10 - 200$	$6 - 80$
Stability issues	Swelling, compaction, mechanical strength	Stability in H_2O	Phase transition	Brittle, oxidising	Stability in CO_2
Poisoning issues	HCl, SOx, (CO_2)		H_2S, HCl, CO	Strong adsorbing vapours, organics	H2S
Materials	Polymers	Silica, alumina, zirconia, titania, zeolites	Palladium alloy	Carbon	Proton conducting ceramics (mainly $SrCeO_{3-\delta}$, $BaCeO_{3-\delta}$)
Transport mechanism	Solution/ diffusion	Molecular sieving	Solution/ diffusion	Surface diffusion; molecular sieving	Solution/ diffusion (proton conduction)
Cost	Low	Low	Low	Moderate	Low

[a] It is a measure of the ability of the membrane to separate two or more gases.

Owing to the properties of the dense metallic membranes, a lot of research has been carried out to check their performance for hydrogen production. Palladium membranes show an outstanding ability to transport hydrogen in its bulk over a wide temperature range. The graph 2.10 shows the hydrogen solubility in different metals (Yun and Ted Oyama, 2011). Developments in Pd and Pd-alloys have been carried out for a long time, among the dense metal materials (Gallucci et al., 2013).

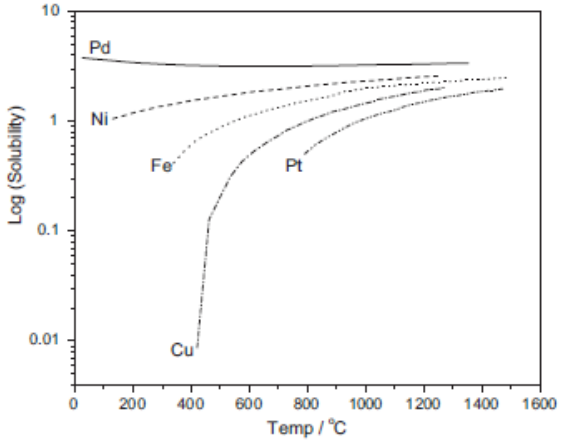

Figure 2.10: H_2 solubility (cm^3 of H2/100 g metal) in different metals at 1 atm (Yun and Ted Oyama, 2011).

For commercial applications, the membranes should have a reasonable cost, high hydrogen selectivity and permeance compared to other gases and steady performance over a long period of time under considerably harsh conditions (Yun and Ted Oyama, 2011). Furthermore, the membranes should have a good thermal stability and they should be resistant to poisoning by substances like H_2S, Cl^-, CO etc. Research shows that Pd or Pd based membranes supported on ceramic and metallic materials showed high hydrogen permeance and selectivity. Also, several Pd and Pd-alloy membranes were reported to be stable for several months in the temperature range of 350 - 500 °C.

In spite of palladium's ability to permeate hydrogen, it suffers some limitations. Adsorption of hydrogen below its critical point of 298 °C and 20 bar, results in two different phases (α/β) of the metal. This leads to bulk and grain boundary defects. Secondly, the exposure of hydrogen can result in the metal loosing its ductility, a process called as hydrogen embrittlement which causes cracking of the metal. Another problem is the palladium surface poisoning by sulphur compounds, CO, H_2O, Cl^-, C, unsaturated hydrocarbons etc. This phenomenon is more significant in thin membranes (Gallucci et al., 2013). To avoid these problems and reduce the membrane cost, palladium can be alloyed with other metallic elements such as Ni, Pt, Ag, Cu and Y. The alloying reduces the critical temperature for the α/β phase transformation (Yun and Ted Oyama, 2011). Pd-alloys mainly Pd-Ag, Pd-Cu and Pd-X-Au are used to decrease the embrittlement effect (Gallucci et al., 2013).

The most effective way to increase the permeability of H_2 through Pd membranes is the reduction in the membrane thickness (Kikuchi, 2000). In recent years, fabrication methods that produce thin selective layers have been developed. The cost of these selective layers are reported to be low to moderate compared to the entire cost of the modules. For instance, Pd membranes are now produced with a thickness in the order of 1 µm (Gallucci et al., 2013).

Common dense metal layer deposition techniques include chemical vapour deposition (CVD), electroless plating (ELP), electroless plating and diffusion welding, physical vapour deposition (PVD, including magnetron spluttering, thermal evaporation or pulsed laser evaporation) (Gallucci et al., 2013). Every techniques has its pros and cons therefore tailoring the deposition techniques with respect to the support material is required in order to obtain a suitable composite membrane.

Membrane configurations
A module is the building block of a membrane system. Gas separation modules are usually based on two types of membrane configurations: planar and tubular. For early laboratory research studies, the planar membranes are often used whereas for medium and industrial scale applications the tubular ones are preferred owing to their higher surface area to volume ratio compared to the planar ones (Gallucci et al., 2013).

Furthermore, membranes can be classified into unsupported and supported structures. Unsupported membrane need to be thick self-standing with thickness more than 50 µm in order to have sufficient mechanical stability. Being thick, the main drawback is a low hydrogen permeance. Furthermore, increasing the membrane thickness means a high material cost resulting in an expensive membrane structure. Therefore, the first industrial membranes preferred are the supported one until further research is carried out to fabricate (thin) unsupported membranes without drastically affecting its performance and cost.

Supported membranes consist of a thin selective film that is deposited onto a support that provides the mechanical stability. As less membrane material is required, the whole membrane cost will be lower than the unsupported one. However, the support costs also are important. Especially when thin film membranes are considered, the pore size of the support should be much lower and also the support must be smoother. These requirements increase the overall cost of the membrane.

The porous support structures can be either metallic or ceramic. Metallic support materials are more robust than ceramic but the tubular ones have lower surface qualities. Ceramic support materials have better surface quality resulting in thinner selective layers. They are more fragile than metallic. Hollow fiber supports are being developed and tested in order to increase the surface area to volume ratio and also improve the surface quality.

Hydrogen permeation mechanism
The mechanism of hydrogen permeation through dense metal membranes follows a solution-diffusion mechanism (Sievert's law), refer figure 2.11. The steps that take places in transporting hydrogen from a high to low pressure region are as follows (Hamstra et al., 2015):

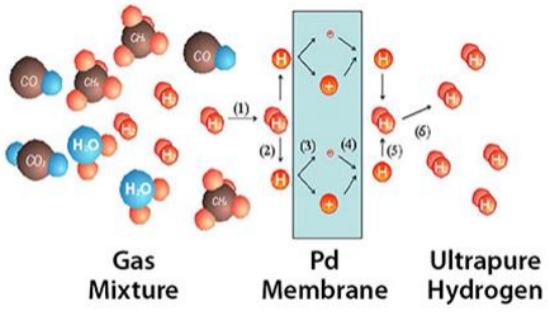

Figure 2.11: Mechanism of permeation of hydrogen through metal membranes (Hamstra et al., 2015).

- Adsorption of H_2 molecule at the gas/metal interface.
- Dissociation of chemisorbed H_2 molecule to hydrogen atoms.
- H atom loses its electron to the palladium structure.
- Diffusion of the H atoms and electrons through the membrane via the lattice structure.
- Re-combination of the hydrogen ions and electrons into molecular H_2.
- Desorption of H_2 molecules from the surface to the bulk gas.

The permeation rate of hydrogen through the membrane is dependant on the mentioned steps. When the diffusion through bulk of the metal is assumed to be the rate limiting step, the hydrogen flux ($J_{H_{2,mem}}$, $kmol/m^2s$) over the membrane can be described by Fick's law (2.4).

$$J_{H_{2,mem}} = -D_{H_2}\frac{dC_{H_2}}{dx} \tag{2.4}$$

where, D_{H_2} is the diffusion coefficient in m^2/s and $\frac{dC_{H_2}}{dx}$ is the hydrogen concentration gradient through the membrane in $kmol/m^4$.

Integrating equation 2.4 over the thickness (δ) of the membrane, we get a new form of the flux equation (2.5)

$$J_{H_{2,mem}} = -\frac{D_{H_2}}{\delta}(C_{H_{2,ret}} - C_{H_{2,perm}}) \tag{2.5}$$

where, $C_{H_{2,ret}}$ & $C_{H_{2,perm}}$ is the concentration of hydrogen ($kmol/m^3$) in the feed and in the permeate respectively.

The hydrogen permeation through a dense palladium membrane is expressed by equation 2.6:

$$J_{H_{2,mem}} = \frac{Q}{\delta}({p_{H_{2,ret}}}^n - {p_{H_{2,perm}}}^n) \qquad 0.5 < n < 1 \tag{2.6}$$

where, Q is the membrane permeability in kmol/m s Pa, $p_{H_{2,ret}}$ & $p_{H_{2,perm}}$ (in Pa) are the hydrogen partial pressures in the retentate and permeate side respectively. The rate limiting step is specified in the equation by the exponent n. The flux can be limited due to surface reactions and diffusion of hydrogen atoms through the membrane. If bulk diffusion is the limiting step, n is set to 0.5. For thinner membranes, surface reactions are the limiting step for which the n value increases towards 1.

Commercialization of dense metal membranes
Different companies have been working on commercialization of dense metal membranes for hydrogen separation. In this section progress of a few companies is presented. Some of these membranes have been successfully used in membrane separators in pilot plants for 20 m^3/h hydrogen production and also in fluidized membrane reactors for methane steam reforming (Gallucci et al., 2013).

1. CRI/Criterion
   Over the last two decades, CRI/Criterion (a company owned by Shell) has made substantial advancements in developing and up-scaling Pd membrane technology. The technology is developed around electroless plating on ceramic-coated tubular metal supports (Enrico Drioli and Giuseppe Barbieri, 2011). The H_2 permeance of these membranes varies in the range of 40-70 $Nm^3/m^2hbar^{0.5}$. Hydrogen flux and selectivity are reported to be stable at temperatures of 300-500 °C and differential pressures of 26-42 bar. H_2 purity of >99% has been demonstrated for periods exceeding 4000 h in high temperature gas separations.
2. TNO Energy Transition (previously The Energy Research Centre of The Netherlands (ECN))
   TNO Energy Transition has been successful in developing hydrogen separation membranes fabricated by electroless plating of Pd-alloys with a thickness of around 3-9 µm on a low-cost (commercially available) ceramic support (Enrico Drioli and Giuseppe Barbieri, 2011). Membrane tube

with length of 0.6 to 0.85 m and a outer diameter of 14 mm were prepared. These membranes were used for single gas permeance test on a bench scale test system that can operate up to 500 °C and 65 bar feed pressure with a membrane area of 50 cm^2. It was recorded that, after initial activation, very high hydrogen permeance values of 50-100 $m^3/m^2hbar^{0.5}$ could be achieved with sufficient perm-selectivity.

TNO Energy Transition made their Pd-based membrane technology pre-commercially available through the Hysep modules. There are three modules available: Hysep 108 (0.06 m2), Hysep 308 & Hysep 1308 (0.5 m2). The nominal capacity of the largest membrane module is reported to be 3.5-6 Nm^3/h, when applying a reformate with 33% hydrogen, inlet pressure of 25 bar and hydrogen outlet pressure of 4 bar. Lifetime of several thousand hours have been reported with hydrogen purity ranging from 99.5% to 99.995% depending on the initial composition (Gallucci et al., 2013). Furthermore, a demonstration project with 10 m^2 hydrogen membrane is in preparation (Hysep ECN).

3. Tokyo Gas
   In the early 2000s, Tokyo Gas developed a MRF test system with a hydrogen production of 40 Nm^3/h, purity of 99.99% and production efficiency of 70%. The membrane modules composed of stainless steel supports and Pd–Y(Gd)–Ag alloy films of less than 20 mm thick. They have also introduced a membrane-on-catalyst (MOC) module. The MOC is a Pd-based membrane prepared on the porous surface of the tubular structured catalyst that has catalytic activity for steam reforming reaction (Gallucci et al., 2013).

2.5.2. Membrane reactors

If chemical reactions are carried out in a membrane module, it is called a membrane reactor. The ability of the membrane to selectively permeate a species through it has a huge advantage when an equilibrium reaction is taking place in the module (Kluiters, 2004). The membrane reactors can bring various advantages as compared to a conventional configuration. Some potential advantages are: improved yields and selectivity; by selectively taking away the products of an equilibrium reaction, membranes can shift the reaction to the product side, reduced downstream costs as the separation is integrated in the reactor. Finally, due to these reasons the capital costs are reduced as the size of the process unit is reduced.

However, reactions taking place in the module complicates it. The success of membrane reactors for hydrogen production depends on the design of innovative reactor concepts which allow integration of energy exchange and separation, reduction of mass and heat transfer resistances and simple housing and sealing process of the membranes (Gallucci et al., 2013). Additionally, the advances in membrane production methods to produce thin membranes that have high hydrogen flux and selectivity is not to be forgotten.

The changes in composition of substances influences the membrane operation due to changes in partial pressure and/or build up of contaminants. Furthermore, catalyst may be required for reactions to take place. The catalyst has to be placed in the membrane reactor. It can be placed inside the feed stream, which is the most simple option and easy to operate with the option to replace the catalyst. The catalyst can be placed in the membrane top layer or inside the membrane also. In this case, replacing the catalyst is difficult and will require replacing the entire membrane (Kluiters, 2004).

The performance of the membrane can also decrease over time due to concentration polarization and fouling. Concentration polarization occurs if a species has limited permeation through the membrane, which results in higher concentration of that species adjacent to the membrane reducing the permeate transport. Usually, this phenomenon isn't very severe for gas separation membranes. Fouling is a phenomenon when species absorb to the membrane surface and pores, which limits or blocks permeation. Common fouling examples are sulphur fouling due to presence of H_2S and SO_2. Purging the membrane with non-absorbing gases is a way to clean the membrane and avoid fouling. Membrane effectiveness can also be affected due to compaction i.e. pore size reduction due to pressurization. Compaction happens in polymer membranes and is usually irreversible. When deciding the optimal

design of the membrane reactor, other practical considerations come into play. Temperature variations cause structural changes in the membrane due to thermal stress. Also, pressure drop increases with length, therefore shorter modules are preferred but will need more seals. Ease of start-up and shut-down should also be considered (Kluiters, 2004).

Additionally, low separation factors, leakage at high temperature, poisoning of catalysts and mass transfer limitations have hindered the commercial application of membrane reactors until recent years (Kluiters, 2004). Tremendous amount of research has been carried out to develop membranes and suitable membrane reactor configurations for feasible hydrogen production. The next section mentions some of the work done on this field of study.

Membrane reactor performance for hydrogen production

A lot of work has been carried out in the past years to determine and improve the performance of membrane reactors for hydrogen production. A few of the relevant research work is presented in this section.

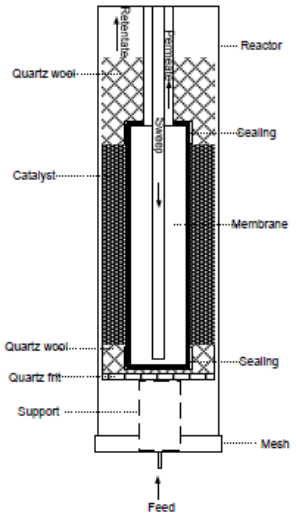

Figure 2.12: Basis sketch of the reactor used by Van Delft et al. (2009).

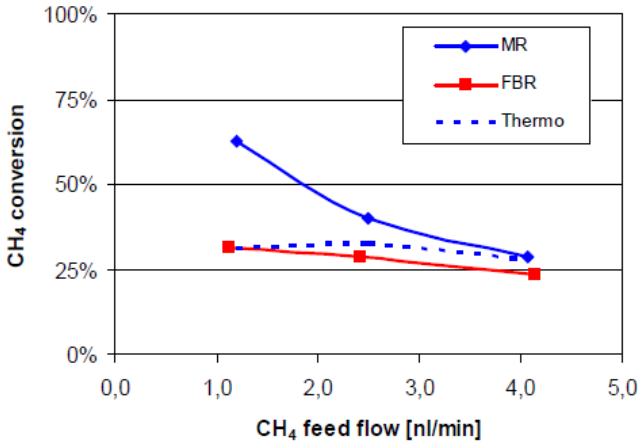

Figure 2.13: Methane conversion with a membrane reactor (MR), fixed-bed reactor (FBR) and equilibrium conversion (thermo) vs feed flow (Van Delft et al., 2009).

Van Delft et al. (2009) investigated the performance of Pd-membrane reactors for large scale hydrogen production. Dense tubular Pd alloy membranes with a high hydrogen permeance made on ceramic supports with electroless plating on 1 m^2 scale were used for this work. The membrane reactor experiments were performed in a single tube membrane reactor with 17.4 cm long PdAg membrane of diameter 1.4 cm (figure 2.12). The membrane was placed in a catalyst bed using commercial low temperature reforming catalysts. Nitrogen gas sweep flow was used in a co-current mode to prevent back permeation of hydrogen. The results showed that methane conversions well above the thermodynamic limits could be achieved at temperature of 600 °C, pressure of 11 bar and S/C ratio of 3 (figure 2.13). The paper also concludes that scaling-up fabrication of thin defect free Pd-membranes and sealing between ceramic tube and fixation in metallic tube are critical items for hydrogen membrane reactor development.

Steam reforming of biogas in membrane reactors for hydrogen production has also been studied in the recent years. The performance of a fluidized bed membrane reactor for production of hydrogen from biogas is analysed by Saebea et al. (2014). The performance of the fluidized bed membrane reactor is compared with the conventional reformer for steam reforming of biogas. The influence of key operating conditions such as temperature, pressure, steam-to-carbon on the performance of the reactor in terms of hydrogen production and purity are studied. The comparison showed that the production rate of hydrogen is higher in the fluidized bed membrane reactor. The steam-to-carbon ratio

had a minor influence on the production, whereas increasing the temperature and pressure (upto a limit) considerably increased the hydrogen production in the fluidized bed membrane reactor.

Di Marcoberardino et al. (2018) investigated the potentiality of membrane reactor for green hydrogen production from raw biogas. A detailed techno-economic assessment was carried out for this innovative system developed within the BIONICO project. This project focuses on the adoption of fluidized bed membrane reactor to produce 100 kg/day pure green hydrogen from biogas. The simulations performed considered two different biogas compositions (from landfill and anaerobic digestion) to access the impact on system performance and costs. Furthermore, two permeate configurations were compared i.e. sweep gas and vacuum. It was found that the resulting efficiency and membrane area for sweep gas configuration were 15% lower at 5 times larger than the vacuum. When compared to the conventional hydrogen production case, the hydrogen production cost for the BIONICO case at 20 bar ranged from 4 to 4.1 €/kg H_2 while reference case resulted in 4.21 €/kg and 6.4 €/kg for SR (steam reforming) and ATR (auto-thermal reforming) respectively. Additionally, the BIONICO case had lower biogas and capital costs but higher efficiency costs compared to the reference SR case whereas it had lower biogas and efficiency costs with respect to the ATR. Between the landfill and anaerobic digestion cases, the latter resulted in the lower costs due to the higher methane content. The work concludes that membrane reactors are a promising technology for green hydrogen production from biogas.

Shafiee et al. (2016) modelled and simulated a multi-tubular metallic membrane reactor for hydrogen production using thin-layer palladium-based membranes. A sequential simulation was done to analyse pure hydrogen and binary hydrogen mixture separations and then scaled-up to simulate an industrial scale unit. A techno-economic analysis was performed for a plant capacity of 300 TPD of hydrogen. The membranes used for this analysis were thin (2.5 µm) defect-free with a selective layer (Pd-Ag alloy). A sensitivity analysis was performed to determine the optimum operating conditions for the lowest cost of hydrogen. Temperature, pressure, steam-to-carbon ratio, amount of catalyst (kg/m^2) were changed. Figure 2.14 shows the calculation methodology used. A similar methodology will be used in this work for determining the optimum hydrogen cost. The cost of hydrogen was calculated to be 1.98 $/kg and the membrane cost was 20% of the total capital cost.

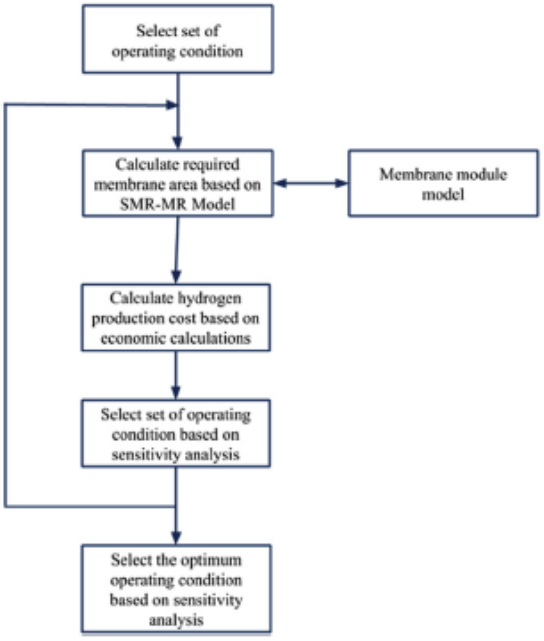

Figure 2.14: Methodology for determining optimum hydrogen cost of a plant (Shafiee et al., 2016).

For commercial use, the membrane reactors developed have to be scaled-up. A recent study by Chompupun et al. (2018) performed experiments for steam methane reforming using Ni/Al_2O_3 catalyst in a membrane reactor to determine the kinetics and formulated a 2-D Pd-reactor model with the

obtained parameters. Furthermore, using the kinetic and permeation data, detailed 3-D membrane reactor models were developed and interesting scale-up strategies were proposed using the model. The membrane reactor configuration and the 2-D axisymmetric model of the membrane reactor are shown in figure 2.15 & 2.16 respectively.

The configuration shown in 2.15 is usually used in laboratories or bench scale experiments and it is impractical to scale-up the annular cylindrical membrane reactor. The solution of this problem, as proposed by Chompupun et al. (2018), is by scaling-up in parallel (enlarging the reactor size) or numbering-up of the same reactor into multi-reactors arranged as a square honeycomb monolith.

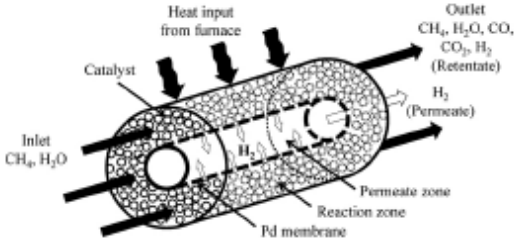

Figure 2.15: Membrane reactor configuration (Chompupun et al., 2018).

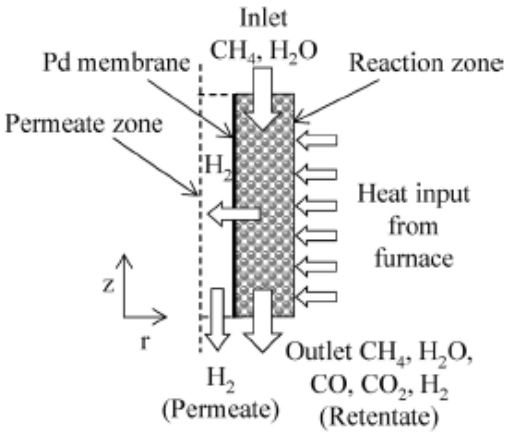

Figure 2.16: Two-dimensional model of the membrane reactor (Chompupun et al., 2018).

Scaling by numbering-up makes the composite honeycomb structure shown in figure 2.17. The cylindrical reactor shown is transformed into a square one (figure 2.17a). The arrangement for thermal integration of heat input (H) for the endothermic reaction is shown in the figure 2.17b. Multiple square packed beds (R) with the inner square annular tube of the membrane permeate zone (M) in the middle make up a scaled reactor. A 2-D unit cell arrangement and a 3-D unit cell honeycomb monolith reactor are shown in figure 2.17c & 2.18 respectively.

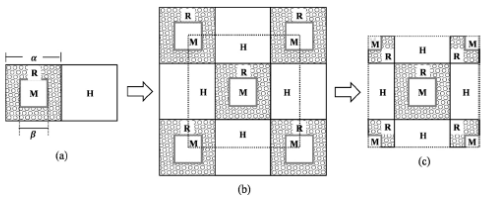

Figure 2.17: Simplified reactor model for scaling-up (Chompupun et al., 2018)

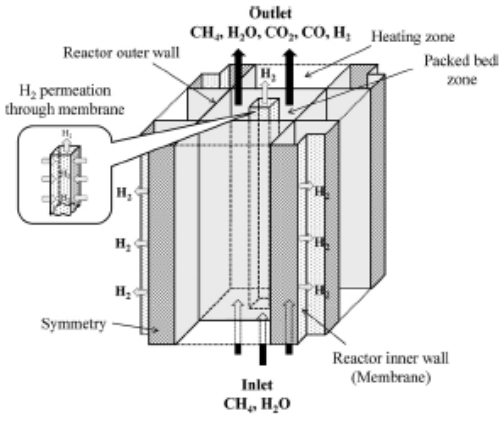

Figure 2.18: 3-D unit cell honeycomb monolith reactor (Chompupun et al., 2018).

Two approaches to determine the performance of an enlarged reactor for scaling up were followed, as seen in figure 2.19. One was keeping the same inner tube size of the membrane tube but this didn't yield the same conversion as the laboratory scale because of insufficient membrane area for hydrogen

separation (refer 2.19a). The other option was keeping the S_{mem}/V_r [4] ratio constant. However, doing this resulted in odd reactor architectures (refer 2.19b). It was agreed that scaling-up by numbering was the preferred solution and the optimum geometric arrangement was examined. Detailed information can be found in Chompupun et al. (2018).

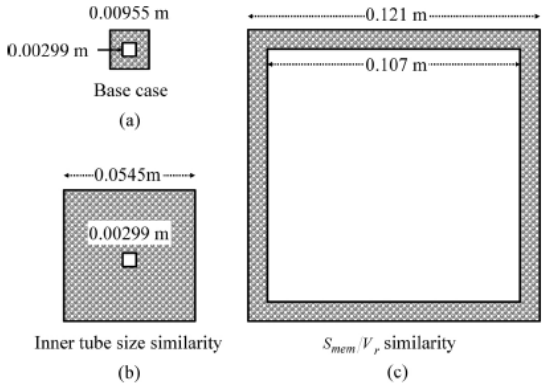

Figure 2.19: Methodology for determining optimum hydrogen cost of a plant (Shafiee et al., 2016).

2.6. Carbon capture and storage

It is widely accepted that one major solution of global warming, as long at the energy economy is based on fossil fuels, is carbon capture and storage (CCS). CCS consists of two challenging technologies: carbon capture & carbon storage. There are three main technological paths for CCS namely post-combustion capture, pre-combustion decarbonization and oxyfuel combustion route (Gallucci et al., 2013). Lately, great interest has been shown for pre-combustion capture technologies, especially for the production of fuel-grade (high purity) hydrogen (National Academy of Engineering, 2004). Removal of CO_2 before the fuel combustion, at high pressure, enables the use of the resulting off-gas in many applications like the production of power, chemicals, pure hydrogen etc. Another way to look at it is that, if CO_2 sequestration is the main aim, the CO_2 stream has to abide to specific composition guidelines (refer table 2.3) and therefore, other impurities need to be removed from the stream.

The stream from which CO_2 has to be recovered contains majorly CO_2 (>50%) with small amounts of other species like H_2O, H_2, CH_4, CO etc. (Atsonios et al.). Water can be easily removed by cooling the stream below the dew point of water. However, the removal of other species is challenging and a cost and energy efficient process needs to be used. The existing and emerging technological options for CO_2 capture from gaseous streams with relatively high CO_2 are summarized in Figure 2.20 (Hartnig and Roth, 2012).

The current commercial CO_2 capture technologies are based on absorption. These processes use solvents that are capable of separating more than 90% of CO_2. Novel technologies i.e. cryogenic separation technology are also being developed and demonstrated (Collodi et al., 2017). In this research work, the performance and feasibility of the cryogenic separation technology, integrated with the membrane reactor, for carbon capture is to be determined. Therefore, the next section will elaborate on this technology and outline the recent research findings.

[4] The ratio between membrane surface area and reactor volume

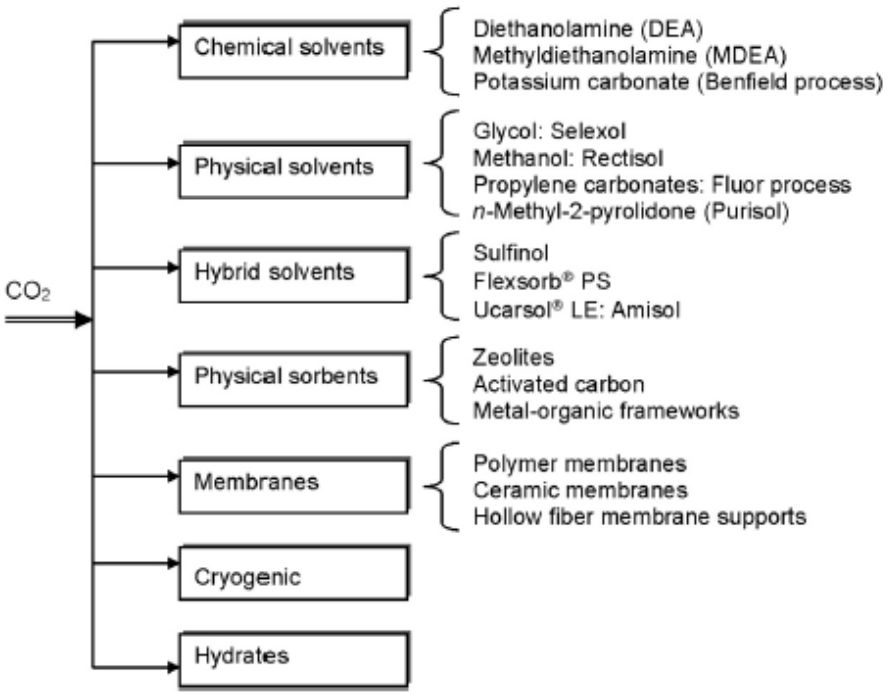

Figure 2.20: CO_2 capture technologies with high concentration of CO_2 (Hartnig and Roth, 2012).

2.6.1. Carbon capture with cryogenic technology

Cryogenic CO_2 separation is based on difference in boiling points of CO_2 and other components in the gas stream. This method is currently widely used in the industry to purify and liquefy CO_2 (Hartnig and Roth, 2012). The gas mixture is cooled below the boiling point of CO_2 (above the CO_2 triple point at 5.2 bar and - 56.6 °C) at a given pressure and the CO_2 is condensed from lighter gaseous components (Voldsund et al., 2016). The retentate stream from the reactor usually has CO_2 partial pressure around its triple point pressure and therefore, suitable for vapour-liquid separation. The CO_2 separation and compression work decreases as the concentration of CO_2 increases. A recovery of 85-90% can be obtained (Voldsund et al., 2016).

The technology has good economy of scale and possibility of direct production of liquid CO_2 that can be pressurized by a pump at low energy cost and transported. The main shortcomings of this technology is that the technology is very energy intensive and a upstream removal of relatively high freezing point components like water is required (Hartnig and Roth, 2012).

Atsonios et al. models a cryogenic method for separation of combustibles from a CO_2-rich stream and evaluates its effects on the systems efficiency. Based on differences in thermodynamic properties (dew point) of each component, the stream is cooled down and the CO_2 is separated in flash separators (figure 2.21) or a distillation unit (figure 2.22). The research showed that applying a distillation column resulted in a higher purity of the product CO_2 stream (>99%) compared to the flash separators. However, separation efficiency for the flash separators is quite high compared to the distillation column as more duty is required due to extra cooling system.

A study by Xu et al. (2014) on cryogenic CO_2 capture technology proposed an improved CO_2 separation and purification system after in-depth analysis of cryogenic separation and distillation theory as well as the phase transition characteristics of gases containing CO_2. Multi-stage compression, refrigeration, separation and distillation technologies are used to produce a high purity CO_2 stream with relatively low energy penalties (figure 2.23). The simulation results showed that specific energy consumption for the CO_2 capture process developed was only 0.425 MJ/kg CO2 with 99.9 % purity. Techno-economic analysis was carried out and the total plant investment was found to be relatively low. Compared to the conventional MEA and $Selexol^{TM}$ absorption methods, the cost of CO_2 capture of the proposed system

was found to be reduced by 57.2% and 45.9% respectively.

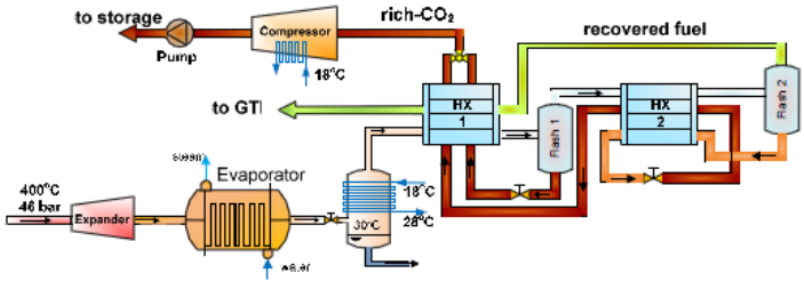

Figure 2.21: Cryogenic CO_2 capture with flash separators (Atsonios et al.).

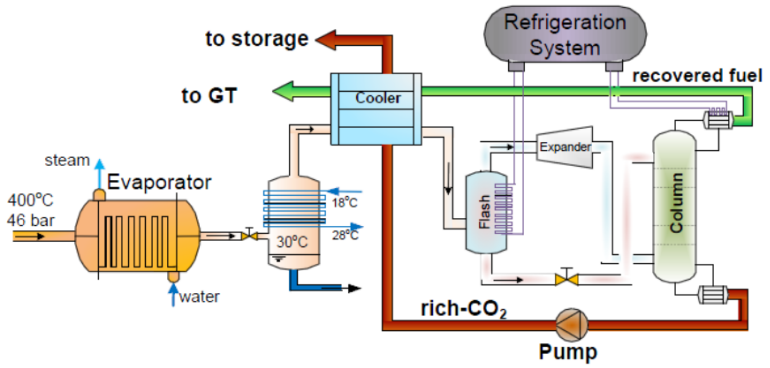

Figure 2.22: Cryogenic CO_2 capture with distillation column (Atsonios et al.).

Baxter et al. reported the performance of a cryogenic CO_2 capture process from flue gas. The work states that the overall energy and economic costs of the process were found to be 30% lower than most of the other conventional processes that involve air separation units, solvents etc. The advantages of the process stem from elimination of the energy and entropy-intensive cyclic separation processes (distillation and absorption), compressing a condensed phase rather than gas, smaller dry volumetric flow rates and other ancillary advantages like energy and water savings.

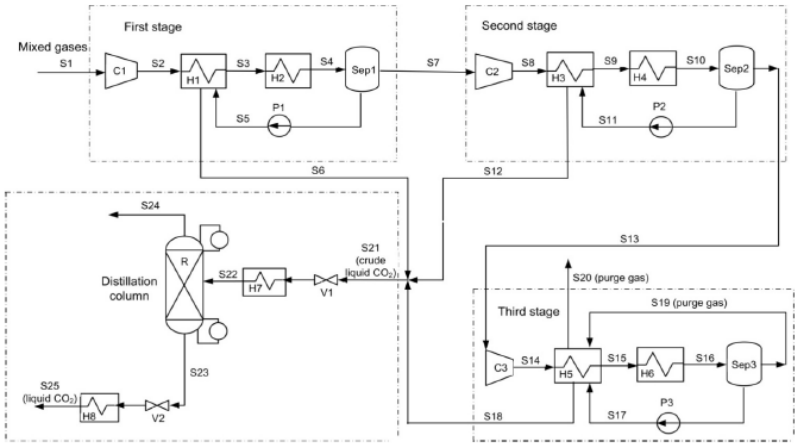

Figure 2.23: CO_2 separation and purification process developed by Xu et al. (2014).

2.6.2. Transport and storage

There are projects being carried out for the transport and storage of carbon dioxide underground and under the North sea in The Netherlands. This work focuses on carbon capture whereas sequestration is outsourced. However, it is important to keep in mind that there are strict guidelines regarding the purity of the CO_2 to be transported and stored. The carbon dioxide captured needs to meet these guidelines. In table 2.3, the specifications for CO_2 storage are mentioned.

Table 2.3: Quality specifications for the CO_2 stream for storage (Alstom UK, 2011)

	Recommended for EBTF	**Aquifer**	**EOR**
CO2	> 90 vol %	> 90 vol %	> 90 vol %
H2O	< 500 ppm (v)	< 500 ppm (v)	< 50 ppm (v)
H2S	< 200 ppm (v)	<1.5 vol %	< 50 ppm (v)
NOx	< 100 ppm (v)	NA	NA
SOx	< 100 ppm (v)	NA	< 50 ppm (v)
HCN	< 5 ppm (v)	NA	NA
COS	< 50 ppm (v)	NA	< 50 ppm (v)
RSH	< 50 ppm (v)	NA	> 90 vol %
Non-condensable components			
N2	< 4 vol % *	< 4 vol % *	< 4 vol % *
Ar	< 4 vol % *	< 4 vol % *	< 4 vol % *
H2	< 4 vol % *	< 4 vol % *	< 4 vol % *
CH4	< 2 vol % *	< 4 vol % *	< 2 vol % *
CO**	< 0.2 vol % *	< 4 vol % *	< 4 vol % *
O2***	< 100 ppm (v)	< 4 vol % *	< 100 ppm (v)

Note: 1 vol % = 10000 ppm (v).
* - x + ∑xi < 4 vol % = total content of all non-condensable gases.
** - health and safety issues.
*** - to avoid ignition.

A property that distinguishes CO_2 from other substances that are transported in pipelines is its low critical temperature of 31.1 °C (Witkowski et al., 2014). Depending on the temperature and pressure conditions in the pipeline, CO_2 can be transported as a gas, as a super-critical fluid or as a sub-cooled liquid. The phase diagram of CO_2 is shown in figure 2.24.

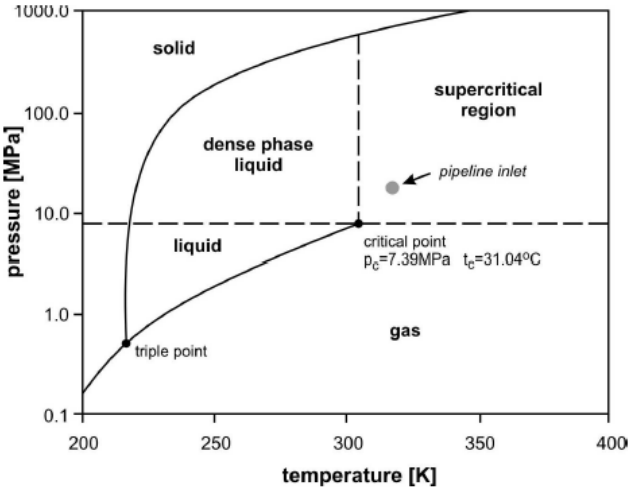

Figure 2.24: Phase diagram of CO_2 (Witkowski et al., 2014).

2.7. Industrial processes

Air Liquide, owning numerous hydrogen plants around the world has developed a solution for CO_2 capture from SMR plants (Terrien et al., 2014). This new technology is called $CRYOCAP^{TM}\ H_2$. It uses cryogenic purification to separate CO_2 from the PSA off-gas stream. This purification step is followed by membrane separation to simultaneously increase the SMR productivity (H_2 recovery) as well as CO_2 capture rate. The extra hydrogen production due to this process is about 10-20%. The first implementation of this technology was suggested to be in the EOR (Enhanced Oil Recovery) application.

$CRYOCAP^{TM}$ technology can be used in many industrial process such as steel plants, thermal power plants, hydrogen production plants. However, $CRYOCAP^{TM}\ H_2$ development has been the fastest having its first industrial deployment in 2015 (Air Liquide). This installation is in Port Jérôme, Normandy, at the largest steam methane reforming hydrogen production unit operated by Air Liquide in France. Figure 2.25 shows the process flow diagram of the process. This process produced food-grade liquid CO_2 and has additional purification steps that aren't needed in the EOR application.

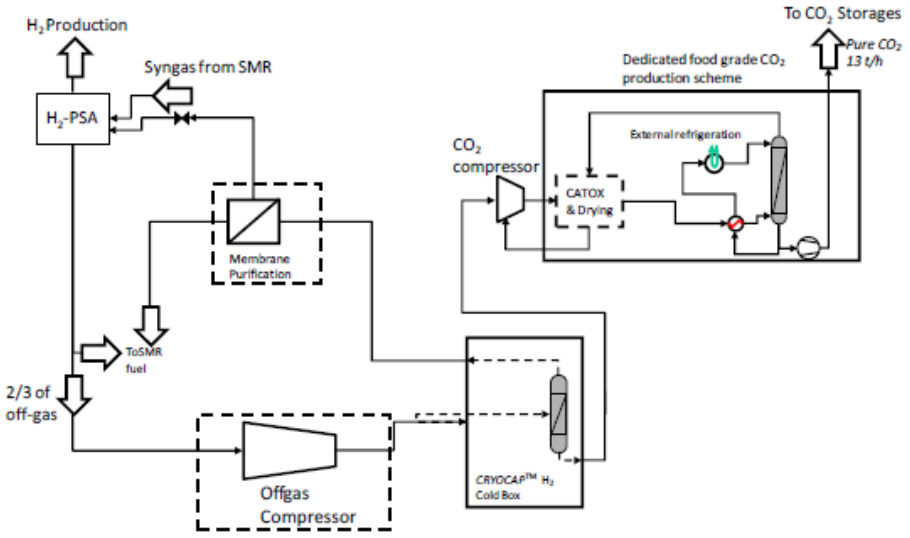

Figure 2.25: Process flow of Port Jérôme plant (Terrien et al., 2014).

The 40 Nm^3/h MRF test system by Tokyo Gas Co Ltd. briefly mentioned before was installed and tested at Senju hydrogen refuelling station in Tokyo. The test unit has a multi-tube rectangular structure with 112 reactor tubes, each having two planar-type membrane modules made of stainless steel support and Pd-based alloy films of less than 20 µm thick. The hydrogen permeability of the membrane was several times as large as the then conventional Pd-Ag alloy membrane. A Ni-based catalyst supported on alumina is used. The system was tested at 495-540 °C at a process gas pressure of 9 bar and a hydrogen product pressure of 0.2-0.4 bar & S/C ratio of 3.0/3.2. The conversion obtained was 80-95% for a natural gas feed flow range of 3.2-11.6 Nm^3/h, while calculated equilibrium conversion without hydrogen separation for the condition is 21-29%. Furthermore, durability of the unit was checked and it was found that after 2100 h of operation time, the impurity concentrations started to increase. The impurity level was less than 3 ppm after 3310h of durability test but long term durability was identified as an important issue.

As seen in figure 2.26, the system installed at the Senju Hydrogen Station was 1/3rd of the previously installed 50 Nm^3/h conventional PSA system. This successful operation and fueling of the FCVs marked a major step towards the efficiency improvement for hydrogen production, which is especially needed for diffusion of FCVs (Shirasaki et al., 2009).

Figure 2.26: Senju Hydrogen Station (Shirasaki et al., 2009).

TNO Energy Transition's Hysep membrane technology was tested in an experimental hydrogen plant at Techimont KT's Chieti test site in Italy in 2010 (ECN, 2010). The hydrogen plant was based on Reformer and Membrane Modules configuration (RMM) integrated with membrane separation and reaction modules. The scale of this test plant was 20 Nm^3/h hydrogen production. TNO delivered a 0.4 m^2 membrane module to perform this test experiment. The flux and the purtiy of hydrogen were closely monitored during the tests. Both were shown to be high for an operation time of 5000 hours and more than 50 thermal cycles.

2.8. Key takeaways

Table 2.4: Key takeaways from the literature study

Hydrogen production	Membrane reforming can result in a high degree of process integration & intensification while achieving higher methane conversions and hydrogen yields at lower temperatures and with higher energy efficiencies compared to conventional steam methane reforming, refer 2.2 & 2.3.
Feed	Natural gas is the conventional feed used currently. Research on hydrogen production using biogas is on the rise at it results in a lower carbon footprint of the process, refer 2.4.
Feed purification	Impurities in the feed harm the membrane and catalyst and decrease their performance. They need to be removed to approx. ppb levels. The most harmful impurity is sulfur, usually present as H_2S, refer 2.4.1.
Membranes (most attractive/ relevant characteristics)	Material: Pd-based dense metallic membranes, refer 2.5.1.1.
	Configuration: Counter-current operation, refer 2.5.
	Structure: Supported resulting in thin, less expensive membranes, refer 2.5.1.2.
	Bulk diffusion through membranes is the limiting step. Hydrogen permeation through metal membranes follows solution-diffusion mechanism (Sievert's law), refer 2.5.1.3.
Membrane reactors, refer 2.5.2.1.	Packed-bed and fluidized-bed membrane reactors are developed and studied for hydrogen production.
	Performance of reactors is mainly determined in laboratory or bench-scale experiments.
	Scaling-up for commercial use can be achieved by numbering-up. However, no large scale demonstration to determine performance.
Carbon capture and storage	Cryogenic carbon capture technology can achieve high capture rates with low energy penalty, refer 2.6.1.
	CO_2 can be transported as a gas, super-critical fluid or sub-cooled liquid through pipelines, refer 2.6.2.
	Strict quality specification for CO_2 storage have to be met, refer 2.6.2.
Hydrogen, refer 2.1	Strict quality specifications have to be met for H_2 to be used as a fuel.
	The fueling pressure for FCVs is 700 bar.
Industrial processes	Air Liquide, Tokyo Gas Co. Ltd. etc. have commercial processes with successful integration of membrane reactors/membranes for separation, refer 2.7.

3

Basis of design

The insights gained from the theoretical research in chapter 2 are used to fix the process design assumptions for the system to be developed. A brief description of the reference system is mentioned followed by detailed description and assumptions of the novel system to be developed. Following which, three configurations are developed. Finally, the key performance indicators that will be used for the performance analysis are defined.

3.1. Value chain definition

The value chain of the novel case and the reference case is defined in this section to get a good perspective of the similarities and differences between the cases during comparison.

3.1.1. Reference system value chain

A reference system needs to be chosen to compare the results of the decentralized novel system to be developed in this work. A conventional steam methane reforming system for hydrogen production was chosen (Spath and Mann, 2001). This reference case is a centralized hydrogen production unit via SMR. Figure 3.1 & 3.2 show the process flow and the value chain of the reference case respectively. It is assumed that the natural gas is readily available at the production site from the grid. It is assumed to be sweetened to remove H_2S to a level of 4 ppmv prior to pipeline transport. The natural gas is further purified to remove any residual H_2S using a zinc oxide bed before feeding it in the reformer. Then, it is compressed, pre-heated and fed to the reforming unit. The composition of natural gas fed into the reformer is 94.5% CH_4, 2.7% C_2H_6, 1.5% C_3H_8, 0.8% N_2, 0.5% CO_2 (Spath and Mann, 2001). The reforming unit is assumed to be steam reforming and run at a capacity of 1.5 million $Nm^3/day\ H_2$ (Spath and Mann, 2001). After the reforming, WGS and purification processes, 500 Nm^3/h hydrogen (same capacity as the novel system) is separated, compressed and stored in cascade storage bullets around 432 bar. Finally, a boost compressor is used to compress the hydrogen to 830 bar and transported to the refuelling stations via pipelines to be refuelled in FCVs at 700 bar (Katikaneni et al., 2014). The higher pressure is to account for pressure loss during pipeline transport. The hydrogen produced by this process is industrial grade with purity >99.5% (Spath and Mann, 2001). The modelling of the conventional production process is out of scope of this study and thermodynamic and economic values are taken from Spath and Mann (2001) & Katikaneni et al. (2014).

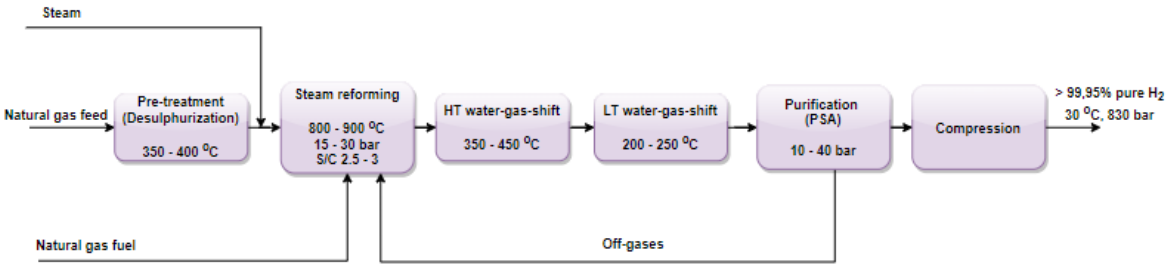

Figure 3.1: SMR process producing 1.5 million $Nm^3/day\ H_2$ (Spath and Mann, 2001).

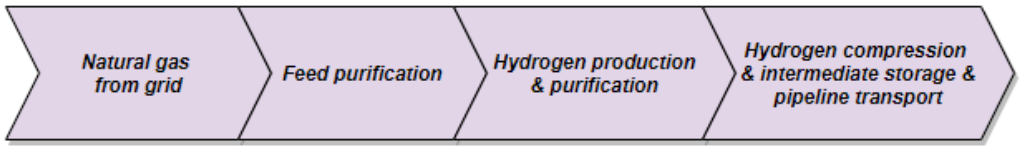

Figure 3.2: Value chain of reference SMR system (Spath and Mann, 2001) & (Katikaneni et al., 2014).

3.1.2. Novel system value chain

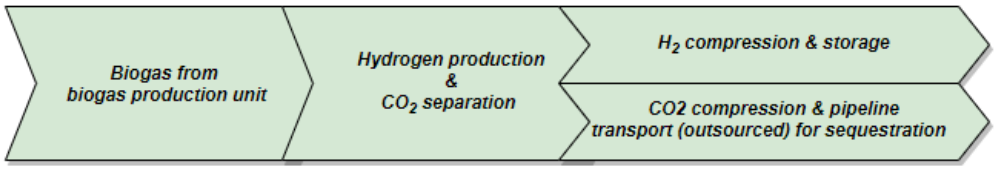

Figure 3.3: Value chain of novel case

It is assumed that pre-treated biogas from the biogas production unit is readily available at the hydrogen production site. The biogas is compressed, pre-heated and fed to the reactor. Hydrogen is produced and separated in the membrane reactor after which it is purified to fuel-grade hydrogen, compressed to 700 bar and stored in cascade bullets ready to be fueled into the FCVs. Simultaneously, the unreacted gases are fed into the cryogenic carbon capture unit which separate the CO_2 into a pure stream. The separated biogenic CO_2 is compressed into a super-critical state (>100 bar and around 30 °C) and transported (outsourced) via pipelines to the storage location. Figure 3.3 shows the value chain of the novel system.

3.2. System description

The process, battery limits, design and modelling assumptions and the configurations generated based on this information are described in this section.

3.2.1. Process description

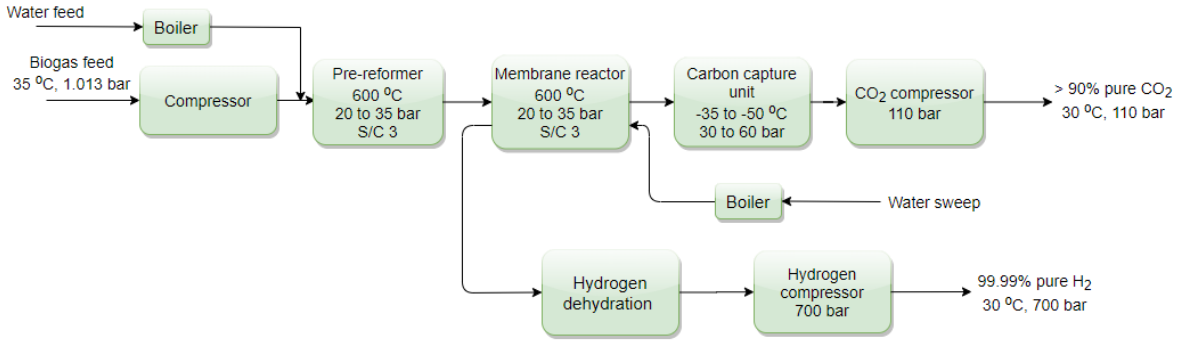

Figure 3.4: Novel process producing 500 Nm^3/h H_2.

Biogas from sewage treatment plant with a composition as in table 3.1 is fed to compressor unit to rise its pressure from 1.013 bar to the desired pressure of the unit. The compressed biogas is heated to 600 °C and fed into the pre-reformer along with steam. A pre-reformer is needed to have the otherwise missing H_2 driving force at the inlet of the membrane reactor. The pre-reformed gas then enters the membrane reactor where most of the reforming takes place and hydrogen is permeated into the permeate side. The reforming temperature for this process is 600 °C and pressure between $20 - 35$ bar. Membrane reforming can achieve high conversions at low temperatures compared to steam methane reforming, however, permeation flux increases with temperature. Therefore, a moderate temperature is a practical choice. Steam is used as a sweep to drive hydrogen out of the permeate side of the membrane reactor. The permeate stream is cooled to around 30 °C to remove water in a knock-out drum. FCVs require very high purity of H_2 as shown in table 3.1, therefore a molecular sieves dehydration unit using zeolite adsorbent is integrated for deep removal of water and contaminants i.e. CH_4, CO, N_2. Two columns are adopted for the purification process for continuous operation. When one is in the adsorption cycle the other is in the regeneration cycle. Temperature swing adsorption technology is used for the regeneration process. Nitrogen gas is heated to 250 °C and passed through the molecular sieves bed to be regenerated. The nitrogen purges (almost) all the contaminants adsorbed to the bed and regenerates them. During this process, 5% of hydrogen is lost. After purification of the hydrogen, it is compressed to 700 bar and stored in cascade storage units.

The carbon capture unit captures CO_2 using cryogenic technology. The process involves a number of different steps. First, the retentate stream is cooled around 30 °C to condensate out most of the water in a knock-out drum. Later, the stream is cooled to a temperature between the triple point and critical point of CO_2 (Seo et al., 2015). The liquefaction temperature of CO_2 is determined mainly by its pressure. The increase in CO_2 pressure enhances its liquefaction temperature, which results in lower energy consumption in refrigeration and prevents the equipment from freezing. Generally, the CO_2 concentration and the total pressure of the gas mixture directly affect the CO_2 pressure in a gas mixture. Depending on the stream conditions, an optimum pressure and temperature is decided. The range is between 30 - 60 bar and -35 to -50 °C (Xu et al., 2014). The liquid CO_2 stream obtained is further purified in a distillation column if required. The pure CO_2 stream obtained is then compressed to 110 bar to be transported via pipelines. The off-gases can be sent to a furnace for combustion to use their energy for the reactor or they can be recycled back into the process.

3.2.2. Battery limits

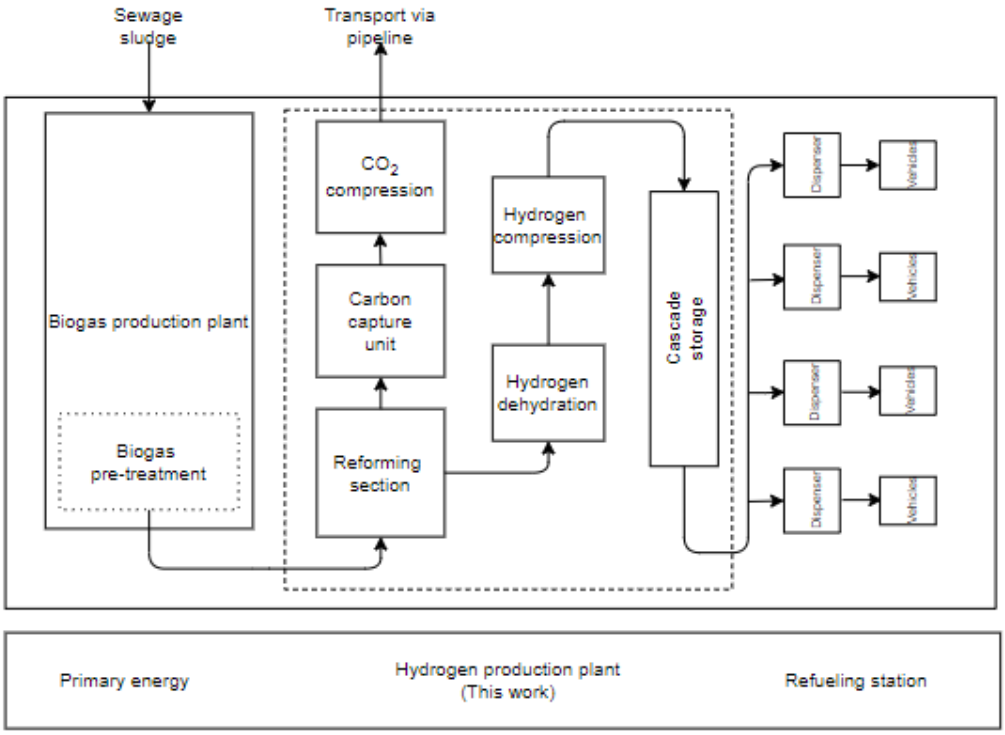

Figure 3.5: Sketch of the whole system from biogas production to refueling station.

Figure 3.5 shows how the biogas production plant, the novel hydrogen production plant and the refuelling station interact with each other. The battery limits of the process developed are shown by the dotted boundary. Pre-treated biogas enters the hydrogen production plant. Hydrogen is stored in cascade storage tanks ready to be fuelled into vehicles. CO_2 is compressed and ready to be transported to storage sites via pipelines.

3.2.3. Design assumptions

The 500 Nm^3/h hydrogen production plant (250 FCVs/day (Katikaneni et al., 2014)) with carbon capture is assumed to be located near a refuelling station in the Netherlands. Currently, there are about 250 cars in operation in The Netherlands and the number is expected to grow exponentially in the near-future (Marcel Weeda, 2020). Therefore, the production capacity chosen will assuredly meed the demand requirements in the future.

Furthermore, the hydrogen production plant is assumed to be close to a sewage sludge biogas production unit. Sludge biogas plants in The Netherlands have capacities ranging from 40 Nm^3/h (HoSt Bioenergy Systems) to several thousand, for example 2050 Nm^3/h in Amsterdam (Dutch Water Sector, 2020). These capacities of biogas would result in 58 Nm^3/h to 3000 Nm^3/h production of hydrogen respectively. These values are in range with the reported capacity of the novel system. A biogas production capacity of around 340 Nm^3/h is required to produced 500 Nm^3/h H_2. Therefore, an average Dutch biogas plant producing 340 Nm^3/h is assumed to be coupled with an H_2 production plant by membrane reactor technology and an H_2 refuelling station for FCV. This scenario is assumed for the study.

The inlet-outlet conditions assumed are mentioned in table 3.1. At the biogas production facility itself, the biogas is purified to the composition mentioned in table 3.1 to meet the membrane reactor specifications (free of impurities such as sulfur compounds). The temperature and pressure values are typical conditions from an anaerobic digester (Di Marcoberardino et al., 2018). The feed water

used for the process is assumed to be demineralized. The H_2 and CO_2 compositions are based on the quality specifications already discussed in the previous chapter. H_2 pressure is in line with the FCV's hydrogen pressure requirement (Katikaneni et al., 2014). CO_2 is assumed to be transported in a super-critical state and the temperature and pressure conditions are taken from the sea-based pipeline requirements of the Porthos project (Porthos Project, 2019). Transportation is out of scope for this work and is assumed to be outsourced.

Table 3.1: Input-output specifications.

Stream (mol%)	
Biogas (available)	63 % CH_4, 35 % CO_2, 1.8 % H_2O, 0.2 % N_2 T = 35 °C, P = 1.013 bar LHV = 19.5 MJ/kg
Water (available)	100 % H_2O T = 15 °C, P = 1.013 bar
Air (available)	78 % N_2, 21 % O_2, 0.96 % H_2O, 0.04 % CO_2 T = 15 °C, P = 1.013 bar
Hydrogen (target)	99.97 % H_2, 5 µmol H_2O/mol H_2, 2 µmol CH_4/mol H_2, 2 µmol CO_2/mol H_2, 0.2 µmol CO/mol H_2 T = 30 °C, P = 700 bar LHV = 120 MJ/kg
Carbon dioxide (target)	> 90 % CO_2, < 2 % CH_4, < 4 % $H_2 + N_2$, < 0.2 % CO, < 500 ppm (v) H_2O T >= 30 °C, P > 100 bar (super-critical state)

The membrane reactor is a continuous plug flow reactor, assuming tube-in-tube configuration with packed bed around the membrane. It is assumed that the membrane reactor is scaled up by numbering up (Chompupun et al., 2018). A counter-current flow configuration is assumed with steam as a sweep agent for hydrogen removal. A counter-current sweep configuration results in high methane conversions and hydrogen recovery, producing a retentate stream containing majorly CO_2 and water. Therefore, efficient carbon capture using cryogenic capture technology is possible considering the scale of the system and also the fact that the retentate stream has a high partial pressure of CO_2 (Sjardin et al., 2006). The refrigeration system type (single-stage or multi-stage) and the refrigerant used depend on the process conditions. The system and the refrigerant selection will be done after the optimum configuration is selected. For the configuration selection, this decision is not important.

Boiler(s) required for steam generation are assumed to be electric as they are more compact, efficient and easy to install than gas boilers. However, electricity is more expensive than gas and therefore the operating costs will be higher. Nonetheless, the environment impact of the electric boilers is lesser and may be even negligible if most of the electricity is produced using renewable sources in the future.

For the dehydration unit, the amount of molecular sieves required is calculated taking into account the water needed to be removed, the other contaminants removed, the adsorption capacity of the sieves, cycle life & time etc. Zeolite molecular sieves 5A are selected for the deep removal of contaminants from hydrogen. 5A molecular sieve is a strong adsorbent and is widely used in the industry for drying and purification of hydrogen due to its high adsorbing quality and speed and high crushing strength (high durability) (Molecular Sieve Desiccants, 2020). They are mostly used for water adsorption in the industry, however, for this work it is assumed that the adsorbent effectively adsorbs water and other contaminants like CH_4, CO_2, CO that may permeate through the membrane. A major advantage of molecular sieves is that they can be regenerated, which reduces the required amount of molecular sieve to economically feasible quantities. TSA is the technology chosen for regeneration of the molecular sieves because it allows removal of impurities down to 0.1 - 1 ppm levels. Pressure swing adsorption is used for less stringent outlet specifications of 100 ppm or more and therefore not suitable for this application. In TSA, the change in the adsorption equilibrium is obtained by increasing

the temperature with the help of a hot gas. Molecular sieves 5A are typically regenerated with a hot gas between 200 °C and 315 °C (Sigma-Aldrich). The maximum velocity of the hot gas in this application is 5 m/min to prevent any channelling or bed lifting (Gas processing and LNG, 2018). The hot gas chosen for this work is nitrogen. Typical specifications of molecular sieves 5A are shown in table 3.2 (ZR Catalyst).

Table 3.2: Typical specifications of molecular sieve 5A (ZR Catalyst).

Performance	**Unit**	
Shape		Sphere
Diameter	mm	2
Bulk density	kg/m^3	680
Water adsorption	wt %	≥ 24

Furthermore, utilities are assumed to be readily available i.e. electricity is available from the grid, cooling water is readily available and refrigerant for cryogenic capture is available.

3.2.4. Model description

For initial results, a basic Aspen model was developed for the membrane reactor which consists of a series of reactor and separator blocks integrated together to model the performance of the membrane reactor (reaction and separation) as closely as possible. This model was used to achieve preliminary results which were refined with a more detailed model developed in the Aspen Custom Modeler. The basic design of the membrane reactor was out-of-scope for this work and a 1-D PFR model already developed was used to estimate the required area to finally estimate the cost, based on publicly available permeance data. In this section, the two models are described.

Membrane reactor Aspen Plus Point model

The Aspen Plus Point model is a 0-D reactor model used to predict the performance of the membrane reactor by achieving quick results for the membrane area, productivity, methane conversion etc. A FORTRAN subroutine is developed in Aspen Plus to calculate the membrane area required. The equations used are as follows:

$$A_{mem} = \frac{\dot{n}_{H_2-perm}}{J_{H_2,mem}} \qquad m^2 \tag{3.1}$$

The flux is calculated using the following equations:

$$J_{H_2,mem} = K_p * DF_{H_2} \qquad kmol/m^2 s \tag{3.2}$$

$$DF_{H_2}{}^{1} = \frac{DF_{in} - DF_{out}}{ln(\frac{DF_{in}}{DF_{out}})} \qquad Pa^{0.5} \tag{3.3}$$

The assumptions and/or limitations of this model are:

1. 0-D model.
2. No kinetics.
3. No permeance.
4. Driving force is fixed (fixed split fraction in the membrane separator block).

[1] where DF_{in} is the driving force at input end of tube $(Pa^{0.5})$ and DF_{out} the driving force at exit end $(Pa^{0.5})$. $DF_{in} = (p_{ret,in})^{0.5} - (p_{perm,in})^{0.5}$ where $(p_{ret,in})$ is the partial pressure on the retentate side at the input end (Pa) and $(p_{perm,in})$ the partial pressure on the permeate side at the input end (Pa). $DF_{out} = (p_{ret,out})^{0.5} - (p_{perm,out})^{0.5}$ where $(p_{ret,out})$ is the partial pressure on the retentate side at the exit end (Pa) and $(p_{perm,out})$ the partial pressure on the permeate side at the exit end (Pa).

Membrane reactor ACM model

The basis of the membrane reactor ACM model used in this work is described below and taken from Lin et al. (2003).

The reactor model was formulated assuming steady-state operation. Isothermal & isobaric reaction conditions were assumed. Furthermore, it was assumed that the permeation of hydrogen through the Pd membrane follows Sievert's law, no boundary layer on membrane surfaces and plug flow on both reaction and permeation sides.

The reactions considered in this model are the reforming reaction 3.4, the water-gas shift reaction 3.5 and the overall reaction 3.6.

$$CH_4 + H_2O \rightleftharpoons CO + 3H_2 \quad \Delta H^{\circ}_{298K} = 206\ kJ/mol \tag{3.4}$$

$$CO + H_2O \rightleftharpoons CO_2 + H_2 \quad \Delta H^{\circ}_{298K} = -41\ kJ/mol \tag{3.5}$$

$$CH_4 + 2H_2O \rightleftharpoons CO_2 + 4H_2 \quad \Delta H^{\circ}_{298K} = 165\ kJ/mol \tag{3.6}$$

The rate expressions for reactions 3.4-3.5 are given below, the unit of each reaction rate is expressed in $kmol/kg_{cat}h$ and the unit of partial pressure p_i is atm.

$$r_1 = \frac{k_1}{p_{H_2}^{2.5}} \frac{p_{CH_4}\, p_{H_2O} - (p_{H_2}^3\, p_{CO}/\, K_{eq1})}{DEN^2} \tag{3.7}$$

$$r_2 = \frac{k_2}{p_{H_2}} \frac{p_{CO}\, p_{H_2O} - (p_{H_2}\, p_{CO_2}/K_{eq2})}{DEN^2} \tag{3.8}$$

$$r_3 = \frac{k_3}{p_{H_2}^{3.5}} \frac{p_{CH_4}\, p_{H_2O}^2 - (p_{H_2}^4\, p_{CO_2}/K_{eq3})}{DEN^2} \tag{3.9}$$

where the adsorption term (DEN):

$$DEN = 1 + K_{adsCO}\, p_{CO} + K_{adsH_2}\, p_{H_2} + K_{adsCH_4}\, p_{CH_4} + \frac{K_{adsH_2O}\, p_{H_2O}}{p_{H_2}} \tag{3.10}$$

the rate constants (k_1, k_2, k_3) , adsorption coefficients ($K_{adsCO}, K_{adsH_2}, K_{adsCH_4}, K_{adsH_2O}$) and equilibrium constants ($K_{eq1}, K_{eq2}, K_{eq3}$) are calculated as follows:

$$\begin{aligned} k_1 &= 4.2248E15\ \ exp\left(\frac{-240100}{8.314\ \ T}\right) \quad kmol\ atm^{0.5}/kg_{cat}\ h \\ k_2 &= 1.9558E6\ \ exp\left(\frac{-67130}{8.314\ \ T}\right) \quad kmol\ /kg_{cat}\ h\ atm \\ k_3 &= 1.0202E15\ \ exp\left(\frac{-243900}{8.314\ \ T}\right) \quad kmol\ atm^{0.5}/kg_{cat}\ h \end{aligned} \tag{3.11}$$

$$\begin{aligned} K_{adsCO} &= 8.23E-5\ exp\left(\frac{70650}{8.314\ \ T}\right) \quad 1/atm \\ K_{adsH_2} &= 6.12E-9\ exp\left(\frac{82900}{8.314\ \ T}\right) \quad 1/atm \\ K_{adsCH_4} &= 6.65E-4\ exp\left(\frac{38280}{8.314\ \ T}\right) \quad 1/atm \\ K_{adsH_2O} &= 1.77E4\ exp\left(\frac{-88680}{8.314\ \ T}\right) \quad 1/atm \end{aligned} \tag{3.12}$$

$$\begin{aligned} K_{eq1} &= 7.846E12\ exp\left(\frac{-220200}{8.314\ \ T}\right) \quad atm^2 \\ K_{eq2} &= 1.412E-2\ exp\left(\frac{37720}{8.314\ \ T}\right) \\ K_{eq3} &= 1.11E11\ exp\left(\frac{-182400}{8.314\ \ T}\right) \quad atm^2 \end{aligned} \tag{3.13}$$

with the partial pressure of each component as:

$$p_i = y_i \, P \tag{3.14}$$

where, y_i is the mole fraction of the component and P is the total pressure.

The component transformation rates are given as, in $kmol/h\ kg_{cat}$:

$$\begin{aligned} \frac{dX_{CH_4}}{dz} &= -r_1 - r_3 \\ \frac{dX_{CO_2}}{dz} &= r_2 + r_3 \\ \frac{dX_{CO}}{dz} &= r_1 - r_2 \\ \frac{dX_{H_2O}}{dz} &= -r_1 - r_2 - 2r_3 \\ \frac{dX_{H_2}}{dz} &= 3r_1 + r_2 + 4r_3 \end{aligned} \tag{3.15}$$

Furthermore, the permeation rate (also known as flux) of hydrogen through palladium membrane is to be calculated. It is expressed as $J_{H_{2,mem}}$. The permeation rate is determined as follows:

$$J_{H_{2,mem}} = K_{p,H_2} \, DF_{H_2} \quad kmol/m^2 s \tag{3.16}$$

where, K_{p,H_2} is the permeance value in $kmol/m^2 s Pa^{0.5}$ and DF_{H_2} is the driving force given as:

$$DF_{H_2} = {p_{H_{2,ret}}}^{0.5} - {p_{H_{2,perm}}}^{0.5} \quad Pa^{0.5} \tag{3.17}$$

where $p_{H_{2,ret}}$, $p_{H_{2,perm}}$ are the partial pressures of H_2 in the retentate and permeate respectively and $n = 0.5$ because it is assumed that bulk diffusion is the rate limiting step as already stated.

In the rate equations 3.7 – 3.9, the partial pressure of H_2 (p_{H_2}) is an important parameter. If the feed-stock to the membrane reactor is hydrogen free i.e. $m^0_{H_2} = 0$, the initial rate of reaction will be infinite because the inlet hydrogen partial pressure is zero. This problem can be solved by having a pre-reformer that converts a small amount of the feed-stock to hydrogen, resulting in sufficient partial pressure of hydrogen at the inlet of the membrane reactor.

3.2.5. Modelling assumptions

The modelling assumptions used to develop the Aspen Plus model for the entire process and also assumptions of the two membrane models used are mentioned in this section.

General process assumptions

The process model is an Aspen model including the reforming unit, dehydration unit, carbon capture unit, feed and products, the utilities required integrated to represent the process design of the novel system. The general unit modelling assumptions for each section to develop the novel process are summarized in table 3.3. The stream modelling assumptions are already mentioned in table 3.1. Furthermore, the modelling assumptions of the two models used in this work are described in the following sections.

Table 3.3: Modelling assumptions used in Aspen Plus simulation[a]

General	
Heat exchanger	Δ p/p = 2% or 0.5 bar Minimum Δ T = 15 °C (gas-liquid) or 30 °C (gas-gas)[b]

Table 3.3 continued from previous page

Biogas compressor	Multi-stage compressor with inter-cooling Outlet temperature doesn't exceed 150 °C [c] Maximum compression ratio = 3 [d] Polytropic efficiency = 0.84 [e] Mechanical efficiency = 0.98
Hydrogen compressor	Multi-stage compressor with inter-cooling Outlet temperature doesn't exceed 135 °C [f] Maximum compression ratio is 2 [g] Outlet pressure is 700 bar[h] Isentropic efficiency = 0.78[i] Mechanical efficiency = 0.98
CO_2 and water pump	Centrifugal pump Efficiency = 0.9
Knock-out drum	Flash drum Q_H = 0 W
Hydrogen dehydration unit	Separator block 99.98 % water removal to 5 µm H_20/ mol H_2 [j] Contaminants removed as per table 3.1. H_2 product loss = 5% Regeneration assumptions (table 3.4).
Reforming	
Pre-reformer	Gibbs free energy minimization reactor Reactor temperature = 600 °C Excess of highly active Ni-based catalyst
Membrane reactor	Aspen Plus Point Model, refer 3.2.5.2 ACM Model, refer 3.2.5.3
Furnace	Gibbs free energy minimization reactor Fuel = Recycle stream and/or biogas Excess air for 100% conversion
Carbon capture	
Compressor	Polytropic efficiency = 0.84 Mechanical efficiency = 0.98
Cooler[k]	Heat exchanger Temperature = -35 to -50 °C
Distillation unit	Short-cut distillation design Partial condenser with all vapour distillate

[a] SRK equation of state is used for the thermodynamic properties.
[b],[c],[d],[e],[i] Sjardin et al. (2006).
[f] According to guidelines of the American Petroleum institute, stated in Sjardin et al. (2006).
[g] According to guidelines of the American Petroleum institute, stated in Sjardin et al. (2006). The low compression ratio per stage reduces the hydrogen discharge temperature and increases the piston ring lifetime.
[h] Fuelling pressure for light weight FCVs (U.S. Department of Energy, 2016).
[j] Maximum allowable limit for PEM fuel cells in road vehicles (Ohi et al., 2016).
[k] The heat is removed by a refrigeration unit with a COP of 1.5 (Luyben, 2017).

Table 3.4: Regeneration modelling assumptions.

Process assumptions	Unit	
Regeneration temperature[a]	°C	250
Hot (purge) gas		N_2
Regeneration flow rate	m^3/min	1/5 of feed flow rate
Hydrogen loss	%	5
Molecular sieves cycle life		1000
Adsorption/regeneration cycle time	hours	16
Water adsorption[a]	wt %	15

[a] The water adsorption capacity of the molecular sieves assumed in this study is a lower value of 15 wt % after taking into account performance loss over the years.

Membrane reactor Aspen Plus Point model
The Aspen Plus point model consists of an RGIbbs block which acts as the pre-reformer. The pre-reformer is followed by a series of reactor and separator blocks integrated together to model the membrane reactor.
The model is formulated assuming:

1. 0-D reactor model.
2. No kinetics.
3. No permeance. Area calculated manually with an assumed permeance value of $6.67E-4$ mol/$m^2 sPa^{0.5}$ (Chompupun et al., 2018).
4. Fixed driving force with fixed membrane split fraction i.e. the permeate stream consists of a fixed fraction of hydrogen generated in the reactor.
5. 100% hydrogen perm-selectivity.
6. Counter current sweep configuration.
7. Steady-state operation.
8. SRK equation of state.
9. Reactor temperature of 600 °C.

Membrane reactor ACM model
The kinetic equations and the basis of the membrane reactor was described in the previous section. In this section, specific modelling assumptions for this work are listed.
The reactor model is formulated assuming:

- 1-D reactor model.
- Packed-bed with tube-in-tube configuration.
- Counter current sweep configuration.
- Steady-state operation.
- SRK equation of state.
- Isothermal & isobaric reaction conditions.
- Driving force is calculated.
- Permeation through Pd membrane follows Sievert's law (refer 2.11).
- Limiting step is the permeation through the membrane (Sjardin et al., 2006).

- An excess of highly active Ni-based catalyst is used to guarantee equilibrium is reached (Sjardin et al., 2006).
- No boundary layer on membrane surfaces.
- Plug flow on both reaction and permeation sides.
- Kinetics from Lin et al. (2003).
- Permeance value of $6.67E-4$ mol/$m^2sPa^{0.5}$ at 600 °C.
- Reactor temperature of 600 °C.
- Perm-selectivity [2] for hydrogen is 1000.

The permeance was measured with a reactor as follows:
An annular cylindrical packed-bed membrane reactor with Pd-coated membrane of 40 µm thickness. The highest permeance value for this membrane was found to be $6.67E-4$ mol/$m^2sPa^{0.5}$ at 600 °C by Chompupun et al. (2018) and is adopted in this work.

3.2.6. Configurations generated

Three process configurations are generated on the basis of the basic process previously described. The aspen models for all three are shown in Appendix A.

In all the three configurations, biogas is compressed to the desired pressure of the unit. In the first configuration, figure 3.6, the compressed biogas is fed into a carbon capture unit directly. Biogas has a high content of CO_2, which reduces the partial pressure of hydrogen and therefore the driving force for permeation, reducing the productivity. Pre-CO_2 separation is interesting because separation of CO_2 from biogas before entering into the reformer will reduce these effects leading to a better performance of the reactor. After most of the CO_2 is removed in the carbon capture unit, the remaining gas containing majorly CH_4 is heated and fed into the membrane enhanced reforming section. In configuration 2 & 3, figure 3.7 and 3.8, the compressed biogas is heated and fed directly to the membrane enhanced reforming section and then CO_2 is separated from the outlet retentate stream. In all the configurations, before entering the membrane reactor, the biogas is pre-reformed. Then the membrane reformer converts most of the feed into hydrogen. Hydrogen permeated through the membrane is cooled and purified to the desired specifications, compressed to 700 bar and stored.

The cryogenic carbon capture unit has stages of compression, cooling and separation, similar in all the configurations with the same operating conditions so that the configurations are comparable. In configuration 1 & 3 however, the CO_2 obtained after the compression stages isn't pure enough and a distillation column is required. The pure CO_2 obtained in all the three configurations is compressed to 110 bar to be transported through pipelines. In configuration 1, the retentate stream is cooled to remove water and then recycled back into the carbon capture unit. The retentate stream contains the produced CO_2 that can potentially be captured and also contains unreacted reactants that can be re-used to increase the efficiency. The heat input required for reforming is obtained by burning additional biogas. In configuration 2, the off-gas from the carbon capture unit isn't recycled but burnt to provide heat for reforming. Additional heat, if required, is obtained by burning biogas. Similar to configuration 1, the off-gas is recycled back in configuration 3 to increase the efficiency and biogas is burnt to provide heat for the reforming reaction. It is important to note that it isn't viable to capture the CO_2 produced from the furnace because it contains very low concentrations of CO_2 (around 15%).

[2] If 1000 kmol/h of hydrogen passes through the membrane, a total of 1 kmol/h impurities (CH_4, CO_2, CO, N_2) will pass through too. In most research work, a 100% selectivity is assumed but a more realistic case is chosen for this study.

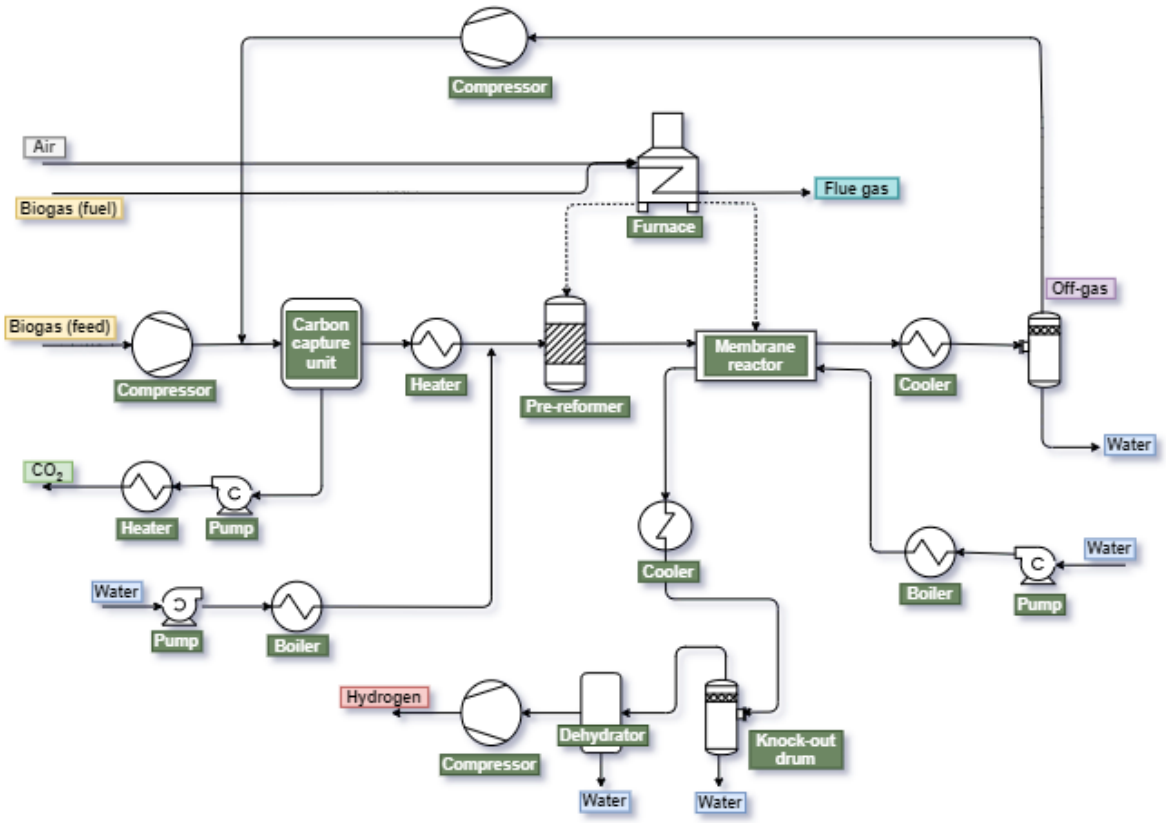

Figure 3.6: Process block diagram (PBD) of Configuration 1: Carbon capture unit before the reforming section.

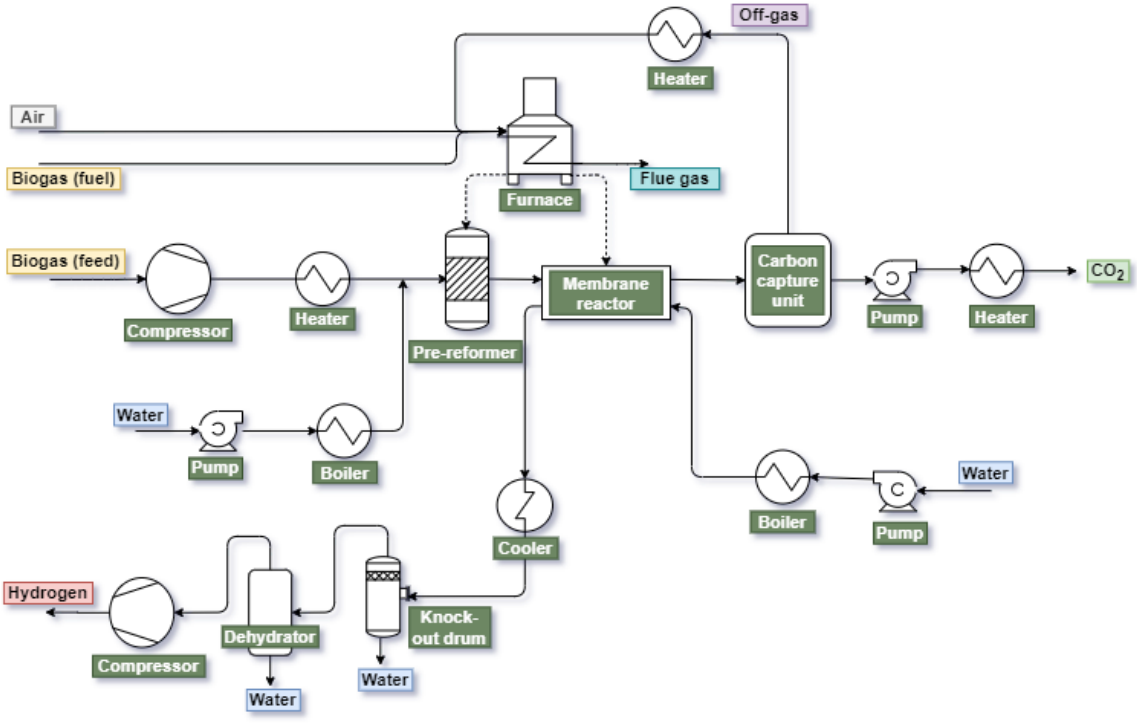

Figure 3.7: Process block diagram of Configuration 2: Carbon capture unit after the reforming section without recycle stream.

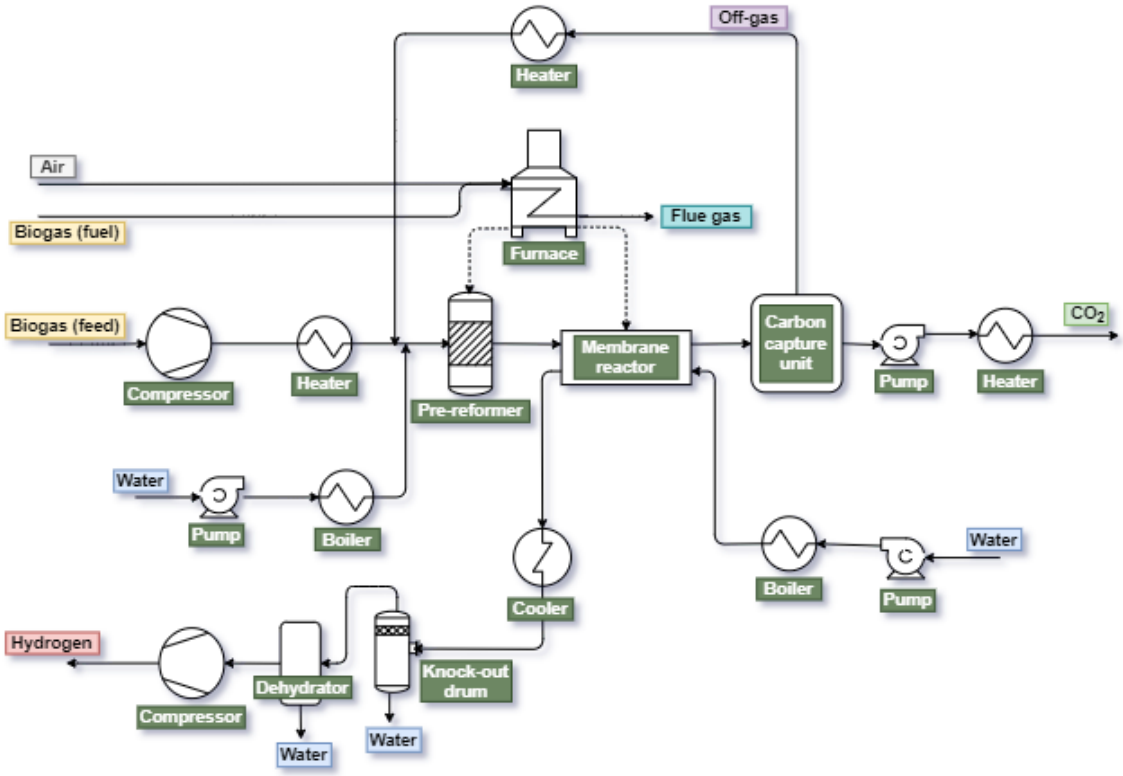

Figure 3.8: Process block diagram of Configuration 3: Carbon capture unit after the reforming section with recycle stream.

Table 3.5: Comparison of the three configurations

Advantages	**Disadvantages**
	Configuration 1
Lower membrane area for the same conversion, hence lower costs.	Lower CO_2 concentration for the carbon capture unit, hence difficult separation. Distillation column required.
Lower chance of coke formation in reactor.	External heat required for reformer.
	More combustion gases released in the air.
	Configuration 2
Energy from off-gas used for reformer. Low/no additional biogas needed.	Dry reforming reactions may take place because of the high concentration of CO_2 in feed, higher steam-to-carbon ratio required.
Lesser combustion gases released in the atmosphere.	Higher membrane area required for same conversion, hence higher costs.
Better separation as high concentration of CO_2 in the feed to the capture unit.	
	Configuration 3
Lower membrane area required, hence less costs.	Dry reforming reactions may take place.
Better separation as high concentration of CO_2 in the feed to the capture unit.	External heat required for reformer.
	More combustion gases released in the air.
	Distillation column required for CO_2 purification.

Table 3.6: Differences between the novel and the reference process across value chain

	Novel process	Reference process
System	Decentralized	Centralized
Feed	Biogas	Natural gas
Feed purification	No (outsourced)	Yes
Reforming	MR	SMR
Carbon capture	Cryogenic	No
Hydrogen purification	Small-scale dehydration unit	Large-scale PSA unit
Hydrogen product purity	99.99% (fuel-grade)	99.95 % (industrial-grade)
Hydrogen compression	700 bar	830 bar
Hydrogen storage	Yes, at the refuelling station	Centralized, before boost compression and transport
Hydrogen transport	No	Yes
CO2 transport	No (outsourced)	-

Table 3.5 summarises the expected advantages and disadvantages of the three configurations. All three configuration have pros and cons and determining the best performing configuration at this stage is unworkable. Therefore, a detailed evaluation of these configurations is done in the next chapter. The aim is to assess the different configurations on their thermodynamic performance in order to determine the most promising one. Then, the chosen process will be optimized taking into account the economic performances. The extent & influence of coke formation in the three configurations isn't researched on in this work and is left for later study.

Furthermore, as the novel process's performance will be compared to the conventional steam reforming of natural gas, it is important to explicitly mention the differences between the two processes for a reasonable comparison. The major differences between the two cases to be compared are mentioned in table 3.6.

3.3. Key performance indicators definition

The key performance indicators used in the work for performance evaluation at different stages are defined below. The KPIs relevant for the evaluation method will be mention in the related chapters.

Thermodynamic performance indicators:

1. Hydrogen recovery factor, %

$$Global\ HRF = \frac{\dot{n}_{H_2-out}}{4\,\dot{n}_{CH_4-feed} + \dot{n}_{H_2-feed} + \dot{n}_{CO-feed}} * 100 \tag{3.18}$$

$$Per-pass\ HRF = \frac{\dot{n}_{H_2-perm}}{4\,\dot{n}_{CH_4-in} + \dot{n}_{H_2-in} + \dot{n}_{CO-in}} * 100 \tag{3.19}$$

2. Methane conversion, %

$$Global\ methane\ conversion = \frac{\dot{n}_{CH_4-feed} - \dot{n}_{CH_4-out}}{\dot{n}_{CH_4-feed}} * 100 \tag{3.20}$$

$$Per-pass\ methane\ conversion = \frac{\dot{n}_{CH_4-in} - \dot{n}_{CH_4-ret}}{\dot{n}_{CH_4-in}} * 100 \tag{3.21}$$

3. CO2 capture rate, %

$$Carbon\ capture\ rate = \frac{\dot{n}_{CO_2-out}}{\dot{n}_{CO_2-feed} + \dot{n}_{CH_4-feed} + \dot{n}_{CO_2-fuel} + \dot{n}_{CH_4-fuel}} * 100 \tag{3.22}$$

4. Global energy efficiency, %

$$\eta_{energy} = \frac{LHV_{H_2}\ \dot{m}_{H_{2-out}}}{LHV_{feed}\ \dot{m}_{feed}\ +\ W} * 100 \tag{3.23}$$

5. Global exergy efficiency, %

$$\eta_{exergy} = \frac{\dot{m}_{H_2}\ \dot{E}_{H_2}}{\dot{E}_{in}} * 100 \tag{3.24}$$

6. Productivity, $kg/m^2\ day$

$$Productivity = \frac{\dot{m}_{H_{2-out}}}{A_{mem}} \tag{3.25}$$

Economic performance indicators:

1. Levelized cost of hydrogen (LCOH), €/ kg H_2

$$LCOH = \frac{(CAPEX * \alpha) +\ c_{OM,f}\ +\ (c_{OM,var} * hours)}{\dot{m}_{H_2}} \tag{3.26}$$

where,
$\alpha = \frac{d}{1-1/(1+d)^n}$ where, $d = rr + i + rr\ i$ (d = after tax rate of return, rr = after tax real rate of return, i = inflation, n = lifetime).

2. CO_2 avoidance cost (CAC), €/ton CO_2

$$CAC = \frac{LCOH_c - LCOH_b}{CO_2 emissions_b - CO_2 emissions_c} \tag{3.27}$$

3.4. Key takeaways

The production capacity of the reference case is 1.5 million Nm^3/day of hydrogen whereas the value chain of the case from natural gas to hydrogen transport is 500 Nm^3/h. The production capacity of the novel case is the same as the value chain capacity of the reference case. The value chain of the novel case is from pre-treated biogas input to hydrogen compression & storage and CO_2 compression, ready to be transported via pipelines (outsourced).

Design assumptions for the novel case are:

1. Capacity: 500 $Nm^3/h\ H_2$.
2. Feed and product specifications: Refer 3.1.
3. Location: The Netherlands.
4. Required utilities: Cooling water, electricity, refrigerant.
5. Membrane reactor configuration: Packed-bed continuous plug flow reactor assuming tube-in-tube configuration. Counter-current flow with H_2O as the sweep agent for membrane reactor.
6. Molecular sieves dehydration unit with TSA regeneration used for hydrogen purification.

Modelling assumptions for the novel case are:

1. The modelling assumptions for developing the entire process in Aspen Plus are shown in table 3.3
2. Two models for the membrane reactor are used. A basic model is developed for initial results, refer 3.2.5.2, and refined results are achieved with a more detailed model developed in Aspen Custom Modeler, refer 3.2.5.3.

With the following assumptions, three process configurations for the novel case are developed. Configuration 1: process with carbon capture unit before the reforming section, configuration 2: process with carbon capture unit after the reforming section without recycle stream and configuration 3: process with carbon capture unit after the reforming section with recycle stream. The expected advantages and disadvantages of the three configurations are summarized in table 3.5. The important differences between the reference case and the novel case are mentioned in table 3.6.

Key performance indicators are defined to evaluate the performance of the configurations developed and select the most promising one, refer 3.3. The KPIs will also be used to evaluate the performance of the (local) optimum process and for comparison with the reference case.

4

Process design & optimization

In this chapter, the performance of the three configurations developed is determined and compared with each other. Firstly, the relevant variables are defined and a number of cases are formulated. The sensitivity of the manipulated variables to the output variables for each of the three configurations is analyzed and presented in Appendix B. Later, one of the three configurations is selected based on comparison of the output variables for the Base case formulated. Finally, the selected configuration's process flow is optimized and heat integration is performed to improve the performance of the process.

4.1. Method for process configuration selection

The process parameters for the base case and the other cases are mentioned in table 4.1. The list below shows the values that are used for the fixed & manipulated variables in the simulation to select the process configuration. The controlled (output) variables are the thermodynamic performance indicators mentioned in chapter 3, section 3.3 (except exergy efficiency). The KPI values obtained are compared case wise for the three configuration defined in chapter 3, section 3.2.6.

1. Fixed variables (assumptions)
   (a) Hydrogen output at 500 Nm^3/h.
   (b) Reforming temperature at 600 °C.
   (c) Reforming pressure at 30 bar .
   (d) Steam-to-carbon ratio of 3.
   (e) Carbon capture temperature, -50 °C.
   (f) Carbon capture pressure, 38 bar.
   (g) Feed composition, refer table 3.1.
   (h) Sweep composition, refer table 3.1.
2. Manipulated (input) variables
   (a) Sweep ratio - 0.1 to 4.
   (b) Permeate pressure - 1.1 to 7 bar.
   (c) Biogas feed - 9.75 to 10.5 kmol/h.
   As the BG feed is changed, the area also changes and from these values the load-to-surface ratio can be found, figure 4.1.
   (d) Recycle ratio - 0.5 & 0.9.

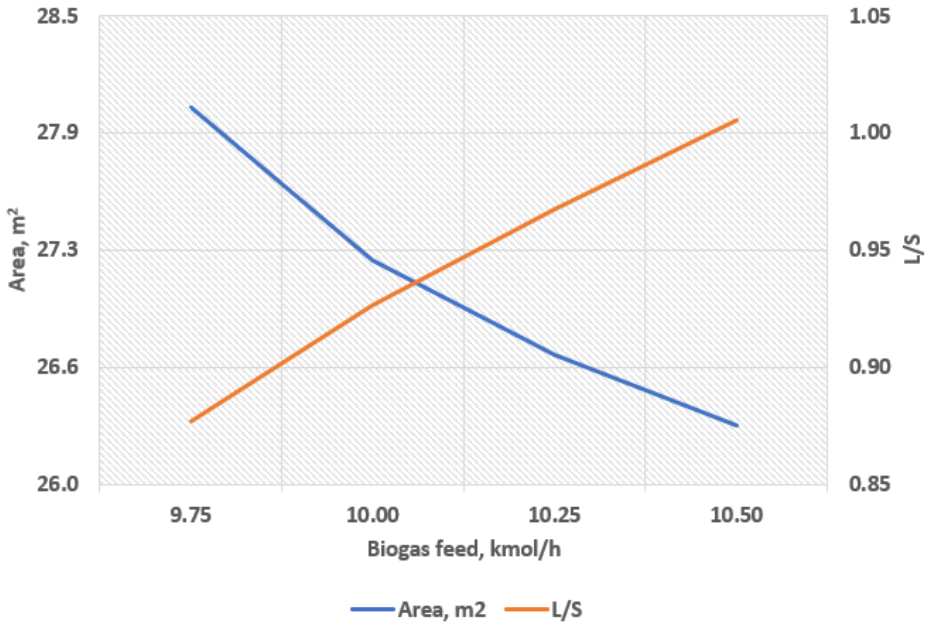

Figure 4.1: L/S & area vs biogas feed.

Table 4.1: Process parameters for different cases formulated.

	Permeate pressure (bar)	Sweep ratio	Recycle ratio
Base case	1.1	1	0.9
Case 2.1	1.1	0.1	0.9
Case 2.2	1.1	0.5	0.9
Case 2.3	1.1	4	0.9
Case 3.1	1.1	1	0.5
Case 4.1	3	1	0.9
Case 4.2	5	1	0.9
Case 4.3	7	1	0.9

4.2. Process configuration selection

The sensitivity of the performance indicators towards sweep ratio, recycle ratio & permeate pressure was analysed for each configuration. The results are presented in Appendix B. However, to choose one process out of the three the results of the Base case are compared in this section.

In figure 4.2 we can see that the global hydrogen recovery factor for all the three configurations is the same. This is because the hydrogen output and the biogas feed for all the cases is the same. However, the configuration 1 has a higher productivity than the other two. This implies that, the membrane surface area required for the same hydrogen recovery is lower.

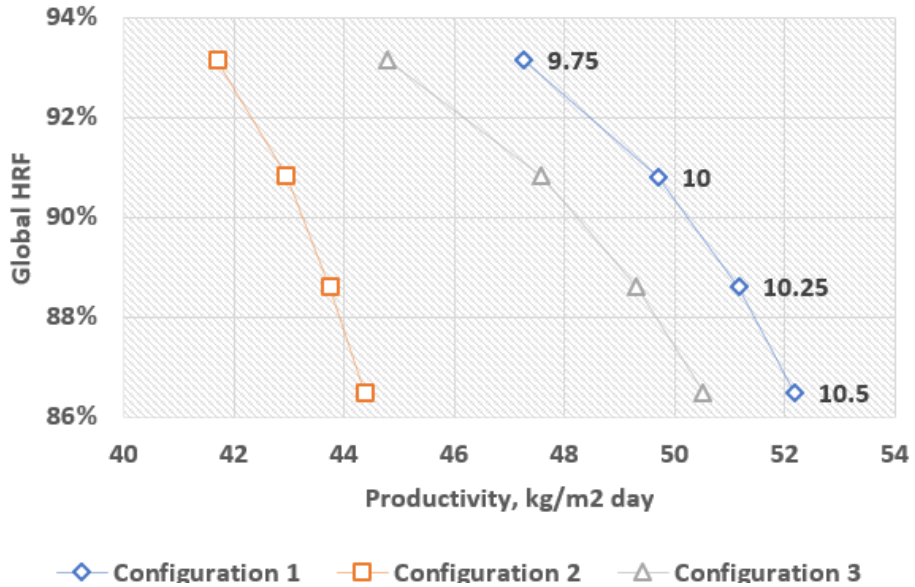

Figure 4.2: Global hydrogen recovery factor for all three configurations varying biogas feed from 9.75 to 10.5 kmol/h.

The carbon capture rate, figure 4.3, for the configuration 2 is the highest compared to the other two. Although, the productivity is lesser (higher membrane surface care required) this configuration is attractive. This is because the operating expenditure is expected to have a larger impact on the cost of hydrogen than the capital expenditure. Furthermore, a higher CO_2 capture rate means a lower carbon footprint.

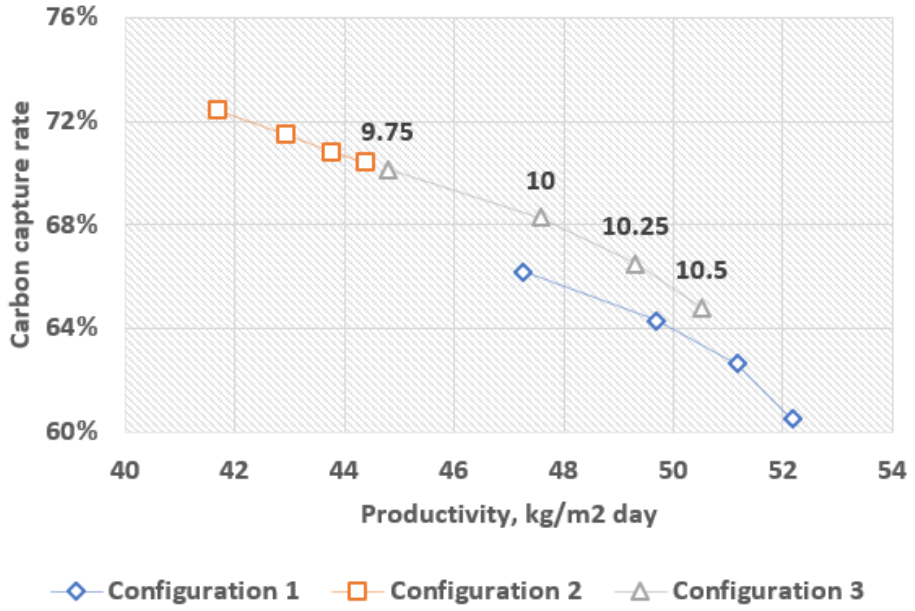

Figure 4.3: Carbon capture rate for all three configurations varying biogas feed from 9.75 to 10.5 kmol/h.

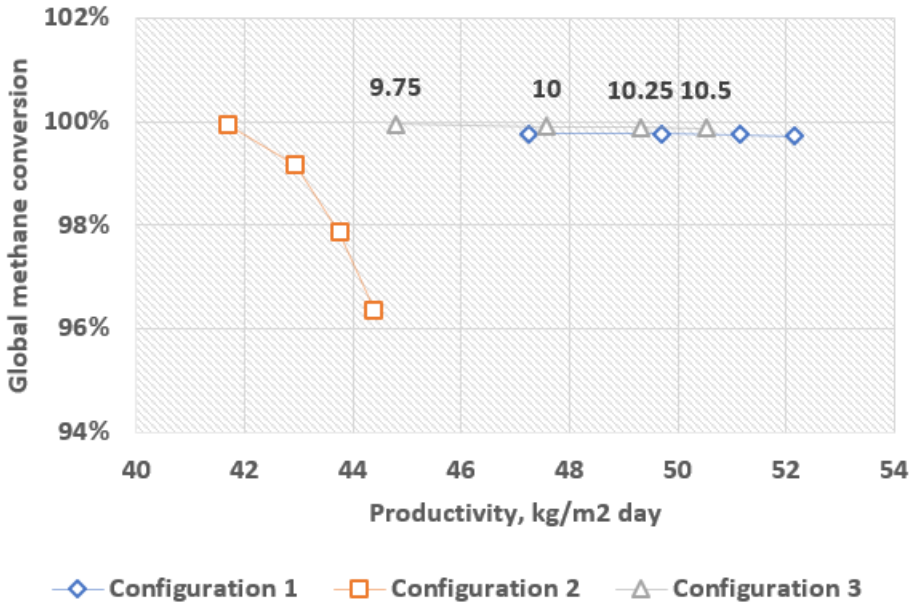

Figure 4.4: Global methane conversion for all three configurations varying biogas feed from 9.75 to 10.5 kmol/h.

The methane conversion values are high for all three configurations, figure 4.4. Configuration 1 & 3 have conversions very close to 100% whereas configuration 2 also has high methane conversions of more than 96%. Furthermore, configuration 1 has the best productivity compared to the other two.

The global efficiency of the configuration 2 is slightly higher than the other two and lesser deviation with changing biogas feed, figure 4.5. However, configuration 2 has a lower productivity.

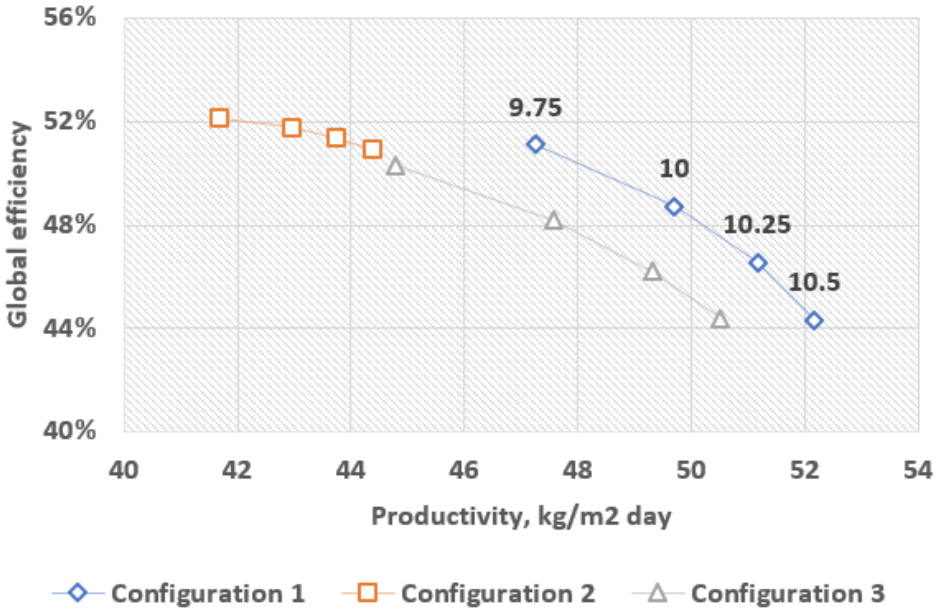

Figure 4.5: Global efficiency for all three configurations varying biogas feed from 9.75 to 10.5 kmol/h.

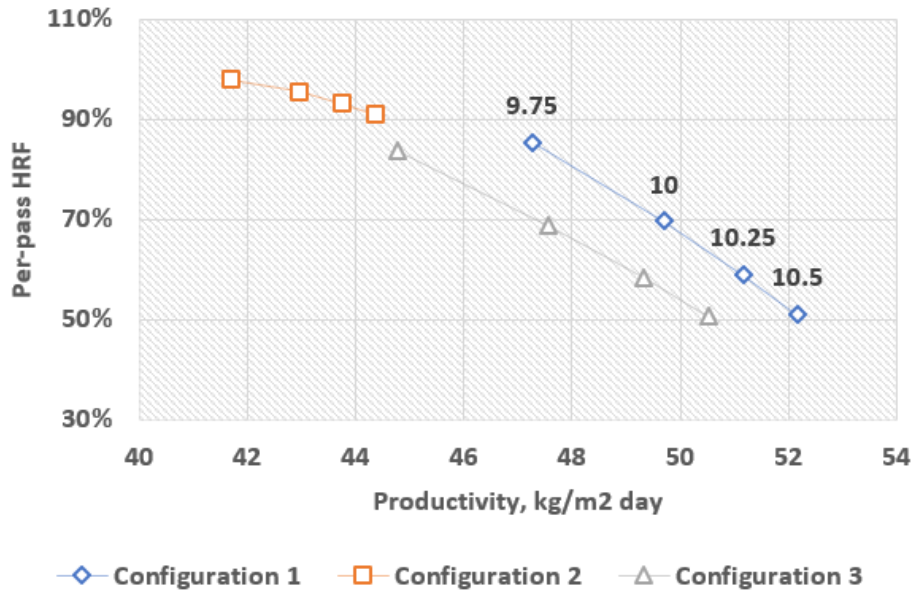

Figure 4.6: Per-pass hydrogen recovery factor for all three configurations varying biogas feed from 9.75 to 10.5 kmol/h.

As seen from figure 4.6, the per-pass HRF for configuration 2 is higher than the global HRF. This is because of the loss of hydrogen during the dehydration stage. The per-pass HRF for the other two configurations is lower than the global HRF. Figure 4.7 presents the per-pass methane conversion of all the three configurations. Furthermore, figure 4.8 shows that the work and heating & cooling duties required for configuration 2 are the lowest because this configuration is a simpler process without recycle streams.

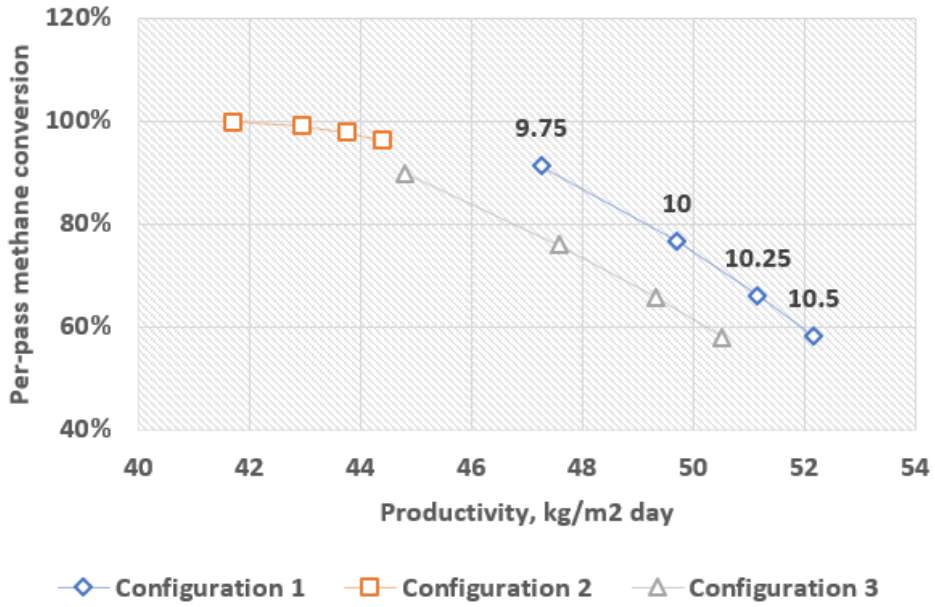

Figure 4.7: Per-pass methane conversion for all three configurations varying biogas feed from 9.75 to 10.5 kmol/h.

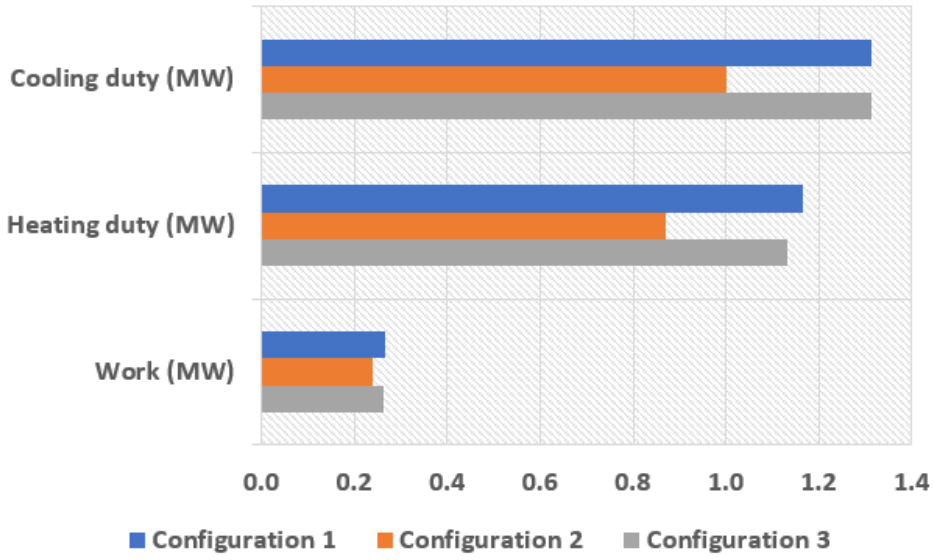

Figure 4.8: Total work & duties of the three different configurations with biogas feed of 10.5 kmol/h.

It is a challenging task to decide which of the three configurations has a better performance as all three perform differently for different performance indications. However, a choice has to be made. Under the assumption that the operating expenditure of the process will have a larger impact on the cost of hydrogen than the capital expenditure and a higher carbon capture rate is required, configuration 2 is chosen: process with carbon capture unit after the reforming section without recycle stream . It is expected that the increase in membrane surface area required will be compensated by the lower work and duties required. Furthermore, without the recycle, the process flow and the plant construction is expected to be simpler.

4.3. Process optimization

For the three configurations to be comparable, the conditions and components used were similar. However, the process design may not be the optimum for the configuration chosen. Some amendments have been made in the carbon capture unit of the process. These changes will be mentioned in this section. Furthermore, after the carbon capture unit has been optimized, heat integration is performed to improve the performance of the process.

4.3.1. Carbon capture optimization

As previously mentioned, the carbon capture unit of all the three configurations was the same except that configuration 1 & 3 has an additional distillation unit to purify the CO_2, whereas the selected configuration didn't need one. The carbon capture process was a 2-staged compression, cooling & separation process for the configuration without recycle: the chosen process. It was found that a single compression and separation stage was sufficient to get the CO_2 purity required for transport and storage. A 2-staged process resulted in a slightly higher recovery & purity of CO_2 but wasn't worth the extra costs.

For the single staged process, the stream is compressed to 38 bar and then cooled to -50 °C which produces liquid, >95% pure CO_2. According to Luyben (2017), a single-staged refrigeration unit is sufficient to remove heat down to -50 °C for our chosen process. An appropriate refrigerant to remove the heat down to -50 °C is to be chosen. The temperature and pressure conditions being -50 °C and 38 bar, R 1270 (propylene) is the preferred option as propylene has a normal boiling point of -53.7 °C and a critical pressure of 45.9 bar. Furthermore, R 1270 is a natural refrigerant, non-toxic with zero ODP (oxygen depletion potential) and very low GWP (global warming potential) therefore negligible impact to the environment (Linde Gas).

Luyben (2017) has designed refrigeration processes at various temperature levels for a refrigeration

load of 1 MW. The paper provides information about the optimum process conditions and the economic results for each process. It also gives guidelines to scale the cost values according to the preferred refrigeration load. The refrigeration cycle shown in figure 4.9 is appropriate for our chosen process and is scaled according to the load requirements. The COP of this particular refrigeration cycle is 1.523 (2.911/1.911) and this value will be used for the next steps of calculations.

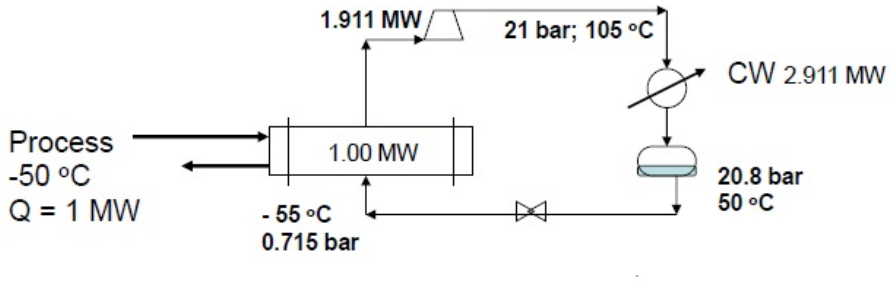

Figure 4.9: Single stage refrigeration cycle using propylene as refrigerant (Luyben, 2017).

4.3.2. Heat integration

The energy requirements of the process can be minimized by heat integration. Pinch analysis is a widely used method to minimize energy consumption and maximize heat recovery of a chemical process. Table 4.2 shows the different streams, their supply and target temperatures and their heat flows. The minimum approach temperature selected is 30 °C which is the maximum heat exchanger Δ T assumed in our model, table 3.3. The values in the table are for the Base case with biogas feed of 10.5 kmol/h.

Table 4.2: Stream information for pinch analysis.

Stream	Stream type	Supply temperature (°C)	Target temperature (°C)	Heat flow (kW)
S1	Cold	30	450	58.0
S2	Cold	15	235.35	110.2
S3	Cold	235.35	235.35	184.7
S4	Cold	235.35	450	47.9
S5	Cold	15	123.53	63.32
S6	Cold	123.53	123.53	277.0
S7	Cold	123.53	600	119.8
S8	Cold	-35	250	5.1
S9	Cold	-35.5	30	18.2
S10	Cold	15	250	8.8
S11	Hot	600	86.62	226.9
S12	Hot	86.62	20	339.3
S13	Hot	600	182.88	96.2
S14	Hot	182.88	20	130.1

The hot pinch and the cold pinch temperature calculated was 71.62 °C and 41.62 °C respectively. The minimum hot utility required was 461.84 kW and the minimum cold utility required was 361.03 kW. The grand composite curve obtained is shown in figure 4.10. The T-Q curves obtained are shown in Appendix C.

Pinch technology is widely used in a lot of industrial processes to minimize energy consumption. Despite the fact, a more practical approach is adopted in this work given the small scale application and limited number of streams of the developed process. Using Aspen Plus, manual heat integration of

streams is performed keeping in mind the objective to reduce energy consumption and avoid unnecessary increase in capital costs (heat exchangers). The minimum hot and cold utility requirements obtained for the Base case with biogas feed flow of 10.5 kmol/h are 493 kW and 392 kW respectively. The hot and cold utility requirements before heat integration for the same process were 893.02 and 792.5 respectively. Therefore, around 400 kW of hot and cold utility is saved, which is 44.8 % of hot utility saved and 50.5 % of cold utility saved from the heat integration. The increase in efficiency after the heat integration is from 50.9 % to 58.73 %.

The results shown are for the base case with biogas feed flow rate of 10.5 kmol/h. With every change in process parameter (different case), the extent of heat integration is expected to vary. For the sensitivity analysis in the next chapter the streams are manually adjusted, whenever required, to optimize the heat integration. For example, the amount of duty required for a stream of water with sweep ratio of 0.1 can be met by a hot outlet stream (permeate for example) but the same hot outlet stream may not be able to provide the duty for a stream of water with a sweep ratio of 4. This change in every case is difficult to document but it is important to keep in mind that the total hot and cold utility required for each case won't necessarily be the same.

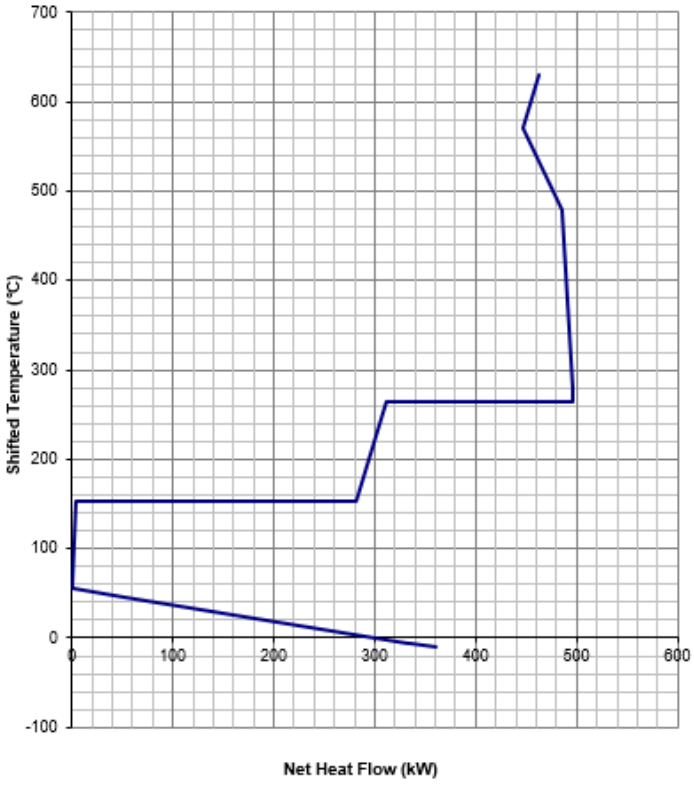

Figure 4.10: Grand composite curve for Base case with biogas feed flow rate of 10.5 kmol/h.

4.4. Conclusion

The global hydrogen recovery factor and the global methane conversion of configuration 2 is comparable to the others. However, the performance w.r.t. the carbon capture rate and global efficiency is better. Furthermore, the work and duty requirements of this configuration are considerably lower than the other two but the productivity is lower. The operating expenditure is expected to have a larger impact on the cost than the capital expenditure. Based on these results, configuration 2 i.e. carbon capture unit after the reforming section without recycle stream is chosen. The carbon capture unit of this configuration is optimized and a single-stage refrigeration unit using R 1270 (propylene) refrigerant is chosen. A realistic approach is chosen for heat integration which increases the energy efficiency of the process by 8% to 58.73%.

5

Techno-economic evaluation

In chapter 4, one configuration was selected based on thermodynamic performances. In Appendix B, the sensitivity of certain process parameters towards the thermodynamic performance indicators was analysed. It is however important to determine the process conditions that result in the optimum performance of the process. The main objective is to achieve the lowest possible levelized cost of hydrogen. Therefore, the optimum process conditions that can result in the lowest LCOH are determined in this chapter. After which, the results of the optimum process are presented and compared with the reference case described in chapter 3.

5.1. Economic factors

Before the sensitivity of variables towards the LCOH can be analyzed and the optimum process conditions determined, the economic factors need to be determined to calculate the LCOH. This section will describe all the cost factors and assumptions made. Referring to equation 3.26, we need to determine the capital expenditure of the plant, the fixed & variable operation and maintenance factors, and investment terms.

5.1.1. General assumptions

General assumptions made to perform the economic calculations are summarized below.

1. The production capacity of the plant is 500 Nm^3H_2/h or 1071 kg/day H_2 .
2. Lifetime of the plant is 20 years with continuous operation of 8760 hours/year. Loss of production time due to equipment failure or other unforeseen events is neglected.
3. The investment cost parameters for the duration are presented in table 5.1
4. Reference year for the cost calculations is 2019.
5. All cost values are converted from dollars to euros with an exchanger rate of \$1 = € 0.91.
6. Plant construction time not taken into account.

Table 5.1: Cost parameters.

After-tax real rate of return	10%
Inflation rate	2%
Annuity factor[a]	13.56%

[a] calculation shown in equation 3.26.

5.1.2. Capital expenditure (CAPEX)

For calculating the total CAPEX of the plant, first we need to determine the total component cost (TCC) of the system. Then, additional factors have to be taken into account like assembly costs, installation costs etc. The cost factors used for this work are explained in this section.

Table 5.2: Capital cost of system components.

Component	Unit	Base scale	Scale factor (R)	Base cost, €	Base year
Compressor[a]	Work (kW)				
Heat exchanger[b]	Area (m^2)				
Boiler[c]	kg H_2O/h	901	0.67	192000	2006
Pump[d]	VFR (m^3/h)				
Pre-reformer[e]	kg H_2/h	4.8	0.7	2616	2002
Membrane reactor[f] **(without membrane tubes)**	kg H_2/h	4.8	0.7	12830	2006
Reactor furnace[g]	kg H_2/h	4.8	0.78	1910	2006
Flash/knock-out drum[h]	kg H_2/h	4.8	0.68	4460	2006
Refrigeration unit[i]	Work (MW)	1	0.6	3.375E+6	2017
Blower[j]	VFR (m^3/h)				
Molecular sieves dehydration unit[k] **(2)**	Volume (m^3)				
Hydrogen cascade storage[l]	kg H_2	140		146510	2014

[a] Centrifugal compressor for biogas and hydrogen. Screw compressor for general. Material assumed is carbon steel (Matches).
[b] Fixed shell and tube, double pipe, water heater depending on the application and area of heat exchanger required (Matches).
[c] The boiler is assumed to be electric. Values from Sjardin et al. (2006).
[d] Positive displacement pump with mechanical seal (Matches).
[e] The cost value is taken from Inc and Francisco (2006) and corrected for material used.
[f],[g],[h] Values from Sjardin et al. (2006).
[i] The total capital costs of the refrigeration unit are taken from Luyben (2017).
[j] Carbon steel axial blower (Matches).
[k] AISI 316L column with a H/D between $0.7 - 3$ (DACE Price Booklet).
[l] Storage size roughly 10 % of daily production to meet the varied hydrogen demand profile (Katikaneni et al., 2014).

The material of construction for the components is SS 316 unless specified otherwise. The membrane reformer is assumed to be a basic reactor resembling the SMR, but since operating conditions are lower less expensive material can be used. The steam methane reformer requires high quality steel alloys like Haynes 556, whereas the membrane reactor can suffice with stainless steel 304 or 316 because of less stringent operating conditions (cost a factor 10 less (Sjardin et al., 2006)). The membrane tubes are an additional cost factor and they need to be replaced within fixed intervals of time. Furthermore, the cost value for the pre-reformer was taken from a SMR plant's economic evaluation. However, the cost is corrected for the material used as the SMR plant assumes Haynes 556 & Incoloy 800H but in our case SS 316 is sufficient (factor of 10 lesser).

The sizing of the molecular sieves unit is done taking into consideration the amount of water & impurities needed to be removed and the adsorption properties of the molecular sieves. The volume of the column is assumed to be 1.5 times the volume of molecular sieves required. Furthermore, the cost of mixer(s) is assumed to be negligible and not accounted for in the total cost of components.

The component cost figures are obtained from literature, websites etc. as mentioned in table 5.2. Some values obtained from literature are for a specific scale. They need to be scaled to the required capacities of the developed system. It is a common practice in engineering economics to use the following scaling equation to calculate the cost at other capacities:

$$c_{new} = c_{known}\left(\frac{Scale_{new}}{Scale_{known}}\right)^{R} \tag{5.1}$$

Table 5.3: Relevant CPECI values for this work.

Year	CEPCI
2002	395.6
2006	499.6
2014	579.8
2017	567.5
2019	603

Values taken from Scribd.

Furthermore, the capital cost values obtained are seldom for the same year, as can be seen in table 5.2. Therefore, the costs need to be calculated for the reference year. This calculation is done using the chemical engineering plant cost index (CEPCI). The CEPCI for relevant years is given in table 5.3 and the cost values of components in year 2019 is calculated as follows (Gas processing and LNG, 2018):

$$c = c_o(\frac{CEPCI}{CEPCI_o}) \tag{5.2}$$

where c is the current cost (€), c_o is base cost (€), CEPCI is the current index & $CEPCI_o$ is the base index.

After the total component cost (TCC) is calculated for the relevant capacity and year (Free on Board cost), additional cost factors need to be taken into account. For example total investment expenditure at the refuelling station, system assembly costs at the production plant & installation costs at the refuelling station need to be determined. Table 5.4 lists the factors taken into consideration and their fractions (Sjardin et al., 2006).

Table 5.4: Installation factors.

Instrumentation & control	13% TCC
Structural support	5% TCC
Assembly	5% TCC
Piping	2% TCC
Total system assembly	25% TCC
Total plant cost (TPC)	**1.25 TCC**
Site preparation	0.5% TPC
Assembly on-site	10% TPC
Tax, insurance and freight	2% TPC
Engineering	5% TPC
Contingency	10% TPC
Fees, overhead and profit	10% TPC
Start-up cost	5% TPC
Total installation	42.5% TPC
Total CAPEX	**1.425 TPC**

5.1.3. Operational expenditure

The OPEX is another factor needed to calculate the LCOH. The OPEX comprises of costs of raw materials, utilities, O&M etc. These costs and assumptions are mentioned in table 5.5.

Determining the membrane tube cost is complicated, not enough cost estimates are available. The costs depend on the membrane surface area, raw material prices, production cost etc. One of the leading manufacturers of palladium membrane tubes have stated that the raw material consists of around 40% of the production cost and the rest is tube manufacturing. The exact cost also depends on the type of support: ceramic, porous metallic support. The latter is more expensive but has advantage of simple connections & noticeable cracks (Sjardin et al., 2006). Furthermore, another author

estimated that the membrane costs could go down to 1500-2000 €/m^2 by 2020 for thin Pd-membranes on ceramic support with a high permeance value (Marcello De Falco). For this work, a value of 2500 €/m^2 is assumed and the economic feasibility of the process, if this value is achieved, is determined.

The costs to replace the catalyst and the membrane tubes also needs to be determined. The lifetime of the catalyst is assumed to be 5 years, i.e. it needs to be replaced 3 times during the lifetime of the plant (Di Marcoberardino et al., 2018). The lifetime of the membrane is an uncertain factor. Sjardin et al. (2006) assumes a lifetime of 3 years which is adopted in this work as well. The membrane tubes have to be replaced 6 times during the lifetime of the plant. Recycling of materials of the membrane isn't considered. The total membrane replacement cost and the catalyst cost is calculated and divided evenly across the lifetime of the plant.

For a well-designed, properly used molecular sieves desorption unit the cycle life is estimated around 24,000 to 40,000 hours (Yuanying Industry Limited, 2015). The adsorption and desorption cycle time considered in this work is 16 hours resulting in 1500 minimum cycles life before recycle. However, a conservative & realistic value of 1000 cycles is taken for this work.

Table 5.5: Operational expenditure factors.

Operational expenditure	Values
Annual load	97%
O&M[a]	4% Total CAPEX
Property taxes[b]	2% Total CAPEX
Insurance[c]	1.5% Total CAPEX
Biogas price[d]	3.46 €/GJ
Electricity price[e]	0.105 €/kWh
Water price[f]	0.35 €/m^3
Deionized water for process[g]	0.91 €/m^3
Refrigeration unit[h]	1.013E+6 €/year (1 MW)
Replacements	
Membranes[i]	2500 €/m^2
Catalyst[j]	1012.83 €/kg
Molecular sieves[k]	2.1 €/kg

[a], [b], [c] Values taken from Sjardin et al. (2006).
[d] Cost of biogas from an anaerobic digester (Di Marcoberardino et al., 2018).
[e] Average electricity cost from DACE Price Booklet.
[f] Value taken from Di Marcoberardino et al. (2018).
[g] Value taken from Mohamad Fahrurrazi Tompang.
[h] the energy costs are taken from Luyben (2017) and scaled linearly according to the load requirement for this work as suggested in the paper.
[i] comparatively higher value than predicted by Marcello De Falco, hence expected to be more realistic and achievable.
[j] Value taken from Sjardin et al. (2006).
[k] Value taken from Alibaba.

It is assumed that besides nominal maintenance tasks, the system can operate unattended and therefore labour costs are omitted. The cost of air required for combustion in the furnace and the nitrogen gas required for regeneration of molecular sieves is assumed to be negligible. The cost influence of the refrigerant required for the refrigeration unit on its total operating cost is also negligible and therefore neglected.

Having all the cost values, the LCOH can be calculated from equation 3.26. Furthermore, the cost is split into two parts: the cost for the reforming section and the cost for the carbon capture unit. The independent influence of process parameters on the two sections can therefore be studied.

5.2. LCOH optimization

First, the relevant variables for the analysis are defined and a finite list of cases to be analyzed are formulated. Next, the results of the formulated cases are presented.

5.2.1. Method for LCOH optimization

The fixed variables are the same as defined in chapter 4, section 4.1 except the reactor pressure, which is a manipulated variable in this analysis. It is expected that a change in the reactor pressure will significantly affect the compression load in the carbon capture unit, and hence the costs. Therefore, the reactor pressure is changed as an attempt to optimize the carbon capture unit. The range of the manipulated variables is shown in figure 5.6. The controlled variables are the thermodynamic and economic performance indicators defined in chapter 3, section 3.3 (except exergy efficiency). The formulated cases for the LCOH optimization are shown in table 5.7.

Table 5.6: Manipulated variables range.

Process condition	Investigated range
Biogas feed (kmol/h)	9.75 to 10.5
Sweep ratio	0.1 to 4
Permeate pressure (bar)	1.1 to 7
Reactor pressure (bar)	20 to 35

Table 5.7: Different cases analysed.

	Biogas feed (kmol/h)	Sweep ratio	Permeate pressure (bar)	Reactor pressure (bar)
Base case	10.75	1	1.1	30
Case 1.1	10.25	1	1.1	30
Case 1.2	10	1	1.1	30
Case 1.3	9.75	1	1.1	30
Case 2.1	9.75	0.1	1.1	30
Case 2.2	9.75	0.5	1.1	30
Case 2.3	9.75	4	1.1	30
Case 3.1	9.75	1	3	30
Case 3.2	9.75	1	5	30
Case 3.3	9.75	1	7	30
Case 4.1	9.75	1	1.1	20
Case 4.2	9.75	1	1.1	25
Case 4.3	9.75	1	1.1	35

5.2.2. Optimization results

The levelized cost of hydrogen obtained for the different cases formulated is presented in this section and the sensitivity of the LCOH with change in process conditions is noted. A summary of the LCOH and thermodynamic results of these cases is shown in Appendix D.

In chapter 4, we have seen that varying the biogas feed results in a change in the load-to-surface ratio (refer figure 4.1). Increasing the biogas feed means having a higher load (more reactants) for the membrane reactor. This results in a lower area required for a fixed output of hydrogen product. The effects are higher biogas feed costs, higher costs upstream the membrane reactor i.e. biogas compressors, heat exchangers costs but lower membrane area costs. It is worthwhile to determine if the lower membrane costs compensate the increase in the upstream costs. Therefore, in Base case & Cases 1.1 - 1.3, the biogas feed is varied to see how sensitive the membrane area is to the change in the load.

The LCOH obtained with varying biogas feed is shown in figure 5.1. The LCOH drops from 5.01 €/kg

to 4.93 €/kg as the biogas feed changed from 10.5 to 9.75 kmol/h. This means that the reduction in the upstream costs over-compensates the increase in the area costs. Furthermore, there is a minor decrease in the carbon capture section costs downstream the membrane reactor due to the reduction in the amount of feed.

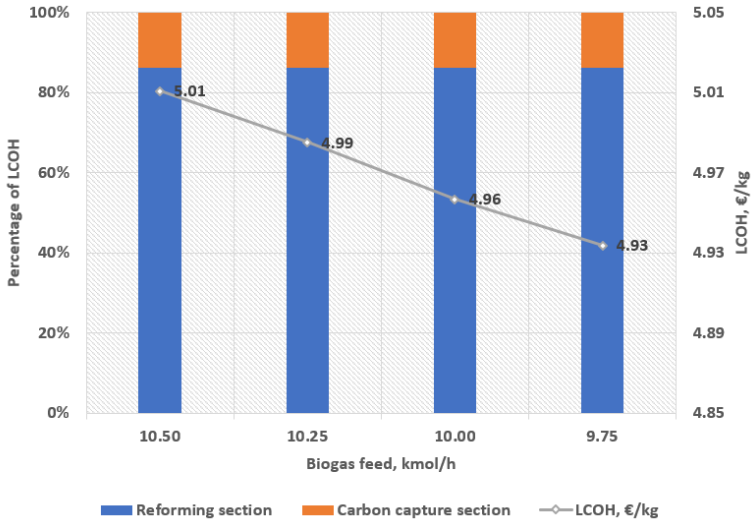

Figure 5.1: Levelized cost of hydrogen with varying biogas feed flow rate.

As the case with the biogas feed of 9.75 kmol/h gives the lowest value of LCOH, the cases analysed henceforth have a feed flow rate of 9.75 kmol/h as shown in table 5.7.

A higher sweep ratio requires lesser membrane surface area for a constant output, hence less membrane costs as seen from the results presented in Appendix B. However, increase in the upstream and downstream load due to a higher sweep ratio results in increase in equipment and operating costs. In Base case & Case 2.1-2.3, the sweep ratio is varied to see the effect of these parameters to the levelized cost of hydrogen.

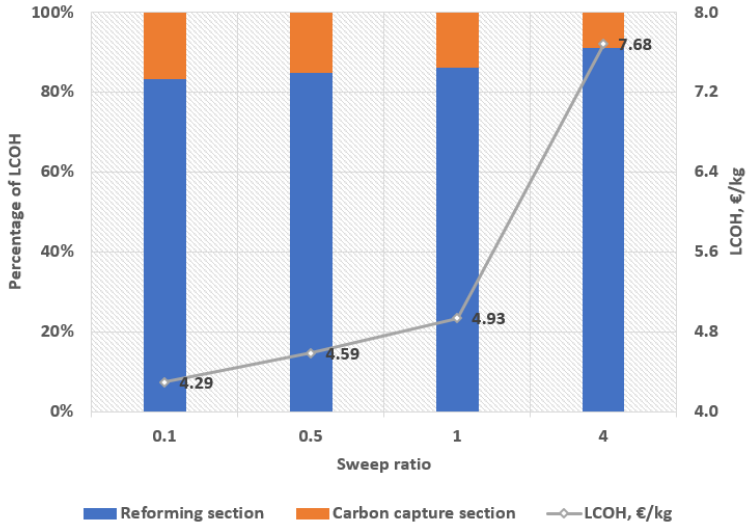

Figure 5.2: Levelized cost of hydrogen with varying sweep ratio.

Figure 5.2 shows the LCOH obtained with varying sweep ratios. While reading the graphs it is important to keep in mind that the x-axis isn't linear, to avoid misinterpretation of the results. The LCOH increases from 4.29 to 7.68 €/kg for sweep ratio from 0.1 to 4, which means that the decrease in mem-

brane costs doesn't compensate the increase in equipment and operating costs for sweep generation and separation from permeate. The percentage cost for the reforming section to the overall LCOH increases from around 84% to 91% with increase in sweep ratio from 0.1 to 4.

The change in membrane surface area and hydrogen compression duty for different permeate pressures is presented in figure 5.3. Therefore, determining a trade-off between increased membrane area costs and decreased hydrogen compression costs for varying permeate pressure is interesting due to the high pressure of hydrogen product required.

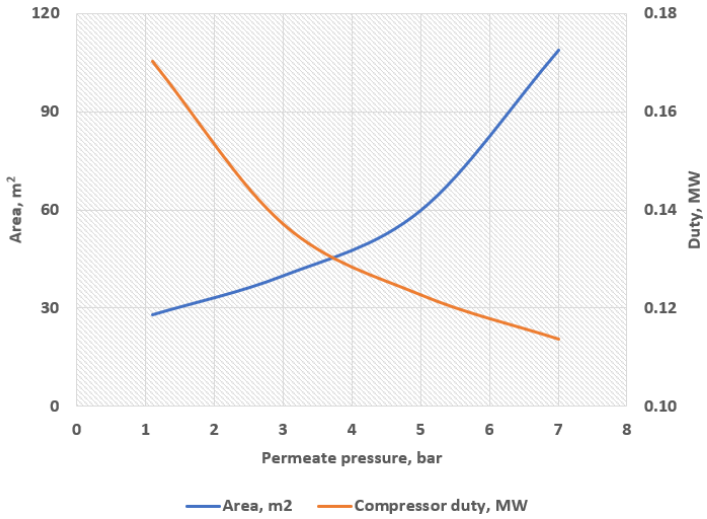

Figure 5.3: Membrane surface area vs hydrogen compressor duty for different permeate pressure.

Figure 5.4 shows the effect of changing permeate pressure on the LCOH. Increasing the permeate pressure from 1.1 to 5 bar results in a decrease in LCOH. This means that the decrease in hydrogen compression costs compensates the increase in membrane area costs. When increasing the pressure from 5 to 7 bar, the increase in membrane area and therefore cost overpowers the decrease in hydrogen compression costs.

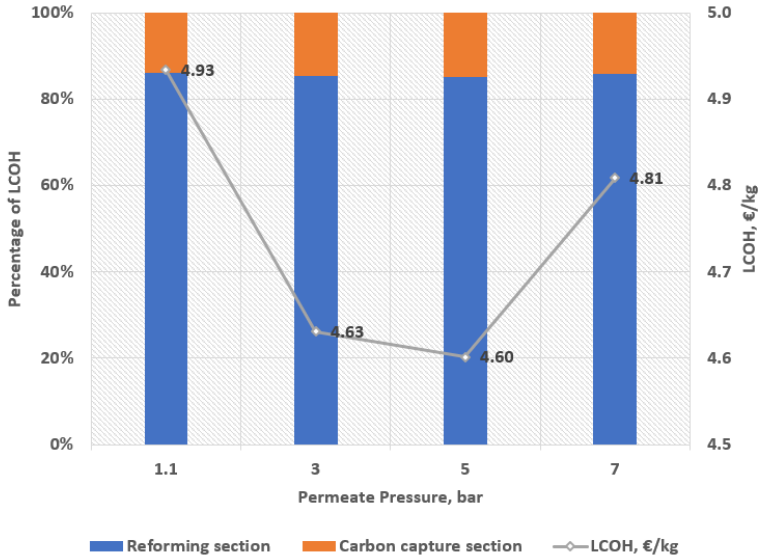

Figure 5.4: Levelized cost of hydrogen with varying permeate pressure.

Furthermore, increasing the permeate pressure considerably reduces the dehydration unit's operating cost as seen in figure 5.5. This is because as pressure increases, latent heat of condensation

of water reduces and more water is removed in the knock-out drum. Therefore, the dehydration unit needs to remove lesser amount of water than it had to at lower pressure, which reduces the operating cost.

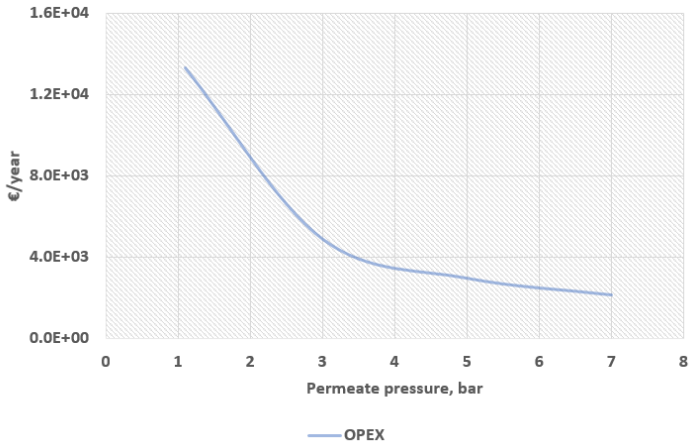

Figure 5.5: OPEX of hydrogen dehydration unit for different permeate pressure.

The effects of change in reactor pressure on the LCOH is also interesting to note. An increase in the pressure results in increase in feed compression costs. However, it also increases the driving force for hydrogen permeation through the membrane (permeate pressure being constant) and therefore reduces the area requirement (refer Appendix D) & cost.

Furthermore, with a higher reactor pressure i.e. higher inlet stream pressure to the carbon capture unit, the compression cost for the carbon capture unit decreases. The effect of the interplay between these variables on the LCOH is shown in figure 5.6. The reduced costs due to reduction in membrane area and carbon capture unit costs compensates the increase in feed compression costs until (at least) the studied reactor pressure range of 35 bar.

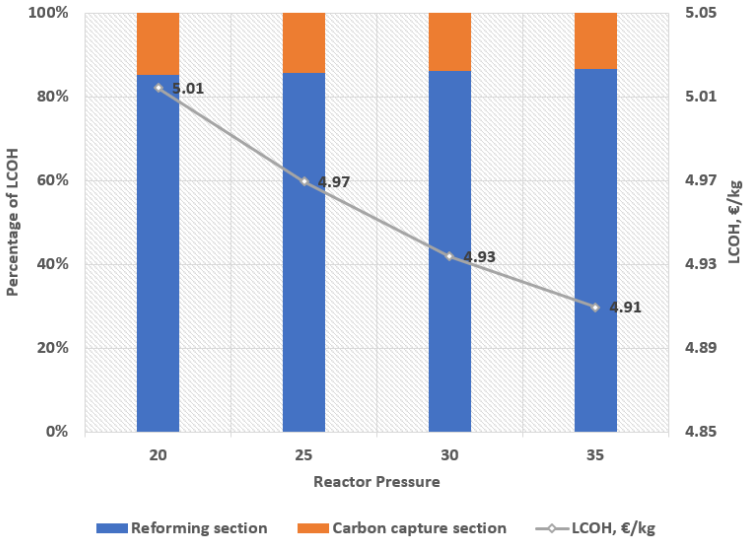

Figure 5.6: Levelized cost of hydrogen with varying reactor pressure.

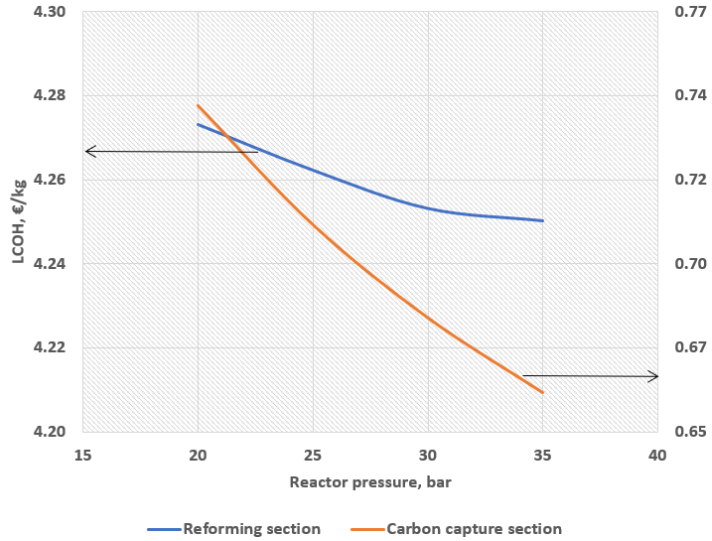

Figure 5.7: Cost changes in the reforming & carbon capture section with varying reactor pressure.

Figure 5.7 shows how the cost of the reforming section and the carbon capture unit change with increasing reactor pressure. With increase in reactor pressure, the membrane area costs reduce (due to the increase in driving force). However, the overall reduction in costs of the reforming section aren't significant due to the increase in compression costs as the reactor pressure increases. As the reactor pressure increases, the line becomes less steeper i.e. the increase in the compression costs have a higher effect compared to the reduction in membrane area costs. Furthermore, the reduction in the carbon capture costs are significant compared to the reforming section and the overall LCOH decreases. For a reactor pressure greater than 35 bar, there may be a point where the reforming section cost increases enough that the carbon capture section cost decrease doesn't compensate the increase, resulting in an increase in the overall LCOH.

5.3. (Local) Optimum result

From the sensitivity results, we expect to obtain the lowest LCOH of the cases investigated for a biogas feed of 9.75 kmol/h, sweep ratio of 0.1, permeate pressure of 5 bar and reactor pressure of 35 bar. It is important to understand that the combination of these operating parameters may not result in a lowest LCOH of all the cases investigated due to a number of interacting factors. A finite list of combinations was formulated to determine to lowest LCOH obtainable, refer Appendix E. Results of the (local) optimum process conditions are presented in table 5.8. The (local) optimum obtained is at biogas feed flow rate of 9.75 kmol/h, reactor pressure of 35 bar, sweep ratio of 0.1 and a permeate pressure of 1.1 bar. With a permeate pressure of 5 bar, the membrane area obtained from simulations was infinitely high, therefore unfeasible. A permeate pressure of 1.1 bar compared to 5 bar results in a higher driving force and therefore lesser membrane area. However, the hydrogen compression costs are higher. The decrease in membrane costs overcompensates the increase in hydrogen compression costs and therefore the (local) optimum is at these process conditions. The Aspen model for this process is shown in Appendix A.

The total annual cost contribution of the (local) optimum process is shown in figure 5.8. Hydrogen compression contributes to the highest costs. This result is expected due to the high fuelling pressure requirement of 700 bar. Annual capital costs followed by the reforming costs are the next highest annual cost contributors. The reforming cost is almost half the cost for hydrogen compression. Membrane replacement, permeate dehydration, carbon capture, biogas input costs contribute to 10.5% of the total annual costs in total. The break-down of these costs is presented in Appendix F.

Table 5.8: (Local) Optimum conditions for the novel process.

Process conditions	
Biogas feed, kmol/h	9.75
Reactor temperature, °C	600
Reactor pressure, bar	35
Steam-to-carbon ratio	3
Sweep ratio	0.1
Permeate pressure, bar	1.1
Biogas fuel, kmol/h	3.73
Results	
LCOH, €/kg	4.26
Hydrogen produced, kg/day	1071
Global hydrogen recovery factor (%)	93.2
Global methane conversion (%)	99.9
Carbon capture rate (%)	72.13
Global efficiency (%)	66.07
Productivity, kg/m^2 day	28.76
Area, m^2	37.34
Load-to-surface area, $kmol/m^2$ h	0.66
CO_2 emitted (biogenic)[a], kg CO_2/kg H_2	3.69

[a] From furnace flue gas.

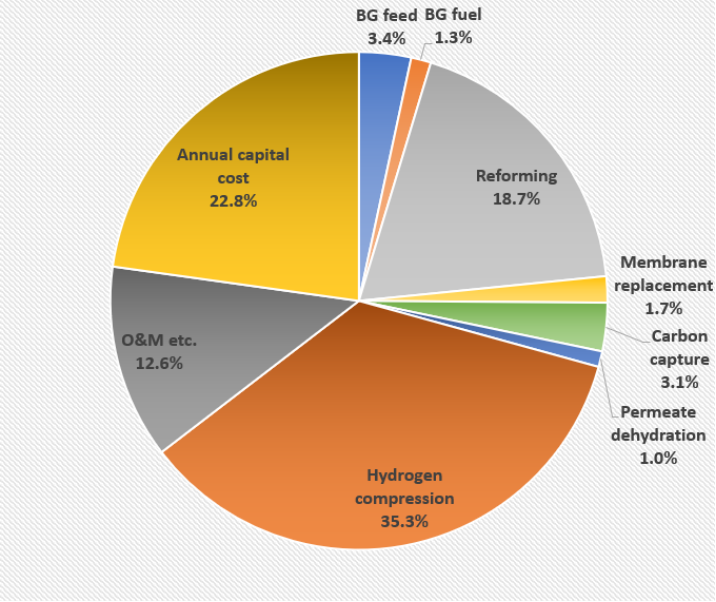

Figure 5.8: Contribution to total annual cost.

5.3.1. Sensitivity analysis on LCOH

To evaluate the effect of potential uncertainties in the main assumptions made to calculate the levelized cost of hydrogen, a sensitivity analysis is performed for a finite list of parameters. The range of the manipulated (input) variables and the reference values assumed for the previous calculations is shown in table 5.9.

Table 5.9: Manipulated variables range.

	Reference value	Range[a]
Membrane cost, €/m^2	2500	1250 - 3750
Biogas cost, €/GJ	3.46	1.73 - 5.19
Electricity cost, €/kWh	0.105	0.0525 - 0.1575
Water cost, €/m^3	0.350	0.175 - 0.525
After tax real rate of return, %	10	5 - 15

[a] $\pm$ 50% from the default value.

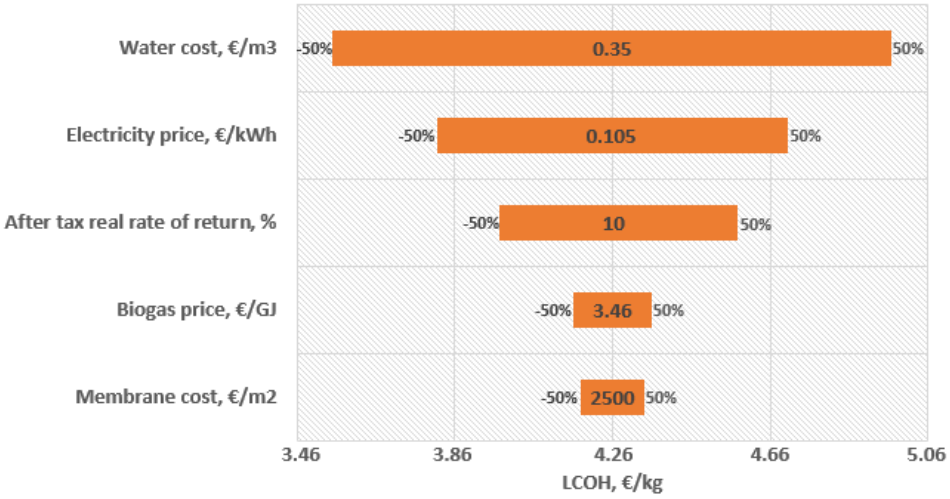

Figure 5.9: LCOH sensitivity for cost variation of $\pm$ 50% from reference value.

Figure 5.9 shows that the LCOH is most sensitive to the water cost, followed by the electricity cost and is least affected by the membrane cost. The cost of water and electricity for industry can vary every year which might affect the LCOH of the process (Frédéric Michas, 2020). The after tax rate of return can change due to a number of factors which are sometimes unpredictable (for example the virus pandemic in 2020). A number of factors can change during the lifetime of the system and the effects of these changes have to be kept in mind to decide if the system will be favourable throughout its lifetime. Furthermore, the assumption in chapter 4 while selecting a configuration that the operating costs will have a higher impact on the LCOH than the capital cost (area) holds true.

5.4. Comparison with reference

The feasibility of the novel system developed is determined by comparing the results obtained with the results of the reference case. The objective of this section is to determine if decentralized bio-hydrogen production (novel case) outperforms the centralized hydrogen production with hydrogen transport (reference case). The performance results of the reference case have been rounded off from 1071 kg/day (which is 500 Nm^3/h) to 1000 kg/day. Therefore, the novel system has also been scaled down to 1000 kg/day for the results to be comparable.

5.4.1. Techno-economic comparison

In addition to the two cases defined earlier, two other cases are defined for a holistic comparison. The four cases compared in this section are centralized production with H_2 transport ($reference\ case_b$), centralized production with H_2 transport + carbon capture ($reference\ case_c$), decentralized production ($novel\ case_b$) and decentralized production with carbon capture ($novel\ case_c$).

Common cost values for MDEA CO_2 capture are taken from literature to define the reference case with carbon capture. MDEA technology is considered because it is commonly adopted in the conventional steam methane reforming processes in the industry for CO_2 capture. An estimate of the amount

of CO_2 emitted by a SMR plant and the percentage of CO_2 captured by the MDEA technology are taken from IEA (2017). A break-down of the LCOH values for both the systems are shown in figure 5.10.

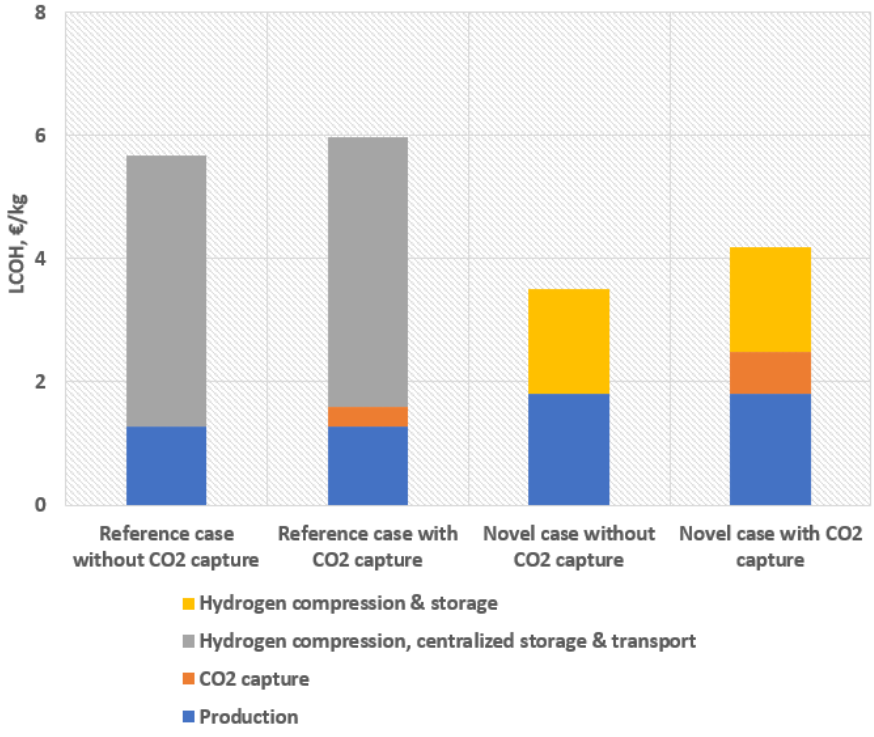

Figure 5.10: Components of LCOH for the four cases.

As seen in table 5.10, the efficiency of the novel cases is higher than the reference cases. The increase in efficiency is due to the intensive membrane reactor reforming compared to the steam methane reforming which has multiple process units, as expected. The efficiency of the $novel\ case_c$ decreases around 1% compared to $novel\ case_b$. Comparing the baseline cases, the LCOH of the novel case is approximately 40% lower than the reference case. With the carbon capture unit, the difference reduces to around 30%. This indicates that the carbon capture unit integrated with the reference system is cheaper than the cryogenic carbon capture unit integrated with the novel system. Figure 5.10 confirms this conclusion as the orange bar in the second column is almost half the size of the orange bar in the fourth column. The production cost for the reference case is 1.274 €/kg. The production cost of the novel case is around 40% higher at 1.81 €/kg. However, the compression, storage & transport costs for the reference system overpower the higher production and carbon capture costs of the novel system. These costs are around 3.5 times the production costs at 4.4 €/kg. Transport distance assumed for the calculation is 161 km (100 miles) (Katikaneni et al., 2014). CO_2 transport cost for the relevant cases isn't taken into consideration but it is assumed the increase in the LCOH for both the reference case and novel case will be the same and won't affect their relative feasibility.

Table 5.10: Comparison of key results.

	Centralized production with H_2 transport Reference case$_b$	**Centralized production with H_2 transport & CO_2 capture Reference case$_c$**	**Decentralized on-site production Novel case$_b$**	**Decentralized on-site production with CO_2 capture Novel case$_c$**
LCOH, €/kg H_2	5.67	5.98	3.51	4.19
Energy efficiency, %	61.64	<61.64	67.86	66.96

The attractiveness of the cases also depends on their carbon footprint i.e. CO_2 emissions of the system. The next section compares the carbon emissions of these cases throughout the value chain.

5.4.2. Carbon footprint comparison

An attempt to evaluate the CO_2 emissions for the entire value chain of the four cases presented in the previous section is made. The value chain with the locations of CO_2 emissions of the two cases with carbon capture is shown in Appendix G. The list of assumptions made to determine the CO_2 emissions of the cases are as follows:

1. The transport mode for feed and products that need to be transported is pipeline transport.
2. The transport distance is 100 km for all substances except biogas. The transport distance for biogas is negligible as the biogas production plant is assumed to be close to the refuelling station.
3. The pipeline transport emissions are 5 g CO_2 / tonne-km i.e. 5 grams of CO_2 will be emitted when 1 tonne of a substance is transported a distance of 1 km (ECTA, 2011).
4. To calculate the CO_2 emissions from biogas production, a number of assumptions are made.
    - The biogas production plant was in operation before the novel process was commissioned.
    - The biogas production plant produced exactly the same amount of biogas required by the novel process.
    - The biogas was used to generate electricity before but is now a feed for the novel process. 4082 m^3/day of biogas produces 7226 kWh/day of electricity as stated in Hanum et al. (2019) and will be scaled linearly for this work.
    - The electricity that was produced by the biogas before, is now taken from the grid (produced with natural gas). Therefore, the CO_2 emissions from electricity production using natural gas are considered the emissions of the biogas production plant.
5. The CO_2 emissions from hydrogen production for the reference system are 9 kg CO_2/kg H_2 (IEA, 2017).
6. For reference case with CO_2 emissions, the MDEA capture technology can capture 54.1% of the CO_2 emissions (IEA, 2017).
7. CO_2e emissions from electricity generation in The Netherlands as calculated on 1-1-2020 are 475 g CO_2/kWh (Milieu centraal, 2020). The absolute CO_2 emissions are calculated depending on the electricity consumption of the system in question.

The input-output specifications of the four cases are mentioned in table 5.11.

Table 5.11: Input-output specifications of the cases.

	$Reference\ case_b$	$Reference\ case_c$	$Novel\ case_b$	$Novel\ case_c$
Feed, kg/kg H_2	3.33	3.33	7.56 (feed + fuel)	7.56 (feed + fuel)
Hydrogen product, kg/h	41.7	41.7	41.7	41.7
CO_2 **captured, kg** CO_2**/kg** H_2	-	5.07	-	8.96
CO_2 **emitted, kg** CO_2**/kg** H_2	10.14	5.45	10	1.4

The CO_2 emissions across the value chain for all the processes along with the carbon avoidance cost is shown in table 5.12 and a break-down of these values is shown in Appendix G. The reference case has significantly higher emissions even after the carbon capture unit is integrated whereas the novel case with carbon capture has comparatively low emissions (The positive 1.4 kg CO_2/kg H_2 emissions are due to the electricity requirement of the process). The $novel\ case_c$ reduces the CO_2 emissions by approximately 90% compared to $reference\ case_b$. This is a favourable result considering the urgency to reduce carbon emissions to mitigate global warming. The $novel\ case_b$ has net emissions lower than the $reference\ case_b$.

The CAC for $reference\ case_c$ and $novel\ case_c$ in comparison with $reference\ case_b$ is 66.1 €$/ton\ CO_2$ and -169.33 €$/ton\ CO_2$ respectively. The negative avoidance cost for the latter is due to the lower

LCOH and massive reduction in CO_2 emissions due to the utilisation of membrane-enhanced reforming for hydrogen production and cryogenic carbon capture technology. The CAC comparing the $novel\ case_c$ with the $reference\ \ case_c$ is $-441.98\ €/ton\ \ CO_2$. The CAC comparing the $novel\ \ case_c$ with the $novel\ case_b$ is 79.1 $€/ton\ CO_2$, higher than the CAC for the reference cases at 66.1 $€/ton\ CO_2$. However, the important takeaway from the CAC calculation is the negative cost of $-169.33\ €/ton\ CO_2$ which indicates that carbon capture isn't actually a cost for the novel case if compared to the $reference\ case_b$, thanks to efficiency improvement. However, it is important to keep it mind that the CO_2 transport costs aren't included and which should be for a complete comparison.

Table 5.12: Comparison of carbon footprint of the different cases.

	$Reference\ case_b$	$Reference\ case_c$	$Novel\ case_b$	$Novel\ case_c$
Net CO_2 emissions, kg CO_2/kg H_2	10.14	5.45	10	1.4
CO_2 avoidance cost (CAC)[a], €/ton CO_2	-	66.1	-	-169.33 -441.98[b] 79.1[c]

[a] The baseline case is $reference\ case_b$ unless specified.
[b] The baseline case is $reference\ case_c$.
[c] The baseline case is $novel\ case_b$.

Although The Netherlands doesn't have a explicit carbon tax in place at the moment, the government as part of the Dutch "climate agreement" has plans to implement a carbon tax system by January 2021 (Loyens & Loeff). According to a statement by the Dutch Government in June 2019, the carbon tax would likely start at 30 €/ton CO_2 in 2021 and rise to 150 €/ton CO_2 in 2030 (Federal News Network, 2019). The Dutch government's measures following the COVID-19 pandemic are uncertain, however the EU Covid-19 recovery plan favouring sustainable and green economies and societies will be favourable for the novel case.

Currently, the electricity is generated majorly from fossil sources. However, in the future there will be a higher mix of renewable sources like wind and solar energy. The CO_2 emissions from renewable sources is negligible and will result in lower and possibly negative CO_2 emissions for the $novel\ case_c$. Two future carbon emission scenarios with 20% and 40% (additional) integration of renewable sources for electricity generation are shown in figure 5.11. The two future scenarios result in net negative emissions for the $novel\ case_c$. Such a scenario, if realized, will significantly benefit in the EU-ETS system. The effective cost of hydrogen produced may drastically decrease as a result.

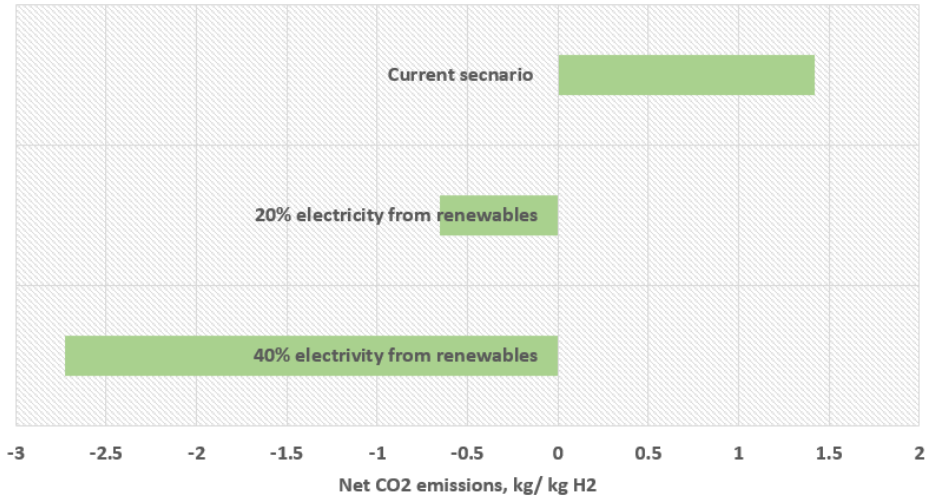

Figure 5.11: Future CO_2 emissions scenario.

5.5. Conclusion

The (local) optimum LCOH for a capacity of 500 Nm^3/h (1071 kg/day) hydrogen is 4.26 €/$kg\ H_2$ at reactor temperature of 600 °C, reactor pressure of 35 bar, S/C of 3, sweep ratio 0.1, permeate pressure of 1.1 bar and biogas feed of 9.75 kmol/h (valid at given assumption). The global HRF, global methane conversion, carbon capture rate, global efficiency are 93.2%, 99.9 %, 72.13%, 66.07% respectively. The major cost contributor is hydrogen compression cost followed by reforming cost due to the high work and duty requirements. Furthermore, the assumption in chapter 4 that the operating costs will have a higher impact on the LCOH than the capital cost holds true: the sensitivity of LCOH is highest for water and electricity costs.

Comparing the optimum results of the novel case with the reference case for 1000 kg/day hydrogen production reveals that the novel case has a better thermodynamic and economic performance and a lower carbon footprint. Four cases are defined i.e. centralized production with H_2 transport ($reference\ case_b$), centralized production with H_2 transport + carbon capture ($reference\ case_c$), decentralized production ($novel\ case_b$) and decentralized production with carbon capture ($novel\ case_c$) and the results are as follows:

Table 5.13: Comparison of novel and reference cases.

	$Reference\ case_b$	$Reference\ case_c$	$Novel\ case_b$	$Novel\ case_c$
LCOH, €/kg H_2	5.67	5.98	3.51	4.19
Energy efficiency, %	61.64	<61.64	67.86	66.96
Net CO_2 **emissions, kg** CO_2**/kg** H_2	10.14	5.45	10	1.4
CO_2 **avoidance cost (CAC)**[a]**, €/ton** CO_2	-	66.1	-	-169.33 -441.98[b] 79.1[c]

[a] The baseline case is $reference\ case_b$ unless specified.
[b] The baseline case is $reference\ case_c$.
[c] The baseline case is $novel\ case_b$.

The LCOH of the novel cases is lower than the reference cases. The higher cost for the reference cases is due to the high transportation costs of hydrogen. Furthermore, the efficiency of the novel cases is higher than the reference cases due to the intensive membrane reactor reforming process compared to the steam methane reforming process which has multiple process units.

The reference case has significantly higher emissions of 5.45 kg CO_2/kg H_2, even after the carbon capture unit is integrated. The $novel\ case_c$ reduces the CO_2 emissions by approximately 90% compared to $reference\ case_b$ (down to 1.4 kg CO_2/kg H_2). This is a favourable result considering the urgency to reduce carbon emissions to mitigate global warming. The important takeaway from the CAC calculation is the negative cost of -169.33 €/$ton\ CO_2$, comparing the $novel\ case_c$ with the $reference\ case_b$, which indicates that carbon capture isn't actually a cost for the novel case if compared to the $reference\ case_b$, thanks to efficiency improvement. However, it is important to keep it mind that the CO_2 transport costs aren't included and which should be for a complete comparison.

The positive 1.4 kg CO_2/kg H_2 emissions are due to the electricity requirement of the process. Scenarios with more penetration of renewable sources for electricity production are formulated to determine the (probable) carbon footprint of the process in the future. A (additional) 20% and 40% integration of renewable sources results in net negative carbon emissions of -0.66 kg CO_2/kg H_2 and -2.73 kg CO_2/kg H_2 respectively.

6

Exergy analysis

This chapter aims to analyze the design of the novel system developed. Optimization of the process after the exergy analysis is out of scope for this work. The process with the most promising results, described in table 5.8 is evaluated in this chapter.

6.1. Definition

Exergy is defined as ”the maximum amount of work obtainable when an energy carrier is brought from its initial state to a state of thermodynamic equilibrium (an inert state) with the common substances of the natural environment by means of reversible processes” (Szargut et al., 1987). In other words, exergy defines the maximum amount of work that can be derived from a process when a substance goes from an initial state to a reference state.

Following the definition, determining the reference state is a very important factor when performing exergy analysis. The reference state conditions are usually the temperature and pressure conditions of the ambient environment. Typical environment conditions are $T_o = 25$ °C and $p_o = 1$ atm.

6.2. Physical & chemical exergy

Exergy of a substance can generally be divided into physical exergy and chemical exergy. The physical part comprises of heat, pressure, kinetic and potential exergies and the chemical part is mostly just the chemical exergy of the substance. Generally assumptions are made so that physical exergy is only related to temperature and pressure, then the exergy is a function of enthalpy, temperature and entropy. When the kinetic and potential terms are ignored, the exergy flow is given by (Moran and Shapiro):

$$\dot{E}_{ph} = h - h_o - T_o(s - s_o) \tag{6.1}$$

where, h & s represent the enthalpy and entropy respectively, at inlet or outlet and h_o & s_o represent the respective values at the reference state.

As seen in the equation above, an increase in entropy of a substance through a process causes a loss of exergy (available work) that can be obtained from the products. Entropy is the enemy of exergy and will always win due to irreversiblilities (Gray and Schlup, 2019). Since physical exergy is a property of enthalpy and entropy, it can easily be calculated for process streams knowing their temperature and pressure conditions.

Chemical exergy is the maximum useful energy theoretically obtainable by a chemical process which turns reactants into products that are in chemical equilibrium with the environment (Gray and Schlup, 2019). Chemical exergy only applies to chemical processes and not the temperature and pressure surrounding the reactants and products. Since there is no single equilibrium state for the chemicals, the final state (reference) must be determined. Generally, chemical exergy is determined in reference to compositions found in the atmospheric air i.e. N_2, O_2, H_2O, CO_2. Once the reference composition

is determined, a series of calculations are required to obtain exergy values of substances of interest. However, these complexities can be sidestepped by using the table for standard molar chemical exergy of (typical) substances by Moran and Shapiro, refer Appendix H.

6.3. Exergy calculation

To calculate the exergy efficiency using equation 3.24, we need to calculate the (useful) exergy out and the total exergy into the process. The exergy out is the total exergy of hydrogen which can be easily calculated knowing its temperature and pressure (physical exergy) and standard molar chemical exergy values from Moran and Shapiro (chemical exergy). The exergy input to the process is majorly total (physical + chemical) exergy of biogas and work.

Table 6.1: Reference state conditions.

Temperature, °C	25
Pressure, bar	1.01325
O_2, %	21
N_2, %	78
H_2O, %	0.96
CO_2, %	0.04

The assumptions for calculating the exergy are listed below:

1. Ideal-gas law.
2. Reference state for all the calculations is mentioned in table 6.1.
3. Kinetic and potential terms are ignored.
4. Physical exergy (exergy flow) values taken from REFPROP (verified by manual calculations, Appendix I.
5. Chemical exergy values taken from Moran and Shapiro, refer Appendix H.

Table 6.2 shows the calculation results of the exergy flow of the process. After calculating the exergy input values, the exergy of hydrogen and the exergy lost in CO_2 and flue gases, the exergy destroyed is easily calculated by writing the exergy balance equation 6.2 (Dincer and Rosen, 2013). The exergy efficiency of the process ($\dot{E}_{H2}/\dot{E}_{in}$) is calculated to be 65.1 % which is quite close to the energy efficiency value of 66.07 % (table 5.8). It is important to note that hydrogen has a smaller exergy content than its lower heating value and methane has a larger exergy content than its lower heating value which result in these values being close to each other.

$$Exergy\ in = Exergy\ output\ in\ product\ + Exergy\ lost + Exergy\ destruction \tag{6.2}$$

Table 6.2: Exergy flow results.

	$\dot{E}$, kW	$\overline{E_T}$, kJ/kg	$\overline{E_{ph}}$, kJ/kg	$\overline{E_{ch}}$, kJ/kg	Percentage of total $\dot{E}_{in}$, %	Temperature, °C	Pressure, bar	Mass flow rate, kg/h
Exergy in	2409.87				100			
Biogas feed	1438.32	20512.11	0.23	20511.88	59.68	35	1.01325	252.434
Biogas fuel	550.25	20512.11	0.23	20511.88	22.83	35	1.01325	96.57
Water (feed)	4.68	50.7	0.72	49.98	0.194	15	1.01325	331.98
Water (sweep)	0.61	50.7	0.72	49.98	0.025	15	1.01325	43.4
Work	405.4				16.82			
Exergy out (Hydrogen)	1569.66	126627.8	8577.8	118050	65.1	30	700	44.625
Exergy lost	131.39				5.5			
Carbon dioxide	77.39	675.58	218.61	456.97	3.2	30	110	412.3
Flue gases	54	232.53	62.97	169.56	2.3	65.27	1.9	836
Exergy destroyed	707.58				29.4			

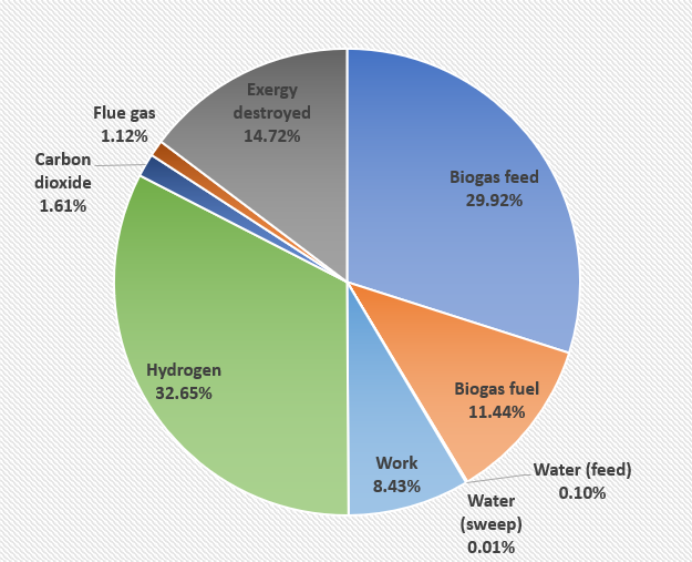

Figure 6.1: Exergy in and out distribution of the system.

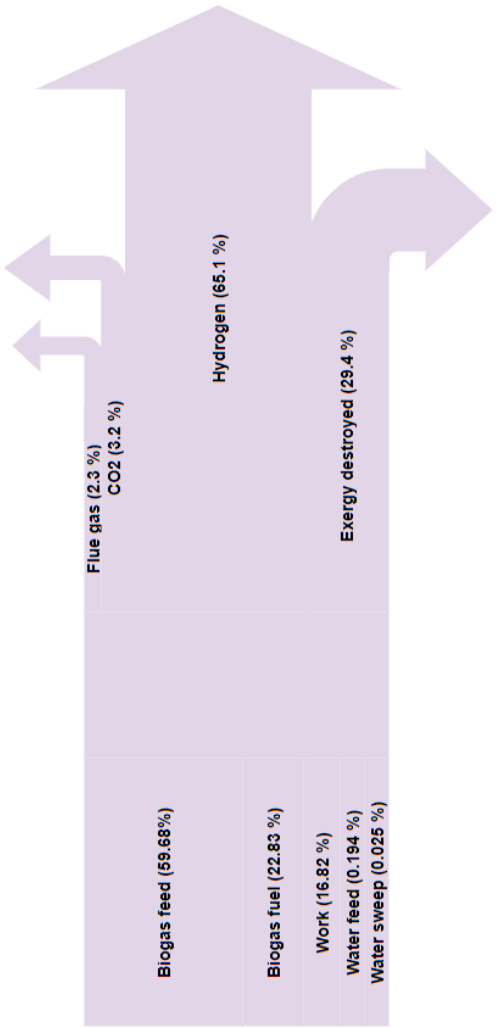

Figure 6.2: Grassmann diagram of novel system.

Figure 6.1 graphically shows the distribution of exergies in and out of the system. The right half of the pie displays the total exergy in and the left half displays the total exergy out. Biogas is the dominant exergy input contributing to 82.51% of the total exergy in. Exergy of feed water and sweep water contributes to a negligible fraction of total exergy in. Majority of the exergy out is carried by hydrogen followed by exergy destroyed due to irreversibilities within the system. The exergy of CO_2 cannot be recovered as it is sequestered. The exergy of flue gas is the lowest exergy out. The temperature of these gases is 65 °C as seen in table 6.2 i.e. most of the exergy is already recovered into the system. First law analysis would lead to a conclusion that most of the heat is lost by the flue gas whereas exergy destruction is the major part of the exergy unused. The exergy distribution illustrated the utility of exergy analysis where these results could help make improvements in the design to reduce unused exergies.

Figure 6.2 represents the Grassmann (exergy) diagram for the novel process developed. The arrows at the upper side correspond to exergy loss of the system whereas the arrows at the lower side correspond to exergy destroyed across each components.

6.4. Conclusion

The exergy efficiency of the process is calculated to be 65.1%. For the calculation, physical exergy is taken from REFPROP and chemical exergy from standard molar chemical exergy values by Moran and Shapiro presented in Appendix H. Major fraction of exergy input is due to biogas feed and fuel at 82.51 %, most of the remaining is work input. Exergy destruction is the major exergy unused at 29.4%. Most of the exergy of flue gas is recovered and the flue gas is released into the atmosphere at 65 °C, resulting in an exergy loss of 2.3%. 3.2 % exergy of CO_2 cannot be recovered as it is sequestered. First law analysis would lead to a conclusion that most of the heat is lost by the flue gas whereas exergy destruction is the major part of the exergy unused.

7

Conclusion and recommendations

Overall, the decentralized membrane reforming system's result is more attractive than the centralized steam methane reforming system.

Three configurations for the novel case have been developed i.e. process with carbon capture unit before the reforming section, process with carbon capture unit after the reforming section without recycle stream and process with carbon capture unit after the reforming section with recycle stream. The process with carbon capture unit after the reforming section without recycle stream (configuration 2) was chosen due to its lower process complexity and superior efficiency for further levelized cost of hydrogen and CO_2 avoidance cost evaluation. The thermodynamic performance of this configuration is better than the other two with comparable global hydrogen recovery factor and the global methane conversion and higher carbon capture rate and global efficiency. Furthermore, the overall cost of this configuration was expected to be lower assuming the operating expenditure would have a larger impact on the cost than the capital expenditure. The results of this configuration, after optimization are compared to the reference case.

The energy efficiency and carbon capture rate of the decentralized system ($novel\ case_c$) are 66.07% & 72.13%, higher compared to 61.64% & 54.1% for the centralized system ($reference\ case_c$). The exergy efficiency of the process is 65.1%, very close to the energy efficiency suggesting a good process design. Major fraction of exergy unused was exergy destroyed at 29.4%. The total LCOH of the $reference\ case_c$ is 5.98 €/kg H_2 and the total LCOH of the $novel\ case_c$ is 4.19 €/kg H_2. The higher cost for the $reference\ case_c$ is due to the high transportation costs of hydrogen. Furthermore, the hydrogen production cost of the reference system is 1.27 €/kg H_2 whereas the novel system is only slightly higher at 1.81 €/kg H_2.

The modelling results also revealed that the novel system has a potential of relatively inexpensive carbon capture. Addition of a carbon capture unit increases the LCOH from 3.51 €/kg to 4.19 €/kg, which means that the carbon capture unit costs 0.68 €/ kg H_2. Furthermore, the energy efficiency drop is roughly 1%, which is a low penalty for a carbon capture unit. This favourable result is due to the high methane conversion of the system which results in low impurities in the retentate and therefore efficient capture of CO_2. Another noteworthy outcome of the research was that the hydrogen purity obtained from the membrane reactor wasn't sufficient for the FCV application. A molecular sieve dehydration unit was integrated into the system at an approximate cost of 0.4 €/kg H_2 to remove 0.15 kg H_2O/kg H_2.

Comparing the carbon emissions of the cases. The reference case has higher CO_2 emissions than the novel case, with and without the carbon capture unit. The CO_2 emissions of the $reference\ case_b$ are unreasonably high at 10.14 kg CO_2/kg H_2. Integrating the carbon capture unit nevertheless results in considerably high CO_2 emissions for the reference case at 5.45 kg CO_2/kg H_2 owing to the low carbon capture rate of the MDEA capture unit. Although the $novel\ case_b$ has similar emissions (10 kg CO_2/kg H_2) to the equivalent reference system, integrating the carbon capture unit results in extremely low

emissions at 1.4 kg CO_2/ kg H_2, approximately 90% lower as compared to $reference\ case_b$. This is a favourable result considering the urgency to reduce carbon emissions to mitigate global warming.

The positive 1.4 kg CO_2/kg H_2 emissions are due to the electricity requirement of the process. Future scenarios with (additional) 20% and 40% integration of renewable sources into the electricity mix will result in -0.66 kg CO_2/kg H_2 and -2.73 kg CO_2/kg H_2 emissions respectively for the $novel\ case_c$. Systems with near-zero and/or negative emissions will be essential for The Netherlands to meet its climate policy to reduce greenhouse gas emissions by 49% by 2030 compared to 1990 levels and a 90% reduction by 2050 (Government of the Netherlands, 2019).

Future prospects to deepen the research are as follows:

- A more integrated optimization of the process taking into account the performance of both the membrane reforming section and the carbon capture unit. For example, analyzing the effect of change in reforming temperature on the carbon capture unit.
- Optimization of the carbon capture unit with sensitivity on the cryogenic temperature and pressure conditions.
- Further research on the process with carbon capture before the membrane reactor.
  - The configuration showed superior productivity.
  - If coke formation is modelled in the membrane reactor, this configuration is expected to have a better performance compared to the others.
- The effect of the carbon tax and the EU-ETS on the attractiveness of the novel system should be considered to access the business case of the technology.
- Optimization based on the exergy analysis to reduce the exergy destruction of the system.
- It will be interesting to compare the fixed bed design with a fluidized bed design by modelling, since contrasting information are available in literature.

Bibliography

Air Liquide. Cryocap™ CO□ cold capture system. URL https://www.airliquide.com/magazine/cryocap-co2-cold-capture-system-unlike-any-other-in-the-world.

Alibaba. 5A Molecular Sieve For Hydrogen Production. URL https://www.alibaba.com/product-detail/High-purity-4-8mesh-5a-molecular_62056502913.html?spm=a2700.7724857.normalList.113.634b64e1N9jhRw&fullFirstScreen=true.

Alstom UK. DECARBit: Enabling advanced pre-combustion capture techniques and plants. Technical report, 2011.

American Gas Association. What Is Natural Gas? URL https://www.aga.org/natural-gas/energy-education/.

Atsonios, K., Panopoulos, K. D., PROFILE Doukelis, S. A., Koumanakos, A. K., Atsonios, K., Panopoulos, K. D., Doukelis, A., Koumanakos, A., and Kakaras, E. Cryogenic Method for H2 and CH4 recovery from a rich CO 2 stream in pre-combustion CCS schemes A review of key environmental and energy performance indicators for the case of Renewable Energy Systems when integrated with storage solutions View project SMart IsLand Energy systems-SMILE View project Cryogenic Method for H2 and CH4 recovery from a rich CO 2 stream in pre-combustion CCS schemes. Technical report. URL https://www.researchgate.net/publication/266052148.

Baxter, L., Baxter, A., and Burt, S. Cryogenic CO2 Capture as a Cost-Effective CO2 Capture Process. Technical report.

Chompupun, T., Limtrakul, S., Vatanatham, T., Kanhari, C., and Ramachandran, P. A. Experiments, modeling and scaling-up of membrane reactors for hydrogen production via steam methane reforming. *Chemical Engineering and Processing - Process Intensification*, 134:124–140, 12 2018. ISSN 02552701. doi: 10.1016/j.cep.2018.10.007.

Collodi, G., Azzaro, G., Ferrari, N., and Santos, S. Techno-economic Evaluation of Deploying CCS in SMR Based Merchant H2 Production with NG as Feedstock and Fuel. In *Energy Procedia*, volume 114, pages 2690–2712. Elsevier Ltd, 2017. doi: 10.1016/j.egypro.2017.03.1533.

DACE Price Booklet. Independent cost estimate data for the process industry. URL https://www.dacepricebooklet.com/.

Di Marcoberardino, G., Foresti, S., Binotti, M., and Manzolini, G. Potentiality of a biogas membrane reformer for decentralized hydrogen production. *Chemical Engineering and Processing - Process Intensification*, 129:131–141, 7 2018. ISSN 02552701. doi: 10.1016/j.cep.2018.04.023.

Dincer, I. and Rosen, M. A. Thermodynamic Fundamentals. In *Exergy*, pages 1–20. Elsevier, 1 2013. doi: 10.1016/B978-0-08-097089-9.00001-2. URL https://linkinghub.elsevier.com/retrieve/pii/B9780080970899000012.

Dutch Water Sector. More biogas from sewage sludge for Amsterdam, 2020. URL https://www.dutchwatersector.com/news/more-biogas-from-sewage-sludge-for-amsterdam.

ECN. Efficient hydrogen production step closer in test with ECN membrane technology, 2010. URL https://www.ecn.nl/nl/nieuws/item/efficient-hydrogen-production-step-closer-in-test-with-ecn-membrane-technology/index.html.

ECTA. Guidelines for Measuring and Managing CO2 Emission from Freight Transport Operations. Technical report, 2011.

Enrico Drioli and Giuseppe Barbieri. *Membrane Engineering for the Treatment of Gases*. 2011. URL https://books.google.nl/books?id=1nIoDwAAQBAJ&pg=PA64&lpg=PA64&dq=cri+criterion+membranes&source=bl&ots=kyQptAetcj&sig=ACfU3U32xamNAem_ClfvVXYbMWG_O94stA&hl=en&sa=X&ved=2ahUKEwiEvLexmv3pAhVM4qQKHej9ArMQ6AEwAHoECAcQAQ#v=onepage&q=cri%20criterion%20membrane.

European Parliament. CO2 emissions from cars: facts and figures (infographics), 2019. URL https://www.europarl.europa.eu/news/en/headlines/society/20190313STO31218/co2-emissions-from-cars-facts-and-figures-infographics.

Federal News Network. Dutch government presents measures to cut carbon emissions, 2019. URL https://federalnewsnetwork.com/world-news/2019/06/dutch-government-presents-measures-to-cut-carbon-emissions/.

Frédéric Michas. Industrial prices for electricity in the Netherlands 1995-2019, 2020. URL https://www.statista.com/statistics/596254/electricity-industry-price-netherlands/.

Gabitto, J. and Tsouris, C. Modeling Sulfur Poisoning of Palladium Membranes Used for Hydrogen Separation. *International Journal of Chemical Engineering*, 2019, 2019. ISSN 16878078. doi: 10.1155/2019/9825280.

Gallucci, F., Van Sint Annaland, M., and Kuipers, J. A. Autothermal reforming of methane with integrated CO2 capture in a novel fluidized bed membrane reactor. Part 2 comparison of reactor configurations. *Topics in Catalysis*, 51(1-4):146–157, 12 2008. ISSN 10225528. doi: 10.1007/s11244-008-9127-7.

Gallucci, F., Fernandez, E., Corengia, P., and van Sint Annaland, M. Recent advances on membranes and membrane reactors for hydrogen production, 4 2013. ISSN 00092509.

Gas processing and LNG. Proper regeneration of molecular sieves in TSA processes—Part 2, 2018. URL http://www.gasprocessingnews.com/features/201804/proper-regeneration-of-molecular-sieves-in-tsa-processes%E2%80%94part-2.aspx.

Go, K. S., Son, S. R., Kim, S. D., Kang, K. S., and Park, C. S. Hydrogen production from two-step steam methane reforming in a fluidized bed reactor. *International Journal of Hydrogen Energy*, 34 (3):1301–1309, 2 2009. ISSN 03603199. doi: 10.1016/j.ijhydene.2008.11.062.

Government of the Netherlands. Climate policy | Climate Act, 2019. URL https://www.government.nl/topics/climate-change/climate-policy.

Gray, T. D. and Schlup, J. An introduction to exergy and its evaluation using Aspen Plus. Technical report, 2019.

Hamstra, P. W., Gallucci, E. F., Zondervan, E., Roghair, I., and Helmi, M. A. A modeling and experimental work on ”Concentration polarization in packed bed membrane reactors”. Technical report, 2015. URL www.tue.nl.

Hanum, F., Yuan, L. C., Kamahara, H., Aziz, H. A., Atsuta, Y., Yamada, T., and Daimon, H. Treatment of Sewage Sludge Using Anaerobic Digestion in Malaysia: Current State and Challenges. *Frontiers in Energy Research*, 7(MAR):19, 3 2019. ISSN 2296-598X. doi: 10.3389/fenrg.2019.00019. URL https://www.frontiersin.org/article/10.3389/fenrg.2019.00019/full.

Hartnig, C. and Roth, C. *In situ characterisation techniques for low temperature fuel cells*. Woodhead Pub, 2012. ISBN 9781845697747.

HoSt Bioenergy Systems. Biogas upgrading at Assen, Netherlands. URL https://www.host.nl/en/case/biogas-upgrading-assen/.

Hou, K., Fowles, M., and Hughes, R. Potential catalyst deactivation due to hydrogen removal in a membrane reactor used for methane steam reforming. Technical report, 1999.

Hysep ECN. Hydrogen Separation Modules. URL https://www.hysep.com/.

IEA. The Future of Hydrogen. URL https://www.iea.org/reports/the-future-of-hydrogen.

IEA. IEAGHG Technical Review - SMR Based Hydrogen Production with CCS. Technical report, 2017. URL www.ieaghg.org.

Inc, N. and Francisco, S. Equipment Design and Cost Estimation for Small Modular Biomass Systems, Synthesis Gas Cleanup, and Oxygen Separation Equipment; Task 2: Gas Cleanup Design and Cost Estimates – Black Liquor Gasification. Technical report, 2006. URL http://www.osti.gov/bridge.

Katikaneni, S. P., Al-Muhaish, F., Harale, A., and Pham, T. V. On-site hydrogen production from transportation fuels: An overview and techno-economic assessment. *International Journal of Hydrogen Energy*, 39(9):4331–4350, 3 2014. ISSN 03603199. doi: 10.1016/j.ijhydene.2013.12.172.

Kikuchi, E. Membrane reactor application to hydrogen production. Technical report, 2000.

Kluiters, S. C. A. Status review on membrane systems for hydrogen separation. Technical report, 2004.

Lin, Y. M., Liu, S. L., Chuang, C. H., and Chu, Y. T. Effect of incipient removal of hydrogen through palladium membrane on the conversion of methane steam reforming: Experimental and modeling. In *Catalysis Today*, volume 82, pages 127–139, 7 2003. doi: 10.1016/S0920-5861(03)00212-8.

Linde Gas. R1270 (CARE 45) Propylene. URL https://www.linde-gas.com/en/products_and_supply/refrigerants/natural_refrigerants/r1270_propylene/index.html.

Loyens & Loeff. The Carbon tax is coming (after all). URL https://www.loyensloeff.com/nl/en/news/news-articles/the-carbon-tax-is-coming-after-all-n19198/.

Luyben, W. L. Estimating refrigeration costs at cryogenic temperatures. *Computers and Chemical Engineering*, 103:144–150, 2017. ISSN 00981354. doi: 10.1016/j.compchemeng.2017.03.013.

Marcel Weeda, R. S. The Dutch hydrogen balance, and the current and future representation of hydrogen in the energy statistics. Technical report, 2020. URL www.tno.nl.

Marcello De Falco, Luigi Marrelli, G. I. Membrane Reactors for Hydrogen Production Processes. URL https://books.google.nl/books?id=-g2huAO89aQC&pg=PA223&lpg=PA223&dq=membrane+costs+van+delft&source=bl&ots=0Gwb7Yhp6J&sig=ACfU3U1UC7hsbsfot7SwW5oc0Zzxqowr9g&hl=en&sa=X&ved=2ahUKEwi8udbGocLpAhWQlqQKHUKHDg4Q6AEwAHoECAcQAQ#v=onepage&q=membrane%20costs%20van%.

Matches. Matches' engineering to chemical energy manufacturing metallurgical industries. URL https://www.matche.com/default.html.

Milieu centraal. Notitie CO2-emissiefactoren stroom. 2020.

Mohamad Fahrurrazi Tompang. Economic Assessment in Bio-process Plant Design. Technical report.

Molecular Sieve Desiccants. Molecular sieve 5A for Hydrogen Purification, 2020. URL https://www.molecularsievedesiccants.com/molecular-sieve-for-hydrogen-purification.

Moran, M. J. and Shapiro, H. N. Fundamentals of Engineering Thermodynamics. Technical report.

National Academy of Engineering. *The Hydrogen Economy: Opportunities, Costs, Barriers and R&D needs. Washington, DC.* National Academies Press, 2004. doi: 10.17226/10922.

Ohi, J. M., Vanderborgh, N., Consultants, G. V., Ahmed, S., Kumar, R., Papadius, D., Laboratory, A. N., Rockward, T., and Alamos, L. Hydrogen Fuel Quality Specifications for Polymer Electrolyte Fuel Cells in Road Vehicles. Technical report, 2016.

Porthos Project. CO2 reduction through storage beneath the North Sea. Technical report, 2019.

Saebea, D., Authayanun, S., Patcharavorachot, Y., and Arpornwichanop, A. Enhancement of hydrogen production for steam reforming of biogas in fluidized bed membrane reactor. *Chemical Engineering Transactions*, 39(Special Issue):1177–1182, 2014. ISSN 22839216. doi: 10.3303/CET1439197.

Sakamoto, F., Kinari, Y., Chen, F., and Sakamoto, Y. HYDROGEN PERMEATION THROUGH PALLADIUM ALLOY MEMBRANES IN MIXTURE GASES OF 10% NITROGEN AND AMMONIA IN THE HYDROGEN. Technical Report 4, 1997.

Scribd. CEPCI | Consumer Price Index | Economic Sectors. URL https://www.scribd.com/doc/121019752/CEPCI.

Seo, Y., You, H., Lee, S., Huh, C., and Chang, D. Evaluation of CO2 liquefaction processes for ship-based carbon capture and storage (CCS) in terms of life cycle cost (LCC) considering availability. *International Journal of Greenhouse Gas Control*, 35:1–12, 4 2015. ISSN 17505836. doi: 10.1016/j.ijggc.2015.01.006.

Shafiee, A., Arab, M., Lai, Z., Liu, Z., and Abbas, A. Modelling and sequential simulation of multi-tubular metallic membrane and techno-economics of a hydrogen production process employing thin-layer membrane reactor. *International Journal of Hydrogen Energy*, 41(42):19081–19097, 11 2016. ISSN 03603199. doi: 10.1016/j.ijhydene.2016.08.172.

Shirasaki, Y., Tsuneki, T., Ota, Y., Yasuda, I., Tachibana, S., Nakajima, H., and Kobayashi, K. Development of membrane reformer system for highly efficient hydrogen production from natural gas. *International Journal of Hydrogen Energy*, 34(10):4482–4487, 5 2009. ISSN 03603199. doi: 10.1016/j.ijhydene.2008.08.056.

Sigma-Aldrich. Molecular Sieves - Technical Information Bulletin. URL https://www.sigmaaldrich.com/chemistry/chemical-synthesis/learning-center/technical-bulletins/al-1430/molecular-sieves.html.

Sjardin, M., Damen, K. J., and Faaij, A. P. Techno-economic prospects of small-scale membrane reactors in a future hydrogen-fuelled transportation sector. *Energy*, 31(14):2523–2555, 2006. ISSN 03605442. doi: 10.1016/j.energy.2005.12.004.

Spath, P. L. and Mann, M. K. Life Cycle Assessment of Hydrogen Production via Natural Gas Steam Reforming. Technical report, 2001. URL http://www.doe.gov/bridge.

Szargut, J., Morris, D. R., and Steward, F. R. Exergy analysis of thermal, chemical, and metallurgical processes, 1 1987.

Terrien, P., Lockwood, F., Granados, L., and Morel, T. CO2 capture from H2 plants: Implementation for EOR. In *Energy Procedia*, volume 63, pages 7861–7866. Elsevier Ltd, 2014. doi: 10.1016/j.egypro.2014.11.821.

UNFCCC. What is the Paris Agreement? URL https://unfccc.int/process-and-meetings/the-paris-agreement/what-is-the-paris-agreement.

U.S. Department of Energy. Hydrogen Pipelines. URL https://www.energy.gov/eere/fuelcells/hydrogen-pipelines.

U.S. Department of Energy. 5 Things to Know When Filling Up Your Fuel Cell Electric Vehicle | Department of Energy, 2016. URL https://www.energy.gov/eere/articles/5-things-know-when-filling-your-fuel-cell-electric-vehicle.

U.S. Department of Energy. Hydrogen: A Clean, Flexible Energy Carrier, 2017. URL https://www.energy.gov/eere/articles/hydrogen-clean-flexible-energy-carrier.

Van Delft, Y. C., Saric, M., Meyer, D. F., De Groot, A., Overbeek, J. P., Dijkstra, J. W., and Jansen, D. Membrane reformer for large scale production of hydrogen TOWARDS THE APPLICATION OF PALLADIUM MEMBRANE REACTORS IN THE LARGE SCALE PRODUCTION OF HYDROGEN. Technical report, 2009.

Voldsund, M., Jordal, K., and Anantharaman, R. Hydrogen production with CO2 capture, 3 2016. ISSN 03603199.

Witkowski, A., Majkut, M., and Rulik, S. Analysis of pipeline transportation systems for carbon dioxide sequestration. *Archives of Thermodynamics*, 35(1):117–140, 2014. ISSN 20836023. doi: 10.2478/aoter-2014-0008.

Xu, G., Liang, F., Yang, Y., Hu, Y., Zhang, K., and Liu, W. An improved CO2 separation and purification system based on cryogenic separation and distillation theory. *Energies*, 7(5):3484–3502, 2014. ISSN 19961073. doi: 10.3390/en7053484.

Yuanying Industry Limited. The service lifetime of molecular sieves, 2015. URL http://www.yyindustry.com/news_show.asp?id=28.

Yun, S. and Ted Oyama, S. Correlations in palladium membranes for hydrogen separation: A review, 6 2011. ISSN 03767388.

Zăbavă, B.-□., Voicu, G., and Ungureanu, N. METHODS OF BIOGAS PURIFICATION-A REVIEW. Technical report, 2019. URL https://www.researchgate.net/publication/330666040.

ZR Catalyst. 5A Molecular sieve adsorbents. URL https://www.zr-catalyst.com/Products/18.html?gclid=CjwKCAjw5cL2BRASEiwAENqAPlYWSwQ3G7Dh-7_HQNMlBzWU-McTdswjztrtVWJTPqTfk5Hiv61-PhoCuc4QAvD_BwE.

A

Aspen models

The aspen model for the optimum process and the three configurations developed is shown here.

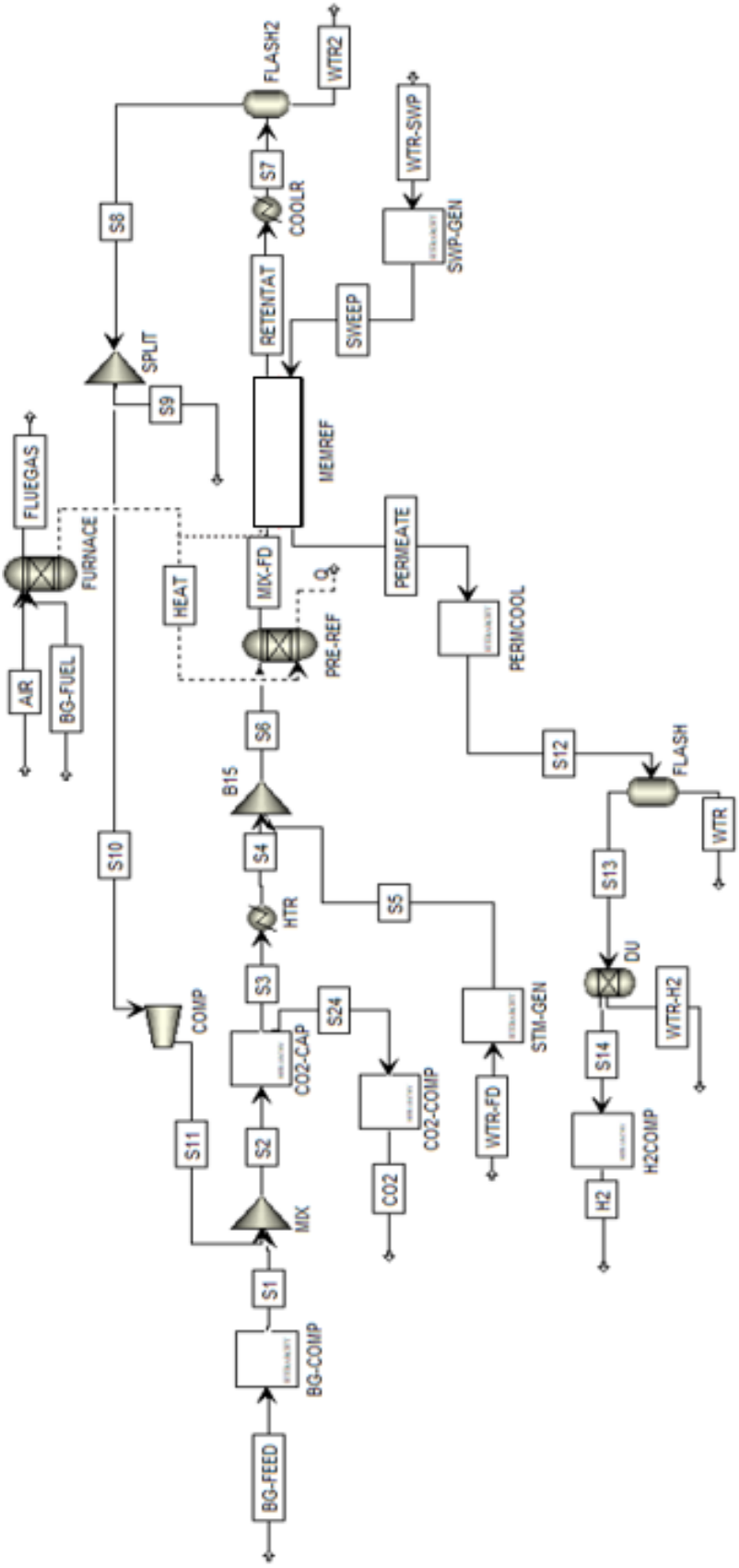

Figure A.1: Aspen model of Configuration 1: process with carbon capture unit before the reforming section.

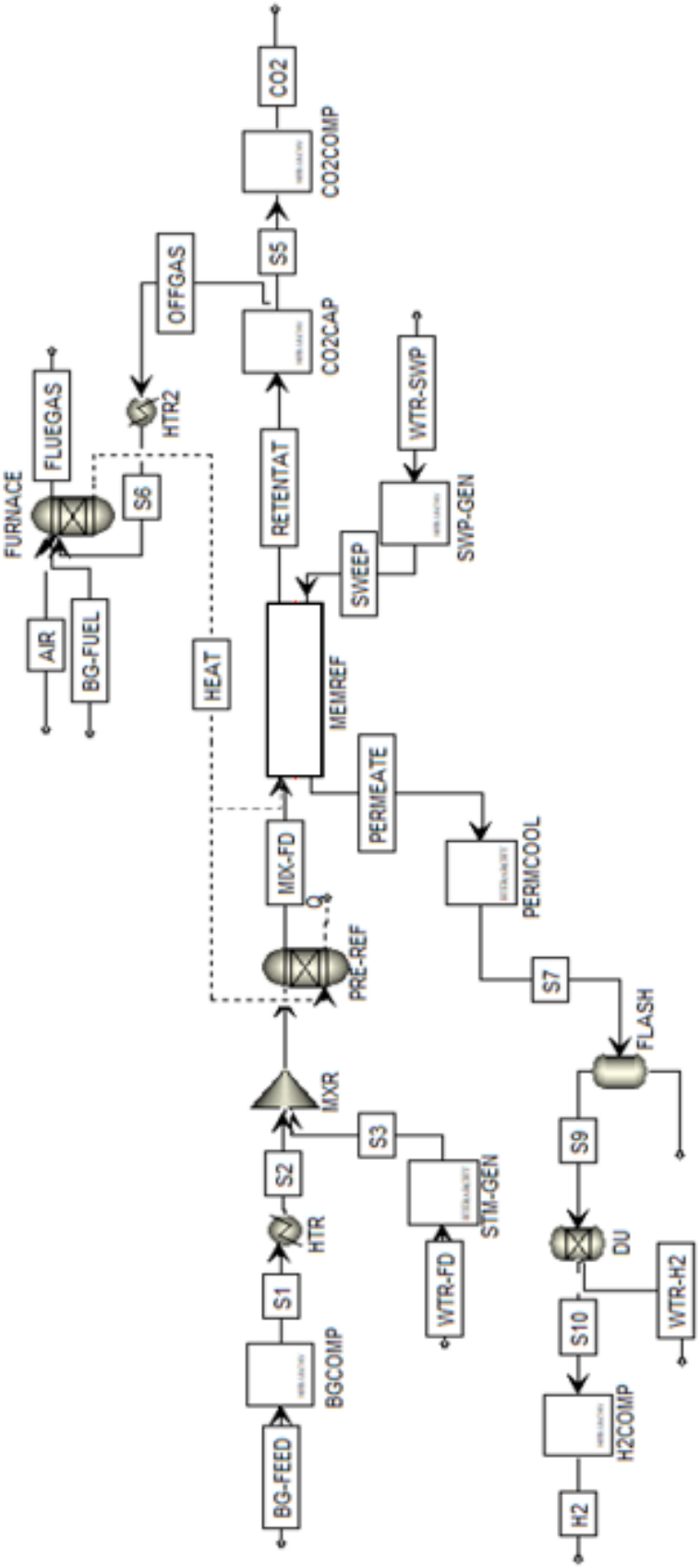

Figure A.2: Aspen model of Configuration 2: process with carbon capture unit after the reforming section without recycle stream.

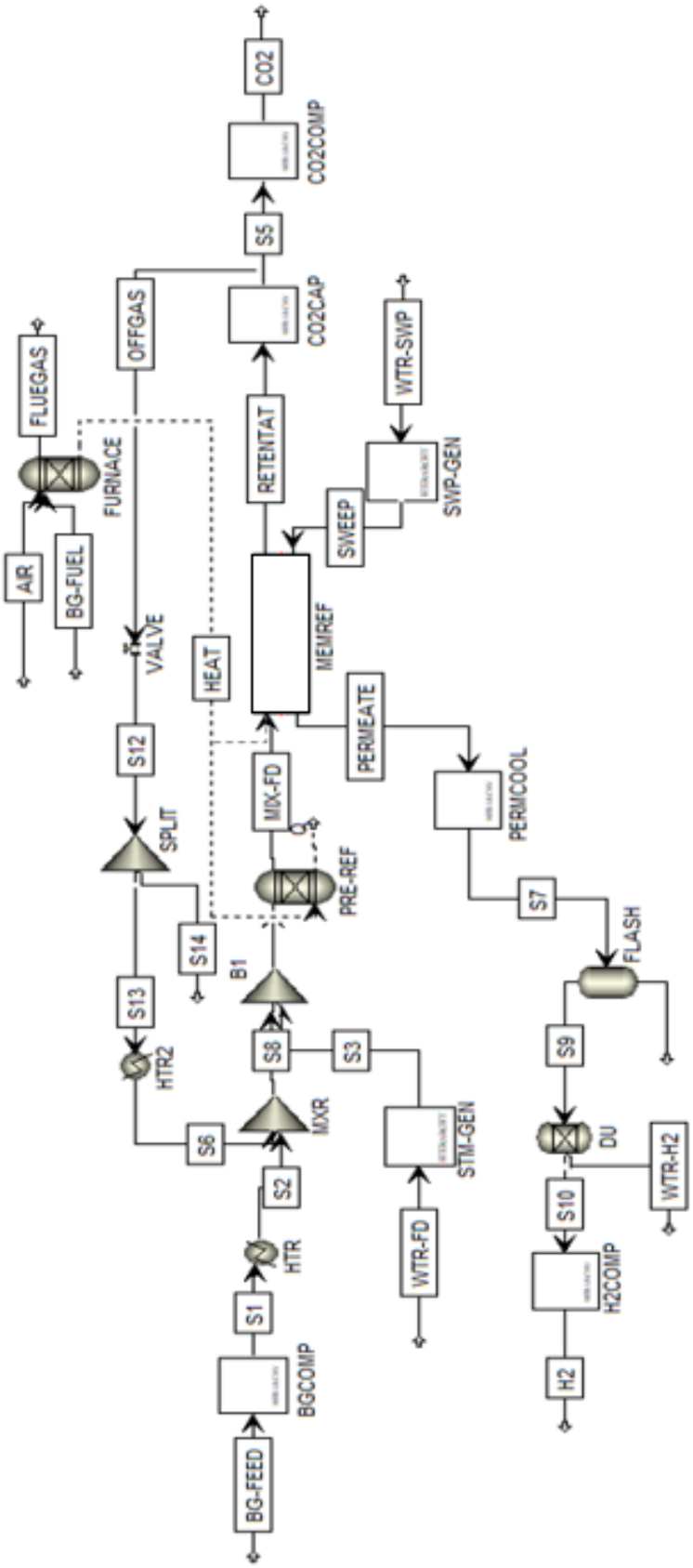

Figure A.3: Aspen model of Configuration 3: process with carbon capture unit after the reforming section with recycle stream.

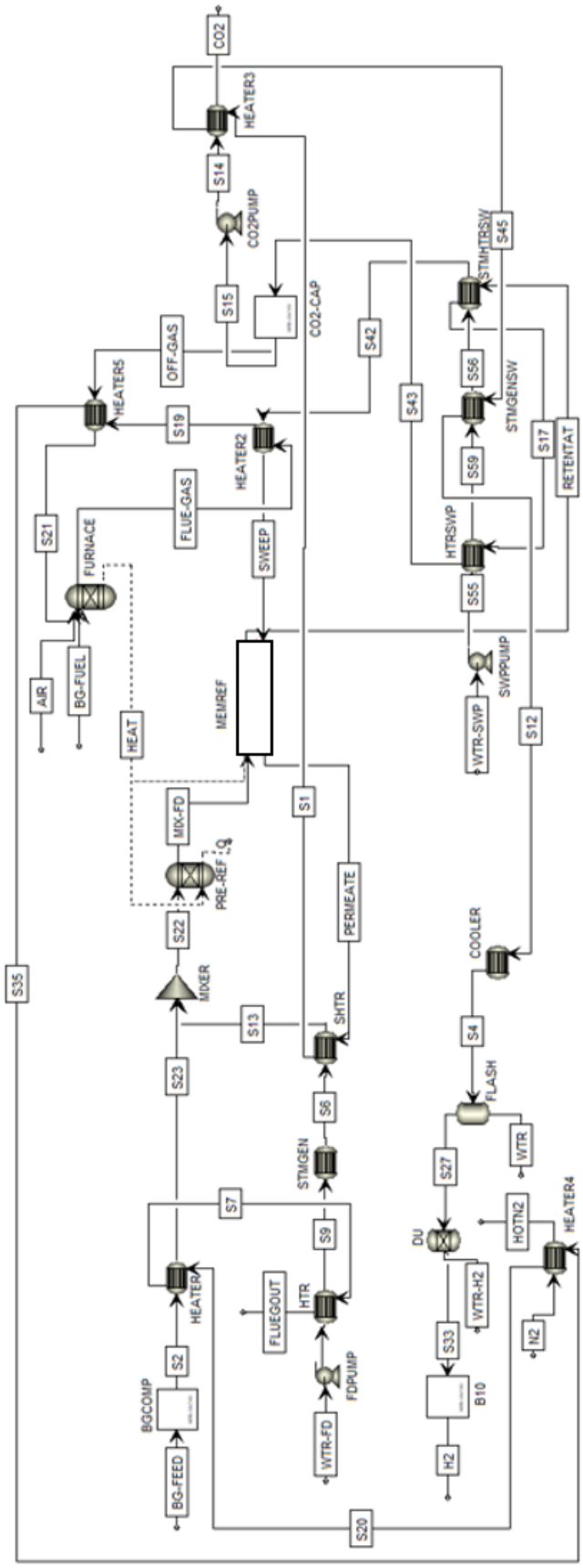

Figure A.4: Aspen model of the optimum process.

The carbon capture unit of the optimum process shown in figure A.4 is expanded in figure A.5.

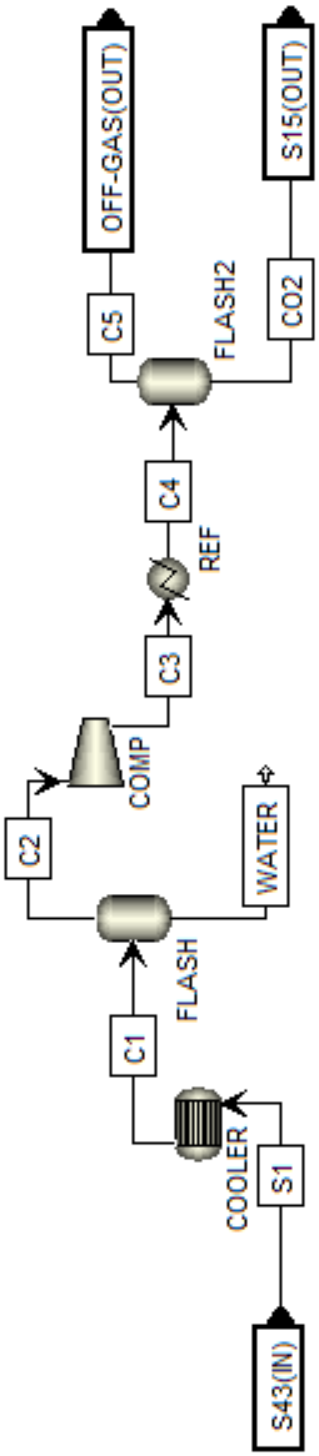

Figure A.5: Aspen model of the carbon capture unit of the optimum process.

B

Performance results of the three configurations

The results of the three configurations based on the cases formulated in chapter 4 are represented here. The sensitivity of KPIs towards change in the process parameters is described.

B.1. Process with carbon capture unit before the membrane reactor

The performance values of different cases for this process will be compared and the trends will be analysed to see how changing certain parameters affects the performance of the process.

B.1.1. Sweep ratio: Base case, Case 2.1, Case 2.2 & Case 2.3

The following graphs B.1 & B.2 display the global hydrogen recovery factor & carbon capture rate vs productivity for different sweep ratios.

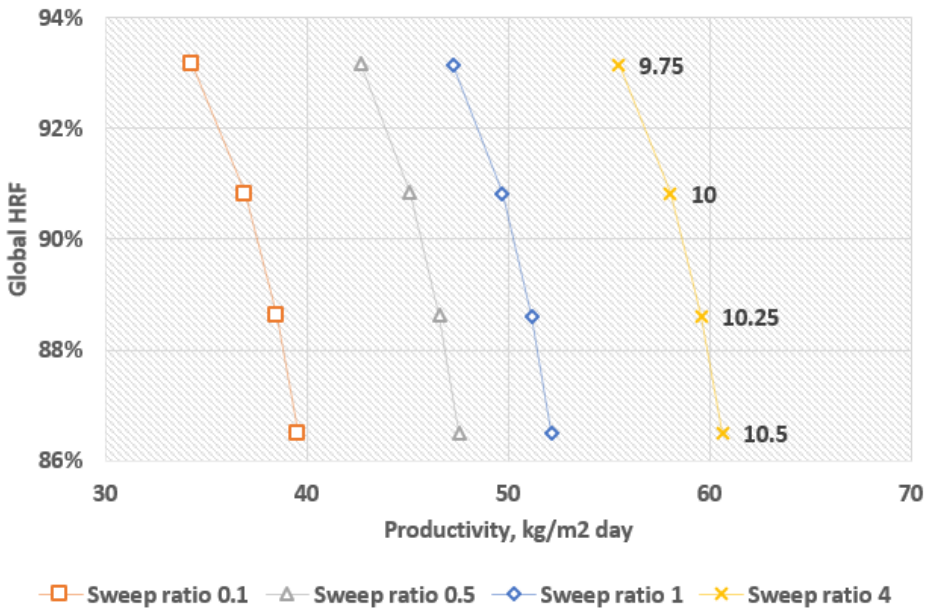

Figure B.1: Global hydrogen recovery factor vs productivity for different sweep ratios, varying biogas feed from 9.75 to 10.5 kmol/h.

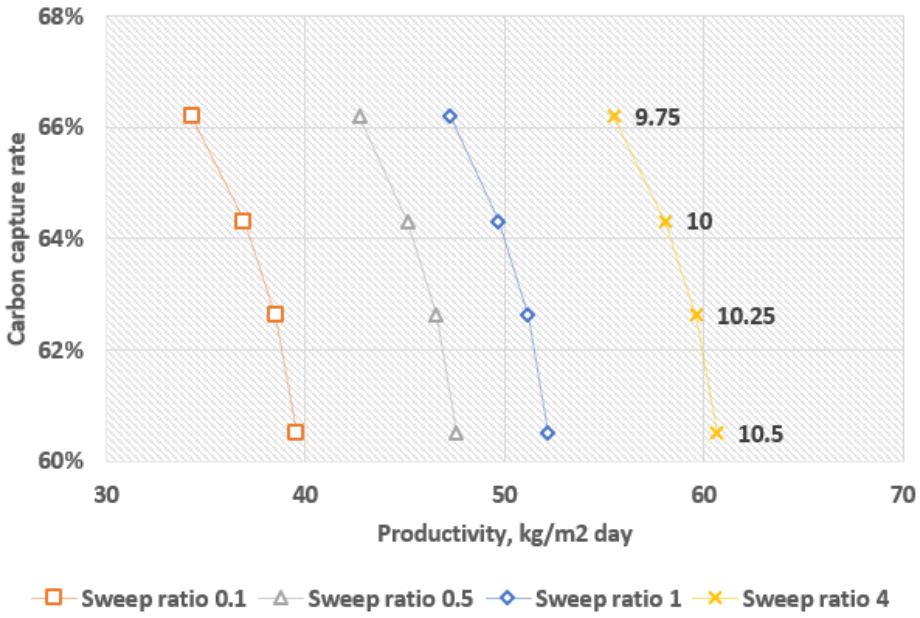

Figure B.2: Carbon capture rate vs productivity for different sweep ratios, varying biogas feed from 9.75 to 10.5 kmol/h.

Considering the global HRF for sweep ratio 0.5 in figure B.1 as a reference, we can see that as the productivity increases the HRF decreases. Productivity is the ratio of hydrogen output to the membrane surface area. As the hydrogen output is constant in all the cases, this in turn means that the HRF decreases with decrease in area, as expected. A higher HRF is obtained with lower biogas flow rate (one would expect to achieve a higher HRF with higher biogas flow rate but that is not the case here because the hydrogen output of the process is constant as mentioned earlier.) However, the membrane surface area is larger compared to the HRF value for biogas feed of 10.5 kmol/h. It is expected that the operating expenditure will have a higher impact on the economics than the capital expenditure. Generally, the membrane cost is considered to be a dominant factor for membrane reforming. However, the membrane cost for this work is selected assuming sufficient technological advancements that reasonably bring down the cost of the membrane. The productivity decrease (area increase) for the lower biogas flow rate isn't very large. Therefore, a higher HRF value with lower productivity is expected to be a better choice. For example, for a sweep ratio of 0.5 a HRF of 93.15% with a productivity of 42.70 kg/m^2 day is preferred over a HRF of 86.5% with productivity of 47.58 kg/m^2 day.

Furthermore, if we compare the results of different sweep ratios, we see that a higher sweep ratio gives a better performance. This is because, although the HRF values do not increase, the productivity increases (area decreases). This is because a higher sweep ratio results in a higher driving force for hydrogen permeation through the membrane, thereby requiring less surface area for the same hydrogen product. Hence, a higher sweep ratio should be selected. However, as seen in figure B.5, the decrease in area for higher sweep ratios is not so significant. Furthermore, a higher sweep ratio would mean more costs to generate steam and in turn to separate the hydrogen product from the permeate stream. Figures B.3, B.4 & B.5 show the change in work, duties and area w.r.t the sweep ratio for a biogas feed flow rate of 10.5 kmol/h (Base case). The trend for other values of biogas flow rate is the same, therefore only one case is shown.

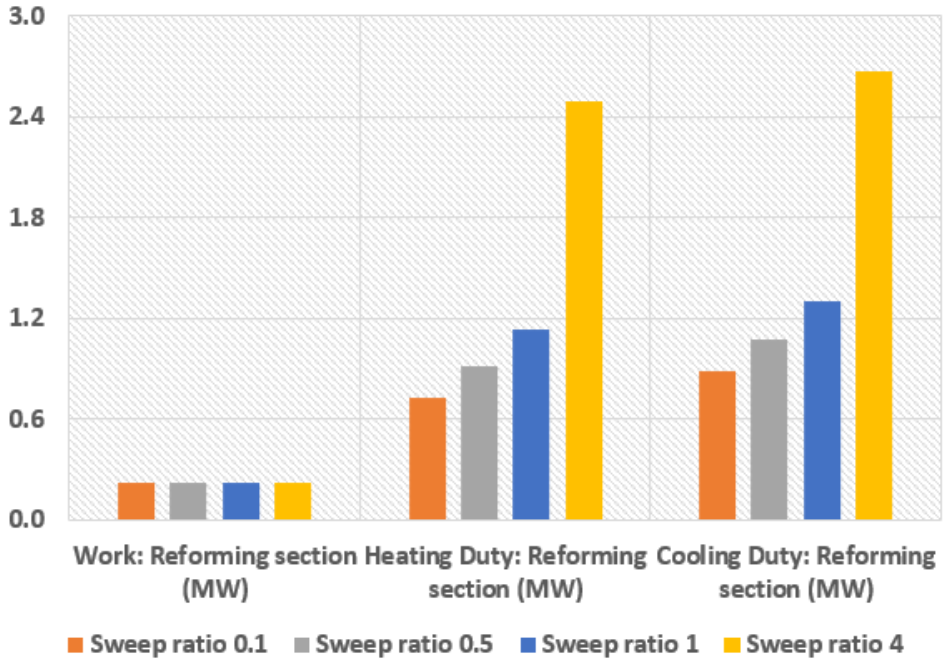

Figure B.3: Work & duties (reforming section) for different sweep ratios with biogas feed of 10.5 kmol/h.

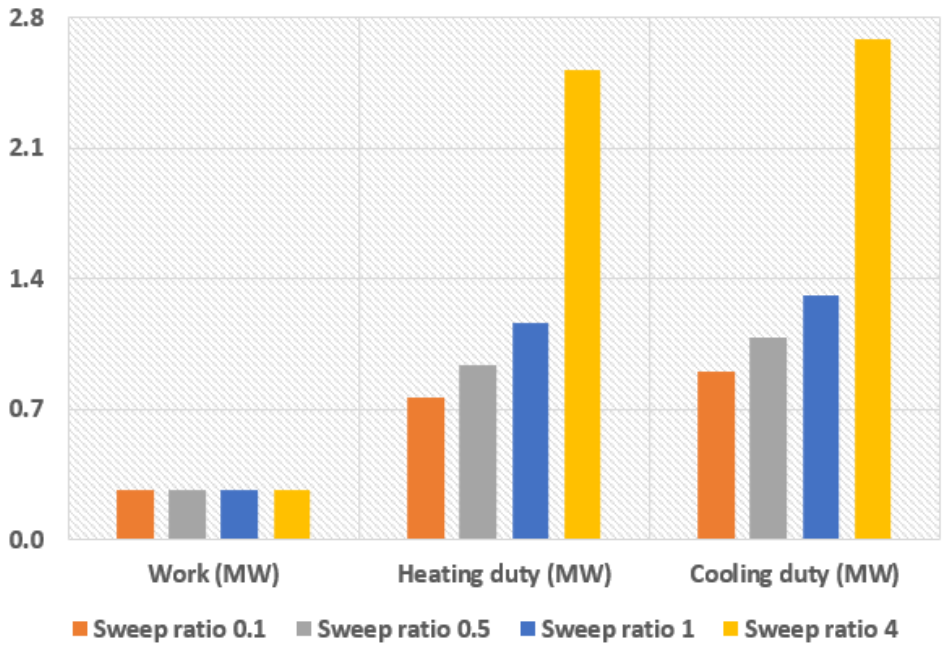

Figure B.4: Total Work & duties of the process for different sweep ratios with biogas feed of 10.5 kmol/h.

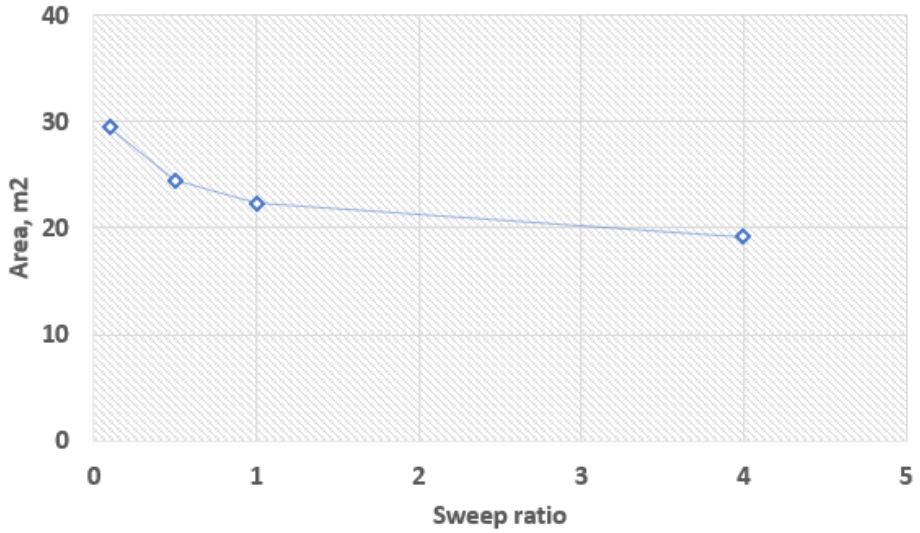

Figure B.5: Membrane surface area vs sweep ratio.

A detailed economic analysis should be performed to determine the best trade-off between reduced membrane area cost vs increased sweep generation & permeate separation costs. This analysis is done in chapter 5, section 5.2.2. A similar trend for the carbon capture rate w.r.t. the sweep ratios is seen in figure B.2 with values ranging from approximately 60.5% to 66% for biogas feed 10.5 to 9.75 kmol/h respectively.

The following graphs B.6 & B.7 display the global methane conversion & global efficiency vs productivity for different sweep ratios.

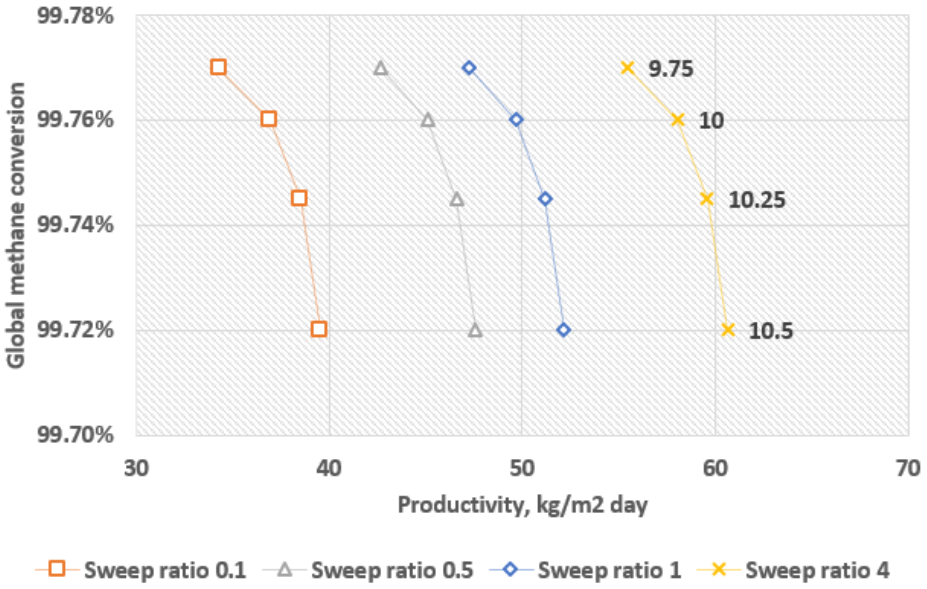

Figure B.6: Global methane conversion vs productivity for different sweep ratios varying biogas feed from 9.75 to 10.5 kmol/h.

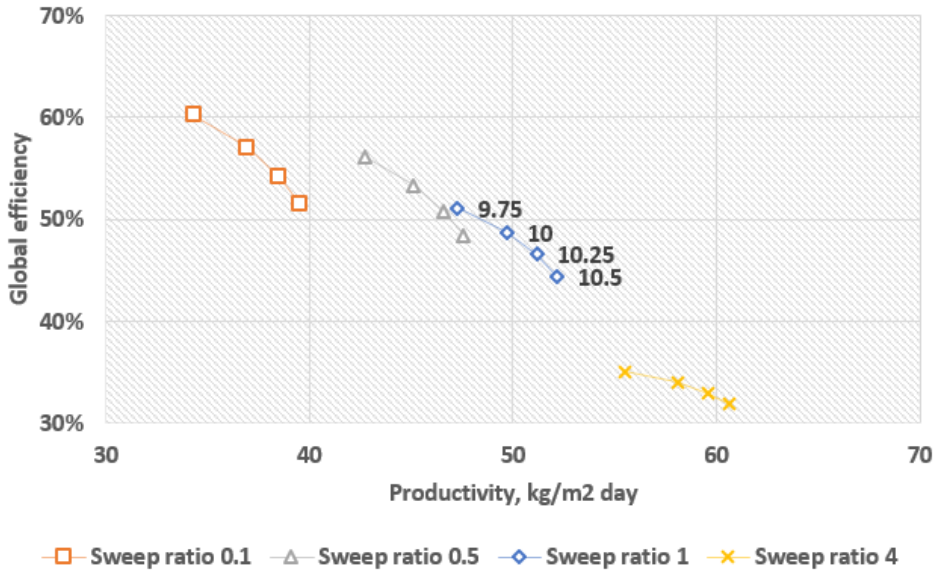

Figure B.7: Global efficiency vs productivity for different sweep ratios varying biogas feed from 9.75 to 10.5 kmol/h.

The global methane conversion w.r.t. sweep ratios also has a similar trend like the global HRF and carbon capture rate. However, the change in value for different biogas flow rates isn't very significant. The values range from 99.72% to 99.77% for biogas flow rates of 10.5 to 9.75 kmol/h, see figure B.6. One would expect the methane conversion to increase with the increase in biogas flow rate. However, it is important to remember that the hydrogen output is constant, which means a biogas flow rate of 10.5 kmol/h will require a lesser conversion than a biogas flow rate of 9.75 kmol/h for the same output of hydrogen. Furthermore, as expected, the global efficiency decreases with increase in the sweep ratio. The efficiency with sweep ratio 4 is considerably low (between 32% to 35%).

In conclusion, assuming the operating expenditure will have a larger impact on the cost of hydrogen, a lower sweep ratio should be chosen and a lower biogas feed (i.e. 9.75 kmol/h) for low levelized cost of hydrogen.

B.1.2. Recycle ratio: Base case & Case 3.1

The performance of this process is analysed when changing the recycle ratio (RR). A recycle ratio lower than 0.5 results in undesirably low carbon capture rates and therefore not worth considering.

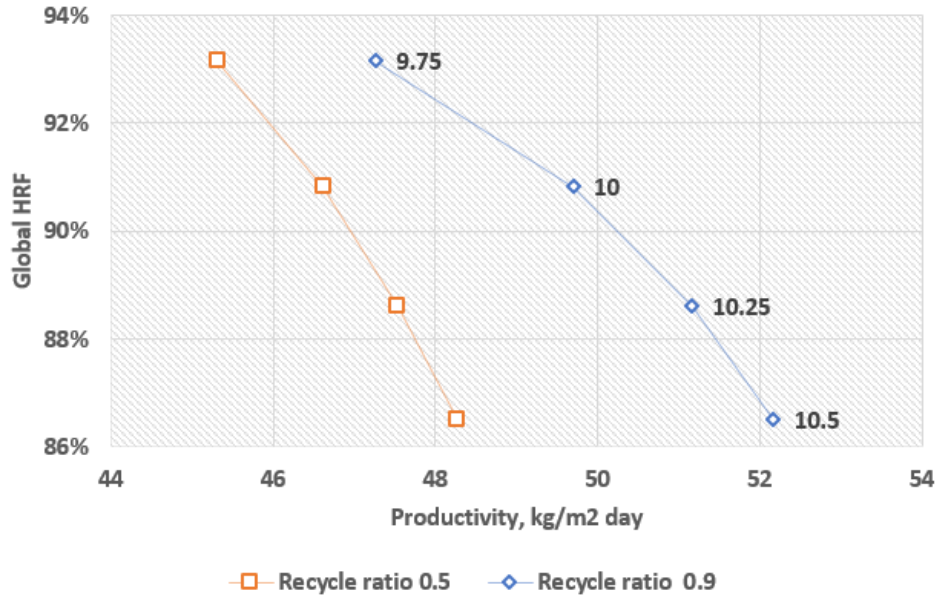

Figure B.8: Global hydrogen recovery factor vs productivity for different recycle ratios varying biogas feed from 9.75 to 10.5 kmol/h.

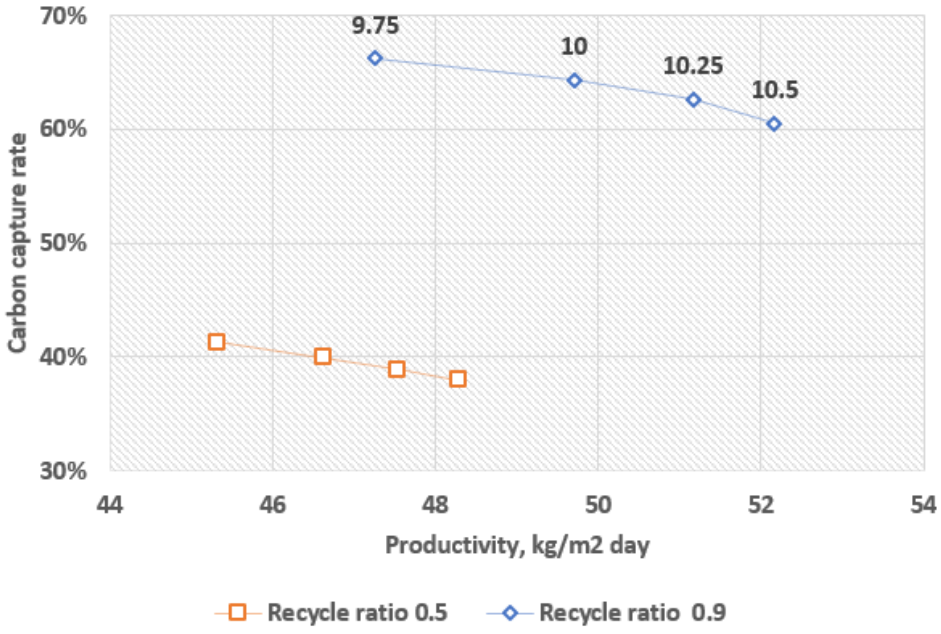

Figure B.9: Carbon capture rate vs productivity for different recycle ratios varying biogas feed from 9.75 to 10.5 kmol/h.

The hydrogen recovery factor for both the cases i.e. recycle ratio 0.9 and 0.5 is the same because the hydrogen output as well as the biogas flow rates for the cases is the same, see figure B.8. However, the productivity for RR 0.9 is higher. This means that the area required for the same output of hydrogen is lower. This is because with a higher RR, more amount of un-permeated hydrogen from the retentate side is fed back into the membrane reactor resulting in a higher driving force for permeation at the inlet. However, higher RR means more amount of recycle stream to be handled resulting in higher operating costs (figure B.14). The per-pass hydrogen recovery factor changes with recycle ratio as shown in figure B.10 unlike when the sweep ratio or the permeate pressure is changed. The per-pass HRF is higher for a lower RR with the same logic as explained for the global HRF.

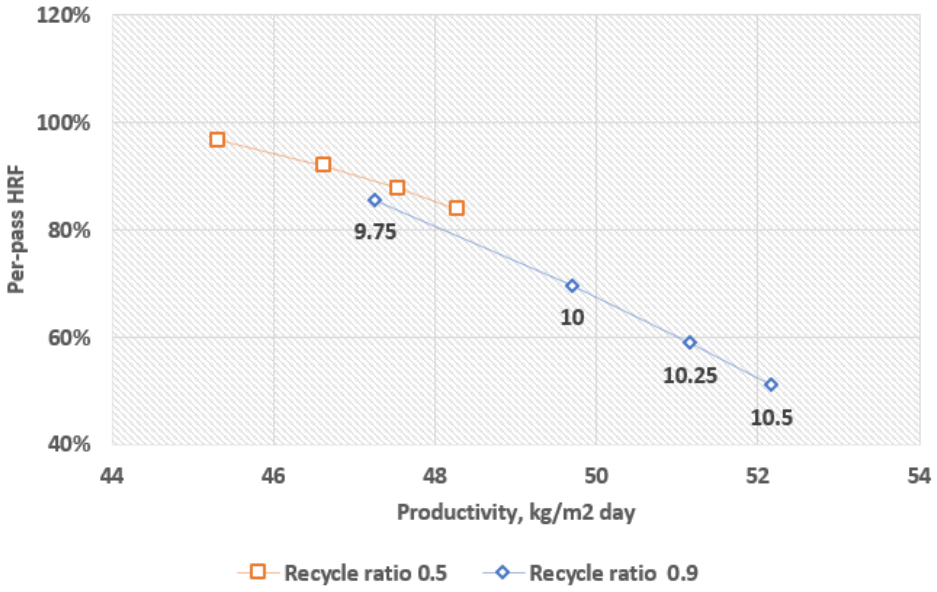

Figure B.10: Per-pass hydrogen recovery factor vs productivity for different recycle ratios varying biogas feed from 9.75 to 10.5 kmol/h.

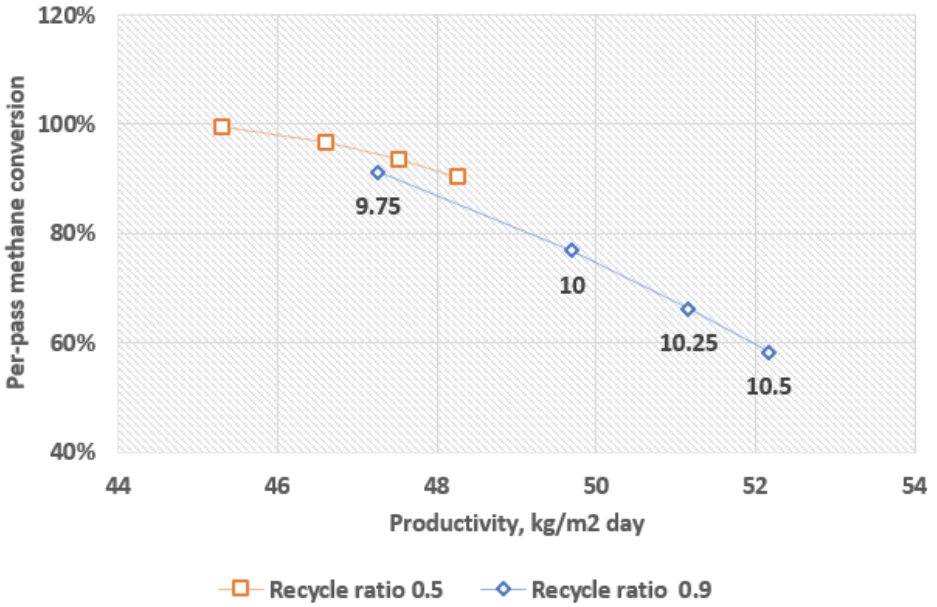

Figure B.11: Per-pass methane conversion vs productivity for different recycle ratios varying biogas feed from 9.75 to 10.5 kmol/h.

In case of the carbon capture rate, figure B.9, a lower RR captures considerably lesser CO_2. This is because, the carbon capture unit is before the membrane reactor & there is considerable amount of CO_2 produced in the membrane reactor. Which means, if a lower percent of the produced CO_2 (retentate stream) is recycled to the carbon capture unit, a lower carbon capture rate is achieved. Furthermore, a higher RR results in a higher productivity with the same logic as explained before. Considering all aspects, a higher RR is preferred.

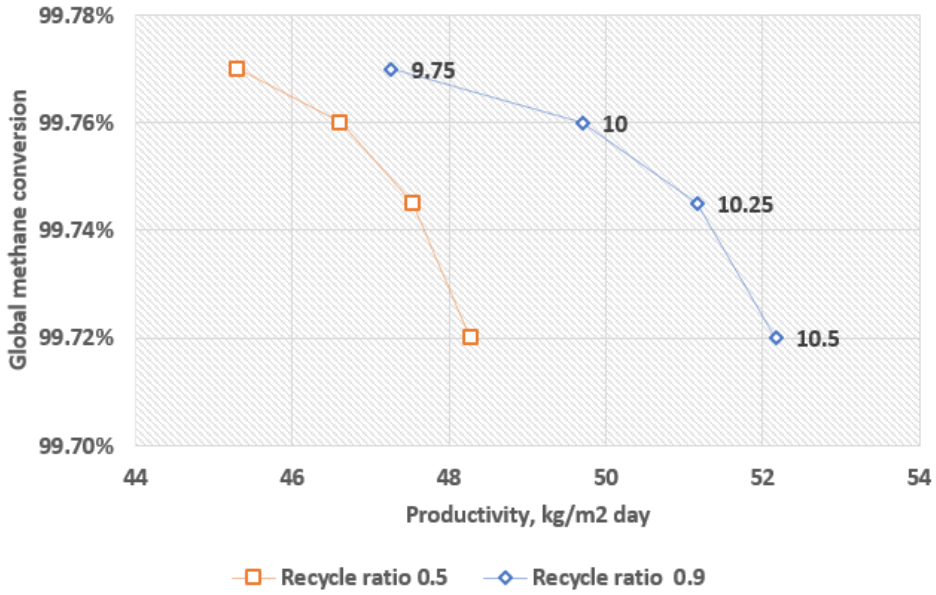

Figure B.12: Global methane conversion vs productivity for different recycle ratios varying biogas feed from 9.75 to 10.5 kmol/h.

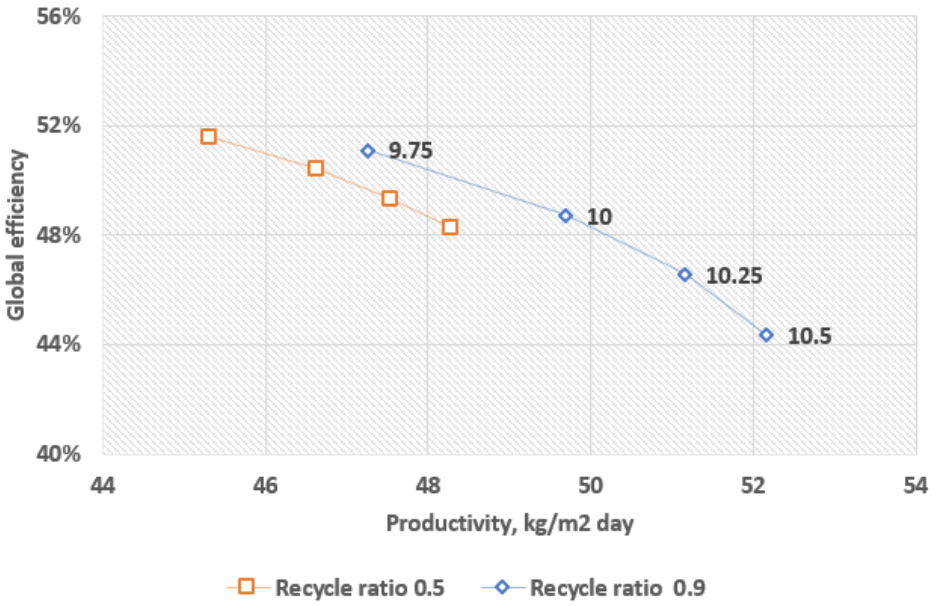

Figure B.13: Global efficiency vs productivity for different recycle ratios varying biogas feed from 9.75 to 10.5 kmol/h.

A similar trend can be seen for the global methane conversion for different RR, figure B.12. The per-pass methane conversion is also shown in B.11. A higher global efficiency for RR of 0.5 is expected as the work & duties required will be lower, considering a lower flow rate. However, the increase in efficiency is not substantial. A case with RR of 0.9 and biogas feed of 9.75 kmol/h gives better efficiency than a case with RR of 0.5 and biogas feed of 10.5 kmol/h.

The work required, heating and cooling duties for the different recycle ratios is shown is figure B.14, B.15 & B.16 for the overall process, the reforming section and the carbon capture section respectively. These values are for a biogas feed flow rate of 10.5 kmol/h.

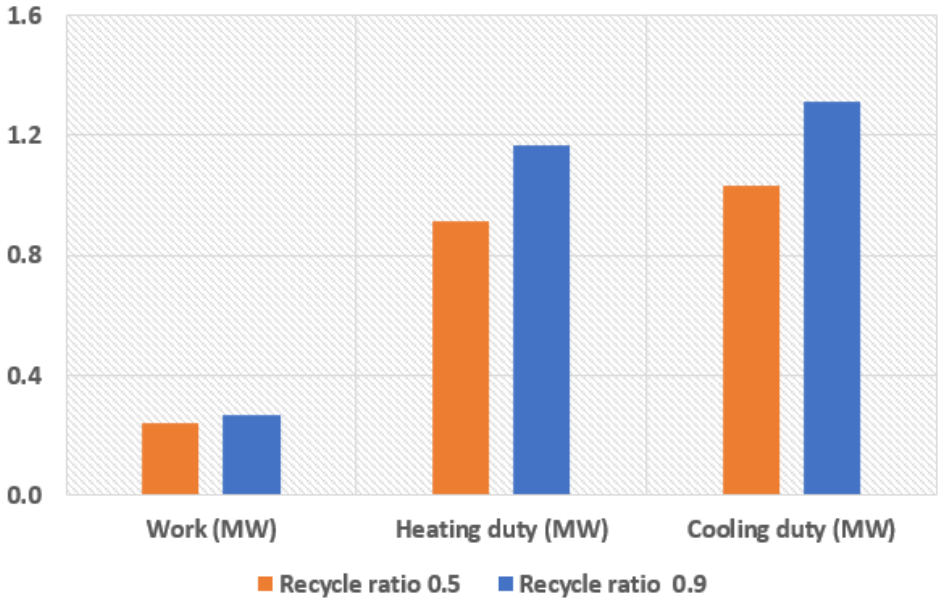

Figure B.14: Total work & duties of the process for different recycle ratios with biogas feed of 10.5 kmol/h.

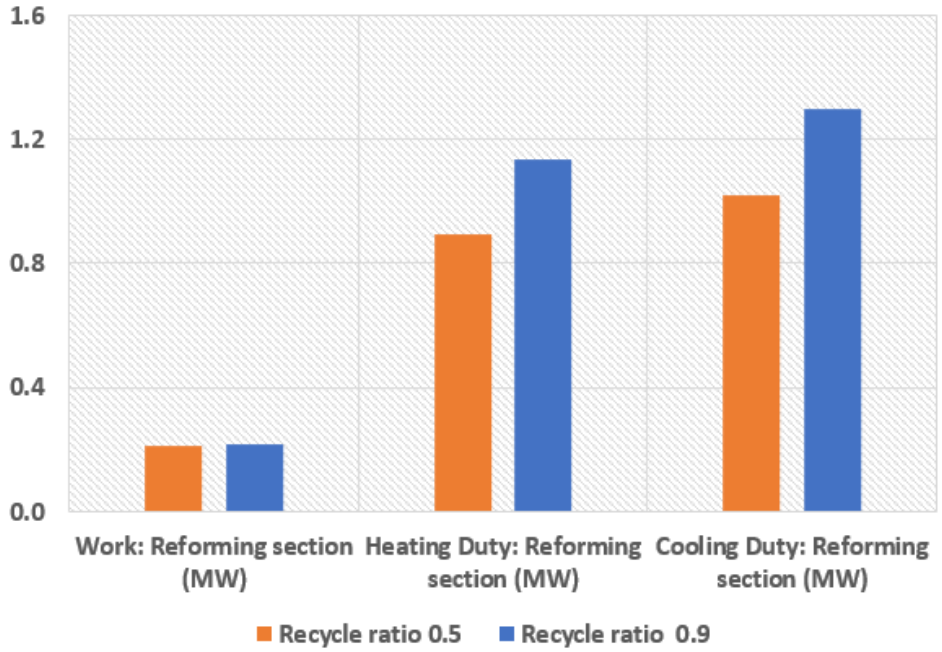

Figure B.15: Work & duties (reforming section) for different recycle ratios with biogas feed of 10.5 kmol/h.

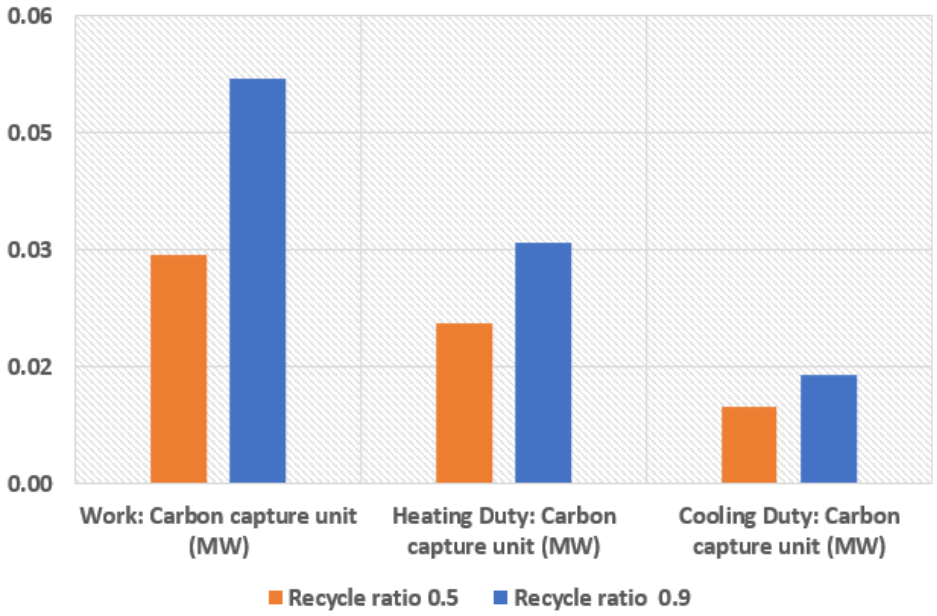

Figure B.16: Work & duties (carbon capture unit) for different recycle ratios with biogas feed of 10.5 kmol/h.

A higher RR results in better performance for most of the performance indicators and the efficiency values aren't significantly different, however the heating and cooling duties are higher. A higher RR will be preferable in terms of economics if the reduction is area costs is more than the increase in cost of duty required. Keeping in mind the unacceptably low carbon capture rates for lower RR, a higher RR is preferred even at higher costs.

B.1.3. Permeate pressure: Base case, Case 4.1, Case 4.2 & Case 4.3

The trend for global HRF, carbon capture rate, global methane conversion is very similar to the cases with changing sweep ratios (Base case, case 2.1 to 2.3).

Figure B.19 shows the methane conversion for different permeate pressures. A higher biogas flow rate gives a lower conversion. This is because the amount of hydrogen output is the same for all the cases, an a higher biogas feed will mean a lower percentage of hydrogen produced and in turn a lower methane conversion. Therefore, for better conversions a lower biogas flow rate should be chosen. However, this results in a slight decrease in productivity (increase in area) because of lower driving force. It is assumed that the increase in methane conversion can compensate the increase the area required as the increase in area isn't significant.

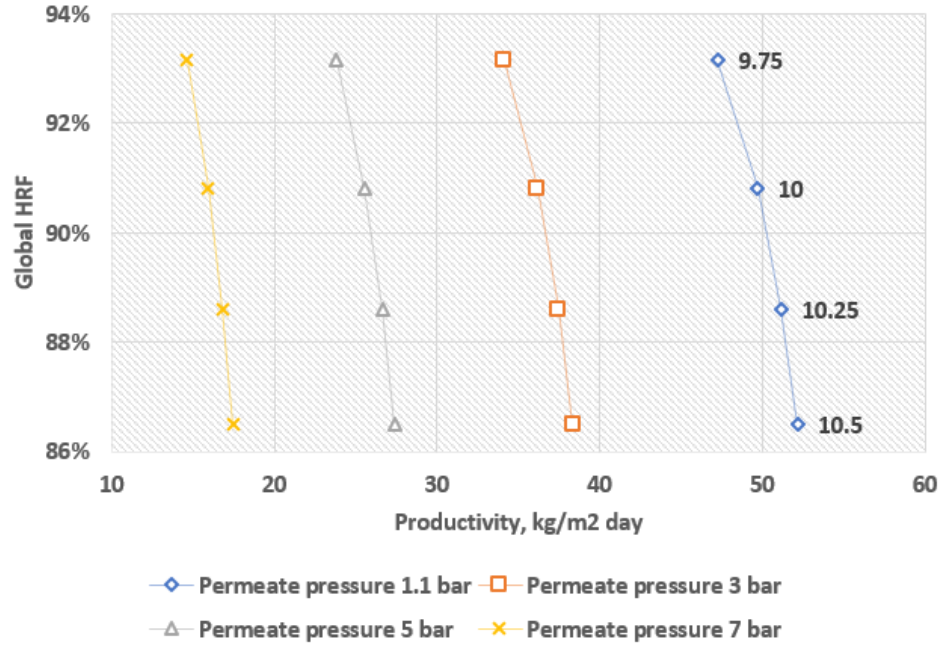

Figure B.17: Global hydrogen recovery factor vs productivity for different permeate pressures varying biogas feed from 9.75 to 10.5 kmol/h.

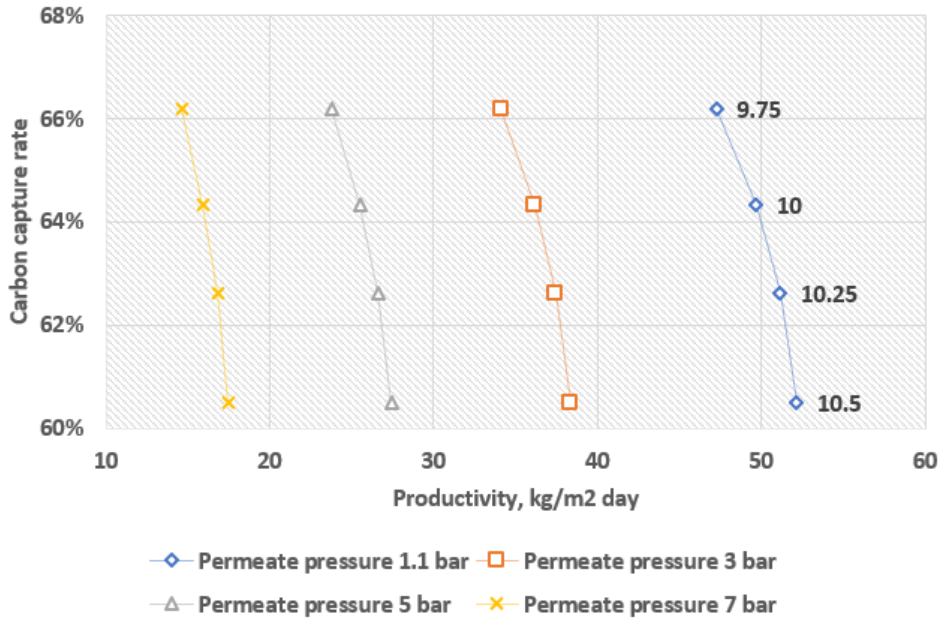

Figure B.18: Carbon capture rate vs productivity for different permeate pressures varying biogas feed from 9.75 to 10.5 kmol/h.

Furthermore, when comparing different permeate pressures, it can be seen that a lower permeate pressure results in a higher productivity. This means a lower area owing to the fact that the partial pressure difference of hydrogen between the feed and the permeate side in higher. A higher difference in pressure requires a lesser amount of area for the same hydrogen output.

However, a lower permeate pressure will mean high hydrogen compressor load resulting in lower efficiencies (figure B.20). As the hydrogen needs to be compressed to 700 bar, even a slight increase in the permeate pressure may result in a considerably lower compressor load, resulting in higher efficiency. A trade-off between increase in area cost and decrease in hydrogen compression cost is

needed to determine the optimum permeate pressure, refer chapter 5, section 5.2.2. The membrane area and hydrogen compression work required for different permeate pressures is shown in figure B.21. The process work and duties required for different permeate pressures at biogas feed flow rate of 10.5 kmol/h is shown in B.22.

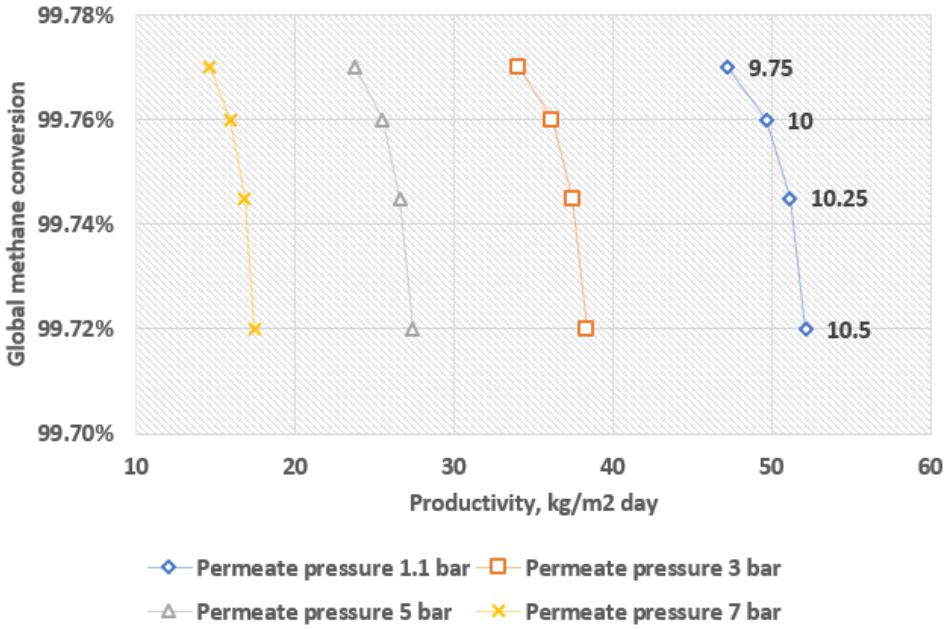

Figure B.19: Global methane conversion vs productivity for different permeate pressures varying biogas feed from 9.75 to 10.5 kmol/h.

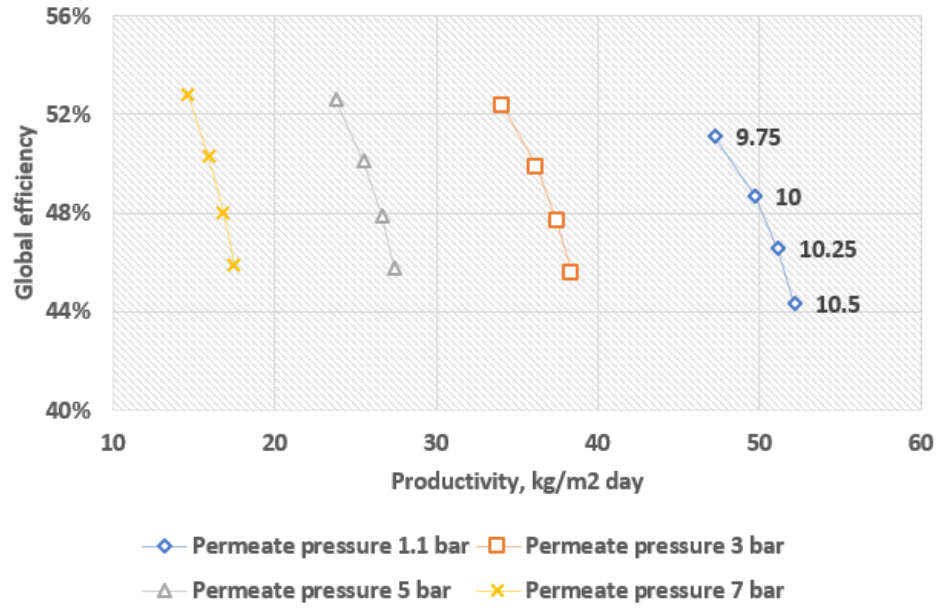

Figure B.20: Global efficiency vs productivity for different permeate pressures varying biogas feed from 9.75 to 10.5 kmol/h.

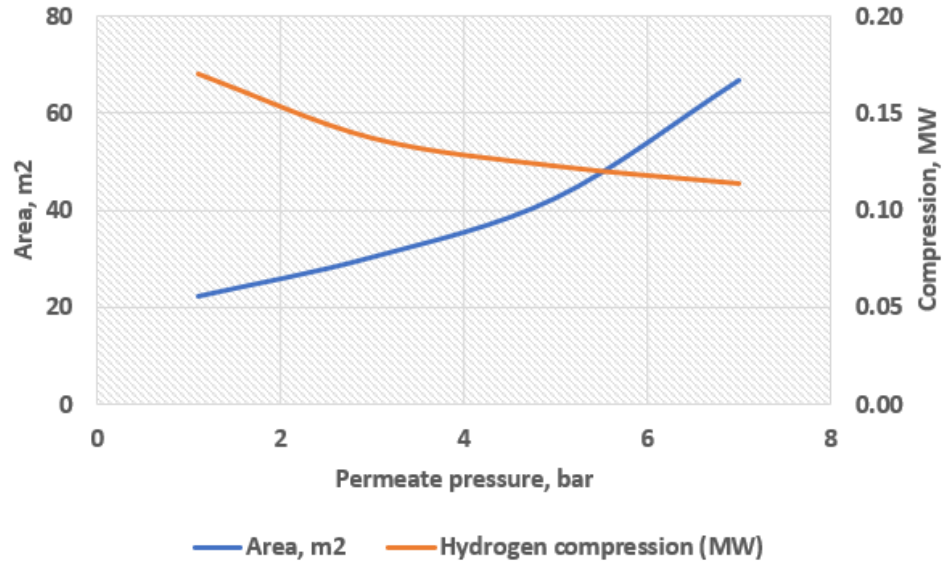

Figure B.21: Membrane surface area vs hydrogen compression work for different permeate pressures.

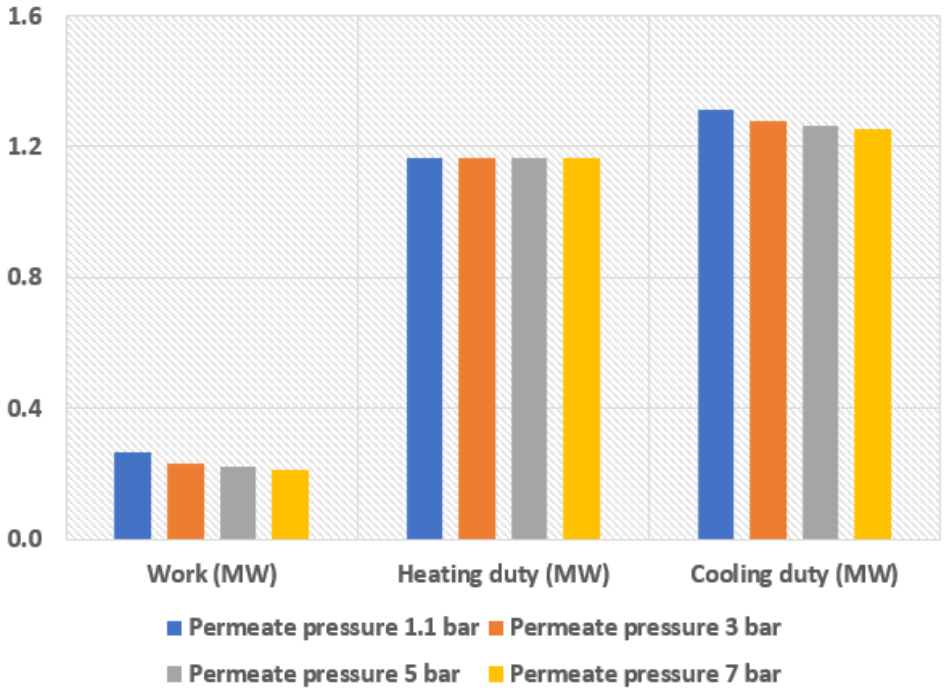

Figure B.22: Total Work & duties of the process for different permeate pressures with biogas feed of 10.5 kmol/h.

The global methane conversion and the global hydrogen recovery factor have the same range for the different cases. The is because the hydrogen output and the biogas feed flow rates are the same for all, which result in the same values.

B.2. Process with carbon capture unit after the membrane reactor: without recycle of off-gases

For this configuration too, similar graphs are presented. The trends for most of the performance indicators are the same. Therefore, elaborate explanations aren't provided.

B.2.1. Sweep ratio: Base case, Case 2.1, Case 2.2 & Case 2.3

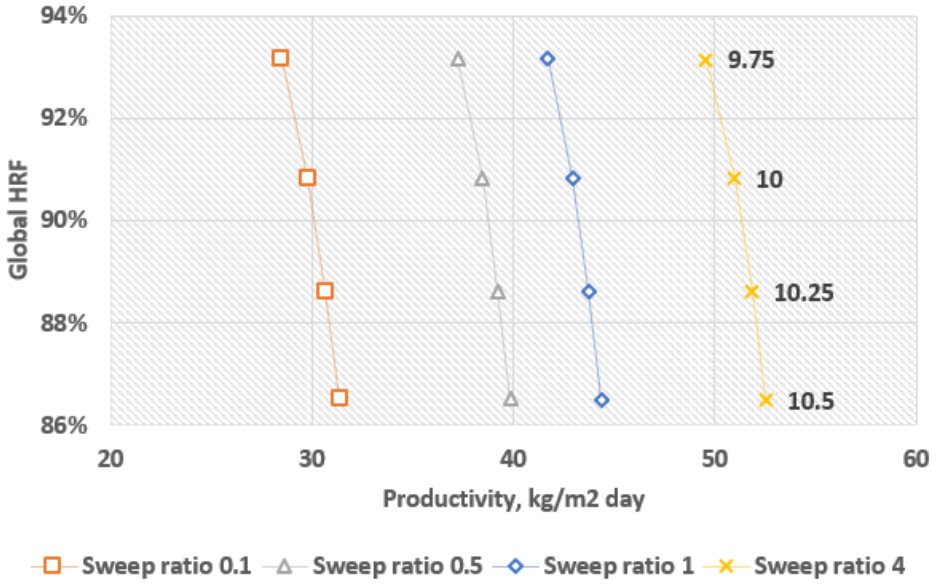

Figure B.23: Global hydrogen recovery factor vs productivity for different sweep ratios varying biogas feed from 9.75 to 10.5 kmol/h.

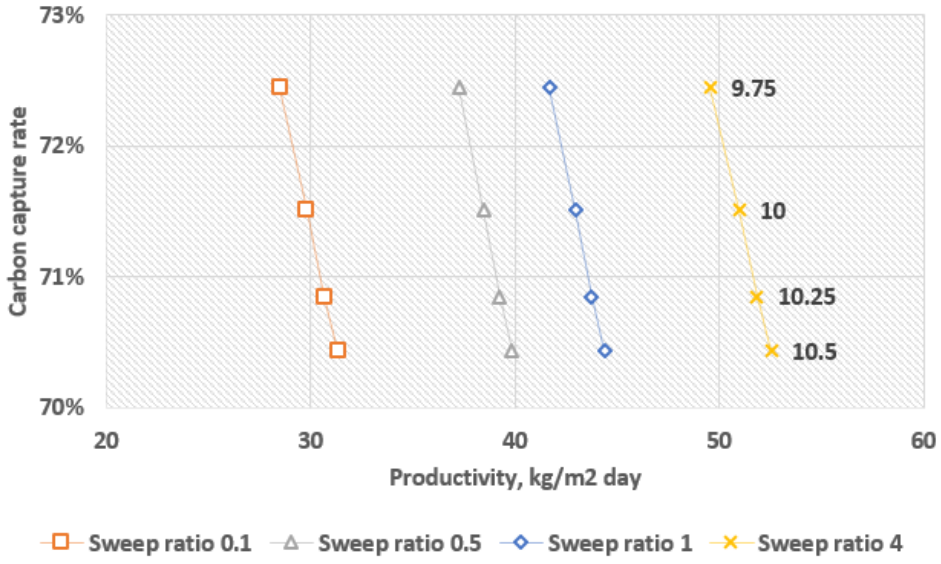

Figure B.24: Carbon capture rate vs productivity for different sweep ratios varying biogas feed from 9.75 to 10.5 kmol/h.

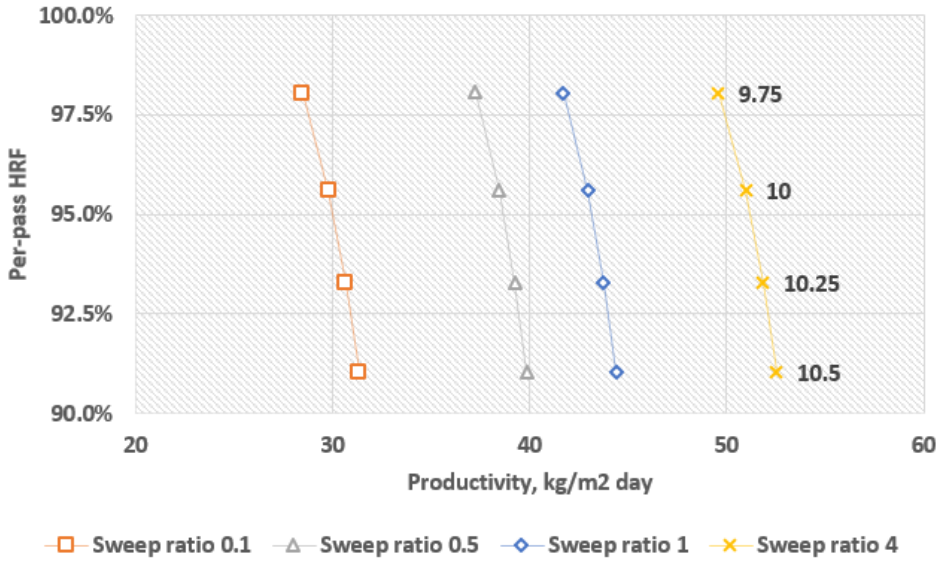

Figure B.25: Per-pass hydrogen recovery factor vs productivity for different sweep ratios varying biogas feed from 9.75 to 10.5 kmol/h.

With no recycle stream, the global and per-pass values for the HRF and methane conversion are expected to be same. However, the global and per-pass HRF aren't the same. This is because, some percentage of hydrogen is lost in the dehydration unit upstream the membrane reactor. Therefore, the per-pass hydrogen recovery across the membrane reactor is higher than the global hydrogen recovery. The per-pass HRF is shown in figure B.25. The same trends for the HRF is obtained for the permeate pressure.

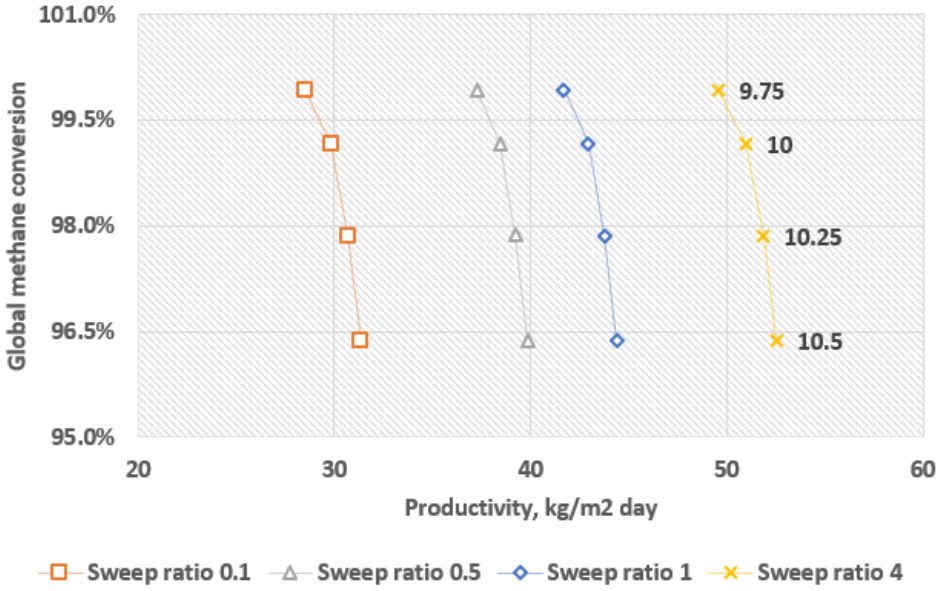

Figure B.26: Global methane conversion vs productivity for different sweep ratios varying biogas feed from 9.75 to 10.5 kmol/h.

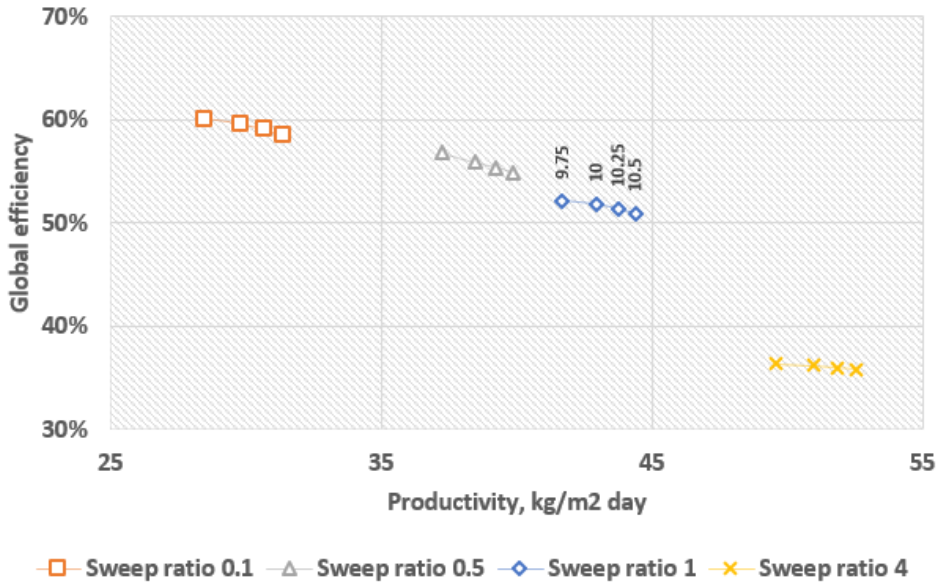

Figure B.27: Global efficiency vs productivity for different sweep ratios varying biogas feed from 9.75 to 10.5 kmol/h.

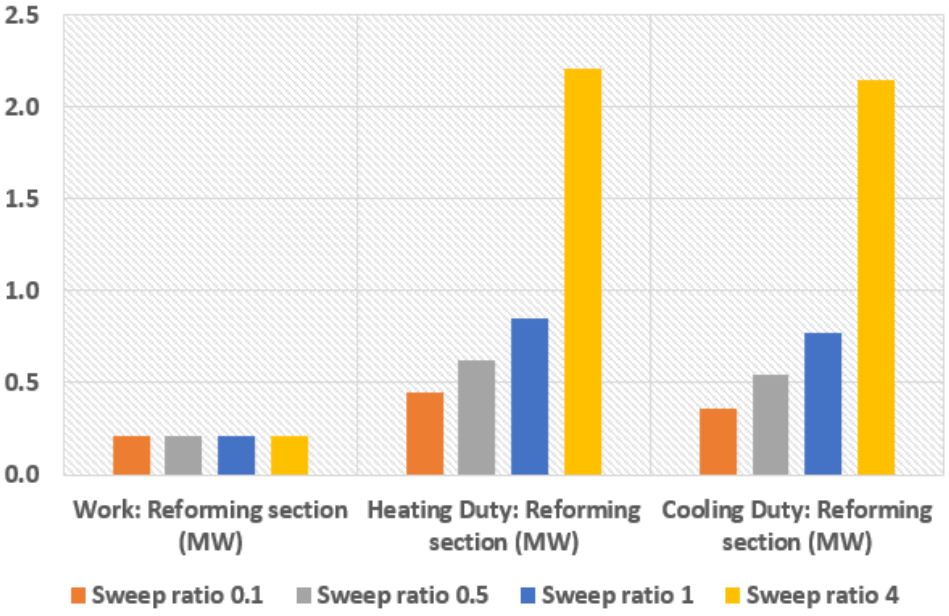

Figure B.28: Work & duties (reforming section) for different sweep ratios with biogas feed of 10.5 kmol/h.

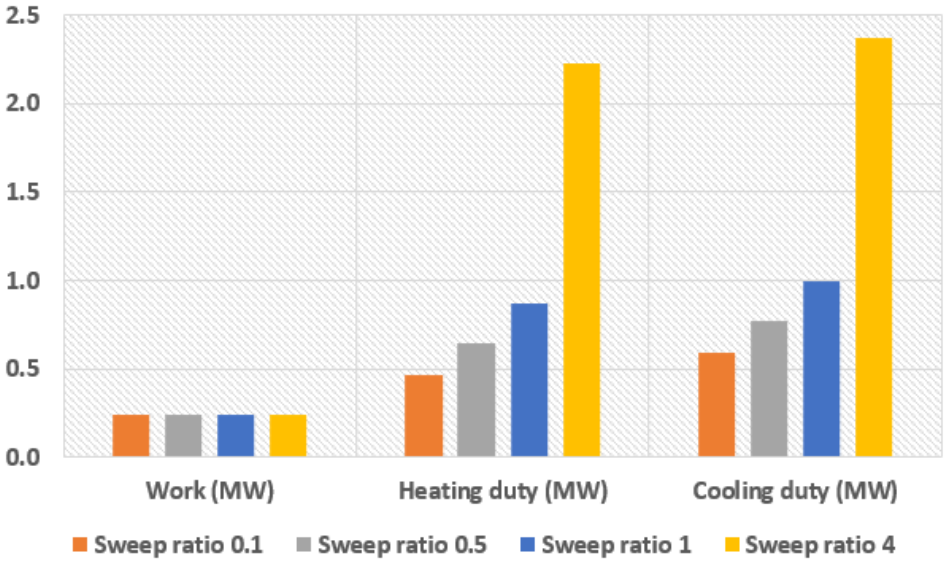

Figure B.29: Total Work & duties of the process for different sweep ratios with biogas feed of 10.5 kmol/h.

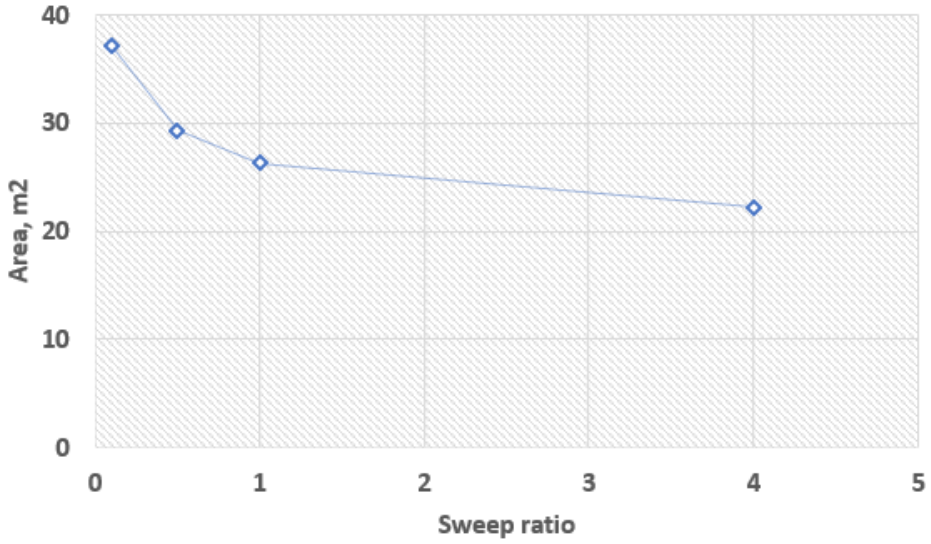

Figure B.30: Membrane surface area vs sweep ratio.

B.2.2. Permeate pressure: Base case, Case 4.1, Case 4.2 & Case 4.3

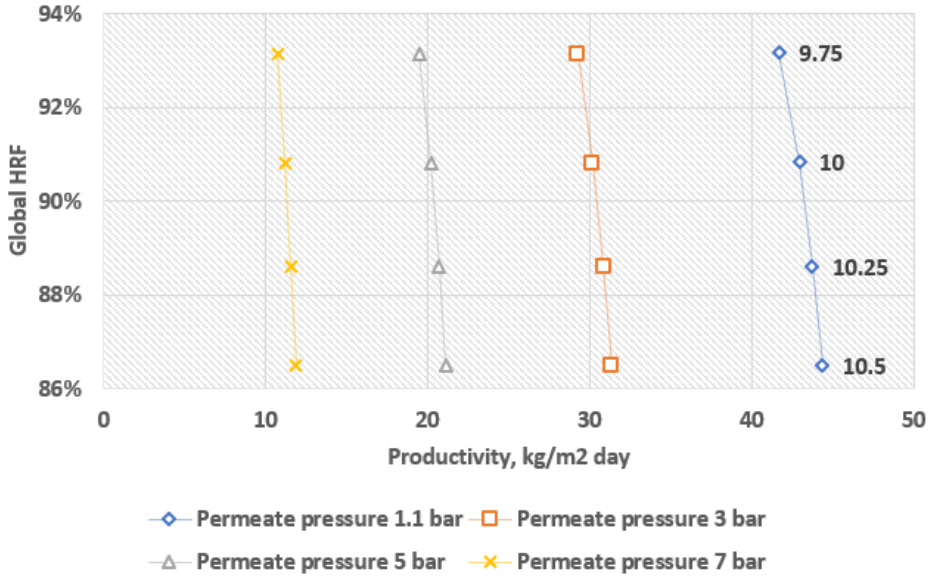

Figure B.31: Global hydrogen recovery factor vs productivity for different permeate pressures varying biogas feed from 9.75 to 10.5 kmol/h.

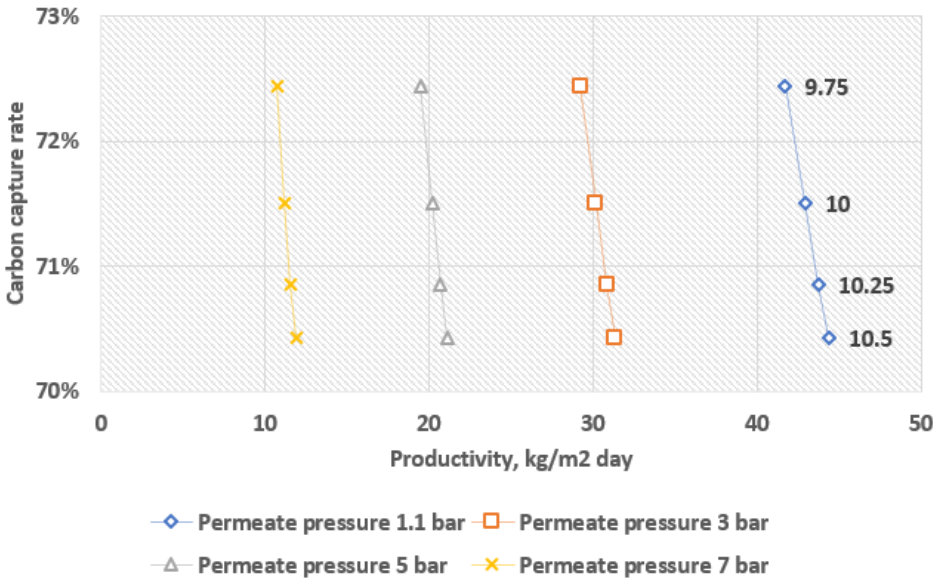

Figure B.32: Carbon capture rate vs productivity for different permeate pressures varying biogas feed from 9.75 to 10.5 kmol/h.

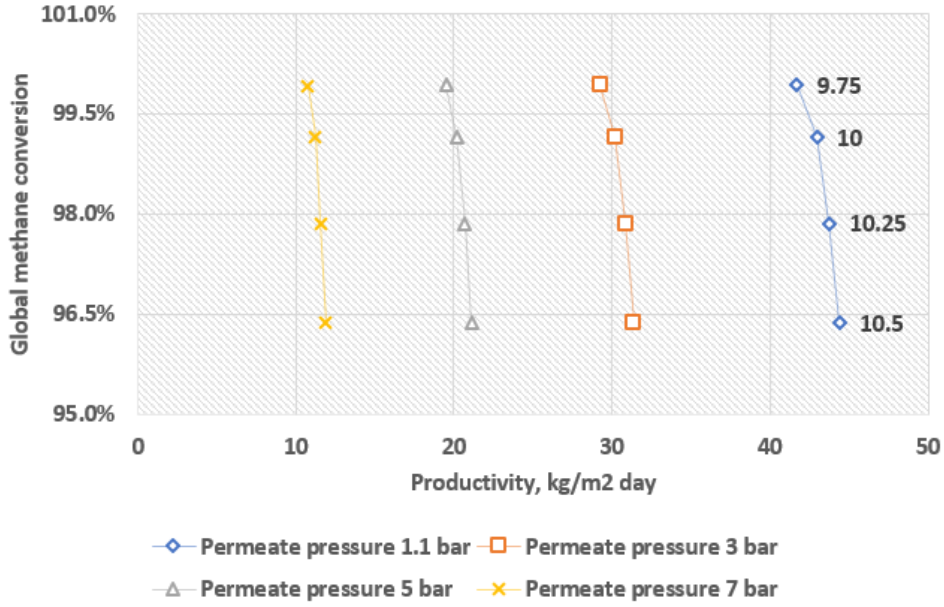

Figure B.33: Global methane conversion vs productivity for different permeate pressures varying biogas feed from 9.75 to 10.5 kmol/h.

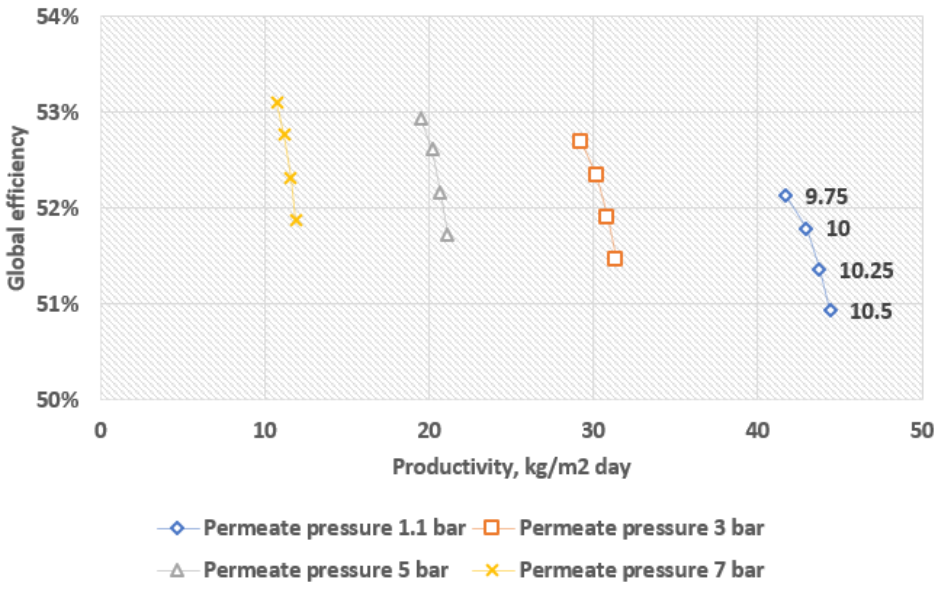

Figure B.34: Global efficiency vs productivity for different permeate pressures varying biogas feed from 9.75 to 10.5 kmol/h.

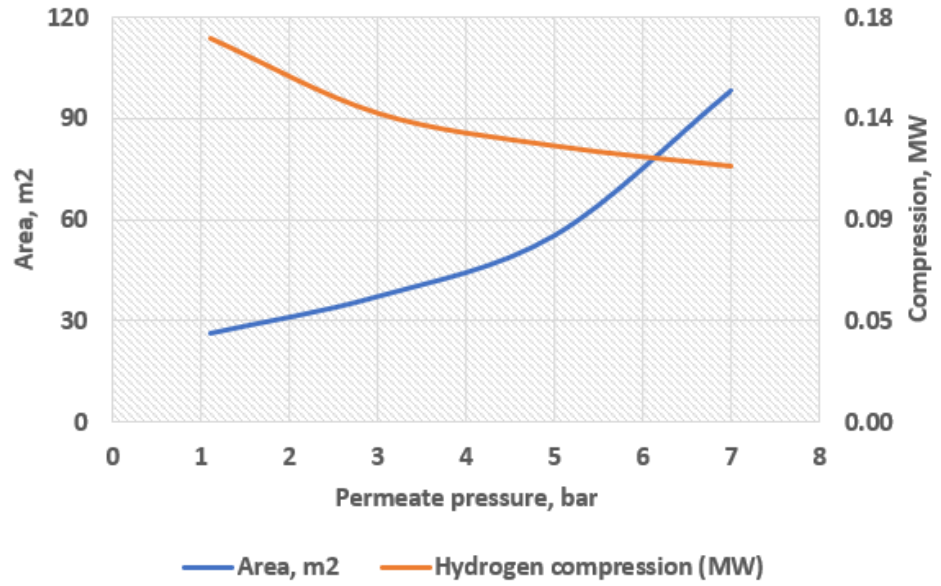

Figure B.35: Membrane surface area vs hydrogen compression work for different permeate pressures.

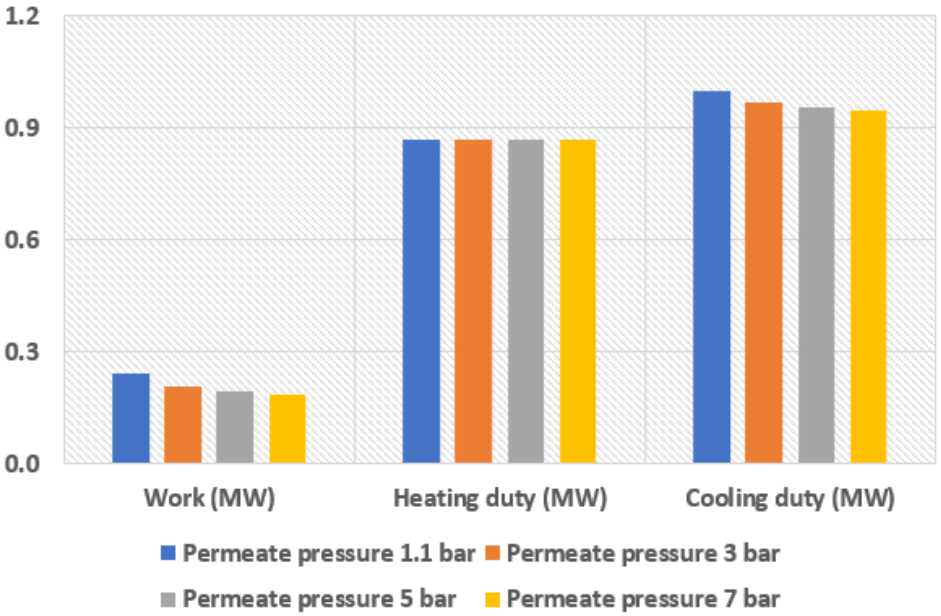

Figure B.36: Total Work & duties of the process for different permeate pressures with biogas feed of 10.5 kmol/h.

B.3. Process with carbon capture unit after the membrane reactor: with recycle of off-gases

For this configuration too, similar graphs are presented. The trends for most of the performance indicators are the same. Therefore, elaborate explanations aren't provided.

B.3.1. Sweep ratio: Base case, Case 2.1 & 2.2 & Case 2.3

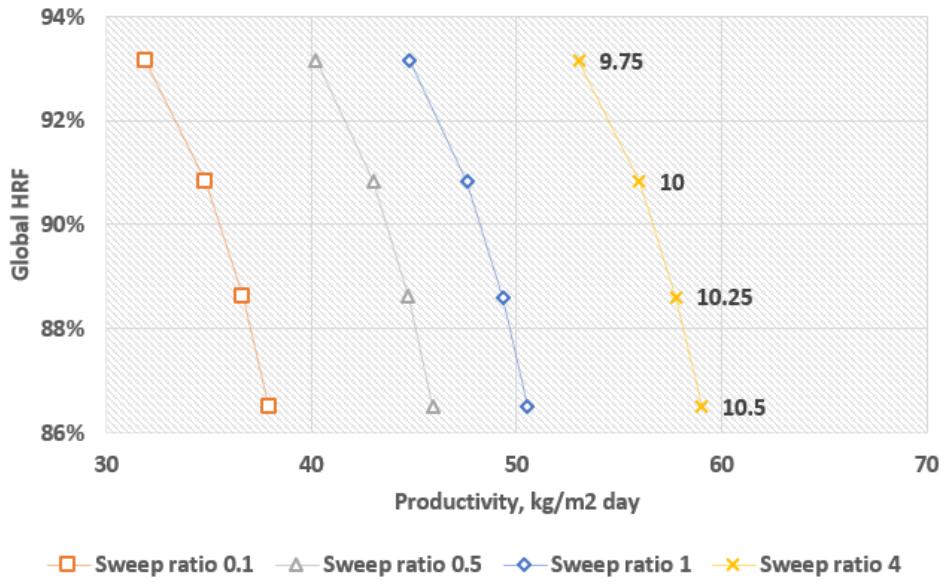

Figure B.37: Global hydrogen recovery factor vs productivity for different sweep ratios varying biogas feed from 9.75 to 10.5 kmol/h.

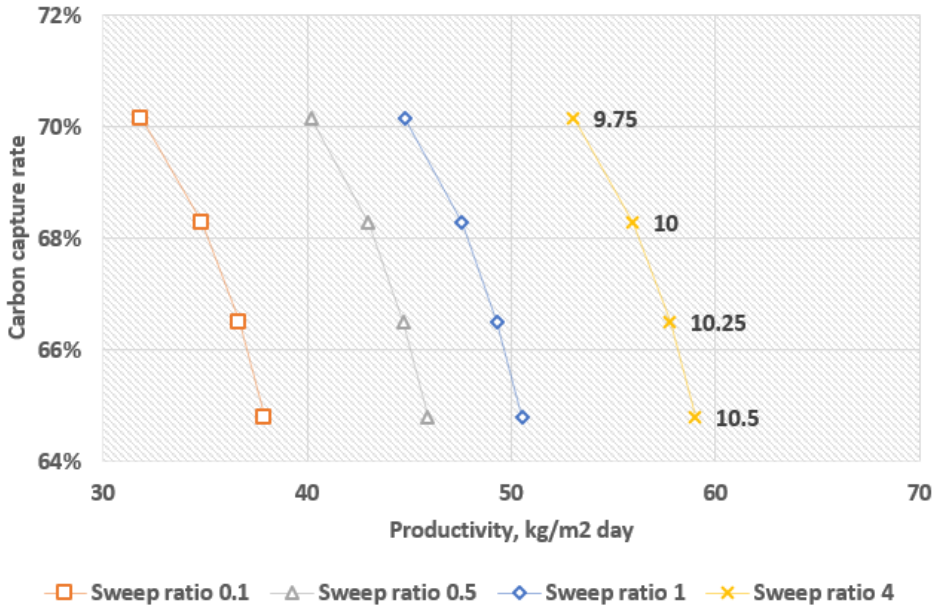

Figure B.38: Carbon capture rate vs productivity for different sweep ratios varying biogas feed from 9.75 to 10.5 kmol/h.

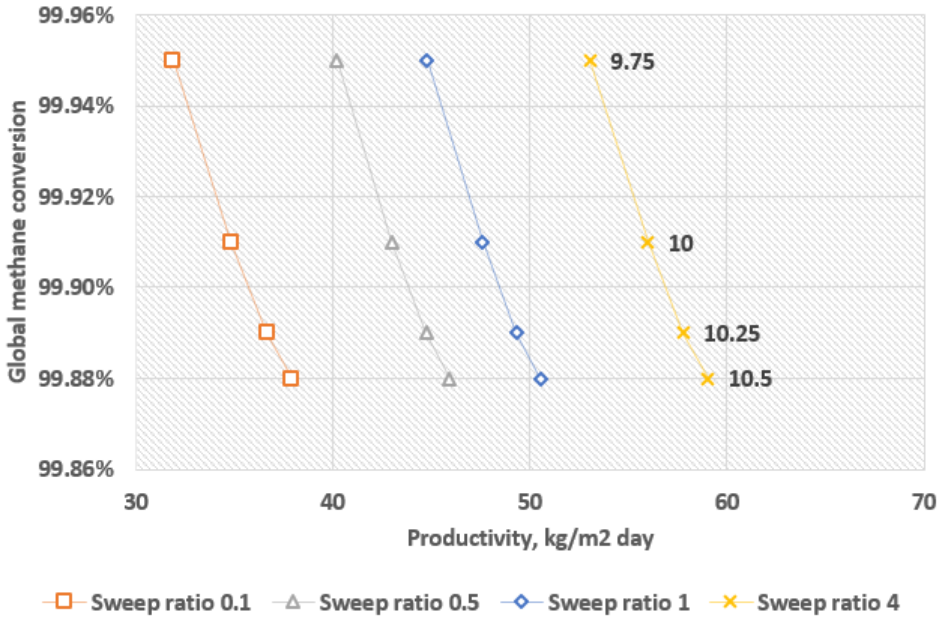

Figure B.39: Global methane conversion vs productivity for different sweep ratios varying biogas feed from 9.75 to 10.5 kmol/h.

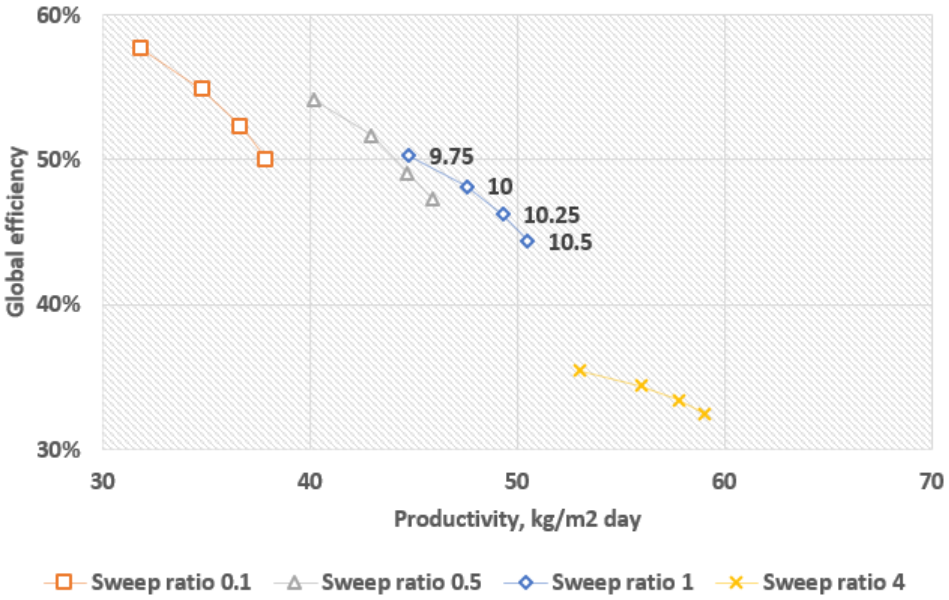

Figure B.40: Global efficiency vs productivity for different sweep ratios varying biogas feed from 9.75 to 10.5 kmol/h.

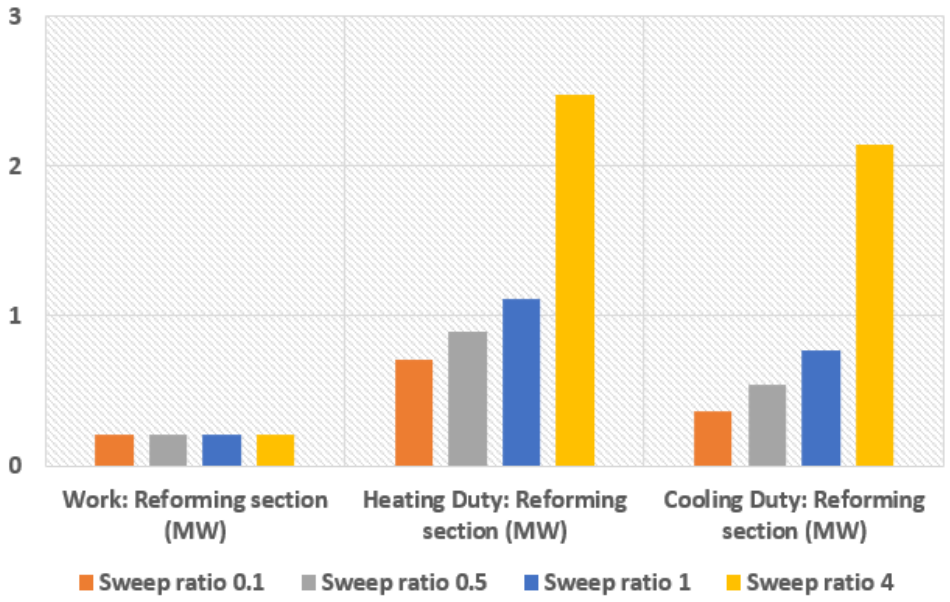

Figure B.41: Work & duties (reforming section) for different sweep ratios with biogas feed of 10.5 kmol/h.

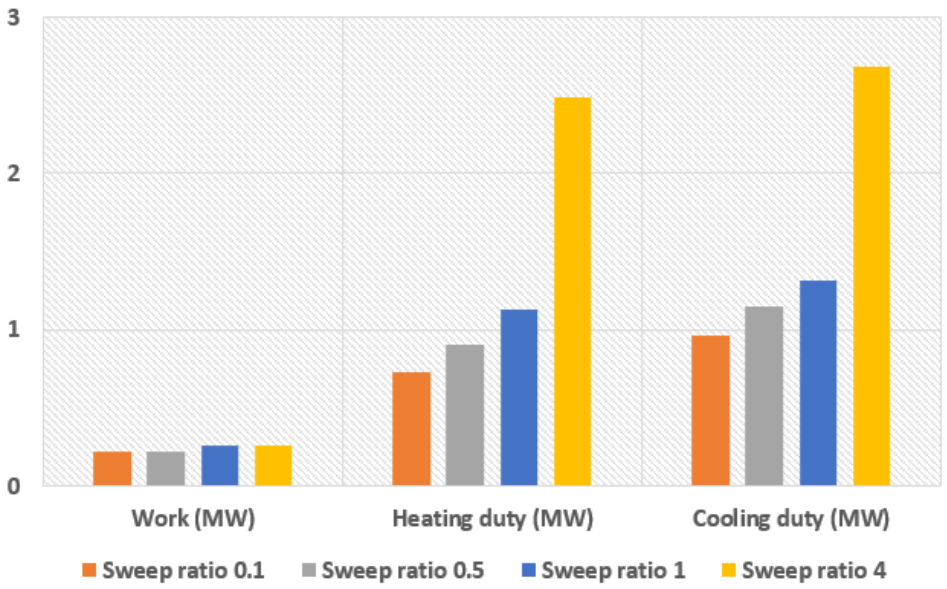

Figure B.42: Total Work & duties of the process for different sweep ratios with biogas feed of 10.5 kmol/h.

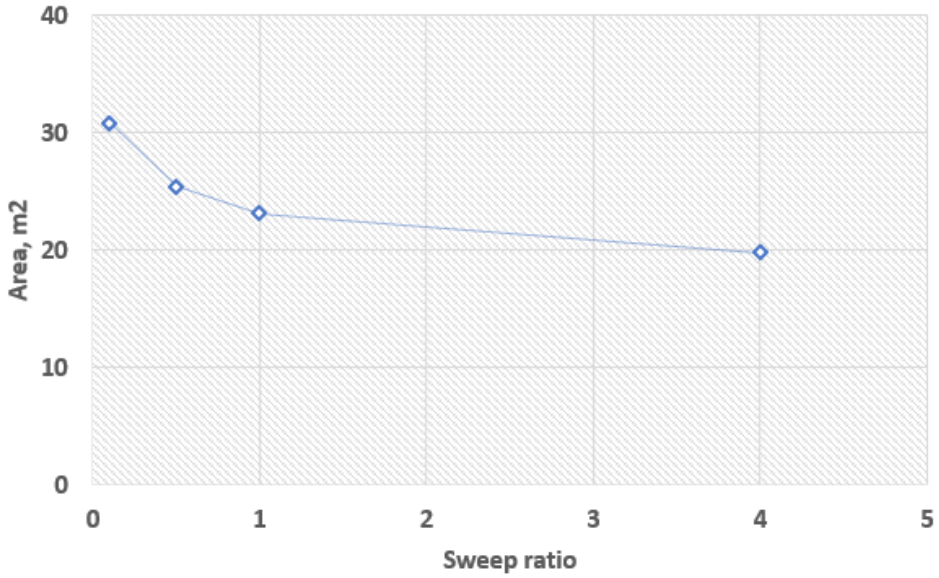

Figure B.43: Membrane surface area vs sweep ratio.

B.3.2. Recycle ratio: Base case & Case 3.1

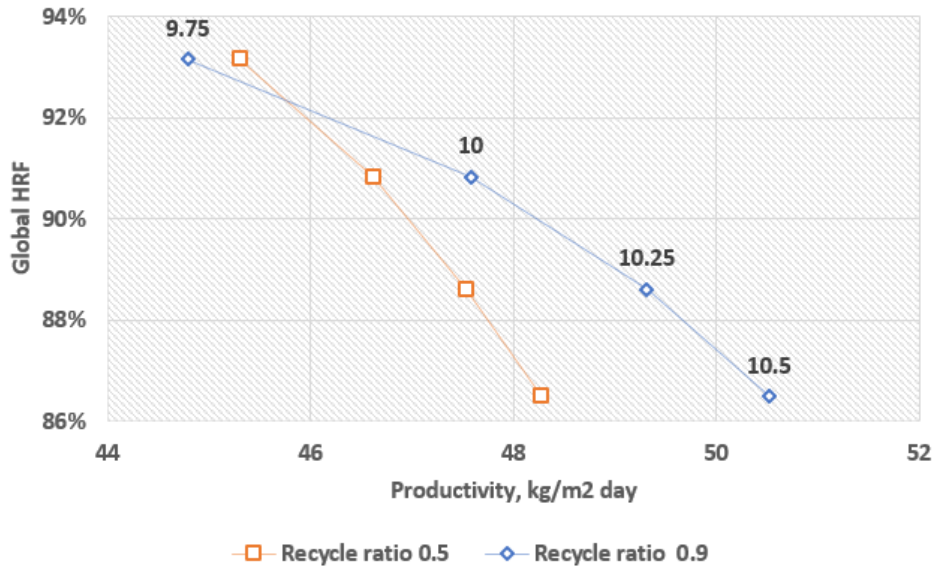

Figure B.44: Global hydrogen recovery factor vs productivity for different recycle ratios varying biogas feed from 9.75 to 10.5 kmol/h.

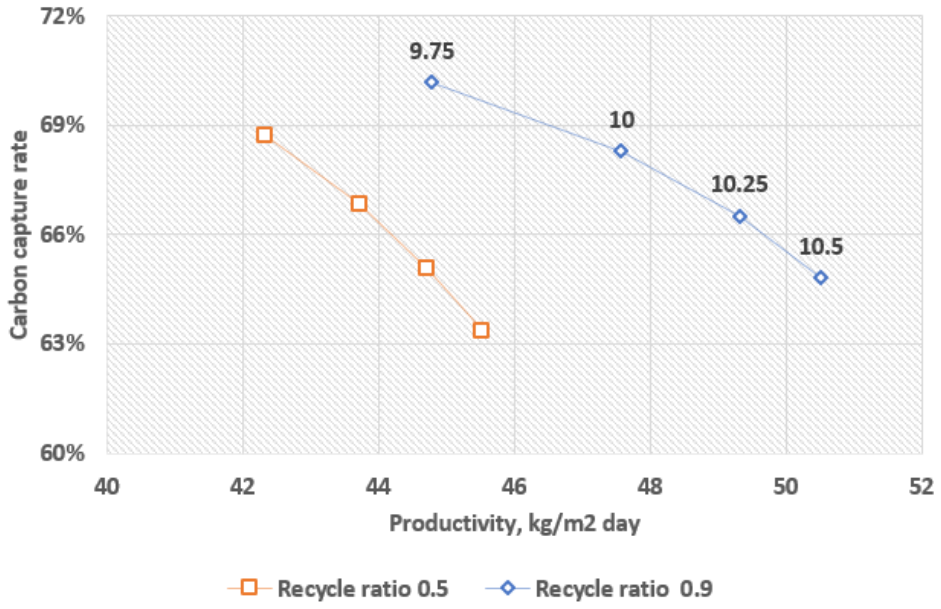

Figure B.45: Carbon capture rate vs productivity for different recycle ratios varying biogas feed from 9.75 to 10.5 kmol/h.

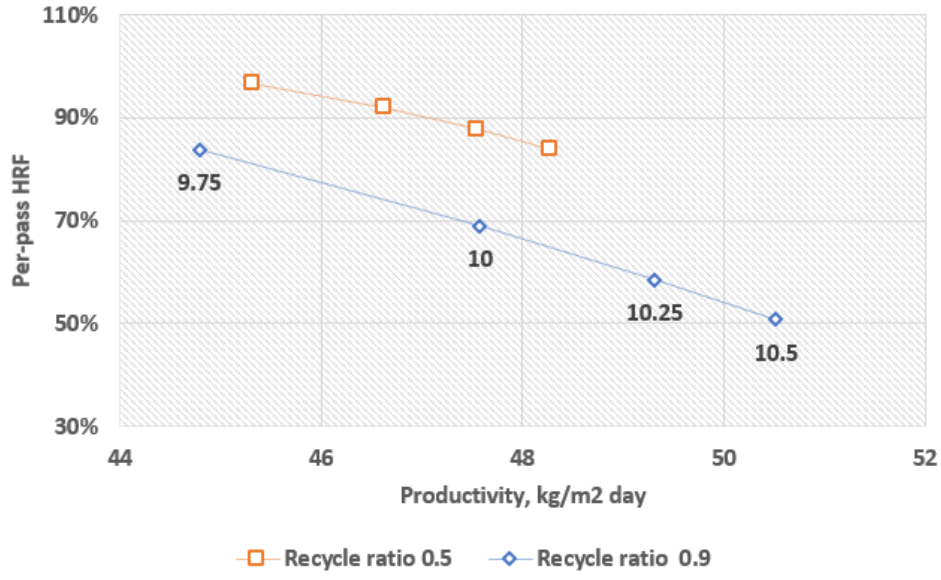

Figure B.46: Per-pass hydrogen recovery factor vs productivity for different recycle ratios varying biogas feed from 9.75 to 10.5 kmol/h.

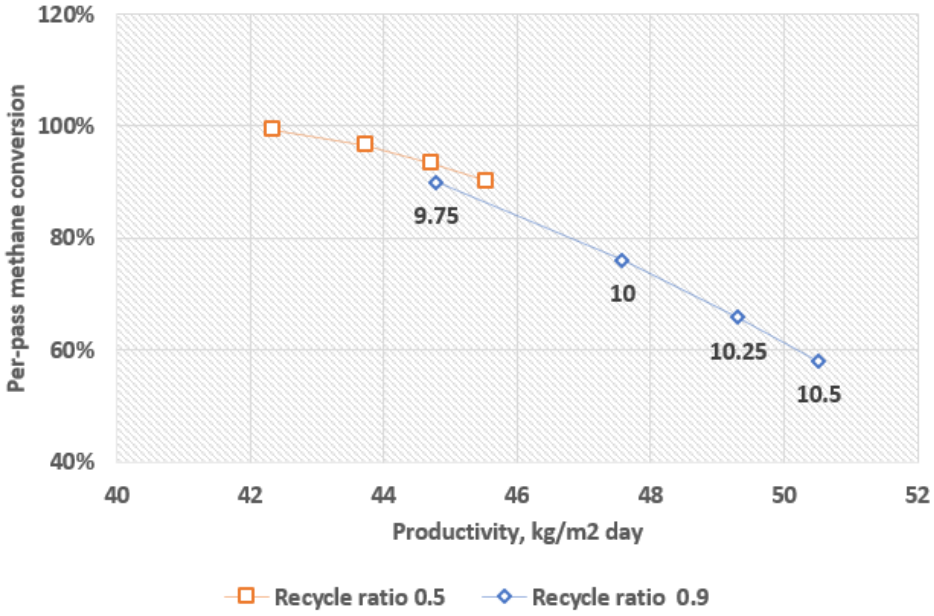

Figure B.47: Per-pass methane conversion vs productivity for different recycle ratios varying biogas feed from 9.75 to 10.5 kmol/h.

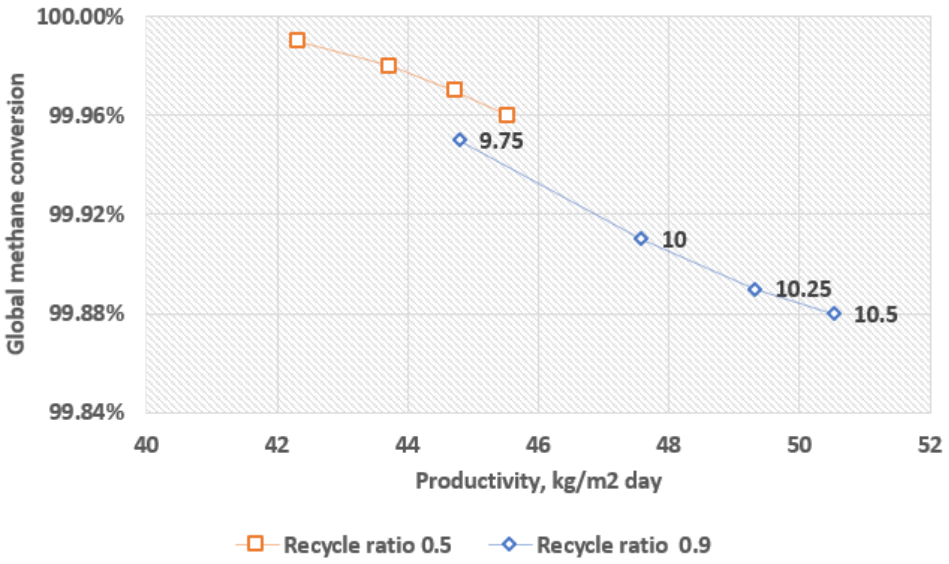

Figure B.48: Global methane conversion vs productivity for different recycle ratios varying biogas feed from 9.75 to 10.5 kmol/h.

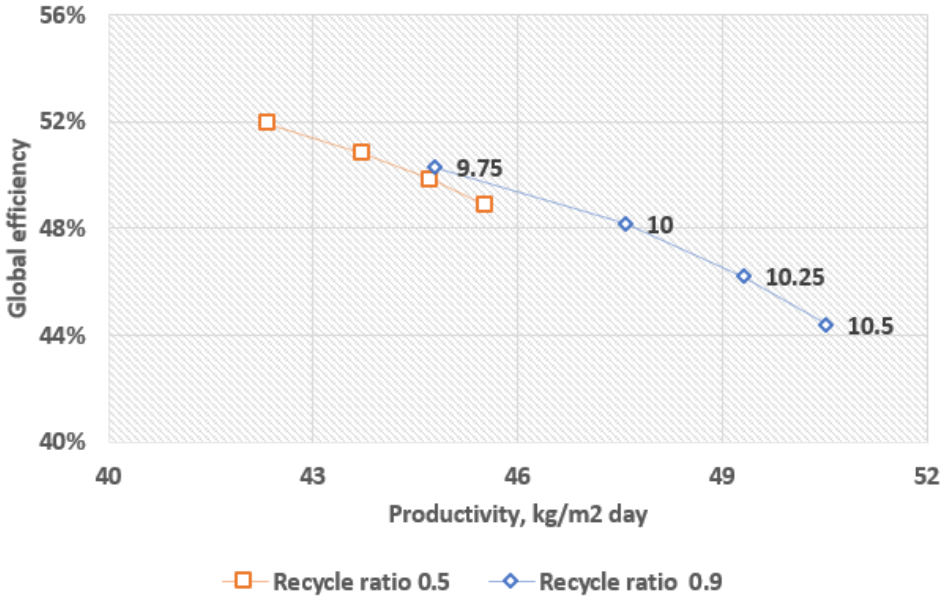

Figure B.49: Global efficiency vs productivity for different recycle ratios varying biogas feed from 9.75 to 10.5 kmol/h.

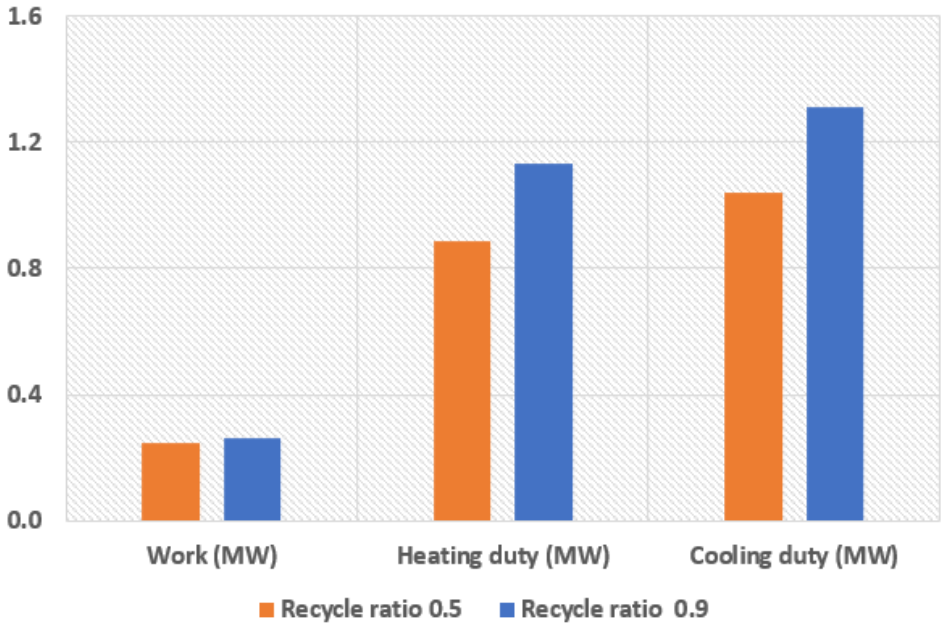

Figure B.50: Total Work & duties of the process for different sweep ratios with biogas feed of 10.5 kmol/h.

B.3.3. Permeate pressure: Base case, Case 4.1, Case 4.2 & Case 4.3

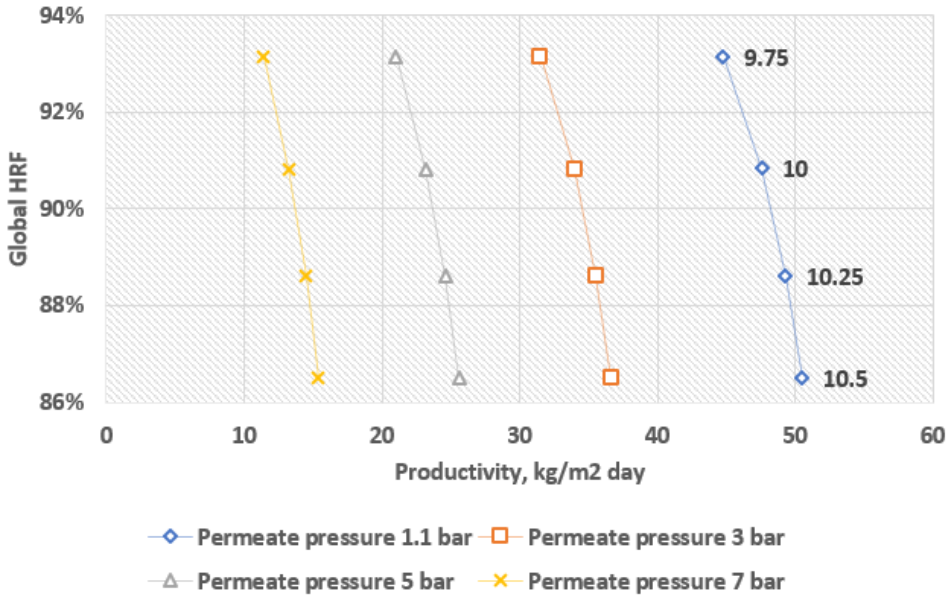

Figure B.51: Global hydrogen recovery factor vs productivity for different permeate pressures varying biogas feed from 9.75 to 10.5 kmol/h.

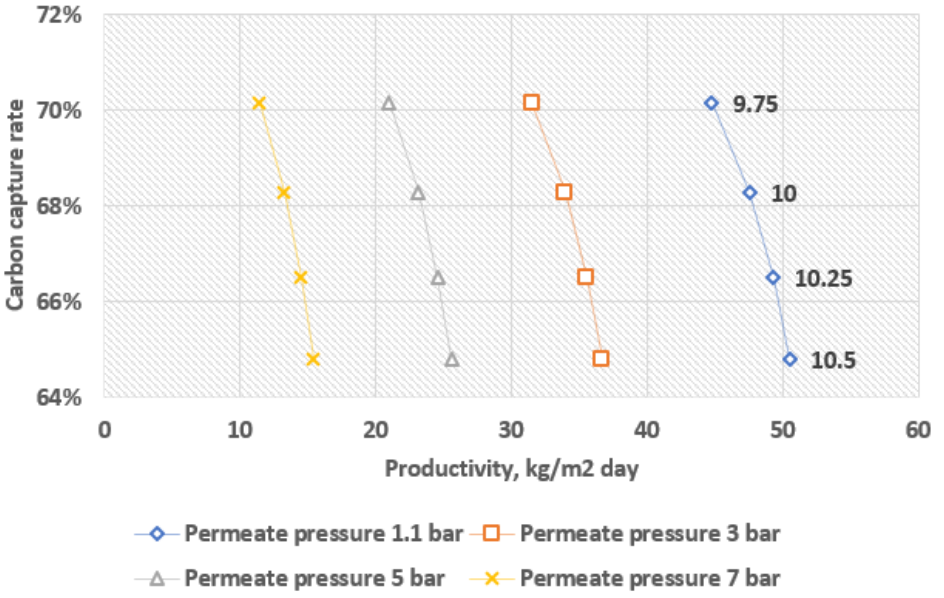

Figure B.52: Carbon capture rate vs productivity for different permeate pressures varying biogas feed from 9.75 to 10.5 kmol/h.

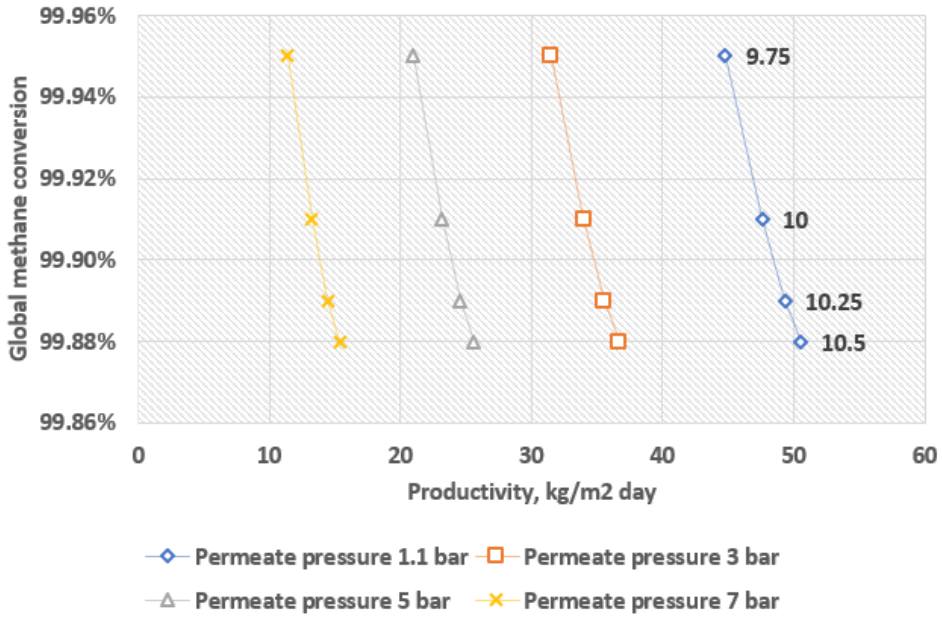

Figure B.53: Global methane conversion vs productivity for different permeate pressures varying biogas feed from 9.75 to 10.5 kmol/h.

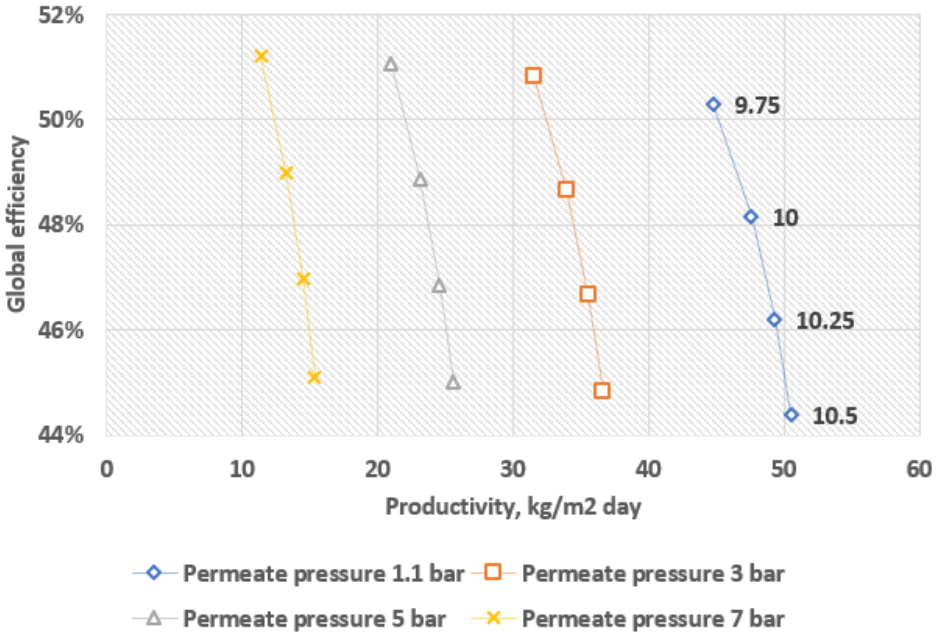

Figure B.54: Global efficiency vs productivity for different permeate pressures varying biogas feed from 9.75 to 10.5 kmol/h.

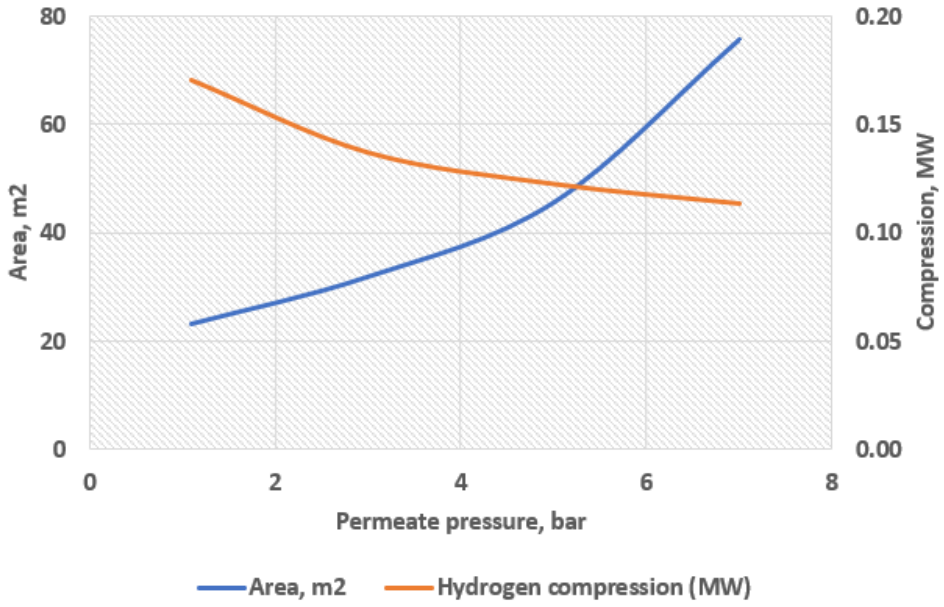

Figure B.55: Membrane surface area vs hydrogen compression work for different permeate pressures.

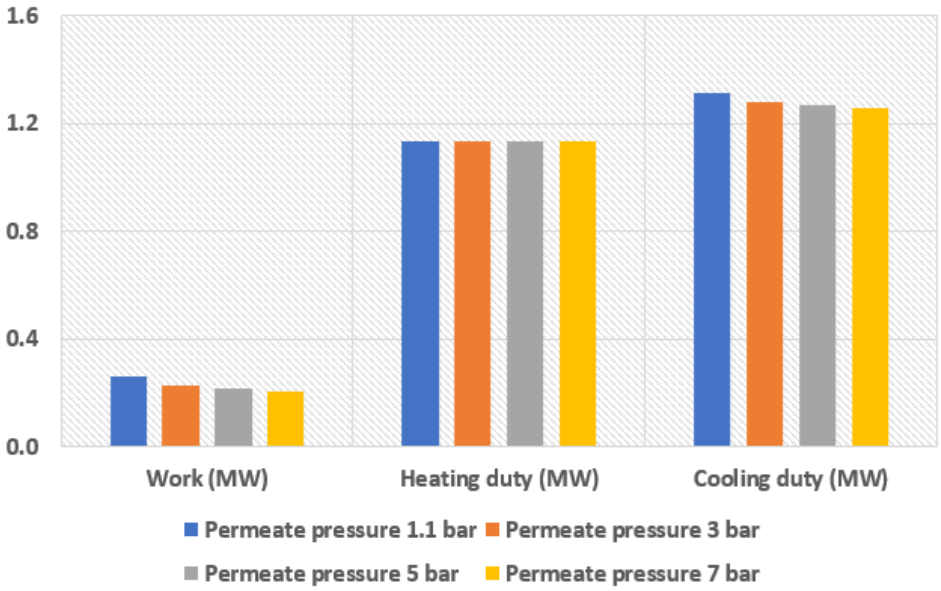

Figure B.56: Total Work & duties of the process for different permeate pressures with biogas feed of 10.5 kmol/h.

The three tables below B.1, B.2, B.3 present all the simulation results of the three configurations designed for easier comparison.

Table B.1: Results of configuration 1.

Carbon capture unit before membrane reactor					
	Biogas flow rate, kmol/h	Global HRF, %	Global methane conversion, %	Carbon capture rate, %	Global efficiency, %	Productivity, kg/m2 day

Table B.1: Results of configuration 1.

Carbon capture unit before membrane reactor						
Base case	10.5	86.50	99.72	60.50	44.33	52.17
	10.25	88.61	99.75	62.63	46.56	51.16
	10.00	90.82	99.76	64.32	48.72	49.70
	9.75	93.15	99.77	66.20	51.10	47.26
Case 2.1	10.5	86.50	99.72	60.50	51.47	39.55
	10.25	88.61	99.75	62.63	54.15	38.49
	10.00	90.82	99.76	64.32	57.03	36.93
	9.75	93.15	99.77	66.20	60.24	34.30
Case 2.2	10.5	86.50	99.72	60.50	48.45	47.58
	10.25	88.61	99.75	62.63	50.82	46.58
	10.00	90.82	99.76	64.32	53.35	45.12
	9.75	93.15	99.77	66.20	56.15	42.70
Case 2.3	10.5	86.50	99.72	60.50	31.92	60.65
	10.25	88.61	99.75	62.63	32.93	59.60
	10.00	90.82	99.76	64.32	33.99	58.06
	9.75	93.15	99.77	66.20	35.11	55.48
Case 3.1	10.5	86.50	99.72	38.01	48.28	48.27
	10.25	88.61	99.75	38.91	49.33	47.54
	10.00	90.82	99.76	39.94	50.43	46.62
	9.75	93.15	99.77	41.31	51.59	45.31
Case 4.1	10.5	86.50	99.72	60.50	45.59	38.36
	10.25	88.61	99.75	62.63	47.68	37.46
	10.00	90.82	99.76	64.32	49.90	36.17
	9.75	93.15	99.77	66.20	52.34	34.10
Case 4.2	10.5	86.50	99.72	60.50	45.79	27.41
	10.25	88.61	99.75	62.63	47.89	26.62
	10.00	90.82	99.76	64.32	50.12	25.51
	9.75	93.15	99.77	66.20	52.59	23.79
Case 4.3	10.5	86.50	99.72	60.50	45.92	17.47
	10.25	88.61	99.75	62.63	48.04	16.82
	10.00	90.82	99.76	64.32	50.30	15.92
	9.75	93.15	99.77	66.20	52.78	14.62

Table B.2: Results for configuration 2.

Carbon capture unit after membrane reactor without recycle						
	Biogas flow rate, kmol/h	Global HRF, %	Global methane conversion, %	Carbon capture rate, %	Global efficiency, %	Productivity, kg/m2 day
Base case	10.5	86.50	96.37	70.43	50.93	44.38
	10.25	88.61	97.86	70.85	51.36	43.75
	10.00	90.82	99.16	71.51	51.79	42.94
	9.75	93.15	99.93	72.44	52.13	41.69
Case 2.1	10.5	86.50	96.37	70.43	58.47	31.36
	10.25	88.61	97.86	70.85	59.04	30.67
	10.00	90.82	99.16	71.51	59.62	29.80
	9.75	93.15	99.93	72.44	60.06	28.48
Case 2.2	10.5	86.50	96.37	70.43	54.86	39.85
	10.25	88.61	97.86	70.85	55.36	39.23
	10.00	90.82	99.16	71.51	55.87	38.45
	9.75	93.15	99.93	72.44	56.75	37.24

Table B.2: Results for configuration 2.

	Carbon capture unit after membrane reactor without recycle					
Case 2.3	10.5	86.50	96.37	70.43	35.77	52.53
	10.25	88.61	97.86	70.85	35.97	51.85
	10.00	90.82	99.16	71.51	36.18	50.97
	9.75	93.15	99.93	72.44	36.34	49.56
Case 3.1	-	-	-	-	-	-
Case 4.1	10.5	86.50	96.37	70.43	51.47	31.36
	10.25	88.61	97.86	70.85	51.91	30.84
	10.00	90.82	99.16	71.51	52.35	30.19
	9.75	93.15	99.93	72.44	52.69	29.24
Case 4.2	10.5	86.50	96.37	70.43	51.72	21.11
	10.25	88.61	97.86	70.85	52.16	20.69
	10.00	90.82	99.16	71.51	52.61	20.19
	9.75	93.15	99.93	72.44	52.94	19.48
Case 4.3	10.5	86.50	96.37	70.43	51.87	11.89
	10.25	88.61	97.86	70.85	52.31	11.57
	10.00	90.82	99.16	71.51	52.76	11.21
	9.75	93.15	99.93	72.44	53.10	10.73

Table B.3: Results of configuration 3.

	Carbon capture unit after membrane reactor with recycle					
	Biogas flow rate, kmol/h	Global HRF, %	Global methane conversion, %	Carbon capture rate, %	Global efficiency, %	Productivity, kg/m2 day
Base case	10.5	86.50	99.88	64.80	44.40	50.52
	10.25	88.61	99.89	66.50	46.21	49.31
	10.00	90.82	99.91	68.28	48.17	47.58
	9.75	93.15	99.95	70.16	50.30	44.78
Case 2.1	10.5	86.50	99.88	64.80	49.99	37.91
	10.25	88.61	99.89	66.50	52.31	36.65
	10.00	90.82	99.91	68.28	54.86	34.83
	9.75	93.15	99.95	70.16	57.65	31.86
Case 2.2	10.5	86.50	99.88	64.80	47.34	45.92
	10.25	88.61	99.89	66.50	49.10	44.72
	10.00	90.82	99.91	68.28	51.66	42.99
	9.75	93.15	99.95	70.16	54.13	40.21
Case 2.3	10.5	86.50	99.88	64.80	32.49	59.02
	10.25	88.61	99.89	66.50	33.41	57.78
	10.00	90.82	99.91	68.28	34.40	55.97
	9.75	93.15	99.95	70.16	35.44	53.05
Case 3.1	10.5	86.50	99.88	63.36	48.88	45.53
	10.25	88.61	99.89	65.06	49.83	44.72
	10.00	90.82	99.91	66.84	50.81	43.72
	9.75	93.15	99.95	68.72	51.93	42.33
Case 4.1	10.5	86.50	99.88	64.80	44.82	36.66
	10.25	88.61	99.89	66.50	46.67	35.55
	10.00	90.82	99.91	68.28	48.67	33.98
	9.75	93.15	99.95	70.16	50.84	31.51
Case 4.2	10.5	86.50	99.88	64.80	45.00	25.59
	10.25	88.61	99.89	66.50	46.85	24.58
	10.00	90.82	99.91	68.28	48.87	23.16
	9.75	93.15	99.95	70.16	51.06	21.00

Table B.3: Results of configuration 3.

Carbon capture unit after membrane reactor with recycle						
Case 4.3	10.5	86.50	99.88	64.80	45.11	15.39
	10.25	88.61	99.89	66.50	46.98	14.48
	10.00	90.82	99.91	68.28	49.00	13.22
	9.75	93.15	99.95	70.16	51.21	11.40

C

Pinch analysts: T-Q curves

The T-Q diagrams (composite curves) obtained for the pinch analysis performed in chapter 4 are presented here.

Figure C.1: T-Q diagram.

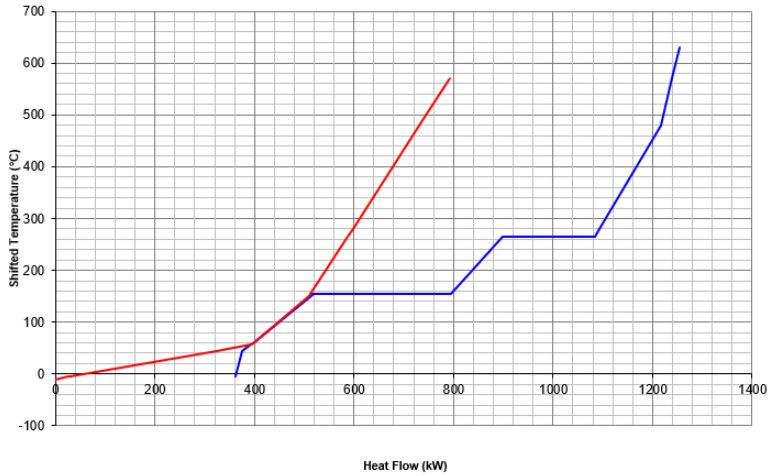

Figure C.2: Shifted T-Q diagram.

D

Results of the cases formulated for LCOH optimization

The key performance indicators for the different cases formulated in chapter 5 are presented here. A summary table with the LCOH and all the performance indicators is also presented for easy comparison.

The results obtained with varying biogas feed is shown in figure D.1. The KPIs are nearly constant with slight increase in membrane surface area and efficiency & slight decrease in productivity with decrease in the biogas feed.

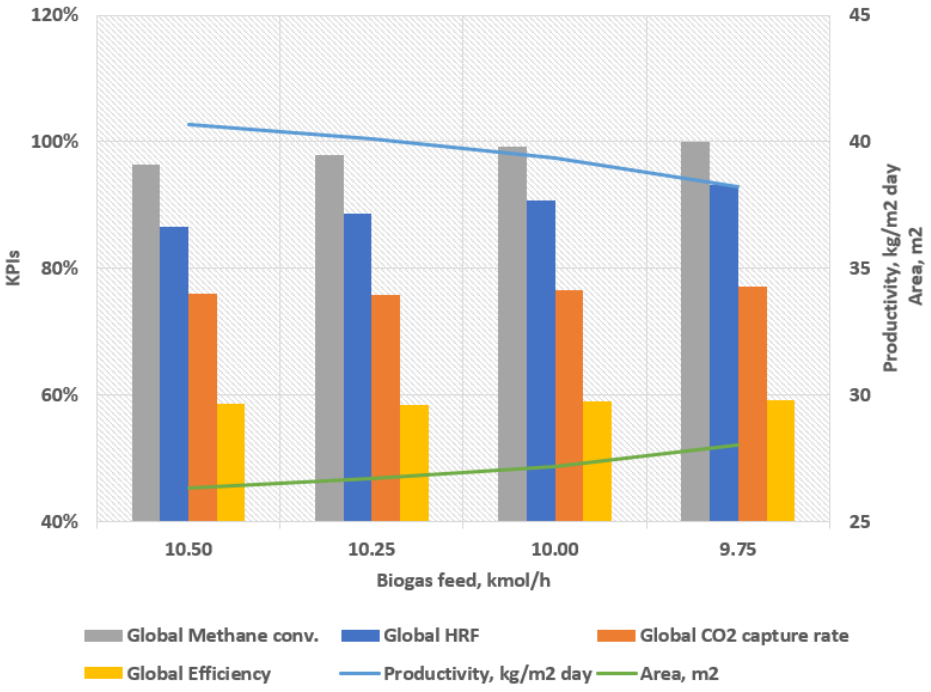

Figure D.1: KPI results with varying biogas feed flow rate.

Figure D.2 shows the results obtained with varying sweep ratios. While reading the graphs it is important to keep in mind that the x-axis isn't linear, to avoid misinterpretation of the results. The KPIs are fairly constant except a decrease in efficiency and area with increase in sweep ratio, and therefore an increase in productivity.

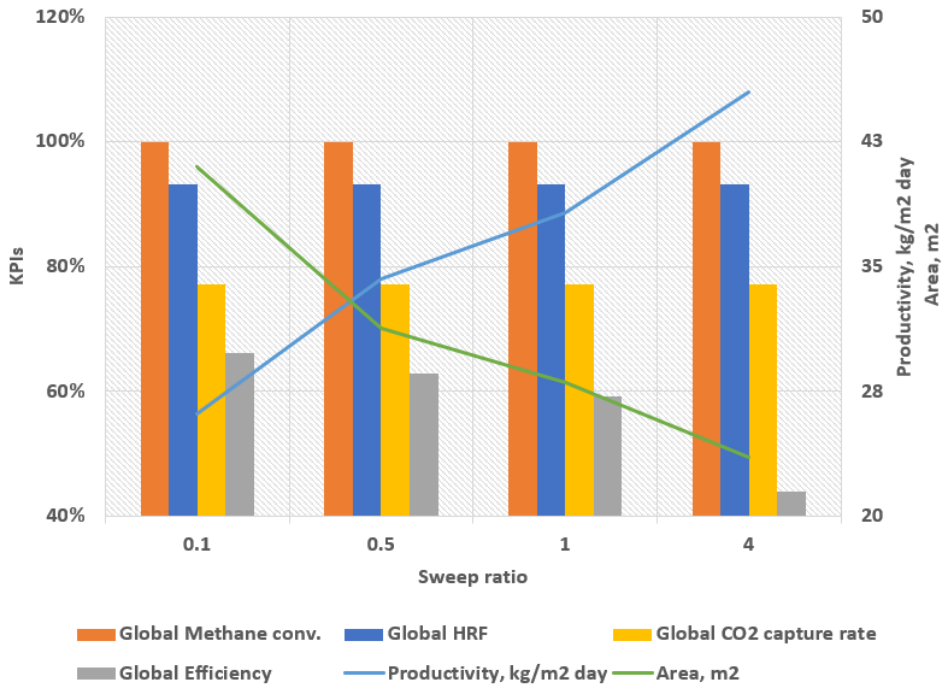

Figure D.2: KPI results with varying sweep ratio.

Figure D.3 show the KPI values for different permeate pressure. The KPI values are fairly constant except that the membrane surface area required increases considerably with increase in permeate pressure.

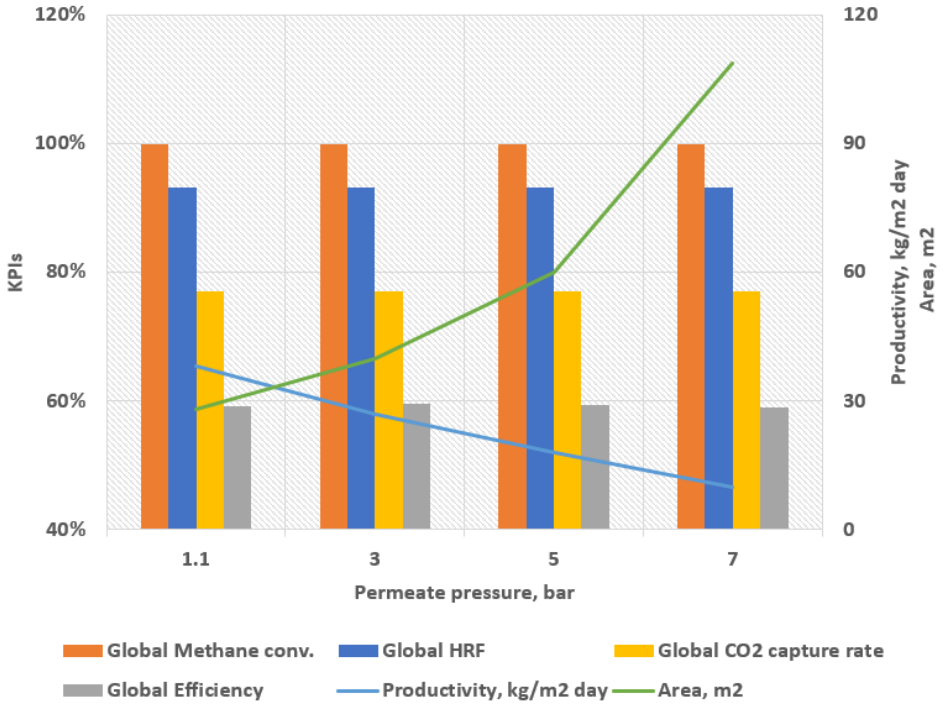

Figure D.3: KPI results with varying permeate pressure.

Increasing the reactor pressure increases the driving force for hydrogen permeation through the membrane (permeate pressure being constant). Therefore, the membrane area required reduces increasing the productivity, figure D.4.

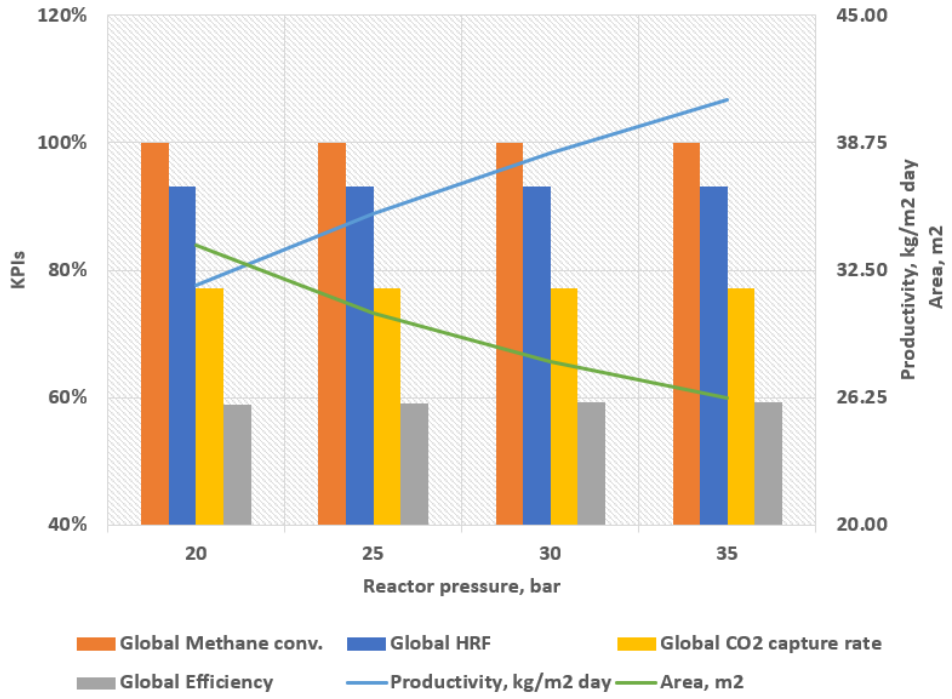

Figure D.4: KPI results with varying reactor pressure.

A summary of the results of these cases is shown in table D.1 below. The ninth column lists the CO_2 released from the furnace which isn't captured in the system.

Table D.1: Summary of the results.

Case	LCOH, €/kg	Global HRF (%)	Carbon capture rate (%)	Global methane conversion (%)	Global efficiency (%)	Productivity, kg/m^2 day	Area, m^2	CO_2 emitted (biogenic)[a], kg CO_2/kg H_2
Base case	5.01	86.50	71.27	96.40	58.73	40.700	26.32	3.86
Case 1.1	4.99	88.60	71.55	98.00	58.52	40.121	26.70	3.82
Case 1.2	4.96	90.80	71.86	99.20	58.97	39.382	27.20	3.75
Case 1.3	4.93	93.20	72.13	99.90	59.22	38.235	28.01	3.69
Case 2.1	4.29	93.20	72.13	99.90	66.20	26.125	41.00	3.69
Case 2.2	4.59	93.20	72.13	99.90	62.91	34.264	31.26	3.69
Case 2.3	7.68	93.20	72.13	99.90	43.84	45.449	23.57	3.69
Case 3.1	4.63	93.20	72.13	99.90	59.54	26.815	39.94	3.69
Case 3.2	4.60	93.20	72.13	99.90	59.36	17.869	59.94	3.69
Case 3.3	4.81	93.20	72.13	99.90	59.03	9.841	108.83	3.69
Case 4.1	5.01	93.20	72.13	99.90	58.92	31.746	33.74	3.69
Case 4.2	4.97	93.20	72.13	99.90	59.10	35.252	30.38	3.69
Case 4.3	4.91	93.20	72.13	99.90	59.34	40.853	26.22	3.69

[a] From furnace flue gas.

E

Cases formulated for (local) optimum process determination

Table E.1: Formulated cases to determine the optimum process conditions.

Case	Sweep ratio	Permeate pressure, bar	Reactor pressure, bar	LCOH, $€/kg$
1	0.1	5	30	-
2	0.1	3	30	4.985
3	0.5	5	30	4.694
4	1	5	30	4.604
5	0.1	1.1	35	4.260
6	0.1	3	35	4.534
7	0.1	5	35	-
8	0.5	5	35	4.466
9	1	4	35	4.540
10	1	5	35	4.529
11	1	6	35	4.555

The process conditions and the LCOH of the formulated cases are shown here. For case 1 & 7, the driving force for hydrogen permeation was too low resulting in a very large membrane area required. Hence, they are not feasible options. The lowest levelized cost of hydrogen obtained was for case 5. The LCOH of this case is slightly lower than Case 2.1 in table 5.7 because of the increase driving force due to the higher partial pressure difference leading to a lower membrane surface area required.

F

Break-down of cost components for the (local) optimum process

In the table below, the break-down of the CAPEX and OPEX is presented which contribute to the levelized cost of hydrogen.

Table F.1: Economic analysis of the (local) optimum process.

	Cost (€)
Capital expenditure (CAPEX)	
Reforming section	
Biogas compressor	42210
Biogas heater	1230
Water pump	12587
Boilers	13566
Sweep pump	10789
Pre-reformer	19439
Membrane reactor	75607
Membrane tubes	93098
Furnace	13498
Knock-out drum	25111
Dehydration unit (2)	360000
Hydrogen compressor	144517
Air blower	5962
N2 blower	1798
Nitrogen heater	947
Additional heat exchangers	10221
Hydrogen storage	146874
Carbon capture section	
Heat exchangers	4827
Knock-out drum(s)	50222
Compressor	3596
Refrigeration unit	499233
CO_2 pump	12587
Total component cost (TCC)	1547919
Total plant cost (TPC)	1934898
Total CAPEX	2757231
Annual cost (OPEX)	

Biogas feed	55493
Biogas fuel	21230
Water feed	2766
Sweep feed	362
Electricity	346452
Cooling water	555726
Reforming catalyst	34031
Membrane replacement	27930
Molecular sieves	839
Refrigeration unit	40338
O&M	110289
Annual insurance and tax	96503
Annual capital cost	373881
Total annual cost	1665840
Hydrogen cost (€/kg)	4.26

The cost figures are presented graphically to get a better perspective of the values compared to each other. The site assembly, installation costs are a major fraction (44%) of the total CAPEX as seen in figure F.1. Figure F.2 shows the contribution to total component cost ignoring the miscellaneous site assembly, installation costs etc. The figure shows that the carbon capture unit is the major contributor to the total component cost followed by permeate dehydration and reforming. The permeate dehydration in figure F.1 & F.3 includes permeate cooling, condensation and separation of water in a knock-out drum and also the dehydration & purification of hydrogen in the molecular sieves unit. The break-down of the permeate dehydration section for both CAPEX and OPEX is shown in figure F.4 & F.5 respectively. The hydrogen compressor and storage costs together account for roughly 19 % of the total component cost.

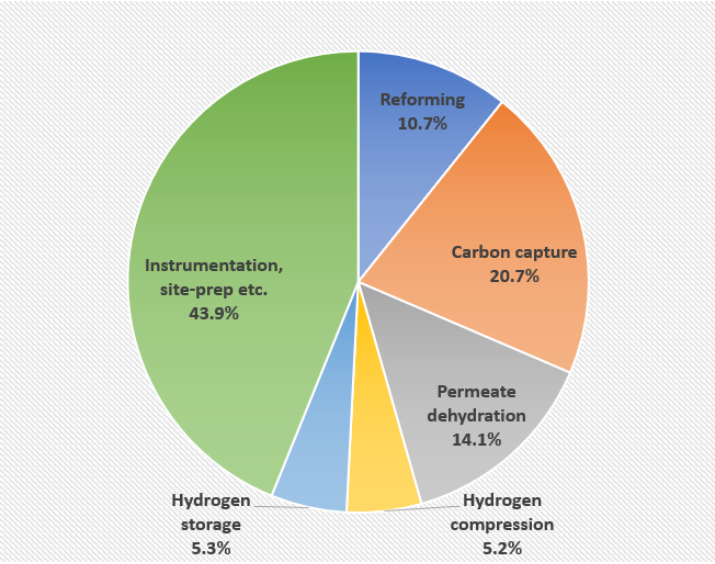

Figure F.1: Contribution to capital expenditure.

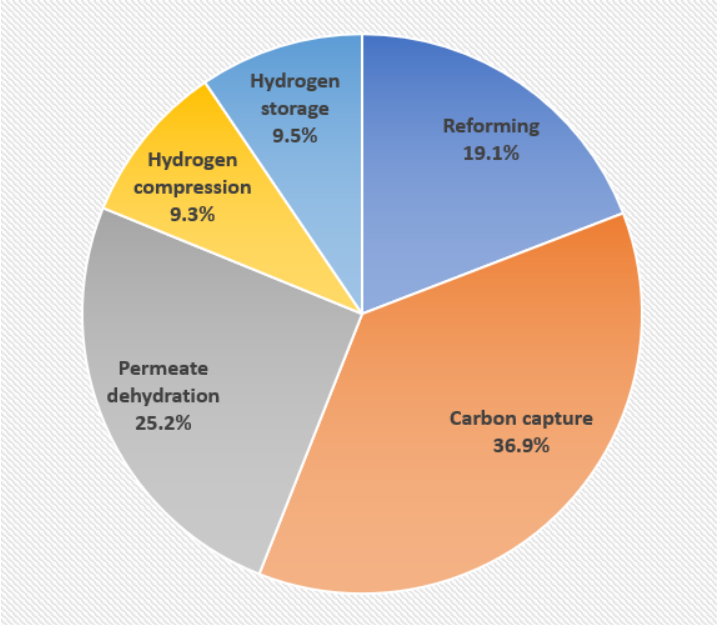

Figure F.2: Contribution to total component cost.

As seen in figure F.3, hydrogen compression is the major contributor to the annual operating cost at 45.8% followed by the reforming section at roughly 24.3%. The cooling water and electricity costs are the major contributors to the annual operating costs as seen in table F.1. The cooling water and electricity required for compression comprising of the largest portion. The reforming costs include biogas feed and fuel costs, biogas compression costs (electricity and cooling water), steam generation costs for feed, initial membrane tube cost & catalyst costs. The high costs for hydrogen compression are expected as hydrogen needs to be compressed to a high pressure of 700 bar.

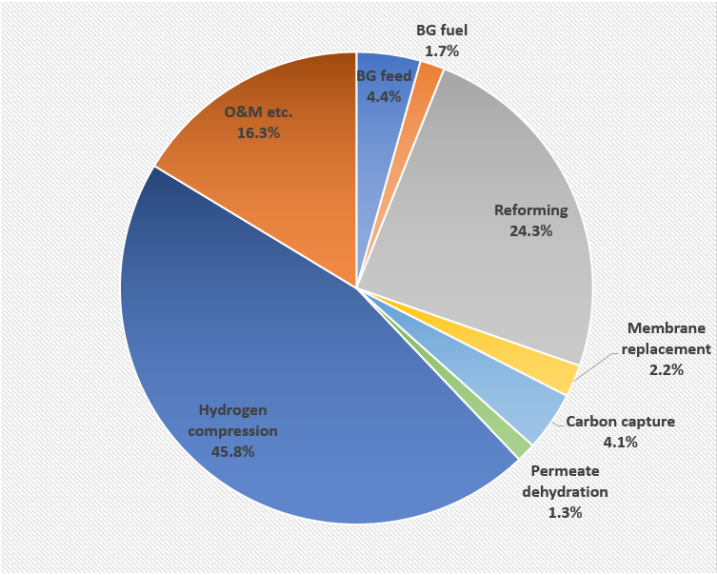

Figure F.3: Contribution to annual costs.

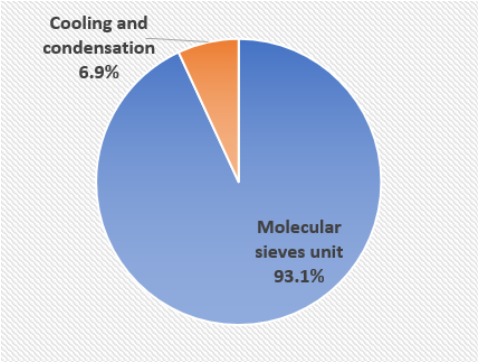

Figure F.4: Break-down of permeate dehydration component cost.

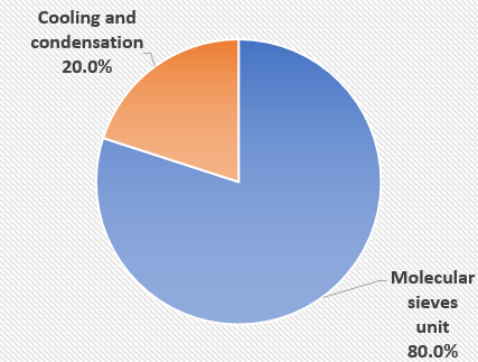

Figure F.5: Break-down of permeate dehydration annual operating cost.

The figures above show that the molecular sieves dehydration unit is the major cost factor in permeate dehydration. The high component cost is because it contains two columns, heat exchanger(s), blower(s) whereas the other part contains only heat exchangers for cooling and a knock-out drum to remove most of the water. The operating costs are high due to the intensive dehydration and regeneration processes requiring molecular sieves, purging etc.

G

Break-down of CO_2 emissions of the four cases

The value chain for the $reference\ case_c$ and $novel\ case_c$ with locations of CO_2 emissions is shown in the following figures. Later, the quantitative break-down of the CO_2 emissions of the four cases formulated in chapter 5 is presented.

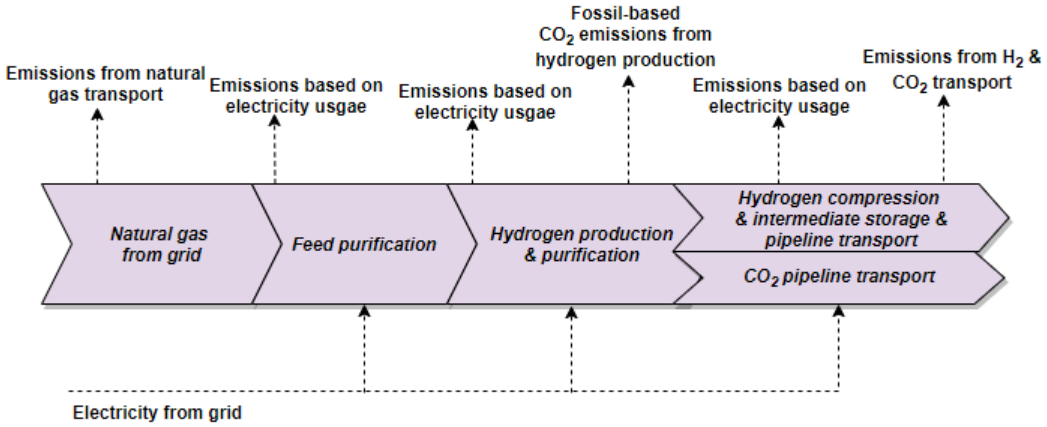

Figure G.1: Value chain of $reference\ case_c$ with locations of CO_2 emissions.

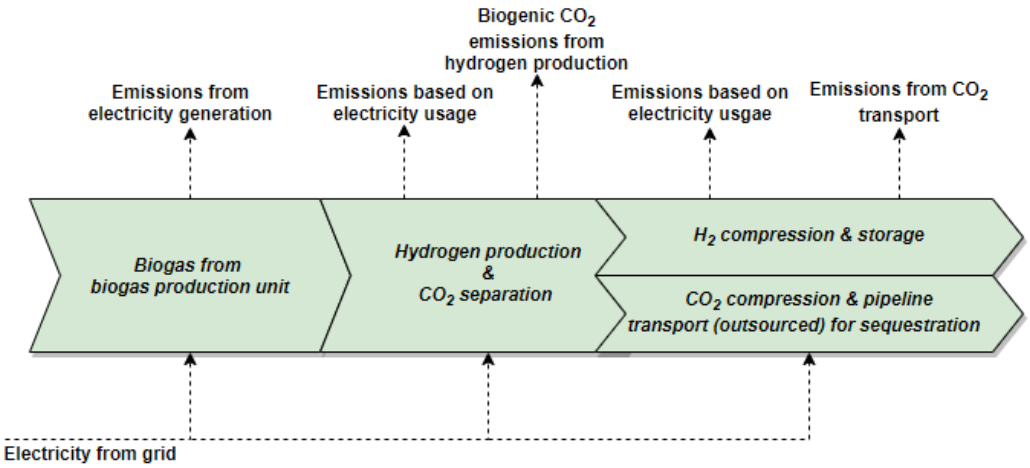

Figure G.2: Value chain of $novel\ case_c$ with locations of CO_2 emissions.

Table G.1: CO_2 emissions of both the processes across the value chain.

	Natural gas transport, kg CO_2/kg H_2	Biogas production, kg CO_2/kg H_2	Hydrogen production & compression, kg CO_2/kg H_2	Hydrogen transport, kg CO_2/kg H_2	CO_2 transport, kg CO_2/kg H_2	Total CO_2 emissions, kg CO_2/kg H_2	Net CO_2 emissions[a], kg CO_2/kg H_2
Reference case without CO_2 capture	0.0017	-	10.14	0.0005	-	10.14	10.14
Reference case with CO_2 capture	0.0017	-	5.44	0.0005	0.0025	5.45	5.45
Novel case without CO_2 capture	-	6.19	16.4	-	-	22.59	10
Novel case with CO_2 capture	-	6.19	7.78	-	0.0045	13.97	1.4

[a] Net CO_2 emissions for the novel cases are calculated as total CO_2 emissions of the process – total CO_2e in biogas (12.57 kg/ kg H_2).

H

Standard molar chemical exergy of selected substances

Table H.1: Standard Molar Chemical Exergy, (kJ/kmol), of selected Substances at 298 K and p_0.

Substance	Formula	Model I[a]	Model II[b]
Nitrogen	N_2(g)	640	720
Oxygen	O_2(g)	3950	3970
Carbon dioxide	CO_2(g)	14175	19870
Water	H_2O(g)	8635	9500
Water	H_2O(l)	45	900
Carbon (graphite)	C (s)	404590	410260
Hydrogen	H_2(g)	235250	236100
Sulphur	S(s)	598160	609600
Carbon monoxide	CO(g)	269410	275100
Sulphur dioxide	SO_2(g)	301940	313400
Nitrogen monoxide	NO(g)	88850	88900
Nitrogen dioxide	NO_2(g)	55565	55600
Hydrogen sulphide	H_2S(g)	799890	812000
Ammonia	NH_3(g)	336685	337900
Methane	CH_4(g)	824350	831650
Ethane	$C2H6$(g)	1482035	1495840
Methyl alcohol	CH_3OH(g)	715070	722300
Methyl alcohol	CH_3OH(l)	710745	718000
Ethyl alcohol	C_2H_5OH(g)	1348330	1363900
Ethyl alcohol	C_2H_5OH(l)	1342085	1357700

[a] $p_0 = 1.019$ atm.
[b] $p_0 = 1$ atm.
For more details and assumptions about the two models, refer (Moran and Shapiro).

Standard chemical exergy values are based on the standard exergy reference environment exhibiting standard reference temperature, T_o and pressure, p_o as already defined. Additionally, for the chemical exergy calculation, the reference state also consists of a set of reference substances with standard concentrations closely representing the chemical makeup of the natural environment. Two alternative standard exergy reference environments are commonly used, called Model I and Model II. For each of these models, the table gives values of standard chemical exergy for several substances, in units kJ/kmol. Either one of the models should be used in a particular analysis.

Exergy calculation verification

Exergy flow values for biogas feed and water feed are verified with manual calculations using equation 6.1. The exergy flow values from hand calculations are similar to the values from REFPROP (refer table 6.2). It is assumed that the REFPROP values are more accurate and therefore, all physical exergy values are taken from the software.

Table I.1: Biogas and water feed exergy flow (hand calculation).

	Mass fraction	**Temperature, °C**	**Pressure, bar**	**Enthalpy[a], kJ/kg**	**Entropy[b], kJ/kg K**	**Exergy, kJ/kg**	**Fraction, kJ/kg**
Biogas							
Methane	0.39037	35	1.01325	21.4618	0.0714755	0.377	0.147
	(reference)	25	1.01325	-0.9722	-0.0025427		
Carbon dioxide	0.594941	35	1.01325	514.39	2.766	0.2047	0.1217
	(reference)	25	1.01325	505.84	2.74		
Water	0.0125	35	1.01325	146.68	0.5053	0.696	8.72E-3
	(reference)	25	1.01325	104.89	0.3674		
Nitrogen	0.0022	35	1.01325	319.7	6.87	0.386	8.36E-4
	(reference)	25	1.01325	309.297	6.837		
Total							**0.278**
Water	1	15	1.01325	62.99	0.2245	0.6842	**0.6842**
	(reference)	25	1.01325	104.89	0.3674		

[a],[b] Values are taken from Moran and Shapiro.